POLITECNICO DI TORINO

Doctorate School

Ph.D. in Mechanical – XXVIII cycle

Doctor of Philosophy Thesis

ReHand:
a portable assistive rehabilitation hand exoskeleton

Ph.D. candidate:
Andrea Lince

Ph.D. Coordinator:

Professor Luigi Garibaldi

Ph.D. Supervisor:

Professor Stefano P. Pastorelli

April 2016

“No. Try not.

Do... or do not.

There is no try”

Yoda “The Empire Strikes Back” (1980)

The thesis contains information relating to an Italian pending patent

(Application 102016000044002)

Area disciplinare A09 – Ingegneria industriale e dell'informazione ING – IND/13
Meccanica applicata alle macchine.

Abstract

This dissertation presents a synthesis of a novel underactuated exoskeleton (namely *ReHand2*) thought and designed for a task-oriented rehabilitation and/or for *empower* the human hand.

The first part of this dissertation shows the current context about the robotic rehabilitation with a focus on hand pathologies, which influence the hand capability. The chapter is concluded with the presentation of ReHand2.

The second chapter describes the human hand biomechanics. Starting from the definition of human hand anatomy, passing through anthropometric data, to taxonomy on hand grasps and finger constraints, both from static and dynamic point of view. In addition, some information about the hand capability are given.

The third chapter analyze the current state of the art in hand exoskeleton for rehabilitation and empower tasks. In particular, the chapter presents exoskeleton technologies, from mechanisms to sensors, passing though transmission and actuators. Finally, the current state of the art in terms of prototype and commercial products is presented.

The fourth chapter introduces the concepts of underactuation with the basic explanation and the classical notation used typically in the prosthetic field. In addition, the chapter describe also the most used differential elements in the prosthetic, follow

by a statical analysis. Moreover typical transmission tree at inter-finger level as well as the intra- finger underactuation are explained .

The fifth chapter presents the prototype called *ReHand* summarizing the device description and explanation of the working principle. It describes also the kinetostatic analysis for both, inter- and the intra-finger modules. in the last section preliminary results obtained with the exoskeleton are shown and discussed, attention is pointed out on prototype's problems that have carry out at the second version of the device.

The sixth chapter describes the evolution of *ReHand*, describing the kinematics and dynamics behaviors. In particular, for the mathematical description is introduced the notation used in order to analyze and optimize the geometry of the entire device. The introduced model is also implemented in *Matlab Simulink* environment. Finally, the chapter presents the new features.

The seventh chapter describes the test bench and the methodologies used to evaluate the device statical, and dynamical performances. The chapter presents and discuss the experimental results and compare them with simulated one.

Finally in the last chapter the conclusion about the ReHand project are proposed as well as the future development. In particular, the idea to test de device in relevant environments. In addition some preliminary considerations about the thumb and the wrist are introduced, exploiting the possibility to modify the entire layout of the device, for instance changing the actuator location.

Contents

Chapter 1 Context and general background

This chapter presents an overview on the actual state of the art on hand exoskeletons. The analysis of the prior art permits to define the principal guidelines to generate novel approaches and technologies in order to design innovative devices that can rehabilitate and/or empower the human hand. The state of the art also allows devices to be compared by principal features and to classify them with the topological criterion.

1.1 What's an exoskeleton?

Since the past, the human being has the dream to improve his physical capability in terms of resistance and force, in ancient Greece as well as in modern age. Nowadays that dream has almost come true by the evolution in the field of exoskeletons or generally in wearable technologies, so the gap between sci-fi literature and reality is reduced (Fig. 1). The growing interest in this research field is mainly caused by the aging of the population and to the steadily increasing quality of health care. In particular, the research on exoskeletons is mainly focused on empowerment, assistance and rehabilitation of impaired people. In the last decades, different technologies have been used in order to realize a large variety of exoskeletons and orthoses for different human limbs. Dollar et al., in (Dollar and Herr 2008), define the difference between the two terms: usually, *exoskeleton* identifies a wearable mechanism that empowers a healthy subject, while the *active orthosis* is typically mentioned to describe a device

that is used to increase the ability of a person who suffers of a certain pathology. In this dissertation, the difference is not so strict for the particular nature of the presented device that can work in both applications.

Fig. 1. Comparison among the sci-fi exoskeleton and an example of real one. In particular, the right figure shows the Cyberdyne HAL®-5 (Hybrid Assistive Limb®).

1.2 Exoskeleton in rehabilitation and assistive process

The traditional rehabilitation is dominated by costly (about 260 €/day/patient) and largely inefficient treatments, often manual, which cause patient's treatment to stop when they recover about 60-70% of the limbs functionality; beyond that percentage, the ratio between cost and benefit is not worthwhile enough to justify continuing. After the treatment the patient, may still requires ongoing care to carry out the usual and normal activities. Those needs are usually carried on by the patient alone or by their family and sometimes it may result very heavy both from the economic and psychological point of view. From a recent Wintergreen report (Curtiss and Susan 2014), robot-assisted rehabilitation is probably the most promising approach to complement current clinical strategies because it permits to increase the intensity of

therapy with affordable costs and offers many advantages such as repeatability and major movement control. The above mentioned report (Curtiss and Susan 2014) consider all the aspects involved in robotic rehabilitation in order to analyse and predict the hospital rehabilitation market in the next five years period (2015-2020) Fig. 2 showing a "dramatical" trend prevision in the rehabilitation market. The health care market and more general in the market of home rehabilitation and services are expected to grow likewise "dramatically" as the robotic rehabilitation market (Fig. 2 b) reported in (Wyndaele and Wyndaele 2006).

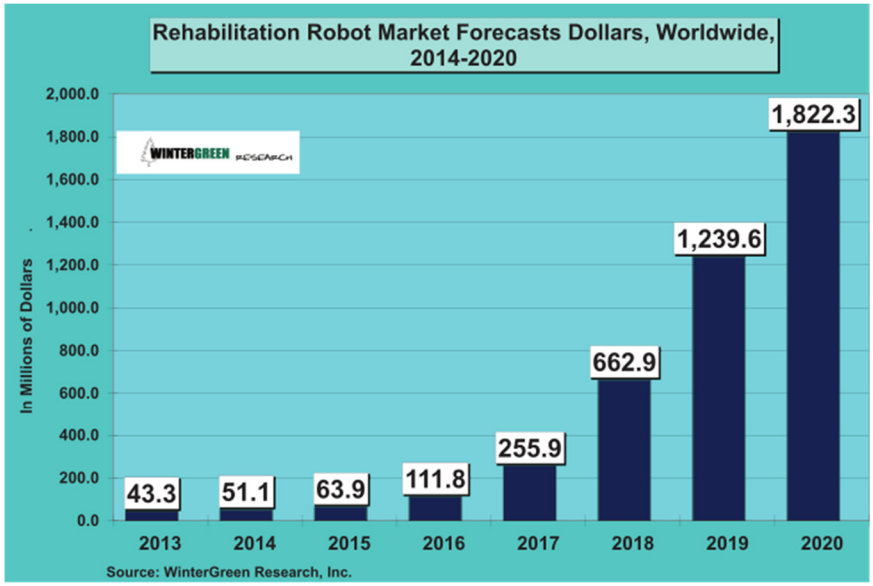

a)

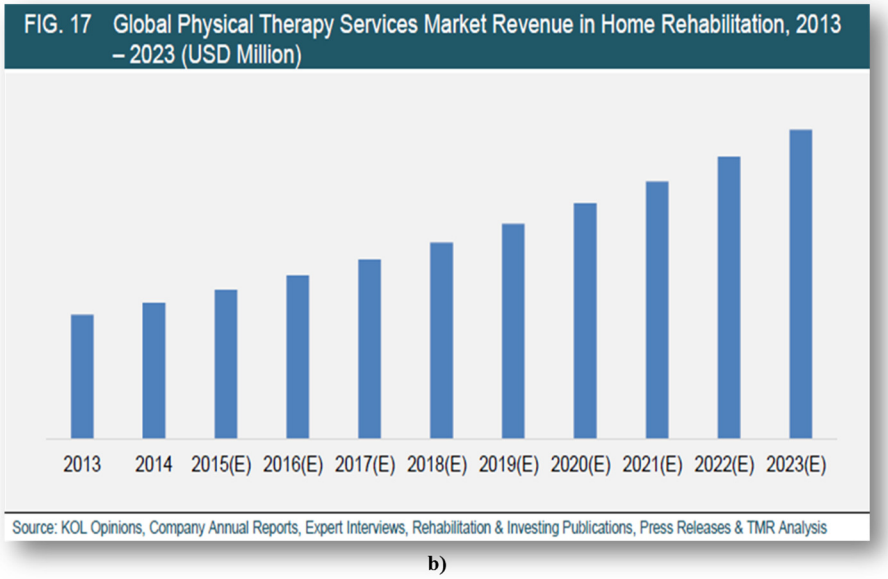

b)

Fig. 2. Prevision on robot rehabilitation market, a) worldwide forecasts from 2014 to 2020, the expected business volume is expressed in millions of dollars; b) home rehabilitation and service market from 2015 to 2023, it is expected that the market amount will be about 176 M€ in 2023.

The principal drivers of this exponential demand are the increasing effectiveness of robotic treatments, the decreasing costs related to a technology that today is new born and the ageing society, which provides a strong imperative to develop these kind of systems.

1.3 Hand impaired pathologies

A recent EUROSTAT report [http://ec.europa.eu/eurostat/web/health/health-care/] estimates that in all EU countries the proportion of the population aged over 65 will rise from 17.1% in 2008 to 30% in 2060 and consequentially also the population aged over 80 will rise from a percentage of 4.4% to 12.1% in the same period. Due to this fact, an increasing number of neurological disorders, e.g. stroke, ALS, traumatic brain and incomplete spinal cord injury, are expected. Moreover another direct consequence of these trends is the decline in the percentage of working population, meaning a shortage of supply for physical therapists and elderly support professionals in general, which will represent a serious problem in the future.

As the number one cause of adult physical disability in the developed world, stroke is a major public health burden. According to the statistical data from the Italian Ministry of Health, only in Italy 200000 strokes take place every year with a 20% mortality rate [http://www.salute.gov.it/portale/salute/p1_5.jsp?lingua=italiano&id=28&area=Malattie_cardiovascolari]. Almost 65% of strokes affect upper limbs mobility, limiting its ability to carry out everyday tasks. Therefore, hand rehabilitation becomes an ever increasing necessity in our country. As of today, there are almost 930000 people in Italy that suffer the consequences of stroke and are thus excluded from a productive and fulfilling life within society [http://www.aliceitalia.org].

Similar projections can be related to the future prevalence of neurodegenerative diseases. Currently, the incidence of illness as ALS (amyotrophic lateral sclerosis) in Europe is about 2.6/100000, with a peak age between 50 and 70 years, with the disease often starting in the hands, with patients losing dexterity and grip strength.

According to the Wyndaele review (Wyndaele and Wyndaele 2006), spinal cord injury (SCI) represents another principal cause of hand impairment. In EU countries, the SCI has a prevalence of about 252 per million. About half of the injuries bring tetraplegia, thus hand impairment, and about half of the injuries are complete (thus there is no possibility of recovery). This means that about 65000 people in Europe suffer hand

impairment due to SCI, and about 50 % of them need a device for assistance whereas also the other 50 % would benefit of a device for rehabilitation.

It is clear, summing all other neurological disorders causing hand impairment, for instance, neuropathies, traumatic brain injuries, incomplete spinal cord injuries, brachial plexus injuries that the number of patients requiring hand rehabilitation is considerable, and will become greater in the future.

In the depicted scenario, machines and robots are invaluable in rehabilitation, they measure patients' progress with great accuracy, are widely used to compare the outcomes and identify the people most likely to benefit from therapies. Some researchers think that machines will transform the way in which treatment is delivered.

As the cost of technology drops while the manual labour one rises, researchers hope that robots will not only lend help to deliver the intensive therapy needed for stroke recovery with increased control and precision, but also will do it more cost-effectively.

1.4 ReHand goal

Nowadays, traditional rehabilitative interventions are mainly focused on passive facilitation of isolated movements or on promotion of movements alternative to those performed before motor diseases. As a consequence of the increasing incidence of stroke patients and the related costs associated to rehabilitation care, it is necessary to establish an efficient rehabilitation protocol, which must definitely start in the hospital but have to possibly continue at home without therapy personnel. Timely and continued rehabilitation are the keys to promote motor functions restoration towards regaining independent living.

The ReHand exoskeleton is a robotic device developed in this thesis project. The robotic device will match with the human upper limb extremity, and consists of two main parts: backhand and finger. In general, the basic idea is to conceive an architecture that is on one hand simple and lightweight, maintaining the capability to assist the human subject when dealing with a huge variety of tasks; it is designed with the aim of minimal interference with natural movements. Regards backhand and four fingers, which show a complex biomechanical structure, the goal of simplicity and flexibility is obtained by means of underactuation: a single actuation unit drives the

whole mechanism that actively adapts to the instantaneous hand configuration. Thus, both lightness and physiological adaptability are addressed thoroughly. In detail, proper velocities/forces are transmitted to each assisted phalange of the fingers, allowing a flexible adaptation to the grasped objects regardless of their shape (Battezzato 2015).

It is noteworthy that the concept of under-actuation mechanically reproduces the strategy of the human brain: starting from a visual input of the object, which must be grasped, the brain determines a motor pattern which does not exploit all actuated DOFs, but adapts the hand to the object (Santello, Flanders, and Soechting 1998). Recent findings argued that the motor system has a modular architecture composed by basic modules (primitives) whose combination allow to express the natural behavior (E Bizzi et al. 2008). These architectures, also referred as compositional, are not unique in biological systems (e.g. DNA) and represent a useful framework for computational approaches. Nevertheless, understanding which rules allow the emergence of complex functions, such as motor behavior, when interacting with natural environments still remain a matter of debate (E. Bizzi and Cheung 2013). Indeed, the motor system seems to act like a modular framework recombining, with different weights, the same basic modules (primitives) to achieve a goal. This architecture has been proposed both as a kinematic (postural synergies) and dynamic model (muscle synergies), but the most of the knowledge available in humans has been collected in the field of dynamic control (i.e. muscle synergies). The ReHand device represents the first opportunity to merge two concepts of kinematic and dynamic downscale in the same device. Because of these needs the natural choice for exoskeleton structure are polymer-based produced by 3D printing. A manufacture based on 3D printing will allow both faster development of the prototypes and fast development of exoskeletal costumed on the single user, only changing few parameters on the general structure design on biometric parameters. There is a number of different 3D printing technique however the most promising in the field of biomedical application are stereolithography (Lu et al. 2006) for the photocurable materials.

In conclusion, the ReHand device, which will be developed in this thesis, is conceived as portable and self-wearable in order to promote home rehabilitation and to be used as assistive device in case of degenerative diseases. Acceptable assistive technologies for individuals with hand weakness (e.g. ALS patients) are currently lacking in routine

clinical care. There are devices available to assist macro movements of the upper arm (e.g. mobile arm supports (Atkins et al. 2008) and the Neater Eater [Neatereater.co.uk]), however even these are rarely used by patients as they are cumbersome and do not provide the level of function that patients find acceptable given by the intrusion of the device.

Chapter 2 Human hand anatomy

The hand is, perhaps, the most important limb for its primary role in *environment exploration, in the touch sensing* and in *object manipulation*. With these important roles, the number of devices to improve and rehabilitate these limbs has increased significantly in the last decades. Nevertheless, the design of hand devices, such as exoskeletons, is one of the biggest challenges for engineers due to complexity of structure and to versatility and dexterity of human hand.

This section describes biomechanical characteristics of the limb, starting from an analysis of the biostructure and its capabilities, continuing with anthropometric data and biomechanics constraints and, finally, listing the taxonomy of grasps.

2.1 Human hand

The human hand is composed by five digits namely thumb, index, middle, ring and little, each of them is composed by phalanges and articulations. In particular, the thumb is characterized by three articulations (from tip to wrist), *interphalangeal – IP, metacharphalangeal – MCP* and *trapezio-metacarpal –TM* respectively, and three links (always from tip to wrist), namely *distal, proximal* and *metacarpal* phalanges. The four fingers are identified by four phalanges: *distal, intermediate, proximal* and *metacarpal* respectively, and the same number of joints, namely *distal interphalangeal*

– DIP, proximal interphalangeal – PIP, metacarpophalangeal – MCP and *Humate-Metacarpal – HM*. The TM and MCP joints are characterized by two DOFs (*flexion/extension* and *adduction/abduction*). The other articulations, instead, can be modelled by a single DOF joint (flexion/extension) (Chen Chen et al. 2013), (Favetto 2014). In addition, the wrist adds two more DOFs to hand, in particular the flexion/extension and abduction/adduction motions. Fig. 3 shows the hand skeleton with the names of interesting bones and articulations. In conclusion, it is possible to consider human hand as a biomechanical structure composed by 24 DOFs.

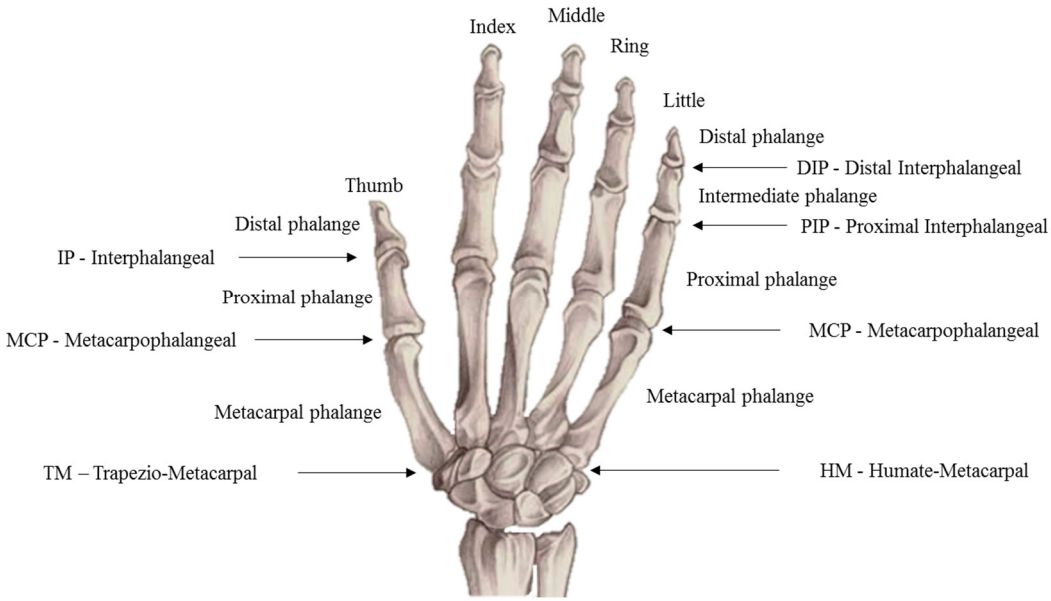

Fig. 3. Anatomical details of the hand skeleton.

The hand is a complex and dexterous limb, which allows different movements as shown in Fig. 4, where the biomedical terminology is illustrated [http://assh.org/].

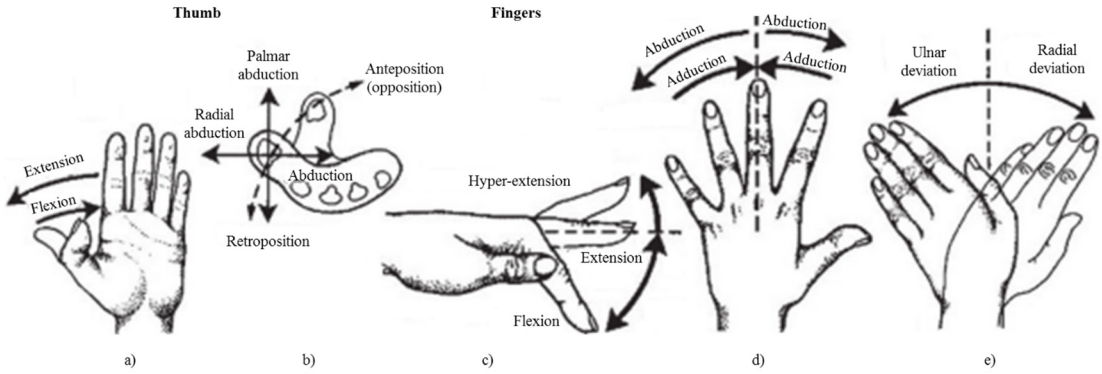

Fig. 4. Hand motion terminology, a) and b) show the terms regarding the thumb; instead c) and d) illustrate the motion of the long fingers and in e) the terminology for the wrist yaw, which assume different connotation according to the forearm bones.

The movements illustrated in the previous figure are driven by the muscles, most of them lie in the forearm and narrow into tendons across the wrist to reach insertions in the bony components. In particular, fingers' flexors are located in the supinator of the forearm; instead, the extensors lie in dorsal side of it. (Taylor and Schwarz 1955) and [http://assh.org/]. Fig. 5 shows the position of the principal extensors and flexors.

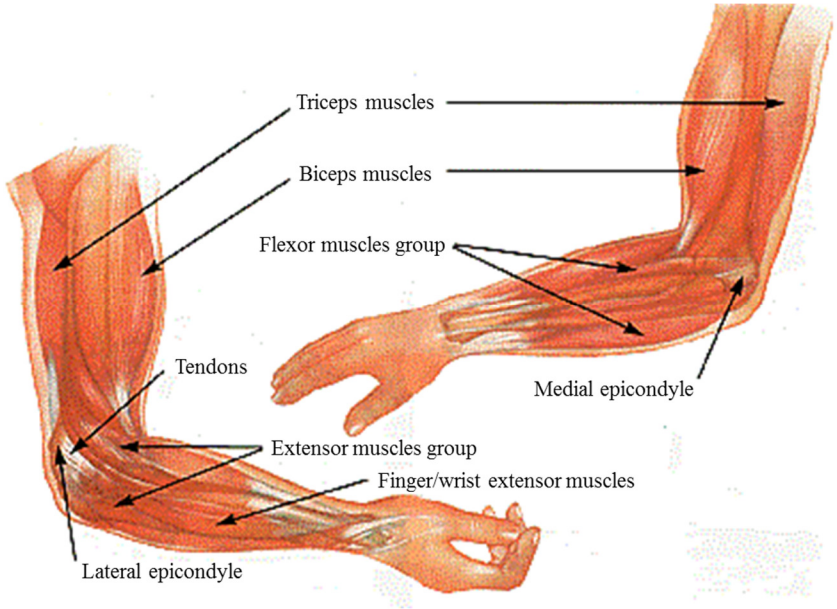

Fig. 5. Position of flexors and extensors for the long fingers.

In literature, it is possible to find several papers, which analyze hand dimensions and mass properties of each digit. In the following section, a summary of these hand properties have been reported. This information is essential in order to create and a

series of guidelines for the design, development and study of the kinematic and dynamic behaviors of a hand exoskeleton system.

2.2 Anthropometric data

Anthropometric information allows practical considerations: not only from a kinematic point of view, but it is also fundamental to predict the dynamic behavior of the whole exoskeleton's system. Starting from the Garrett's studies (Garrett 1970; Garrett 1971), it is possible to make a brief overview of anthropometric data, reported in the followed table (Tab. 1).

Tab. 1. Mean of hand dimensions measured on a sample of 148 men and 211 women (USAF members).

		Length (mm)			
		Mean	**St. d.**	**< 5 %**	**< 95 %**
Male	**Length**	197.2	9.3	183.2	211.5
	Breadth	89.6	4.0	83.2	97.1
	Metacarpal Circ.	215.9	9.0	200.2	230.8
	First Circ.	296.1	13.5	273.4	318.6
	Wrist Circ.	175.0	9.4	159.9	190.9
	Wrist Breadth	67.8	3.7	62.6	73.3
	Thickness	32.9	2.0	29.8	36.1
	Depth	61.9	4.5	55.0	70.2
Female	**Length**	179.3	8.6	165.3	192.7
	Breadth	77.1	3.8	70.6	83.2
	Metacarpal Circ.	187.1	8.3	174.5	201.5
	First Circ.	248.3	13.1	228.6	271.8
	Wrist Circ.	149.8	9.8	138.5	162.1
	Wrist Breadth	58.3	3.3	53.6	64.4
	Thickness	27.6	1.8	24.6	30.5
	Depth	51.7	3.9	45.3	58.2

Tab. 1 shows right hand dimensions referred to Fig. 6. The measurements are performed on 148 male and 211 female healthy subjects. Table reports also mean value, standard deviation and dimension values of 5 and 95 percentiles.

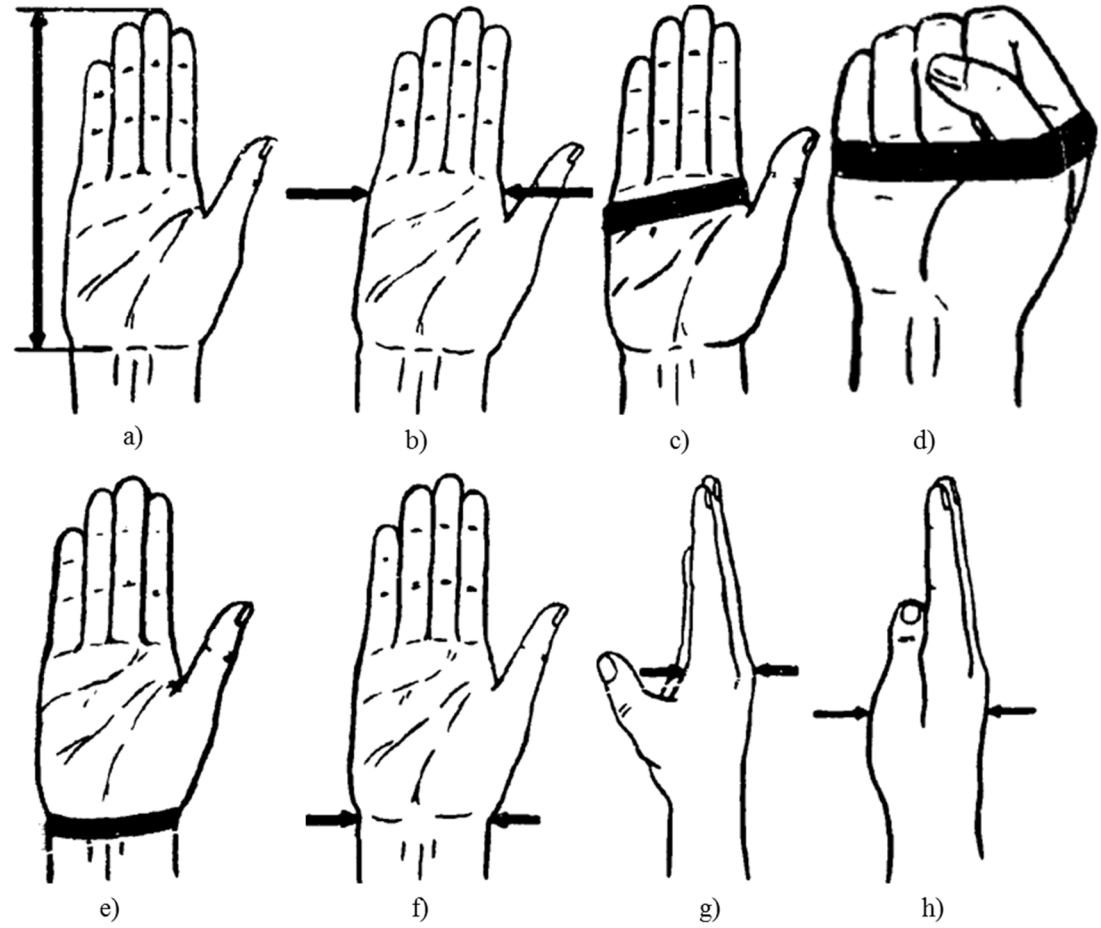

Fig. 6. Reference of analyzed hand dimensions in particular: a) hand length, b) hand breadth, c) hand circumference, d) metacarpal (or first) circumference, e) wrist circumference, f) wrist breadth, g) hand thickness, h) hand depth.

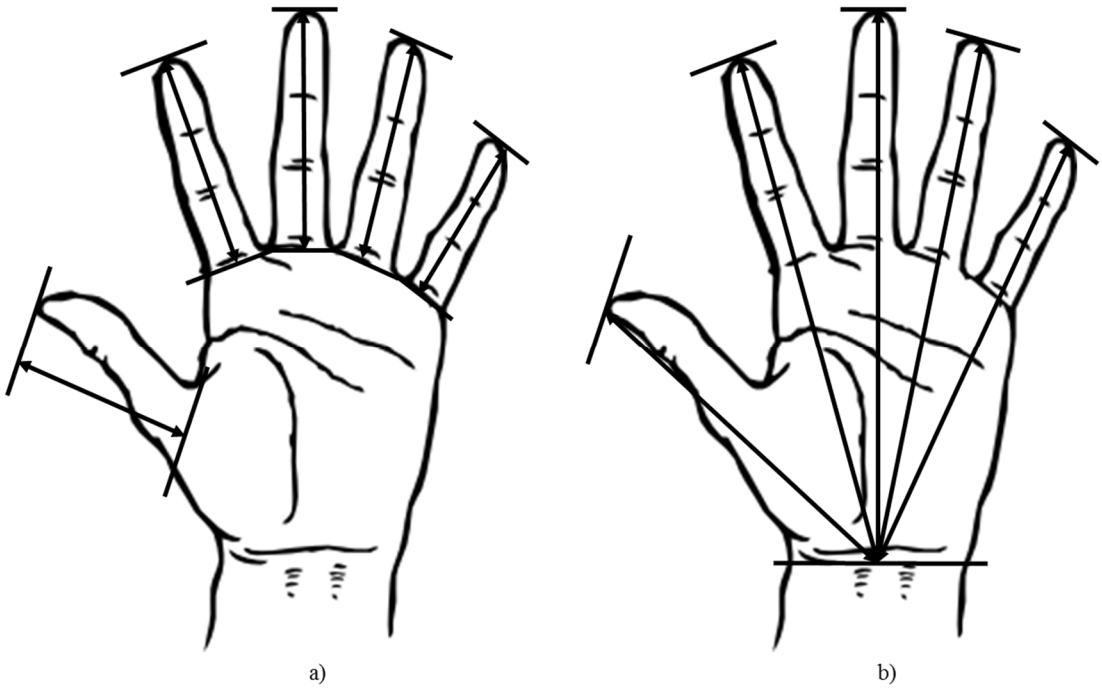

Fig. 7. Distance between fingertips to, a) crotch, b) to wrist crease.

2.2 Anthropometric data

Tab. 2. Length of entire human hand, 148 male and 211 female subjects.

		Length (mm)							
		Fingertip to crotch				**Fingertip to wrist crease**			
		Mean	**Std.**	**<5 %**	**<95 %**	**mean**	**Std.**	**<5 %**	**< 95 %**
Male	**Thumb**	58.7	4.5	50.7	65.7	127.0	11.3	110.5	146.8
	Index	75.3	4.6	68.3	81.9	185.2	8.8	173.3	200.6
	Middle	85.7	5.1	78.2	97.4	195.2	9.2	181.0	210.4
	Ring	80	4.7	74.4	89.3	187.2	9.1	175.2	202.8
	Little	61.4	4.7	54.4	69.9	166.1	9.1	151.1	181.0
Female	**Thumb**	53.7	4.4	46.8	61.2	110.5	10.0	95.1	128.3
	Index	69.0	5.2	61.0	78.0	166.7	8.9	152.1	181.4
	Middle	77.9	5.1	70.1	86.8	176.5	8.7	162.2	190.5
	Ring	73.1	5.2	65.2	82.2	167.6	89.4	152.8	182.0
	Little	54.6	4.4	48.0	62.4	146.4	9.2	131.1	161.2

Tab. 2 reports typical values used to describe the human hand (Fig. 7), which are called crotch to fingertip and wrist crease to fingertip. The crotch to fingertip length is the dimension evaluated along a hypothetical axis of the finger from the midpoint of its tip to the corresponding webbed crotch between fingers. Similarly, the wrist crease to tip dimension is the measured along a hypothetical axis passing through the fingertip midpoint in to the wrist crease baseline.

Tab. 3. Mean values of long finger phalanges lengths.

		Length (mm)											
	Hand	**Index**			**Middle**			**Ring**			**Little**		
		Distal	**Middle**	**Proximal**	**Distal**	**Middle**	**Proximal**	**Distal**	**Middle**	**Proximal**	**Distal**	**Middle**	**Proximal**
M	**Right**	23.2	23.7	26.5	26.0	27.8	28.0	22.9	25.6	27.6	19.6	19.2	25.1
	Left	23.2	23.9	26.1	26.0	28.2	27.5	23.0	25.9	27.8	19.5	19.8	24.9
F	**Right**	22.3	22.4	24.5	24.4	25.5	25.6	21.2	23.4	25.2	17.9	17.4	22.6
	Left	22.0	22.4	23.5	22.4	24.3	25.3	21.3	23.6	24.9	17.7	17.7	22.6

Tab. 3 describes the results of Habib et al. studies (Habib and Kamal 2010) about long finger phalanges lengths; the statistical analysis is performed on a large sample of subject varying by age and gender; in particular, authors analyzed phalanges length of 159 candidates (82 males and 77 female) with different age (18 - 25 years).

Tab. 4. Long finger weight properties, the inertia is estimated considering the approximation to a solid cylinder.

	Proximal		**Middle**		**Distal**	
	Mass (*g*)	**Inertia (*gmm²*)**	**Mass (*g*)**	**Inertia (*gmm²*)**	**Mass (*g*)**	**Inertia (*gmm²*)**
Index	30	9798	14	1899	7	1128
Middle	33	10778	16	2171	7	1803
Ring	22	7185	15	2035	7	1558
Little	18	5879	7	950	4	538

Finally, in order to develop a dynamic model of the exoskeleton system, the long fingers weight properties are introduced in the previous table (Tab. 4). The mass data are outcome of Biryukova et al. studies, about the dynamic behavior of human hand, and major information are reported in (Biryukova and Yourovskaya 1994). All the presented data, outcome of Garrett, Habib and Biryukova studies are fundamental in order to provide an idea about human hand dimensions. In particular, these data are collected on healthy subjects but can be used also for post-stroke patients, assuming in first approximation that the injury does not change the finger dimensions.

2.3 Hand grasps

The hand is the most important limb in terms of interaction with the surrounding environment; in fact, a human being can *touch*, *manipulate* and *feel* objects with different shape, dimension and surfaces. The structural complexity and the dexterity of hand makes the standard classification of its function a challenging exercise to be defined. In past years, several researchers proposed some standardization guidelines to classified the hand grasp, as Kapandji in (Kapandji I.A. 1970), Edwards in (Edwards, Buckland, and McCoy-Powlen 2002) and Cutkosky in (Cutkosky and Howe 1990). In particular, Kapandji and Edwards publications define, respectively, 21 and 20 types of grasps, while, in Cutkosky work, a list of 16 types of hand grasps is presented. For its simplification, in terms of grasps' types, the Cutkosky classification is largely used in the fields prosthetics and of robotic grippers (Fig. 8).

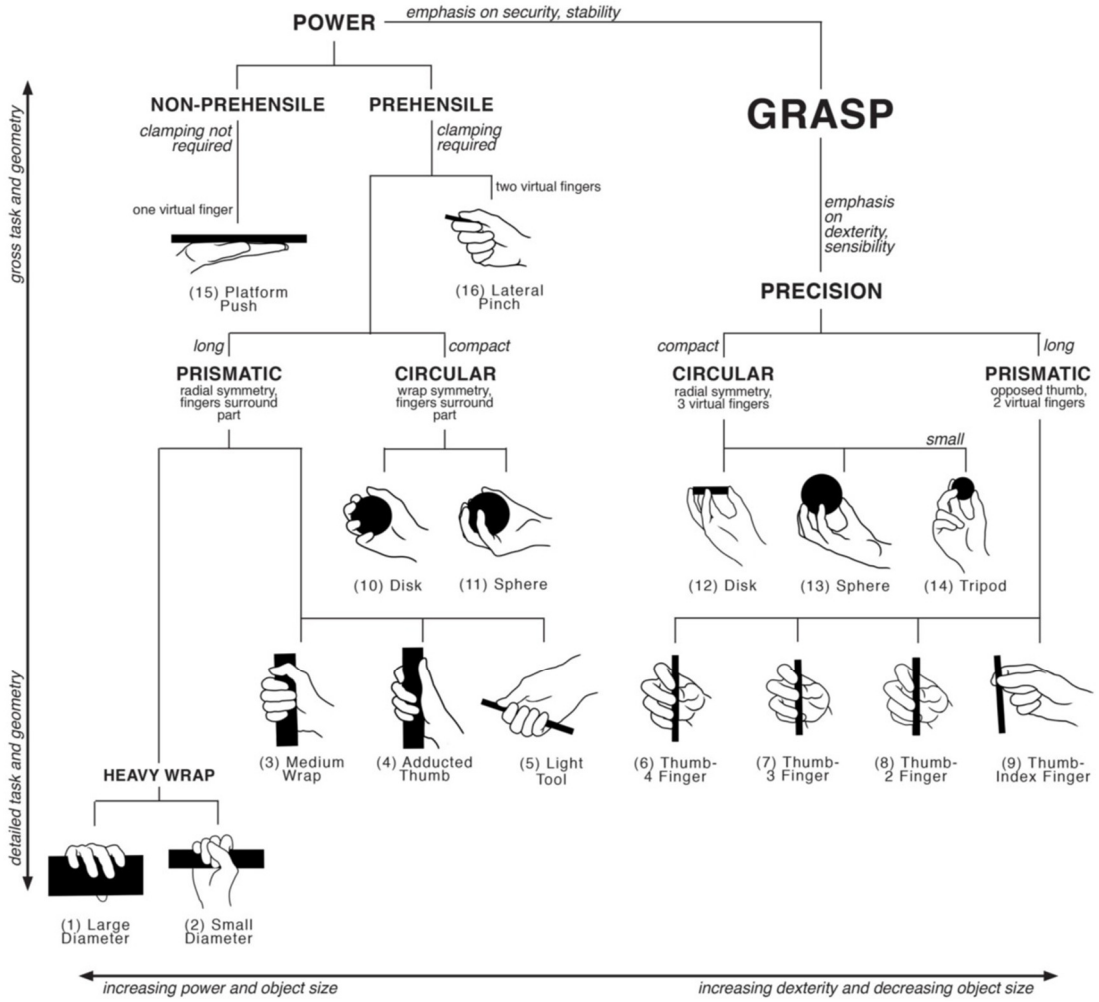

Fig. 8. Cutkosky and Zheng grasp three taxonomy (Cutkosky and Howe 1990) (Zheng et al. 2011).

Nonetheless, the previous publications do not give a clear and final definition of grasp from a bioengineering point of view. A suitable classification is given within GRASP project [http://grasp.xief.net/], which proposes new grasp taxonomies[1].

Before entering in the details of the proposed grasp taxonomy, it is necessary to define what a grasp is. Feix et al. in (Feix et al.) define a grasp as: *"…every static hand posture with which an object can be held securely with one hand, irrespective of the hand orientation…"*. The definition implies that the grasp stability has to be insured independently from the relative force and direction between hand and object, so under this assumption, Feix et al. have defined a more complete taxonomy, collects 33 grasp types, depicted in Fig. 9.

[1] Taxonomy: a branch of biology which concerns the classification of organisms into groups based on similarities of structure (Dictionary 1989).

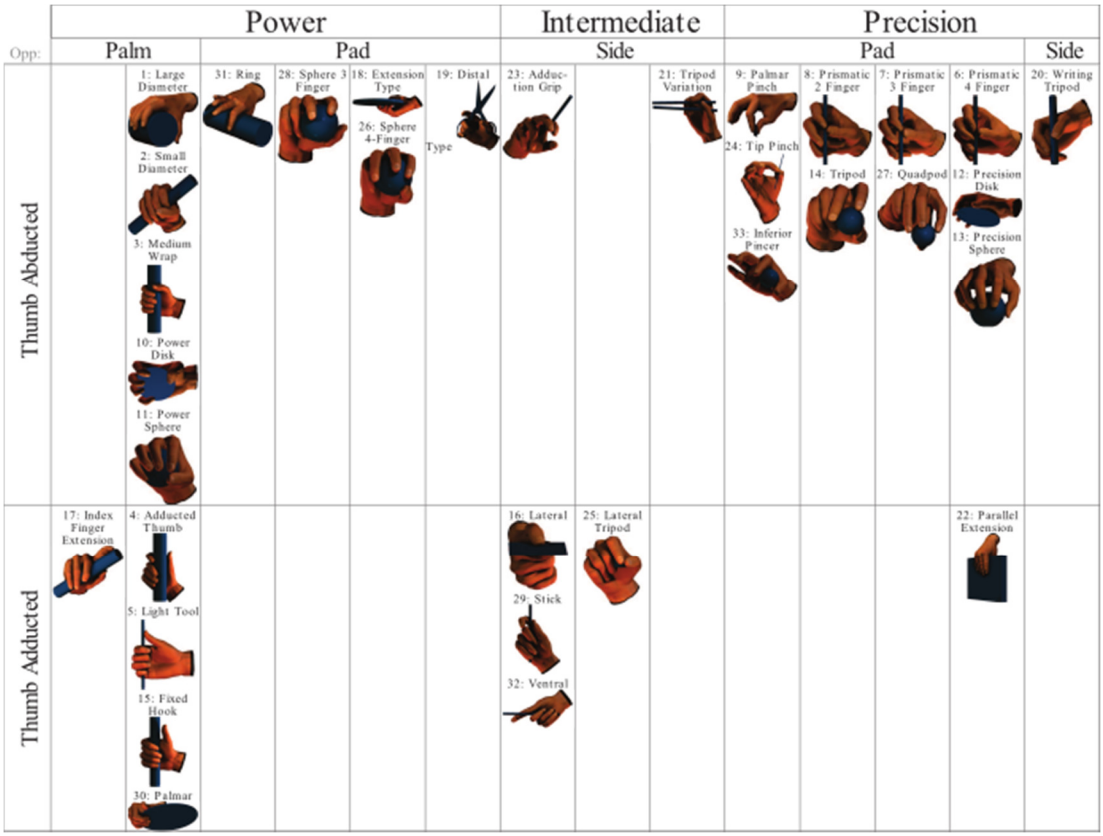

Fig. 9. Grasp taxonomy proposed by Feix et al (Feix et al.). *The grasps are categorized in the columns according to their assignment into power, intermediate and precision grasps, and the opposition type. Finally, the rows are classified by the thumb position (abducted or adducted).*

Fig. 9 reports the Feix et al. taxonomy. The grasps are arranged in columns according from power[2] to precision[3] grasps passing through the intermediate[4]; in addition, another differentiation concerns the opposition type (palm, pad or side). Finally, the thumb position defines the difference between rows, abduction and adduction of the thumb respectively. Considering the similarity of the properties (opposition type, thumb position, virtual fingers[5], etc.) of several grasps, it is possible to reduce the 33 grasp types into 17, without considering the object shape and dimension.

[2] Power grasps: Landsmeer in (Landsmeer 1962) proposed a power grasp definition; it is a handling where a rigid relation between the hand and the hold object is done.
[3] Precision grasps: according to Landsmeer (Landsmeer 1962), the precision grasp is defined as a handling where is possible perform intrinsic movements on the object without moving the arm.
[4] Intermediate grasps: the intermediate grasps is added in the Kakamura (Kamakura et al. 1980) and Skerik (Skerik, Weiss, and Flatt 1971) works. This category presents both power and precision elements in the same quantity.
[5] Virtual finger (VF): is a functional unit, proposed in (Iberall 1997). Fingers belong to the same virtual fingers if they apply forces in the same direction and act in simultaneously. The number of VF depends on the grasp type, the number of real fingers in contact and hand part.

2.4 Finger constraints

Every day we use the hands and fingers to interact with the surrounding environment, and it is very easy to verify that the phalanges' motions are not completely decoupled between each other. Even executing a simple and completely controlled movements, it is notable that other not planned actions are performed. This particular behavior is due to the presence of internal elements like tendons, ligaments and soft tissues that prevent a completely decoupling of the physiological joints. Several studies analyze the hand and finger constraints, which reduce the theoretical capability of them. These limitations can be summarized in two types: static and dynamic constraints; the latter in turn can be divided in inter-finger and intra-finger constraints. Inter-finger constraints concern the joints limitation among different fingers; while, the intra-finger ones regard the constraints belonging to different articulations on the same finger. These limitations reduce the effective hand degrees of freedom during motion. The constraints are described here, with aid of tables and pictures and the aim to analyze the hand limitations and capabilities, in order to develop a device with a compliant design.

2.4.1 Static constraints

"Static constraints generate limitations of the movement of the specific joint, independently from the position of the other articulations of the hand" (Favetto 2014). The human Range of Motion (RoM) collects all the static constraints; it is possible to define a finger RoM as the maximum and minimum value of physiological angle. In bioengineering, the physiological RoM is something ambiguous because it depends on personal characteristics and involves different elements, which are very difficult to express in closed form. Cobos et al. collected in (Cobos, Ferre, and Ortego 2008) the principal static limitations of the human hand. A survey of static constraints is reported in Tab. 5.

Tab. 5. Human hand static constraints.

Finger	*Joint*	*Flexion (°)*	*Extension (°)*	*Abd/Add (°)*
Thumb	TMC	50 - 90	15	45 - 60
	MCP	75 - 80	0	5
	IP	75 - 80	5 - 10	5
Index	CMC	5	0	0
	MCP	90	30 - 40	60
	PIP	110	0	0
	DIP	80 - 90	5	0
Middle	CMC	5	0	0
	MCP	90	30 - 40	45
	PIP	110	0	0
	DIP	80 - 90	5	0
Ring	CMC	10	0	0
	MCP	90	30 - 40	45
	PIP	120	0	0
	DIP	80 - 90	5	0
Little	CMC	15	0	0
	MCP	90	30 - 40	50
	PIP	135	0	0
	DIP	90	5	0

2.4.2 Dynamic constraints

Cobos et al. in (Cobos, Ferre, and Ortego 2008) (Cobos et al. 2007), collects, describes and models the hand dynamic constraints during grasping. This type of constraint can be categorized in intra-finger and inter-finger limitations. Intra-finger constraints are limitations that couple different articulations on the same finger; in addition, these kinds of limitations are studied in order to reproduce a specific grasp, for instance, cylindrical or prismatic power grasp (Cutkosky and Howe 1990). The inter-finger limitations involve different articulations belonging to different fingers: in other words, the inter-finger constraints are studied in order to detect the articulations' dependencies between index, middle, ring and little fingers. These dependencies are notable when

the finger moves from an initial configuration to another one (Lin, Wu, and Huang 2000). An example of dynamic intra- and inter-finger constraint for circular grasp is reported in the following table (Tab. 6).

In the table below, the Greek character ϑ represents the physiological angle followed by three nested subscripts that specify the finger, the joint and the movements involved. Concerning the motion, the flexion/extension is indicated as (f/e), while the abduction/adduction as (a/a).

Tab. 6. Inter-finger and intra-finger dynamic constraint during circular grasp.

	CMC	***MCP***		***PIP***
Thumb (t)	$\vartheta_{t_{CMC}} = \frac{11}{10}\vartheta_{t_{MCP}}$	$\vartheta_{t_{CMC}} = \frac{4}{5}\vartheta_{t_{PIP}}$		-
Index (i)	$\vartheta_{i_{CMC}} = \vartheta_{m_{MCP}}$	-	$\vartheta_{i_{MCP_{f/e}}} = \frac{4}{3}\vartheta_{i_{PIP}}$	$\vartheta_{i_{PIP}} = \frac{3}{2}\vartheta_{i_{DIP}}$
Middle (m)	$\vartheta_{m_{CMC}} = \vartheta_{r_{MCP}}$	$\vartheta_{m_{MCP_{a/a}}} = \frac{1}{5}\vartheta_{i_{MCP_{a/a}}}$	$\vartheta_{m_{MCP_{f/e}}} = \frac{4}{3}\vartheta_{m_{PIP}}$	$\vartheta_{m_{PIP}} = \frac{3}{2}\vartheta_{m_{DIP}}$
Ring (r)	$\vartheta_{r_{CMC}} = \vartheta_{l_{MCP}}$	$\vartheta_{r_{MCP_{a/a}}} = \frac{1}{2}\vartheta_{r_{MCP_{a/a}}}$	$\vartheta_{r_{MCP_{f/e}}} = \frac{4}{3}\vartheta_{r_{PIP}}$	$\vartheta_{r_{PIP}} = \frac{3}{2}\vartheta_{r_{DIP}}$
Little (l)	-	-	$\vartheta_{l_{MCP_{f/e}}} = \frac{4}{3}\vartheta_{l_{PIP}}$	$\vartheta_{l_{PIP}} = \frac{3}{2}\vartheta_{l_{DIP}}$

Static and dynamic constraints are very important because they allow the researcher to design and to develop physiological devices. On the other side, the dynamic limitations cannot be generalized because they are strictly related to the shape and dimension of the grasped objects and to the physiological differences among the human beings. In addition, the knowledge of the dynamic constraints is essential because it allows, in particular cases, to reduce the number of degrees of freedoms with the consequent reduction of device's complexity.

2.5 Hand capabilities

In this sub-section the human hand capabilities in terms of forces and velocities have been described. This knowledge is essential in order to dimension a suitable actuation strategy for a multi-fingered device. It must be kept in mind that these capabilities are strongly influenced by the training of the subjects. In addition, the collected data only give us an idea about the hand capabilities of each person.

2.5.1 Finger force and torque

In literature, several researchers analyzed the maximum force exchanged between the hand and the grasped object. These properties are important during the dimension the actuation module. An et al. in (An, Askew, and Chao 1986) performed a measurement of all normal forces applied on each phalange of each finger during a cylindrical maximum strength power grasp, using a system composed by a series of strain gauge sensors deployed in the mid-point of each phalange. The measurement results are reported in Tab. 7.

Tab. 7. Maximum forces exerted by the human phalanges during cylindrical power grasp, taken from (An, Askew, and Chao 1986)

	Maximum force (N)		
	Proximal	**Middle**	**Distal**
Index	42	22	62
Middle	24	40	68
Ring	15	28	44
Little	7	20	31

Other experimental results are performed by Lowe et al. in (Lowe, Kong, and Han 2006). The results consist in the average distribution of force during a circular power grasp. The experimental setup concerns in 20 force sensors based on conductive polymers, mounted in a thin leather glove, and located in the mid-point of phalanges. The table below (Tab. 8) reports the average forces expressed in Newton.

Tab. 8. Average forces exerted by the human phalanges during cylindrical power grasp, taken from (Lowe, Kong, and Han 2006).

	Average force (N)		
	Proximal	**Middle**	**Distal**
Index	21	26.1	45.9
Middle	29.3	36.5	64.1
Ring	22.3	27.8	48.8
Little	11.6	14.5	25.4

It is important to notice that results are referred to the same grasp type. Each tests performed by the author are different by subjects and experimental setups: so, the

results are suitable to give only an idea about the magnitude of the phalange forces and joint torque exerted during a power grasp.

Starting from the knowledge of phalange forces and the hand shape, it is possible to evaluate the finger torque, obtaining the position vector of the application point and making a simple cross product. The position vector describes the application point of the force and it give the contribution of each joint torque. Tab. 9 shows the maximum joint torque estimated by An's work.

Tab. 9. Maximum joint torque presented in An's work.

	Maximum joint torque (Nmm)		
	MCP	**PIP**	**DIP**
Index	2700	2280	775
Middle	3220	2890	850
Ring	2030	1800	550
Little	1260	1200	398

In conclusion, it is possible to notice that index and middle finger's performance results to be the strongest and it generates the biggest part of the force during the grip. These observations are very important because they imply different strategies for the development of the future device.

2.5.2 Velocities

The knowledge of the maximum speed of finger articulations gives us additional constraint regarding the tolerable velocities that have to be applied by the exoskeleton devices in order to replicate the human hand performances. Darling et al. in (Darling and Cole 1990) measured the fingers' joints velocity (except the DIP ones) during their works on dynamical fingers analysis. The measurements were performed on 4 subjects and the conclusions of these publications are reported in the following table (Tab. 10).

Tab. 10. Joints velocities.

	Speed (rad/s)		
	Peak	**"Natural"**	**Slow**
MCP	18	~10	3 - 6
PIP	12	~10	3 - 6

Several researchers confirm these results, as Saliba et al. in (Saliba, Camilleri, and Farrugia 2005), which measured the maximum velocity of MCP around 17 (rad/s) and estimated the peak PIP velocity around 18 (rad/s).

Chapter 3 State of the Art

As previously stated, the realization of a dexterous and versatile hand exoskeleton is one of the most significant challenges in rehabilitation robotics due to the above-mentioned reasons. Nowadays, the technology level allows to realize exoskeletons for elderly and impaired people, especially concerning arms and lower limbs, where a sort of standard has been reached. On the contrary, the hand exoskeletons are still very rare although the number of prototypes is increasing in the last decade. Before entering in the specific overview of hand mechanisms, it is necessary to make an analysis the most used technologies in this field, in order to organize the results of this survey on the current hand exoskeletons.

3.1 Hand exoskeleton technology

Exoskeletons are complex mechatronic systems; usually, as shown in Fig. 10, they are composed by one or more actuators and transmission modules to generate the power, a set of sensors to control the system and a mechanical structure or mechanism to connect together all the components and guarantee a properly kinematics and dynamics of the system.

In this section, the most used technology for exoskeleton devices will be described, in a synthetic way, with particular attention on finger/hand systems. In particular, the

different types of finger mechanisms will be observed, with the description of the working principle of actuators and transmissions as well as the type of used sensors.

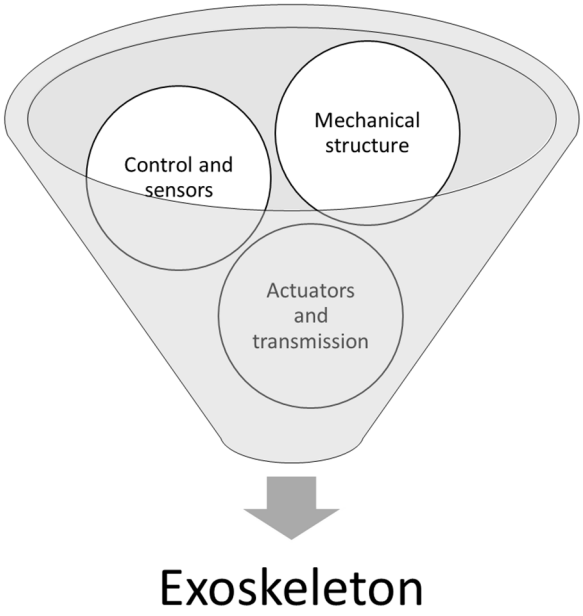

Fig. 10. General modules that compose an exoskeleton.

3.1.1 Mechanisms

Concerning mechanisms, Heo et al. (Heo et al. 2012) proposed a classification of the most used mechanisms in hand exoskeletons. The direct matching mechanisms (Fig. 11 a) is the simplest one and consists in a series of linkages connected to each other by mechanical joints placed in correspondence of the physiological ones. Such structure is built on the finger side and this fact is its main drawback; in fact, the structure can be used mainly for thumb, index and little fingers. This method is not ideal for a multi-fingered hand because it requires additional space among the fingers, moreover this solution does not overcome the issue of the finger crotch (that negate the access of the middle and ring MCP joint). In order to overcome the limit of the previous mechanism, different solutions have been developed. Fig. 11 b) shows a mechanism with remote center of motion (RCM). A generic RCM mechanism is located away from the finger joint in order to reduce the size on the finger side and it does not requires the correspondence between mechanical joints and human ones. A particular type of RCM is the redundant linkage mechanism shows in Fig. 11 c). In this case, the redundant DOF is eliminated by the constraints given when the mechanism is attached to the finger. Another example of RCM mechanism is the serial

linkage attached to the distal phalange, reported in Fig. 11 f). Beside RCM mechanisms, there are also two types that are hybrid with the type of transmission and actuation. Fig. 11 d) and Fig. 11 e) show the finger mechanisms actuated by a bending actuator attached on the finger's joints and by a tendon driven mechanism respectively. It is possible to combine different types of mechanisms in order to obtain some specifications; for instance, a tendon-driven mechanism with the redundant linkage structure.

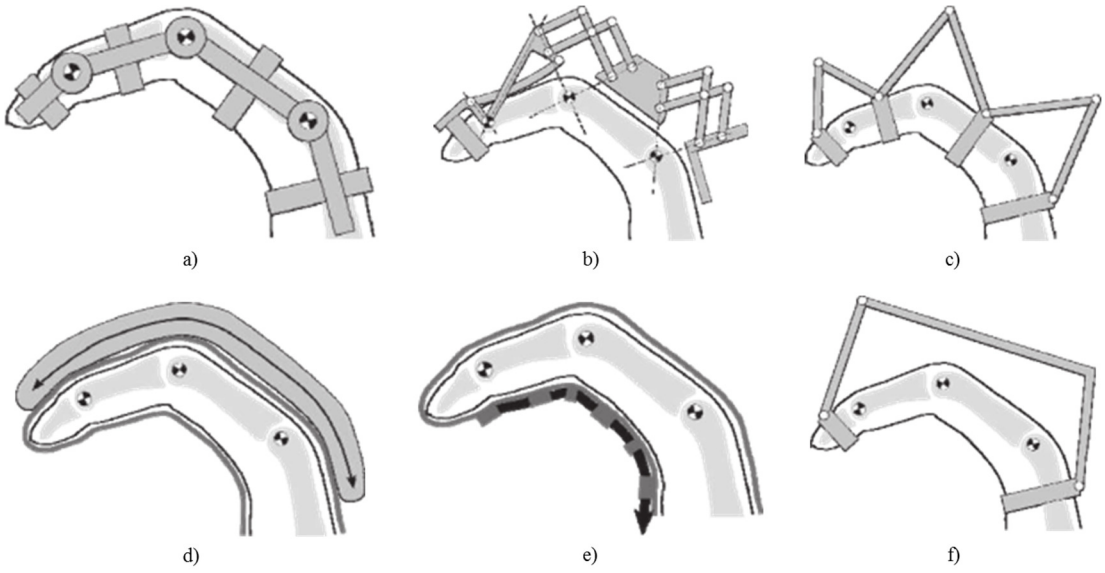

Fig. 11. Common mechanisms used in hand exoskeletons; a) direct matching of joints axis; b) remote center of motion (RCM); c) redundant linkage mechanism d) bending mechanism; e) tendon-driven mechanism and f) serial linkage attached to the distal digit.

3.1.2 Transmission

The second fundamental part on the hand exoskeleton device is represented by the transmission. Usually it is not possible to attach the actuators directly on the joint, so a suitable transmission method is necessary in order to remote the location of the actuators. Remoting the actuators allows to manage overall dimension and weight properties. Usually, when electrical motors are employed, it is necessary to use two transmission steps: the first one is used in order to reduce the speed and increase the torque; and generally, gearhead, screw or rank-pinion types are applied. After this reduction step, usually, another transmission mechanism is used in order to reach the joints. In particular, wires, linkage and bending mechanisms (as Bowden cable) are

used. On the contrary, other type of actuations as bending actuators or shape memory alloys can be used directly on the mechanical structure or substitute it, as described in the following sections.

3.1.3 Actuators

Generally, the actuation system is a critical point during the development of robotic devices, and particularly in hand exoskeleton, where dimension, weight and power are tight constraints. In the last decades significant progress in the development of actuation technologies has been made. Nowadays, it is possible to find several types of actuators in the market (Fig. 12), and in the recent years, the related research activity was focused mainly on variable stiffness actuators in order to develop safe devices in human environment. The actuator choice require to take in account several properties as the generating power and the speed, in order to guarantee a good level of dexterity. Moreover, due to the space limitations of this project, features like power to volume and power to weight ratios are very important.

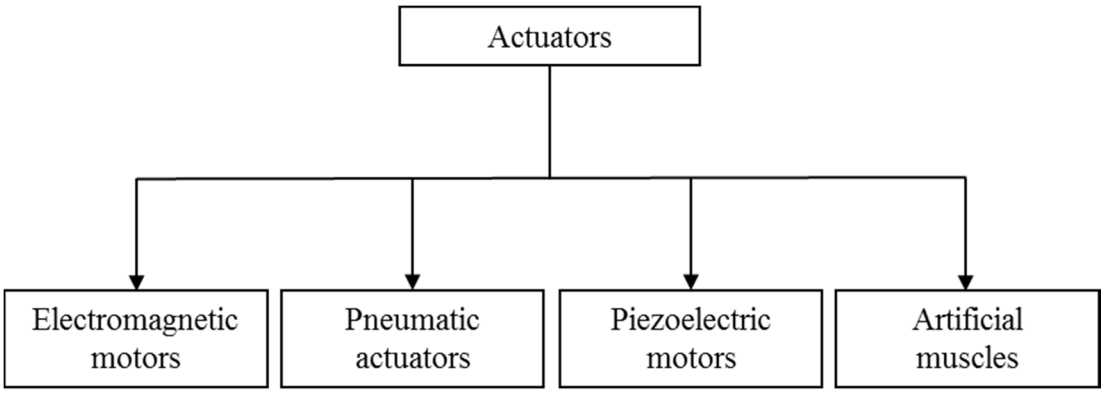

Fig. 12. Categorization of actuators collected by working principle.

Electromagnetic actuators

A large amount of electromagnetic actuators is available in the market. The most common electric drives can be categorized in direct current actuators (DC motors) and alternative current actuators (AC motors). Beside these two main categories, there are also voice coil actuators, steppers and brushless motors. In the following figure (Fig. 13) a categorization of electric drivers is reported. From a functional point of view, there are no differences between them, because the torque is generated by the

interaction between the magnetic fields of the stator and the one of the rotor. The main difference concerns the generation of magnetic field, which can be produced by coils, permanent magnets or electromagnets. The distribution of magnetic field in the gap between rotor and stator is strictly related to the generated torque; in particular, this gap limits the maximum magnetic flux density and then the maximum current that could be provided to the coils. Usually, the maximum theoretical torque is available only for limited time due to thermal constraints the actuating time can be increased reducing the torque magnitude or reducing the temperature. This kind of actuators needs to have a dissipative or cooling system in order to prevent overheating during the operation time. For the above-mentioned reasons, usually, it would better to have electromagnetic motors with low torques and high speed, but this limitation is overcame with the use of gearboxes, which amplify the output torque decreasing the speed. The main critical aspects regarding this technology is its weight, relatively low power density, heat dissipation and the undesirable characteristic of friction backlash at the standpoint, resulting from the coupling of motor and gearbox. On the other hand, the easy of supply and control and its well-known behavior make this technology the most popular choice in the exoskeleton and prosthetic field.

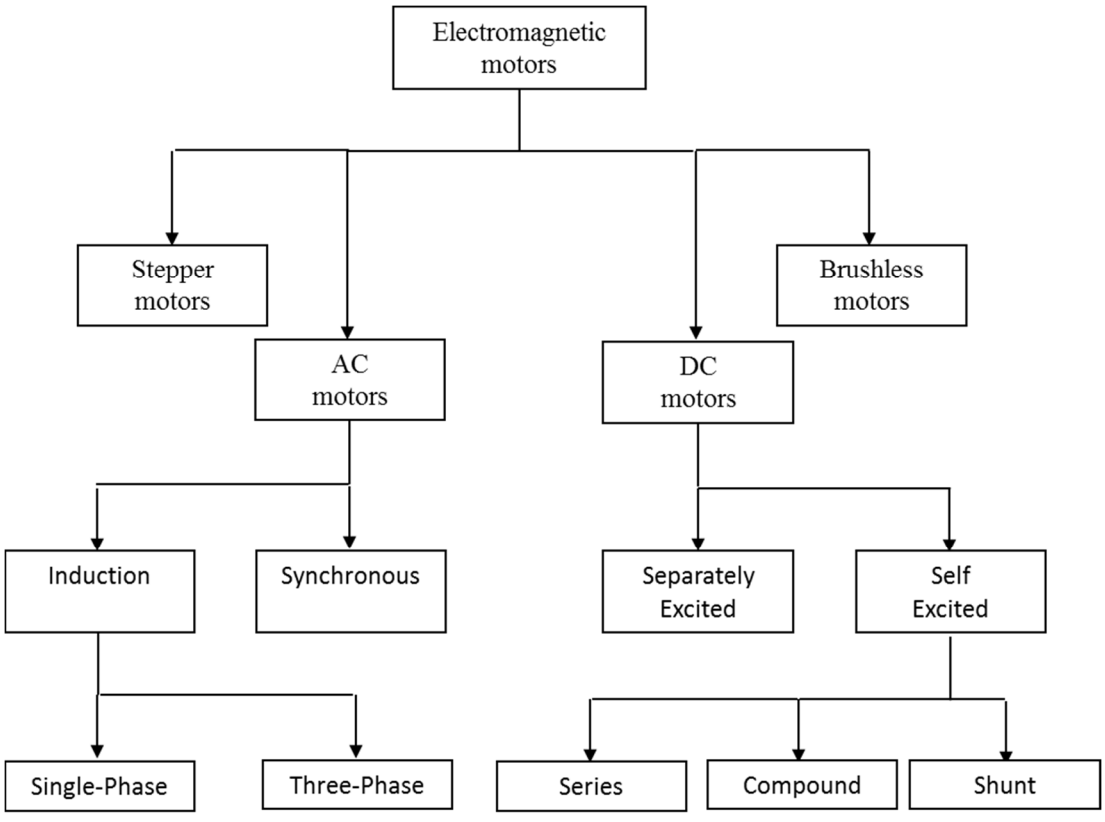

Fig. 13. Categorization of electromagnetic actuators.

Pneumatic actuators

Pneumatic actuators transform the energy stored up by pressurized air into mechanical power. Air is usually pressurized by compressors, which are generally bulky and noisy. The noise issue can be overcome using pre-compressed air storage. Moreover, the size of pneumatic actuators and valves cannot be easily reduced due to the storage air chamber volume and problems related to leakages that require a careful design. The pneumatic actuators can generate a linear motion or a rotational one, and they are usually composed by a piston driven by pressurized gas. Another type of pneumatic actuator, called McKibben artificial muscle, will be described in the section about artificial muscles. In general, pneumatic actuators have advantages of good power to mass ratio, good velocity performance and reduced weight in loco; in contrast, issue regarding the supplier represents its major disadvantage. Nevertheless, pneumatic actuators are often used in lower mobility systems and several hand exoskeleton driven by pneumatic actuators can be found in literature, as presented in the following section.

Piezoelectric actuators

Piezoelectric actuators transform vibrations generated by piezoelectric materials in linear or rotational displacement: for instance, linear micro-stepper and ultrasonic motors. The vibrations are generated by a differential of voltage applied on the crystal surfaces of the material. Similarly, when an external force stresses piezoelectric material, it answers generating an electrical charge proportional to its deformation. Usually, the deformation on the piezoelectric material is not suitable to be used directly, so a large number of mechanisms are designed in order to amplify these properties. Piezoelectric actuators, as said before, transform the vibration motion in linear or rotational displacements, using frictional forces in order to generate the output forces/torques. Usually, this kind of technology is suitable to be used directly without reduction stages but high precision is requested during the fabrication process, increasing the costs. Usually these actuators are driven with a frequency modulation strategy and it can happen that used frequencies are in the audible specter causing annoying and hazardous noises.

Artificial muscles

This sub-section describes the principal actuators that mimic the physiological behavior of muscles. These three types are shape memory alloys, electro-polymers and McKibben muscles. These types have similar external behavior, thus contracting themselves, but have completely different working principles.

The McKibben muscle is the most known Pneumatic Artificial Muscle (PAM) and it works by filling of pressurized air an inflatable elastic bladder, surrounded by an un-stretchable mash. When the air is blown up, the device contracts itself, as a muscle, due to the different layers' elastic module. In particular, the different layers force the volume expansion into a linear contraction along the actuator axis.

Shape-Memory Alloy Actuators, or simply SMAA, are based on the physical effect called shape memory. The shape-memory alloys are able to change their shape as consequence of an external specific stimulus and return to an un-deformed state, previously memorized, when the stimulus is over. The memory effect is guaranteed by the transition between two phases: the martensitic and the austenitic phases, during the external excitation. Usually, this materials are sold as wires and the external stimulus is a thermal variation obtained through Joule effect. It is important to notice that while it result very easy provide heat to an object, it is more tricky to remove it; this fact is one of the most problematic aspect of SMA and usually cause a strongly asymmetric behavior. The main advantage is the power weight ratio, which is very high compared with traditional actuators. In contrary, the major disadvantages are related to the cooling system.

The last group of artificial muscles is the electroactive polymer actuators (EPAs). The electro-polymeric actuators convert the electrochemical energy into mechanical one with a behavior similar to human muscles. The electro-polymeric materials are able to change their shape, bend, or contract as consequence of an external stimulus as the SMAA. This technology has today many limitations due to its infancy, and EPAs are not used yet for robotic applications due their difficult control.

Variable compliance actuators

The classical actuators have good performances in terms of power respect to muscles, on the contrary, the biological muscles are excellent in terms of power to weight and

force to weight ratios, compliance, and control as said by Van Ham et al. in (Van Ham et al. 2009). Among all the differences Alexander states that the key difference between classical actuators and muscles is the compliance (Alexander 1990). In fact, in the last years, the research activity on actuators has increased its interest on variable compliance actuators. The growing interest in this field is due to the increasing success of wearable robotics but is also fundamental for the development in rehabilitation devices or, more in general, in those applications where a certain level of safety is required because there is physical interaction between man and machines (Van Ham et al. 2009). Vanderborght et al. in (Vanderborght et al. 2013) give us the VIA (Variable Impedance Actuator) definition starting by the description of classical actuators. A stiff actuator is a device able to move and follow a predefined path, when the final position is reached: ideally, the actuator holds this position independently from external applied loads. This behavior is given to traditional actuators by their own stiffness. On the contrary, a VIA is a device able to deviate from its equilibrium position, depending on external loads and on the mechanical properties of the actuator. In this case, the equilibrium is defined at a virtual position (Hogan 1985) where the actuators generate zero force. The variability of compliance can be obtained in several manners as proposed in the following figure, (Fig. 14) from a revision of the Vanderborght categorizations (Vanderborght et al. 2013).

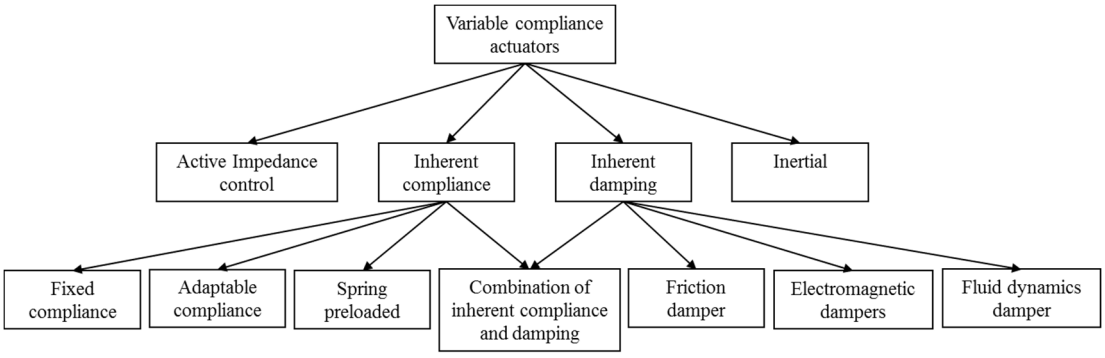

Fig. 14. Categorizations of VIAs.

In conclusion, the main advantages of VIAs can be summarized in the following points:

a) Efficiency;
b) Robustness to external perturbation and unpredictable dynamics;

c) Adaptability and force accuracy in the interaction with the operator;
d) Safety for humans.

3.1.4 Sensors

A network of sensors is fundamental in order to create robotic devices. In particular, type and amount of sensors defines the control strategy, as well as their placement, size and number affect the design of the whole device. In exoskeleton and prosthetics field, it is necessary to detect the motion intention of the limbs and its interaction with the environment: this goal can be accomplished with several different sensing methods. The market presents several types of sensors, which are suitable for the above-mentioned applications. Different physical principles can be adopted, either to control the articulation attitude, the intention of movement and to detect the exchanged force with the environment. Obviously, there is not only one correct solution: several types of sensors can be used, according to project constraints and actuation system. Regarding the aim of this project the sensors are chosen considering the imposed constraints as size, working space, and energy consumption. In this section, the sensors are classified on the basis of the types of measured signals; in particular, they are divided in motion, force and bioelectrical sensors.

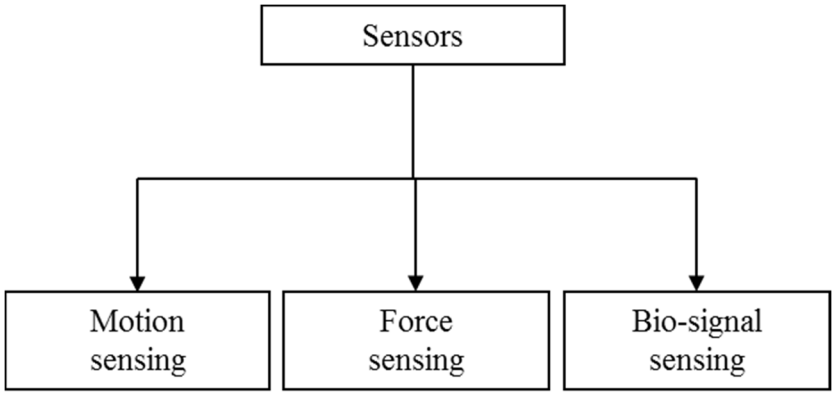

Fig. 15. Categorization of sensors used in this dissertation.

Motion sensing

The articulation's angle can be used as feedback signal for a position control of assistive exoskeletons. Usually, with this kind of control, it is necessary to implement a master-slave configuration. Generally, the finger angle can be measured with flexible electrogoniometers, bend sensors and rotary encoders.

Electrogoniometer

Electrogoniometers are resistive transducers that convert a joint angle into a voltage; usually, the output signal is obtained by means of potentiometers or strain gauges. The operating principle of an electrogoniometer exploits the presence of a variable resistor, which varies its resistance according to the joint angle. The electrogoniometer based on potentiometer, results bulky for rehabilitation purposes and constrains the patients' movements: in addition, the instrument's precision can be compromised by its inability to follow changes in the rotation axis. Flexible electrogoniometers are based on strain gauges and take advantage of strain gauges deformation to change, proportionally, the electrical resistance with the consequent voltage variation. Flexible goniometers have several advantages as low weight, and small size; furthermore, they are easily applicable on injured patients: due to these characteristics, they are the most used in biomedical engineering.

Bend or flex sensors

Flexible or bend sensors are a type of position sensors. As the goniometers, they are usually composed by piezoelectric materials or carbon elements. They change their nominal resistance proportionally with the bending radius. In particular, the smaller the radius is, the greater is the electrical resistance. Bending sensors are suitable for exoskeleton applications because they are very compact, lightweight and low cost. In order to take advantage of all the measurement potentials, the sensors require an accurate deployment.

Rotary encoders

Rotary encoders convert an angle rotation of a shaft into an analog or digital signal; this type of sensor can be absolute or incremental (or relative), and it can be built with several operating principles. The most common technologies divide the encoders in mechanical, optical, magnetic and capacitive ones. Generally, these sensors are accurate and precise; in the market, there are several dimensions available but the miniaturized ones are very expensive. On the contrary, placement is a big issue since it is not always possible to directly measure the articulation angle and sometime a mechanism is required in order to remote the bulky frame.

Force sensing

Another method used to detect the movement intention is based on the measurement of forces generated by the users at the interface between human limb and exoskeleton.

This method is used for the control of many assistive exoskeletons and usually the force sensor is located at the fingertip level. Force sensing resistors (FSRs), pressure sensors and strain gauge sensors are the most common choices to implement a force control.

Load cells

Load cells are a huge slice of the force sensors market thanks to their good accuracy and repeatability. These sensors can exploit different technologies such as strain gauges, piezoelectric, piezoresistive, hydraulics and pneumatics. These sensors create an electrical signal, proportional to an external load. In strain gauges load cells, the variation of the force exploits the change in electrical resistance as a consequence of the strain gauges deformations. Usually, load cells are composed by four strain gauges in a full Wheatstone bridge configuration but also other configurations are available as quarter bridge configuration (only one strain gauge in the bridge) and half bridge (when two strain gauges are used in the bridge). The strain gauge load cells can fail with high dynamic measurements. The piezoelectric load cells overcome this issue: these sensors are based on piezoelectric materials, which generate an output tension proportional to the load cell deformation. The piezoresistive devices generate an output tension due to the change of electrical resistance caused by the deformation of the devices. The main issues for these sensors is the overload, the nonlinearity at the end of their scale and the mechanical mounting.

Flexible force sensors

Using the piezoresistive effect, a series of flexible force sensors have been developed in the last ten years. In order to reduce the product cost and the sensors dimension, the flexible force sensors are fabricated using special piezoelectric or piezoresistive inks, resulting in a thin (< 0.50 mm) and flexible device, easily adaptable on the hand surface.

Tactile sensors

Tactile transducers are sensors capable to detect external stimuli from mechanical stimulation and in general, temperature and pain. Usually, tactile sensors exploit capacitance effects, in particular, the external stimulus varies the capacitance values, and consequently the tension output. On the market, it is possible to find pressure arrays, which provide a high resolution of the contact surface. Tactile sensors arrays can be built from conductive rubber, polyvinylidene fluoride (PVDF) and metallic capacitive sensing elements.

Bio-signal sensors

Use of bio-signals as detection of the human intention is another developed method to command exoskeletons and it is the state of art of commercial prosthesis control. There are several bio-electrical signals in human's body but the most used for this purpose is the surface electromyography (sEMG). The sEMG observes the bio-potential coming from the brain to the muscles measured on the skin surface. The EMG signals are related to the force that the human body intends to apply with the muscles. As previously mentioned, the finger muscles are placed in the forearm except for the thumb, allowing the sensor system to be located away from the hand. On the contrary, the main disadvantages concern the complex post processing treatment of signals and the requirement of an accurate placement of sensors on the skin.

3.2 Hand exoskeletons

In this section, recently developed hand exoskeletons will be investigate.. According to (Heo et al. 2012) and (Foumashi, Troncossi, and Castelli 2011), various criteria can be use in order to classify the hand devices such as: actuator type (pneumatic, electric, SMA etc.), purpose, power transmission (link, cable, direct actuation) or control input (EMG, force etc.). In this dissertation, the hand exoskeletons will be classified by its purpose, in order to discriminate several guidelines for the development of the ReHand exoskeleton mechanism.

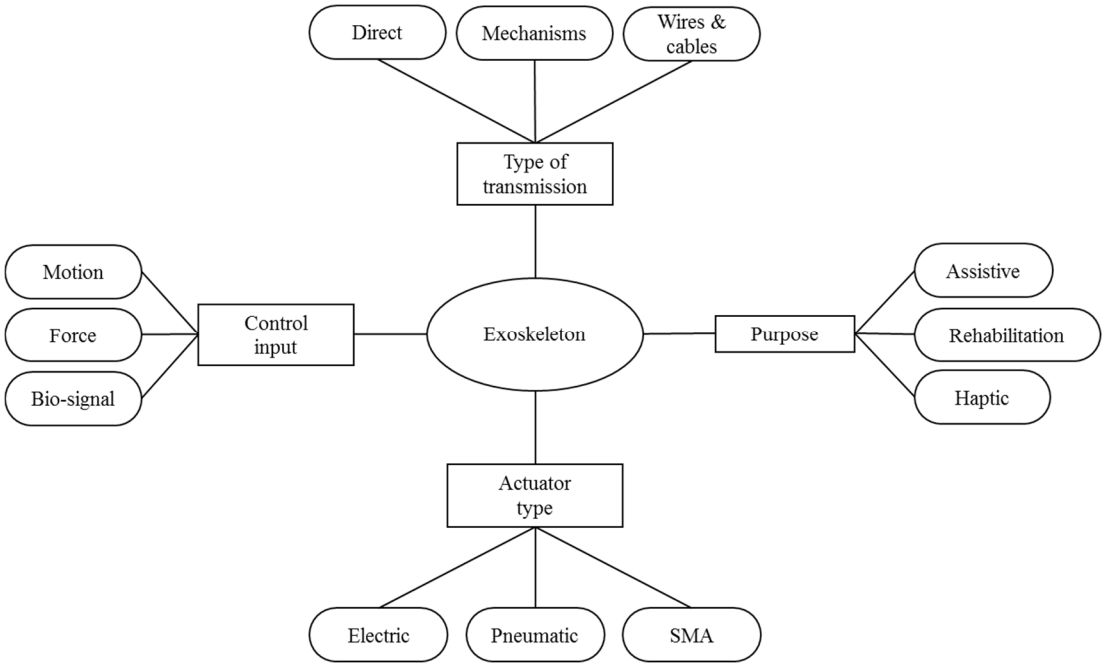

Fig. 16. Scheme of possible classifications of exoskeleton devices.

3.2.1 Rehabilitation exoskeletons

This section shows the principal hand exoskeleton devices, studied in the last decade, developed with the aim of helping the therapists during the rehabilitation of impaired subjects. Usually, during the rehabilitation treatment, patients cannot move the hand due to pathologies and/or injury. In this case, actuators substitute the human muscle in order to move the hand.

Technical University of Berlin rehabilitation hand (Wege and Hommel 2005; Wege, Kondak, and Hommel 2006)

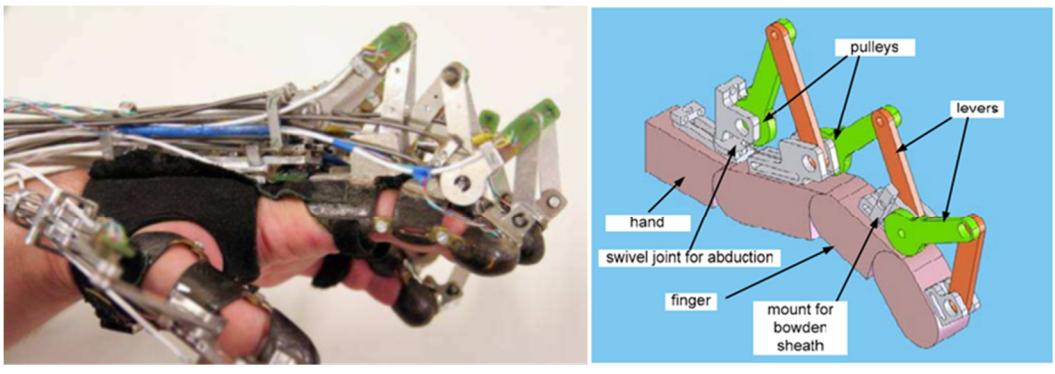

Fig. 17. Prototype and functional scheme of finger; a) photo of developed rehabilitation hand made by University of Berlin, taken from (Wege, Kondak, and Hommel 2006)*, b) drawing of finger module attached to simplify finger dummy; each pulley is actuated by two Bowden cables to allow bidirectional movement, picture taken from* (Wege and Hommel 2005).

The Wege et al.'s exoskeleton was made around 2005 at University of Berlin for the rehabilitation of hand injuryed patients. The mechanism assists the movement of the four long fingers and the thumb: the exoskeleton allows the motion of four degrees of freedom for the long finger and three for the thumb with a structure composed by a series of four-bar mechanisms. The single finger mechanism is made by three main parts: orthopedic attachment, mechanical links and actuator unit. Concerning the actuator unit, each long finger needs four actuators to move four degrees of freedom. The transmission is made by Bowden cables; the end of each Bowden cable is attached to a pulley, which is moved by a DC motor with transmission gears. The cable transmission needs also several tensioning devices for each path, in order to keep cables under tension. Fig. 17 b) shows the functional scheme of the long finger module. Obviously, one side of mechanism is attached to the dorsal part of the hand and the other side is connected to each of the fingers' phalanges. The base point of the link can be adjusted granting adaptability to different hand's size. Thanks to a swivel joint, the mechanism allows the abduction movement. Each lever ends into a pulley where the ends of the two the Bowden cables are connected: the movement of the cables leads to a rotation of the pulleys, thus in a rotation of finger joints. The lengths of the external bars are chosen in order to optimize in term of applied force, and to allow the movement of the finger inside the entire range of motion without any accidental collision. Concerning the control, the device provides also several speed and force sensors in the mechanical structure in order to implement two different control strategies, the first one is based on the position control, the second one is based on force control. Another implementation of the control foresees also the use of EMG (electromyography) sensors, with the aim to improve the rehabilitation efficiency.

HANDEXOS (A. Chiri et al. 2009; A. Chiri et al. 2012)

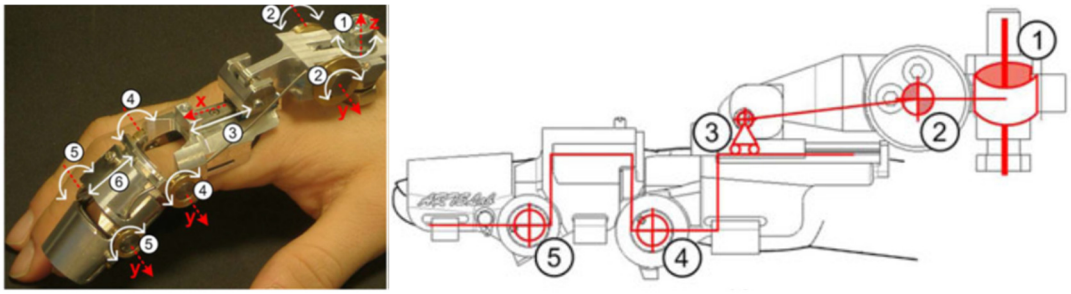

Fig. 18. Prototype and finger functional scheme; a) image of the realize prototype of a single finger; b) functional scheme of mechanism, figure taken form (A. Chiri et al. 2009).

The basic idea of HANDEXOS consists in five independent modules, one module for each finger. Every module is made of three links, one for each phalange. The links are connected with each other by means of active and passive DOFs. Fig. 18 b) shows the scheme of the joint position, the joint named 1 is a passive DOF that allows the MCP abduction/adduction. The flexion/extension of MCP is provided by slide-crank-like mechanism that is represented by joints 2 and 3 (3 is a translational passive joint). The movement of the fourth and fifth joints allow the flexion/extension of the human phalanges. In addition, to allow small adjustments on the distance between the PIP (joint 4) and DIP (joint 5) joints can be changed with a mechanism based on a screw and a prismatic joint. A Bowden cable actuates the finger extension running across idle pulleys, which are deployed in each finger joint, and fixed at the distal phalange. The DC motor pulls the cable by a linear slider placed in the backhand, whereas the finger flexion is passively obtained by a set of three antagonistic cables (one for each phalange joint) connected to three compression springs. The actuation system is designed in order to be lightweight, modular, simple, reconfigurable and remotely located respect to the hand. The prototype permits also a reconfiguration of the intra-finger transmission: in particular, the finger module can be actuated with only one motor, using the underactuation principle, or using one DC motor for each finger.

Finger exoskeleton for treatment of tendon Injuries (Ertas et al. 2009)

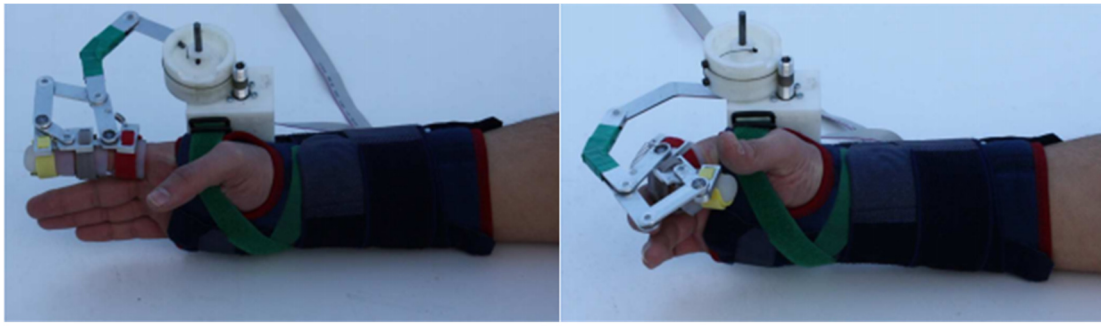

Fig. 19. Underactuated finger exoskeleton for treatment of tendon injur, photos taken in (Ertas et al. 2009).

The treatment of tendon injuries requires the use of an exoskeleton that allows to reach the natural finger range of motion both in flexion and extension. Eratas at al. propose an underactuated finger exoskeleton for the therapy of the tendon injury patients, whit a kinematic scheme similar to (Lionel Birglen, Laliberté, and Gosselin 2008). The kinematics of the finger exoskeleton is similar to the kinematics of four/six-bar linkages that are coupled to each other by means of compliant springs. The springs are used to ensure a coordinate motion of the finger bodies. The springs maintain the second and third phalange fully extended until the first one meets an obstacle or achieves a mechanical limit of motion. Fig. 19 shows the realized prototype in two different configurations, a) fully extended finger and b) and flexed configuration. The mechanism is attached to the phalanges with soft silicon rings tight by Velcro straps, and a DC motor, equipped with an optical encoder, actuates the exoskeleton. The rehabilitation foresees several therapy modes: passive, active, active-assisted, and active-constrained. In the passive mode, the finger exoskeleton moves the injured finger on predetermined trajectories while the patient remains completely passive. In the active case, the injured finger is active and the patient follows desired finger trajectories while the device is passive, this mode is used when early mobilization needs to be exercised. In the active-assisted mode, the finger exoskeleton encourages the patient to stay active during flexion/extension, instead in the active-constrained mode, the finger exoskeleton applies resistance to keep the patient passive during flexion (or extension) of the injured finger while the patient finger is active during extension (or flexion). In order to have an efficient rehabilitation the device can simultaneously measure finger movements, interaction forces, and muscle activities.

HEXOSYS-II (Iqbal, Tsagarakis, and Caldwell 2011)

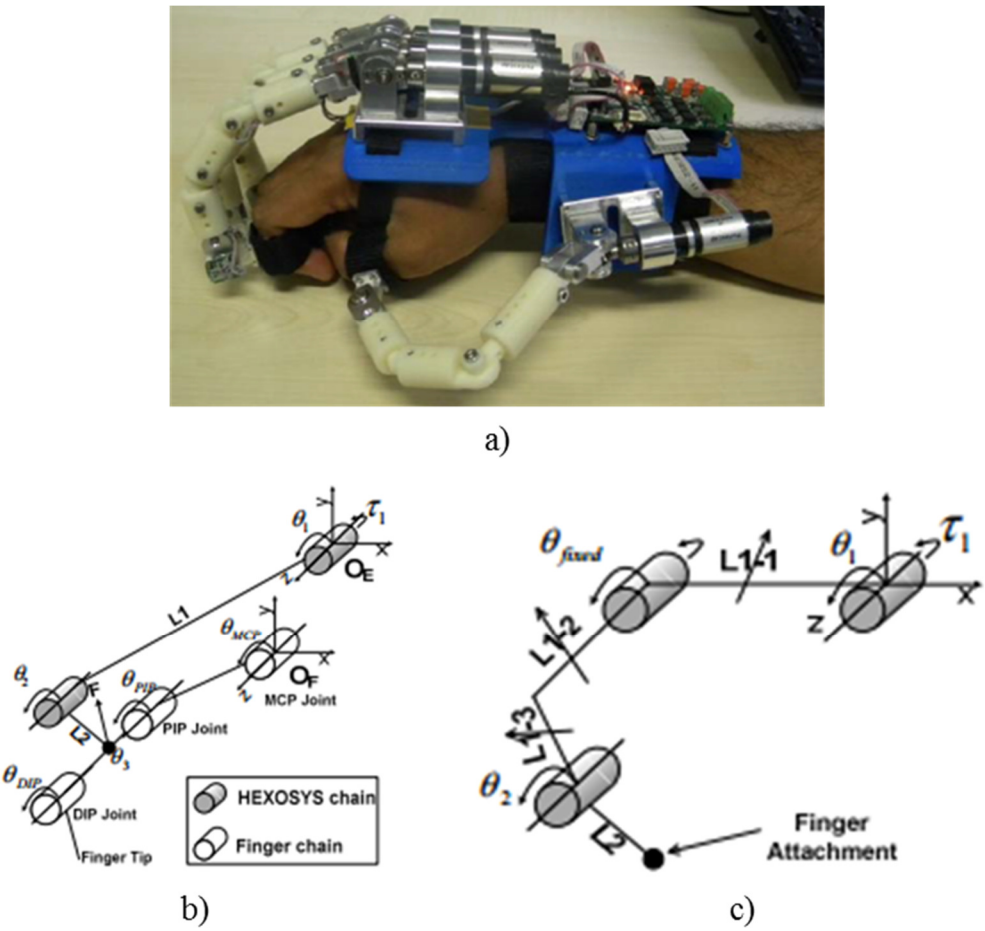

Fig. 20. HEXOSYS-II; a) picture of realized prototype, b) scheme of the kinematic mechanism coupled with the finger; c) optimized mechanism scheme, images taken from (Iqbal, Tsagarakis, and Caldwell 2011).

The Iqbal et al. rehabilitation device assists five fingers and it supports small adjustments to fit different hand sizes. The finger's structure is based on serial linkages attached to the distal phalange, according to the classification structure of Heo et al. in (Heo et al. 2012). The application of the above-mentioned structure, together with the chosen transmission, allows to have a bi-directional distribution of forces on the finger. In addition, using a direct transmission between the finger structure and the actuation allows to have a compact and portable exoskeleton device. Fig. 20 b) shows the underactuated finger mechanism: that is formed by two serial revolute joints structure. The serial manipulator is attached to the finger at a single point in a distal phalange neglecting the distal one; Fig. 20 a) shows it and in addition, it shows that the structure is attached to the intermediate phalange with Velcro straps. As described in (Iqbal, Tsagarakis, and Caldwell 2011) the structure is optimized in terms of transmitting

force between finger and exoskeleton. Fig. 20 c) reports the optimized structure, it is possible to notice that the first link is splitting into three segments and the angle between the sub-segments L1-1 and L1-2 allows only adjustments and is maintained fixed during the use.

Hand exoskeleton using a three-layered sliding spring mechanism (Arata et al. 2013)

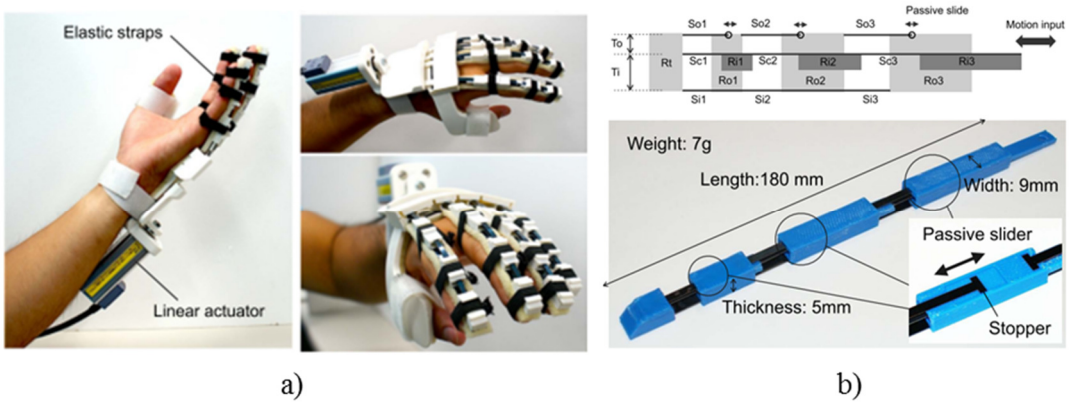

Fig. 21. Three sliding spring mechanism hand exoskeleton; a) image of prototype; b) schemes of working principle.

Arata et al in (Arata et al. 2013),propose a novel design for a rehabilitation device based on the deformation of the mechanism body, in order to obtain a compact and lightweight exoskeleton. The mechanism is designed to distribute one linear actuated DOF into twelve rotational joints, three DOFs for each finger (MCP, PIP and DIP). Fig. 21 b) shows an overview of the presented mechanism. The finger system consists in three-layered sliding spring and rigid bodies (R_t, R_i, R_o). The inner spring (S_i) is located on the bottom of the mechanism and it is fixed to the rigid bodies R_t and R_o; therefore, the spring blades S_{i1}, S_{i2}, S_{i3} are connected to the rigid bodies at each end. The center spring (S_c) is driven through a slit in the outer bodies (R_o). The inner rigid bodies (R_i) are fixed separately to the spring, so the connection spring function as independent springs. The S_o spring blades, which are connected between the outer rigid bodies. Each proximal end of S_o are equipped with a passive slider mechanism and a stopper. Applying a linear motion input to R_{i3} in the long axis toward the mechanism, the device performs the bending motion. The backhand transmission, as the fingers, is based on underactuated principle; in particular, motor action provides the input action for each finger using a sort of spring loaded slider. The devices is designed to provide

therapy in ambulatory and not ambulatory environments. Concerning the control strategy, the device can be commanded by the user by mean of bio-signals; in particular, several tests are performed with ENG (ElettroNeuroGraphy) signal in a mirror control.

Exoskeleton hand SMA (Tang et al. 2013)

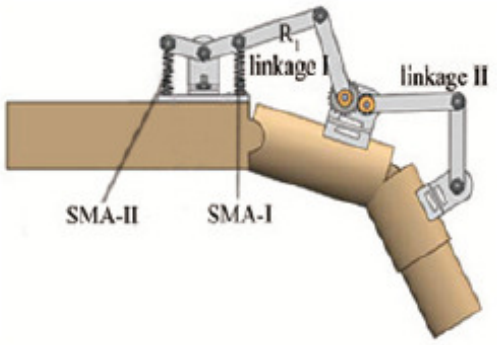

Fig. 22. Finger exoskeleton actuated by SMA springs.

The peculiarity of this rehabilitation exoskeleton is not represented by the kinematic structure, already well known (Wege and Hommel 2005), but it is given from its actuation: the prototype is in fact driven by two shape memory alloy (SMA) springs. The device is based on two successive four-bar mechanisms, in order to adapt itself to different finger dimensions. The linkage I and linkage II are used to drive the MCP and PIP respectively. The first linkage is driven by the SMA springs and the second is coupled to first one by means of two gears. The gear transmission is designed in order to obtain a speed reduction on the PIP joint of $\frac{3}{4}$ with respect to the MCP joint motion. The designed mechanism allows to reach all the physiological range of motion and in addition, for safety issues the input torque should be as small as possible. The actuation system is made by two opposite SMA springs (Fig. 22) in particular, SMA-I performs the finger flexion whereas SMA-II performs the extension. The modularity of the finger module allows to extend the design to whole hand thumb.. To enhance rehabilitation, the control input signal is based on surface electromyography (sEMG).

Cable Actuated Finger Exoskeleton (CAFE) (Jones et al. 2014)

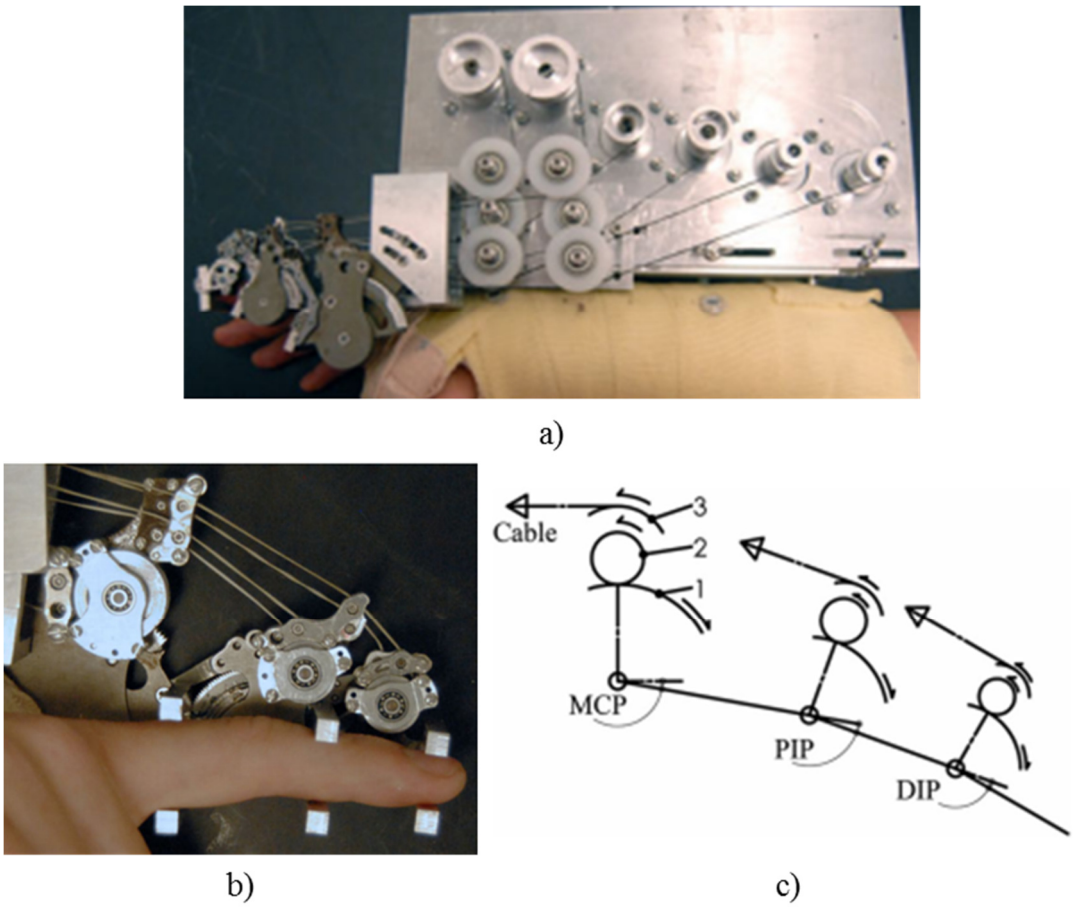

Fig. 23. CAFE prototype, a) entire exoskeleton system, b) and c) shows the picture and the scheme of the finger mechanism.

In this rehab device, three rotational joints of the exoskeleton are aligned with the finger axes by means of a mechanism that runs along the radial side of finger. The connection among the exoskeleton and finger is obtain through parallel bars. In addition, the exoskeleton has three actuated joints, one for each finger phalange. Fig. 23 b) and c) shows the functional principle of the mechanism, in particularly the body named 1 (joint concentric gear) is attached to first phalange, body 2 (small mating gear) that is united by body 3 (joint pulley) transmits the movement on body 1. The joint pulley (body 1) is moved by an actuated cable. The mechanism is repeatable for each digit. Fig. 23 a) presents the whole exoskeleton system, in particular, it is possible to notice that for each actuated joint two actuators are needed, and the motor action is transmitted to the phalanges by Bowden cables. This rehabilitation device can perform a predetermined trajectory for each phalange.

Tokyo hand (Yamaura et al. 2009)

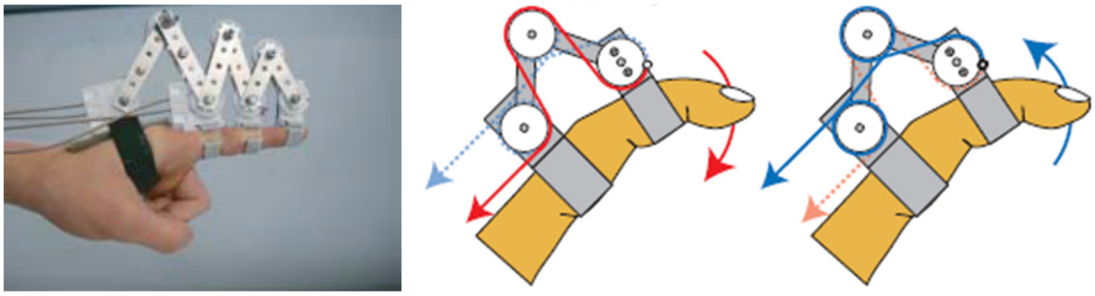

Fig. 24. Tokyo Hand, a) the realized prototype, working principle on finger flexion b) and during the finger extension c).

Tokyo hand is an exoskeleton designed with the intention to develop a rehabilitation device; in particular, the device is designed in order to rehabilitate patients with paralysis and or contractures. The Tokyo hand is composed by three four-bar mechanisms, which assist the three human joints. The active movement is performed for the first articulation by a servomotor placed remotely, while the other two are coupled and a single actuator is used. The wire transmission allows to transmit the power from the actuators to the four-bars. In particular, this device controls joint movements in both directions (flexion Fig. 24 b) and extension Fig. 24 c)). Each wire ends onto a fixed pulley that cannot rotate. The force applied on the wire generates a deformation in the four bar mechanism, causing the approach of two opposite vertexes, and thus the motion of the human articulation. The exoskeleton is designed in order to perform the MCP, PIP and DIP motion. In particular, for an index finger the performed RoM is about 70°, 80° and 60° respectively for MCP, PIP and DIP. The exoskeleton is controlled by the healthy hand that wears a data glove in order to perform a "mirrored motion" control. In particular, the data glove acquires position signals originated form the healthy hand/fingers, which drive the exoskeleton position. This prototype had a strong influence on the future development of the ReHand2 device, in particular for the wire-driven transmission that performs both flexion and extension movements. In addition, the four-bar structure allows the device to be easy attached and adjusted to different finger sizes.

3.2 Hand exoskeletons

In recent years, several rehabilitation exoskeleton prototypes have become commercial products, the most widespread are Hand of Hope (Rehab-Robotics ®) and Gloreha (Idrogenet).

Hand of Hope (Ho et al. 2011; K. Y. Tong et al. 2010).

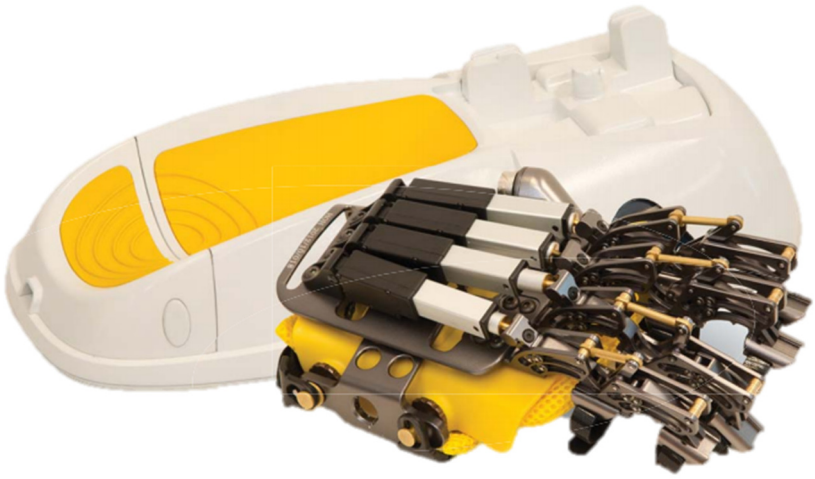

Fig. 25. Hand of Hope power by Rehab-Robotics.

Hand of Hope, is a wearable exoskeleton device for hand rehabilitation that includes a hand brace. The device is composed by five digits and each one is driven by a single linear actuator. The exoskeleton finger assists all three human joints and the phalanges of each finger are connected in order to realize a specific closing trajectory. Each motor is mounted in close proximity to the external platform and has one end connected to the external platform and another end coupled to its proximal follower, assembled by means of a ball joint in order to facilitate the force transfer and to minimize mechanical stress on the other parts of the device. From a rehabilitation point of view, the device can perform a series of tasks, either controlled by a PC or by sEMG signals. The main advantages are the use of a linkage that allows the device to control both flexion and extension of the hand, and the use of sEMG control. In contrast, the use of five actuators generates a bulky and heavy (700 - 800 g) device, which requires an external platform and it is not a portable device.

Gloreha [www.gloreha.com/]

Fig. 26. Gloreha powers by Idrogenet.

Gloreha is a lightweight five fingers exoskeleton created by Idrogenet. The exoskeleton consists of a soft glove and each finger is actuated by a pneumatic actuator deployed remotely in a bulky frame because it requires a compressor unit. The power is transmitted from the actuator to the fingertip by means of Bowden cables, that allows both flexion and extension movements; thus exhibiting a low impedance actuations. Concerning the motion, the finger flexion is performed by pushing the cable while the extension is actuated by pulling the cable. With this device is possible to perform both single finger movements and whole hand gestures. Gloreha can perform task oriented rehabilitation and virtual reality exercises, with visual and audio stimulation and feedback. The main advantages of this exoskeleton are the very low weight and an high comfort, on the contrary the use of Bowden cables does not allow an efficient use of the pneumatic power due to the intrinsic limitations of cables.

3.2.2 Assistive exoskeleton

The follow section shows an overview on hand exoskeletons designed as assistive devices. These devices are defined assistive because they can help elderly and impaired subjects during all the activities of daily life (ADLs). As sees before, several rehabilitation devices can be used also as assistive devices.

Five-fingered assistive hand (Hasegawa et al. 2008)

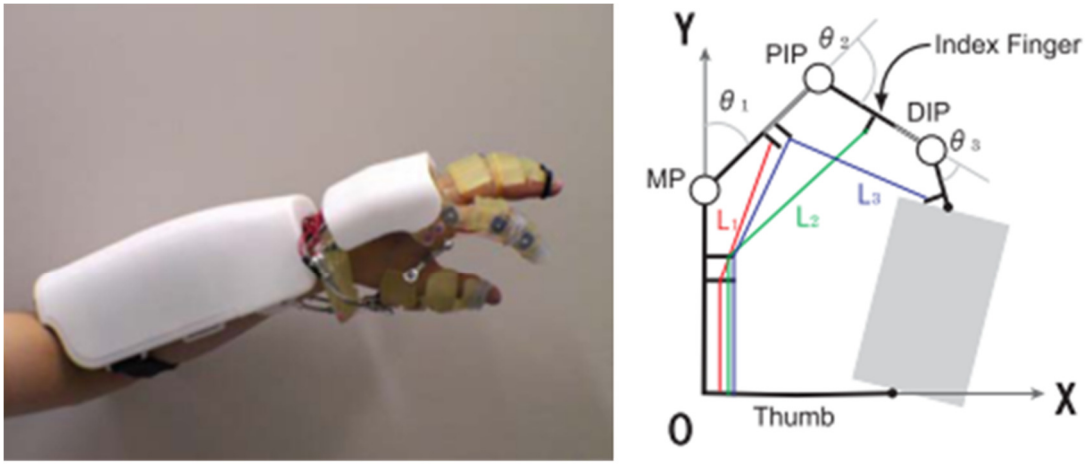

Fig. 27. University of Tsukuba hand exoskeleton, a) five-fingered assistive hand composed by a forearm module where the actuation controllers are located, a finger module and a parallel mechanism for the wrist movements deployed between forearm module and the exoskeleton; b) scheme of tendon-driven index finger.

Hasegawa et al. present this assistive device in (Hasegawa et al. 2008). The exoskeleton controls eight DOFs, three for the flexion/extension of the index finger as well as the combination of middle, ring and little; the remaining two DOFs, instead, assist the thumb movements. Eight DC motors actuate the same number of DOFs and, the transmission is tendon-driven. The actuation modules for the long "fingers" are deployed on the backhand, instead the thumb's one is located in the forearm module with the controllers. In Fig. 27 b) the tendon scheme for the index finger is shown. The main mechanical feature concerns the position on hand. In fact, the finger structure is placed on the finger side so that the finger and exoskeleton joints coincide as Fig. 27a) shows. This kind of structure allows to have a low complex structure and less friction forces. On the other hand, the major drawback concerns the impossibility to implement this kind of structure for all fingers, because it can be implemented only on thumb, index and little finger. The mechanism also allows a passive abduction/adduction movement of the long "fingers". The device is also equipped with position and force sensors in order to implement the control strategy. The device permits to control the finger movements with two different strategies called finger-following control and grasping force control. In fingers-following mode, the device is kept passive in order to not influence the fingers' motion. Grasping force control provides the force transmission by the mechanism and the finger.

UoA hand exoskeleton (Tjahyono et al. 2013)

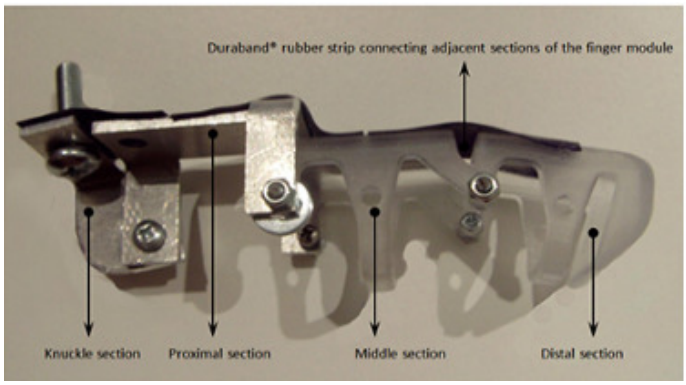

Fig. 28. UoA hand exoksletont for index finger, it possible notice the presence of an elastic band in order to obtain the MCP joint.

The UoA hand exoskeleton uses 10 PAM (pneumatic artificial muscles) and 1 linear electric actuator to obtain 15 DOF. Focusing our attention on the finger module; it is possible to see the use of the direct matching of joint centers. Without sacrificing the functionality of the hand, the MCP joint is unassisted. The transmission mechanism works only in flexion (contraction of PAMs), whereas for the finger extension a strip of DuraBand, placed on top of each joint, is used.

HX (Cempini et al. 2013)

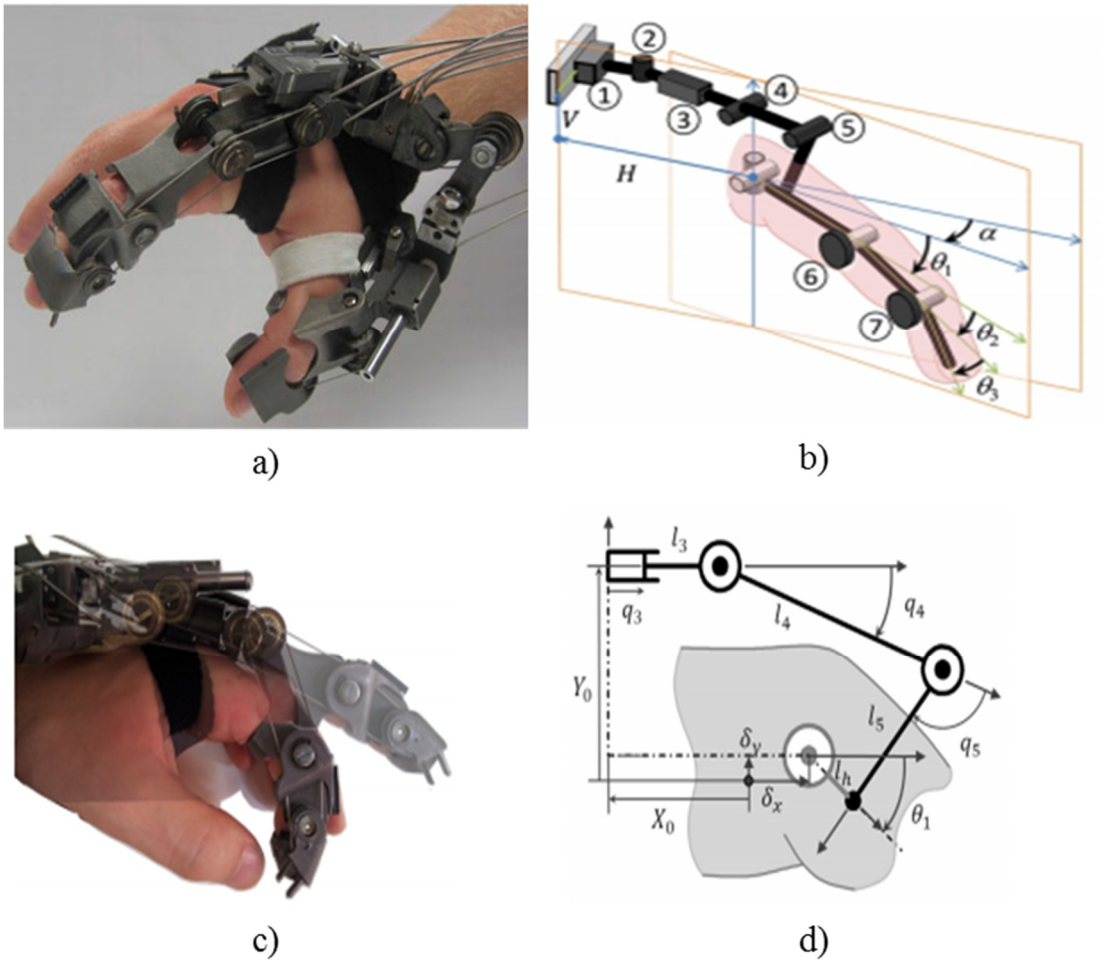

Fig. 29. HX exoskeleton, a) realized prototype, b) full kinematic scheme of finger plus exoskeleton, c) e d) Flexion/extension kinematics for the MCP joint.

The HX mechanism is formed of index and thumb fingers, with four and three active DOFs respectively, Fig. 29 a) shows the index mechanism, joints 1 and 2 allow the abduction/adduction of the finger and the other joints are used to move the human finger in flexion/extension. Focusing our attention on the flexion/extension of the MCP, the choice to use a PRR (Prismatic Revolute Revolure) manipulator of the exoskeleton structure, as shown in Fig. 29 b) is interesting.

In last five years, several assistive exoskeletons have become commercial products, in particular in this category it is possible to mention the Power Grip (Broadened Horizons), the SEM (Bioservo Technologies AB) and the ExoHand (Festo).

Power Grip [www.broadenedhorizons.com/powergrip]

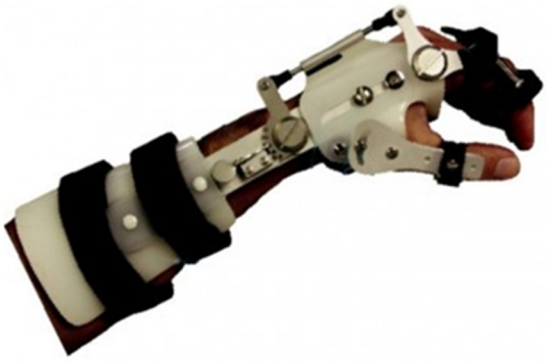

Fig. 30. Commercial active orthotic system namely Power Grip, powered by Broadened Horizons

Power Grip is an active orthotic system for grasping, designed for ADLs. The thumb is held fixed with an orthotic splint while the index and middle finger are moved together by means of a linear actuator, which performs opening and closing movements. All is connected to a small battery pack which can be embedded on a wheelchair or in a backpack. The device is composed by two parts, an orthopedic splint which must be realized ad hoc by an orthotist and the power grip system, which must be mounted on the splint. The principal advantages are that it is an effective wearable system for everyday assistance and that it can be triggered by any kind of signal (even sEMG). On the other hand, it has no flexibility (only one rigid grasp is feasible).

SEM (Soft Extra Muscle) Glove [http://www.better-grip.co.uk/]

Fig. 31. Bioservo Technologies AB soft assistive glove.

The SEM Glove is a glove based on soft robotics which assists weakened hands. The

thumb, middle and ring fingertips in the SEM Glove are equipped with force-sensitive sensors that recognize when the user grasps an object. A microcontroller calculates how much force should be added to perform a standard grasp. This product is developed for users that present a week hand grip but have no major spasticity, contractures, or severe pains. The sensors in the fingers respond to the user's intention and ability to apply pressure to the object being gripped. If the person cannot use the fingers at all or cannot exert enough force to grip an object then the device cannot be trigged because is unable to sense the user's intention. Finally, the soft glove is lightweight, and reaches a weight of about 700 g with the power unit. The main advantages of the SEM Glove are wearability and lightness, which make it ideal for assistance in ADLs. Disadvantages include the fact that it cannot be used for rehabilitation purposes, since it only enhances people with limited hand strength and that it cannot be used by subjects who are unable to generate grasping force (augmentation starts when a force is detected by means of pressure sensors on the fingertips).

Festo ExoHand [https://www.festo.com/]

Fig. 32. Festo ExoHand, pneumatic hand exoskeleton for rehabilitation and assistive scopes.

Festo ExoHand is an exoskeleton developed by Festo designed in order to perform both assistive and rehabilitation tasks. The mechanical structure is made in polyamide by SLS (selective laser sintering) process. The mechanism can be considered an hybrid between direct matching mechanism (for DIP and PIP joints) and remote mechanism for the MCP joint. The power unit is composed by 8 pneumatic cylinders, which assists five fingers. In particular, the system assists the thumb and the index with two cylinders (abduction/adduction and flexion/extension movements) and the

flexion/extension of middle, ring and little fingers are performed with the other four cylinders. The system allows a single finger control: moreover, the whole hand system allows to adapt itself to the grasped object. The power unit requires also 16 piezo proportional servovalves. Concerning the control strategy, several methods can be applied, e.g. brain control and position control. The system embeds 8 linear potenziometers and 16 pressure sensors in order to measure the finger displacement and the finger forces respectively.

Others Exoskeleton devices

In the previous sections, several type of hand exoskeletons have been described in detail, starting from those with rehabilitation purposes passing to assistive ones, and finally describing the commercial ones. Nevertheless, in literature it is possible to find many other prototypes of hand exoskeletons used for rehabilitation and/or empowerment. According to previous statements, this kind of devices can be classified according to the number of actuated degrees of freedom. For instance, (Jones et al. 2014) implemented a fully actuated device, which has the main advantage of obtaining a dexterous system, but on the other hand it is very heavy due to the number of used actuators and the control complexity to exploit all the actuators represents a severe limitation, together with the energy consumption. Other researchers reduce the number of active degrees of freedom in order to decrease the complexity and bulk (Fontana et al. 2009) (Shields et al. 1997). However, this solution usually implies great simplification on the versatility of the devices allowing, sometimes, only a single grasp mode. Other devices are designed using the underactuation principle (see Chapter 4), this choice allows to obtain a weight reduction with a consequent improvement of the wearability and comfort but at the same time grant a very wide grasping possibilities. Usually, the exoskeletons are associated with prosthetic devices and robotic grippers, where the underactuation has already been widely investigated (L. Birglen and Gosselin 2006) (Lionel Birglen, Laliberté, and Gosselin 2008) (Catalano et al. 2012) (Dollar and Howe 2007). The underactuation principle in exoskeleton is widely used in relation of single fingers interaction as in (de Visser and Herder 2000) (Stergiopoulos, Fuchs, and Laurgeau 2003). However, this principle has never been adopted to perform interaction at inter-finger level, with the exception of (In et al. 2011), which proposes a soft glove architecture with tendon-driven transmission. The

exoskeleton state of the art is also focused on the interaction between man and machine: in fact, the necessity of command signals that reflect the human intention is of fundamental importance. In this particular context, the surface electromyography (sEMG) has achieved promising results in the prosthetic and exoskeleton fields. The benefits, in this last case, are related not only to the controllability of the device but can also be extended to rehabilitation efficiency, as shown in (Hu et al. 2013). In fact, a rehabilitation workout is more effective when it involves a voluntary effort instead of simple passive movements. There are a lot of sEMG-driven exoskeletons, designed specifically with the only aim of performing slow opening and closing cycles for the hand rehabilitation (Ho et al. 2011) (Loconsole et al. 2013) (Mulas, Folgheraiter, and Gini 2005). In recent years, the exoskeleton systems go further, exploiting the characteristics of electromyography in terms of decoding the intention of movement in order to achieve an active rehabilitation, or "functional" one. Not only it permits slow hand movements, but it also allows object grasping, and more in general the interaction with the external world. Therefore, it descends that the current hand exoskeletons are eligible both for rehabilitation and assistance, i.e. permitting the user to perform activities of daily living (ADLs).

3.3 Design requirements of a rehabilitation exoskeleton device

From the previously section, after an accurate analysis of the state of the art in hand rehabilitation and empowering devices, it is possible to highlight several common requirements:

1. Limiting the range of motion to the physiological one with mechanical stops for safety;
2. Coincidence of the exoskeleton's center of rotation with the rotational axis of the humans joints;
3. Small size;
4. Low weight;
5. Simple structure and easy attachment;
6. Actuation of the main degrees of freedom for each finger;
7. Free palm, in order to allow the interaction of the human body with the environment.

As pointed out in the previous list, it is possible to define and explore some guidelines for the design of a new generation of rehabilitation and assistive hand exoskeleton. According with (Pons 2008) and (Iqbal and Baizid 2015) it is possible to summarize the design requirements in the following bullets:

- Range of motion;
- Compactness;
- Energy consumption;
- Comfort-ability and wear-ability;
- Force levels;
- Intention movements control;
- Safety.

Let's go deeper in the details of each point:

Range of Motion (RoM): this first constraint concerns the shape and the dimension of the *workspace*. For exoskeleton devices where the mechanisms are connected with human limbs, the workspace must follow as much as possible with the human *range of motion (RoM)*. In particular, the exoskeleton's *RoM* must be at least a physiological subset of the human one, but in any case, the *RoM* of the device cannot constrain the limb with accidental and unnatural movements.

Compactness: a rehabilitation or empowering exoskeleton should be compact, in order to perform both grasps and manipulability tasks. The compactness considers structural weight and inertia of the links, and the size of the device. The device's size is most important also from the safety point of view and for the comfort- and wear-ability.

Energy consumption: the energy consumption is a big issue for every portable device, where the energy issue is strictly connected with the number and the size of the actuators. In rehabilitation, this issue can be partially solved by reducing the number of actuators, introducing self-balance and passive mechanisms for an optimization of the energy consumption.

Comfort-ability: exoskeletons or in general rehabilitation devices need to be comfortable in order to be worn and used for many hours without generating pain or suffering on the users. The comfort-ability and wear-ability are also connect with the weight and dimensions of the device.

Force levels: in order to obtain an efficient rehabilitation, the exoskeleton must generate a sufficient force level to allow the limb movements, without generating undesirable reaction as muscle cramps caused by fast movements. In addition, the force level must be high enough to help the user in empowering tasks.

Intention movement control: another important aspect regards the control strategy of rehabilitation devices is the easy to use; in fact, the efficiency of the rehabilitation is conditioned by the control. In particular, the use of bio-signals, as input signals, is better than other types as it enhances the recovery of the neural network paths (Fig. 33).

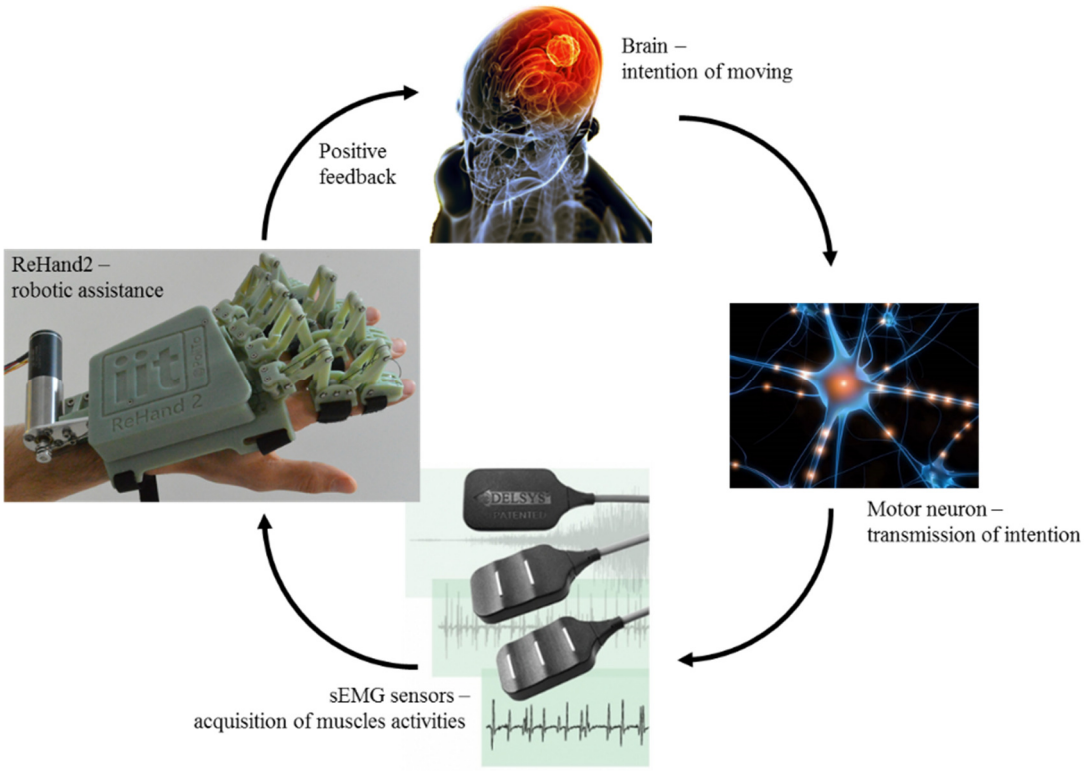

Fig. 33. Path form the intention (brain) to active assistance (ReHand2) passing to intention transmission (motor neurons) and the acquisition of muscle activities (sEMG sensors).

Safety: all the previous requirements are intrinsically conditioned by the safety requirement. For instance, in order to avoid injuries is important to reduce the weight and the inertia and provide a compliant *RoM*. In general, any medical device has to strictly satisfy restrictions related to risks (Bien and Stefanov 2004). In particular, ISO 14971:2012 collects the standards related to the risks management in order to determine the safety of medical devices.

Finally, after an accurate reasoning of the design requirements, we chose to develop a hybrid exoskeleton able to perform functional rehabilitation and empowering tasks, for stroke patients (rehabilitation feature) and for elderly and SLA patients (empowering feature), aiming to recover the normal hand functionality or to help suffering people during all the *activities of daily living* (*ADLs*). In particular, we chose to exploit the principle of *underactuation*, already used in the prosthetic field with excellent results. The underactuation permits to coordinate multiple outputs (in our case the fingers) with only one actuator, thus with a simple control strategy, as will be described in next chapters.

Chapter 4 Thinking underactuated

This chapter introduces the principle of underactuation, with a detailed description of the most common differential elements joined with the transmission topologies. The underactuation principle is followed by the description of its application in hand exoskeleton device and prosthetic limbs.

4.1 Thinking towards underactuation

"The idea behind underactuation in grasping is to use an ingenious mechanical system that can adapt to the shape of the object automatically."

L. Birglen, T. Laliberté, & C. Gosselin: Underactuated Robot

The idea behind underactuation is an old concept in automation and robotics as shown in (Fig. 34); nonetheless it is not completely exploited yet. Formerly Leonardo Da Vinci implemented the underactuation concept in several of his inventions. The principle expresses the property of a system to have a number of inputs lower than the number of output (Lionel Birglen, Laliberté, and Gosselin 2008). Practically speaking in robotic fields, it means that the number of actuators is fewer than the number of degrees of freedom (DOF). This practical consideration allows to obtain innovative and lightweight structures and devices that are very attracting for industrial application

(De Luca et al. 2002) and (Seifried 2014). In an underactuated multibody system, the actuated joints are replaced by so-called passive or flexible joints, in the latter case the underactuated DOFs are the result of the body elasticity, which yields in most case undesired structural vibrations.

In the last decades, the underactuation principle was also used with great success in hand prosthetics and in the grasping robotics fields. The motivation behind the use of this principle in such fields is very simple and well explained by Birglen et al. in (Lionel Birglen, Laliberté, and Gosselin 2008), where they assert, *"it is desirable to be able to grasp objects using a simple control rather than having to command and coordinate several actions."* Therefore, the application of underactuation permits to design mechanisms that can adapt themselves to the shape of the grasped object, and the differential elements are the basis of this mechanical intelligence (Hirose and Umetani 1978), (Hirose and Ma 1991), (Carrozza et al. 2004), (L. Birglen and Gosselin 2006) (Lionel Birglen, Laliberté, and Gosselin 2008).

In this section, the underactuation principle will be described in detail, followed by the analysis of the main type of differential elements and the needed mathematical tools for the application of underactuation.

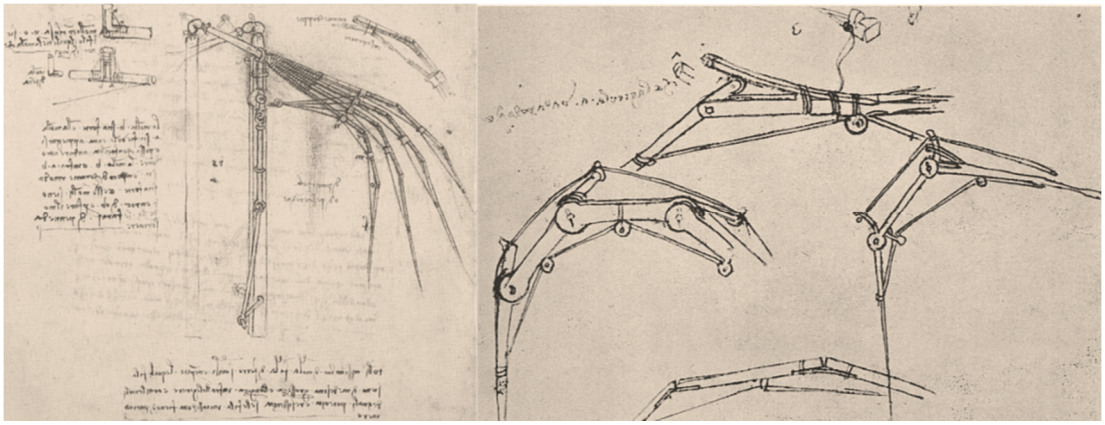

Fig. 34. Articulated wing taken form Da Vinci, Codex Atlanticus (ca. 1496).

4.2 Underactuation concept in grasping tasks

As stated before, the underactuation concept sounds to be suitable in grasping and prosthetic robotics with the purpose to grasp and manipulate objects with different shape without complex control strategies. In underactuated hands, this mechanical intelligence could be embedded in the hand by means of differential mechanisms (a

generic transmission differential cell is shown in Fig. 35). In this case, the working principle is quite simple: when a finger touches an object and stops, the others could continue to close and wrap the object (L. Birglen and Gosselin 2006) and (Xu et al. 2015).

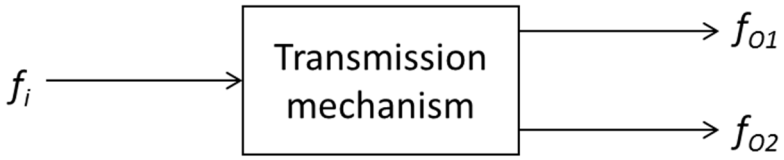

Fig. 35. Differential mechanism cell.

Starting from the definition of degree of actuation (DOA) give in (Lionel Birglen and Gosselin 2004), which in first approximation could be confuse with the number of actuators, it is possible define a system as underactuated "*if the number* $\boldsymbol{m}$ *of input* $\boldsymbol{u} \in \mathbb{R}^{\boldsymbol{m}}$ *is smaller than the number of degree of freedom* $\boldsymbol{f} > \boldsymbol{m}$ *of the system.*" (Seifried 2014).

A grasping robotic device can be considered as divided in two modules: inter- and intra-finger levels. In this dissertation, the inter-finger term is used to specify the module used to share the input action in several outputs; usually it is composed by several differential elements and represent the massive part of the "mechanical brain" of the device. The intra-finger module is referred to the finger's mechanism. In literature is possible find the application of the underactuation principle at both levels. Generally, the transmission on underactuated fingers (intra-finger level) is *serial*. This fact is due to the physical layout of robotic fingers where the phalanges are joint to each other in series. Concerning the inter-finger module the transmission tree is not strictly related to a single architecture. In the following section, the principal differential systems and the most used layouts are presented.

4.2.1 Differential elements

The differential elements can be considered as the main part of the "mechanical brain" in order to reach the above-mentioned properties. According to IFToMM terminology (IFToMM Commission 1991), the differential element is a 2-DOF mechanism capable to split a single input action into two output actions. The ratio among the outputs is determined by the geometrical parameters of the differential element.

Classical differential mechanisms

The classical differential mechanisms are based on planetary and bevel gear transmissions (Fig. 36) and are widely used in underactuated grippers as shown in (Laliberté and Gosselin 2001) and (L. Birglen and Gosselin 2006).

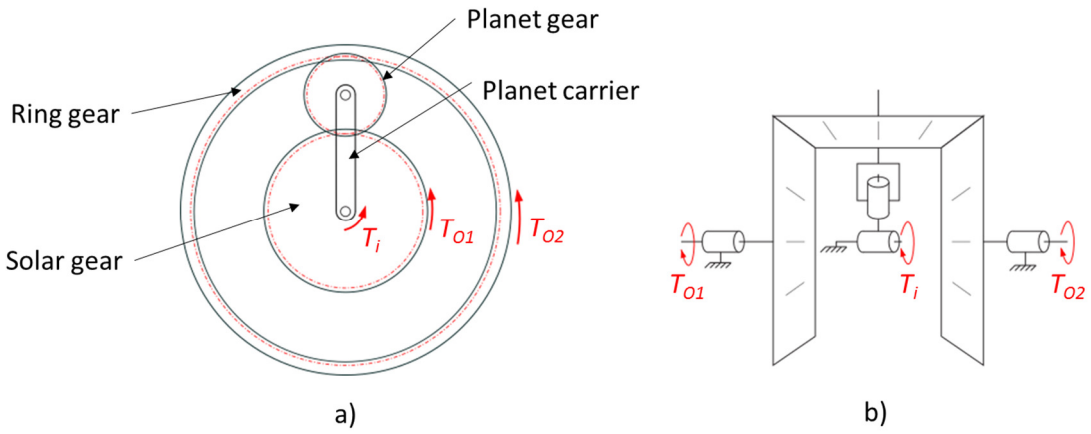

Fig. 36. Classical differential mechanisms: a) planetary gear differential and b) bevel gear transmission.

As Fig. 36 a) shows, the input torque T_i acting on planet carrier while the output torques, T_{O1} and T_{O2}, act on the sun and ring gears respectively. The planetary gear differential has the property to keep the output independent from the position. In Fig. 36 b) a particular case of the planetary differential of the bevel-gear transmission is reported. The (4.1) allows to define the outputs amplitude by means of the force transmission matrix ($[\boldsymbol{T}]$) and the torque input, for the planetary gear differential.

$$\begin{bmatrix} T_{O1} \\ T_{O2} \end{bmatrix} = \begin{bmatrix} \dfrac{r_s}{(r_s + r_c)} \\ \dfrac{r_c}{(r_s + r_c)} \end{bmatrix} T_i \qquad (4.1)$$

Where T_{Oj} with $j = 1, 2$ are the outputs torques, T_i is the input torque and r_s and r_c are respectively the ring and sun pitch radii respectively. The bevel gear differential is a particular case of the planetary gear differential; in this case, the outputs are global force-isotropic and are equal to one half of the input torque. In the last few decades, several differential mechanisms are proposed for grasping devices; figure below (Fig. 37) shows the most used elements in this field.

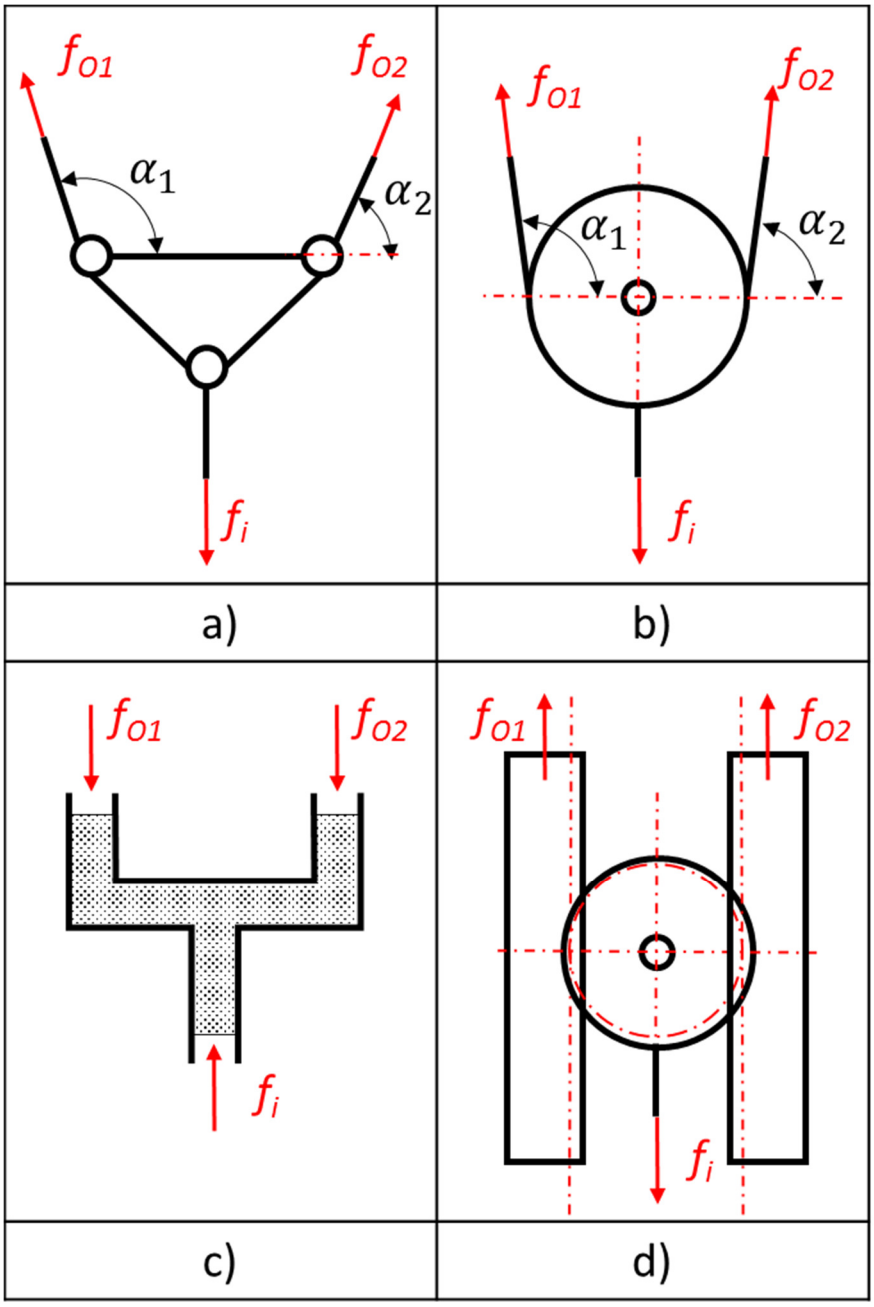

Fig. 37. Several type of differential mechanism used in the design of prosthetic hand and gripper, a) seesaw mechanism, b) a movable pulley, c) a fluidic stage, and d) a pinion-based one.

Seesaw element

A *seesaw* element is illustrated in Fig. 37 a). The input force f_i acts on a pin and generates two output pulling forces f_{O1} and f_{O2}. The generated forces depend on the external loads; in particular, when the external loads are equal, the two outputs are also equal and the seesaw translates along its path without any rotation. Vice versa, when the external loads are unbalanced and the seesaw tilts. The output with major load will

be stopped whereas the other will continue its motion. The force transmission matrix related to the seesaw element is shown in (4.2):

$$\begin{bmatrix} f_{O1} \\ f_{O2} \end{bmatrix} = \begin{bmatrix} \dfrac{b_2}{b_1 sin(\alpha_2) + b_2 sin(\alpha_1)} \\ \dfrac{b_1}{b_1 sin(\alpha_2) + b_2 sin(\alpha_1)} \end{bmatrix} f_i \tag{4.2}$$

The equation is related to the geometric set used in the previous equation is the same presented in Fig. 37 a).

Movable pulley element

Fig. 37 b) shows the differential pulley element. The working principle is almost the same as the seesaw. The pulling force acts on the center of the pulley and generates two pulling actions. Also in this case, when the external forces are not balanced, the side with major load will stop while the other one, exposed to smaller load, will continue to rotate. With reference on Fig. 37 b), it is possible to define the matrix [$\boldsymbol{T}$] and the magnitude of output forces as:

$$\begin{bmatrix} f_{O1} \\ f_{O2} \end{bmatrix} = \begin{bmatrix} \dfrac{1}{sin(\alpha_2) + sin(\alpha_1)} \\ \dfrac{1}{sin(\alpha_2) + sin(\alpha_1)} \end{bmatrix} f_i \tag{4.3}$$

Fluidic differential element

In Fig. 37 c) a fluidic T-pipe is shown. According to IFToMM, the mechanism distributes the input action into two outputs. The fluidic stage takes advantage of the compressibility/deformability of a fluid to separate its flow into two distinct streams. This transmission element is often used for industrial grippers where high grasping forces are required and the use of fluid power is not a relevant problem. The equilibrium equation, in this case, can be written as:

$$\begin{bmatrix} f_{O1} \\ f_{O2} \end{bmatrix} = \frac{1}{S_a} \begin{bmatrix} S_1^a \\ S_2^a \end{bmatrix} f_i \tag{4.4}$$

In the previous equation it is possible notice that the outputs depend on the respective section areas of the input and of primary and secondary output pipes (respectively S_a, S_1^a, S_2^a).

Pinion based differential element

Fig. 37 d) shows a rack-pinion transmission mechanism, the working principle is strictly similar to the movable pulley. In particular, the input acts on the center of the pinion while the external loads are applied at the sliding racks where the output forces are generated. The output forces can be calculated using the following equation:

$$\begin{bmatrix} f_{O1} \\ f_{O2} \end{bmatrix} = \begin{bmatrix} \frac{1}{2} \\ \frac{1}{2} \end{bmatrix} f_i \qquad (4.5)$$

Continuum differential element

Besides the traditional differential elements, there is also another type, called continuum differential element, presented in (Xu et al. 2015). This mechanism (Fig. 38) consists by a fixed frame, a flexible driving backbone, where the input force (f_i) acts, two flexible driven backbones and an end link. All backbones are attached to the rigid end bar and pass through the holes in the fixed frame. When the external load is unbalanced and the input continues to push, the two flexible driven bodies will be bent generating the differential outputs.

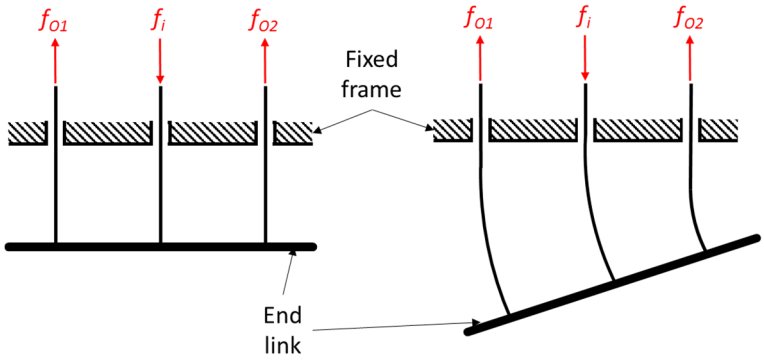

Fig. 38. Continuum differential element.

The traditional differential elements can be deployed in different types of transmission trees, as will be describe in the following section, and their reliability is major than the continuum elements, thanks to their property to generate differential translational outputs, compared with continuum elements. The characteristic of the continuum elements to generate differential outputs with different pattern can require a large amount of space in backhand. These kind of differential elements can be suitable in the prosthetic hand but not for actuated orthosis and industrial gripper where one of the major constraints are connected with the mechanism dimension or generating forces.

4.2.2 Inter-finger transmission

In underactuated prosthetics and grippers, the inter-finger mechanisms have the goal to distribute one input action into several outputs, where usually the number of outputs is strictly major than two. In the past years, several researchers conceived different mechanisms, which can be based on the application of several differential elements or using completely different designs such as the floating platform or a spring loaded slider.

Inter-finger transmission tree

Hirose et al. in (Hirose and Umetani 1978) and (Hirose and Ma 1991) proposed the idea to connect several differential elements with the goal of producing multiple output systems without losing the peculiarity of adaptability. As explained in (L. Birglen and Gosselin 2006) and (Lionel Birglen, Laliberté, and Gosselin 2008), in order to obtain *n* outputs, usually from three to five in robotics, *n-1* transmission stages are required. Each differential mechanism generates two outputs for one input, so inserting a differential element in the transmission tree gives an additional output to the system.

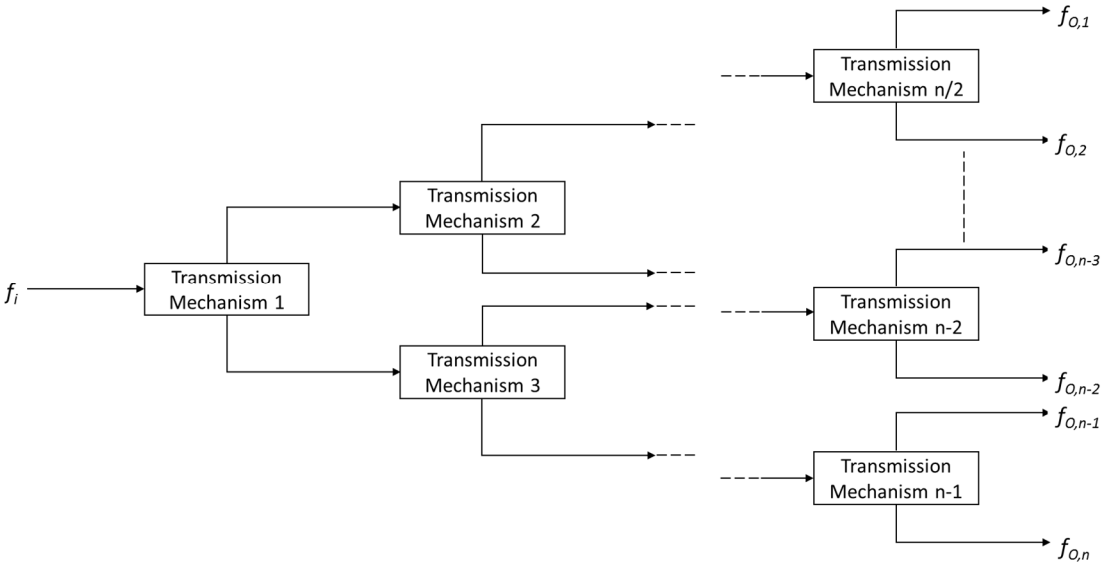

Fig. 39. Strictly parallel (or symmetrical) transmission tree.

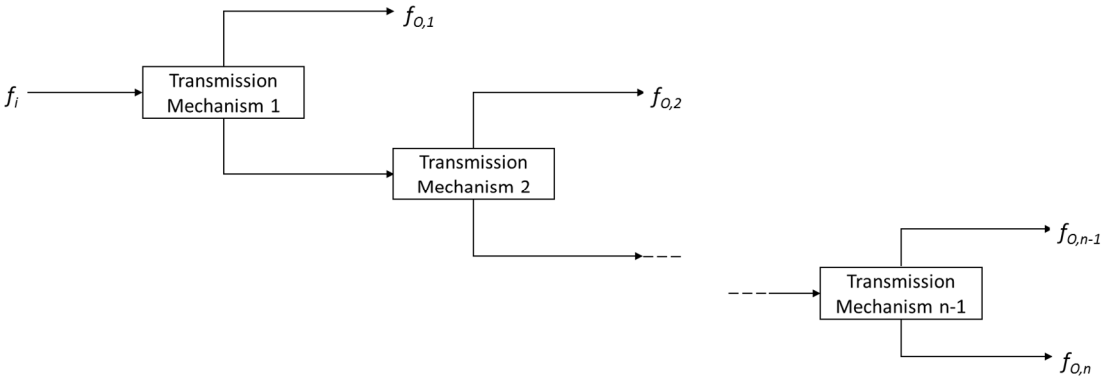

Fig. 40. Strictly serial transmission layout.

In the figures above (Fig. 39 and Fig. 40) two different types of transmission layout are shown. In particular, Fig. 39 shows the symmetrical (or parallel) multi-output mechanism, whereas Fig. 40 shows a serial layout.

In the parallel transmission, the outputs of the first differential element are the inputs of the second step of transmission, and only in the last transmission stage the outputs are connected to the fingers. The previous explanation can be translated in mathematical form as follows:

$$\begin{bmatrix} f_{O,1} \\ f_{O,2} \\ \vdots \\ f_{O,n} \end{bmatrix} = [\boldsymbol{T}] f_i \tag{4.6}$$

Where the force transmission matrix $[\boldsymbol{T}]$ can be written as follows:

$$[\boldsymbol{T}] = \prod_{k=1}^{\frac{\log n}{\log 2}} \begin{bmatrix} \boldsymbol{T_{2^i-1}} & & \boldsymbol{0} \\ & \boldsymbol{T_{2^i-1}} & \\ \boldsymbol{0} & & \boldsymbol{1_{n-2^i}} \end{bmatrix} \tag{4.7}$$

The term $[\boldsymbol{T_k}]$ is the force transmission matrix for the $k-th$ differential element, $[\boldsymbol{1}]$ is the identity matrix of dimension h, and $[\boldsymbol{0}]$ is the null matrix.

The serial tree transmission foresees that at least one differential element output is connected to a finger; instead, the other one is the input of the following differential mechanism. The serial tree transmission follows the equation (4.6), but changes its $[\boldsymbol{T}]$ matrix, which shows the following form:

$$[\boldsymbol{T}] = \prod_{k=1}^{n-1} \begin{bmatrix} \boldsymbol{1_{n-1-k}} & & \boldsymbol{0} \\ & \boldsymbol{T_{n-k}} & \\ \boldsymbol{0} & & \boldsymbol{1_{k-1}} \end{bmatrix} \tag{4.8}$$

An example of a generic transmission with seven outputs is shown in Fig. 41. It can be observed that after the first transmission stage, the upper branch is based on a parallel transmission and the lower branch is made by a serial layout.

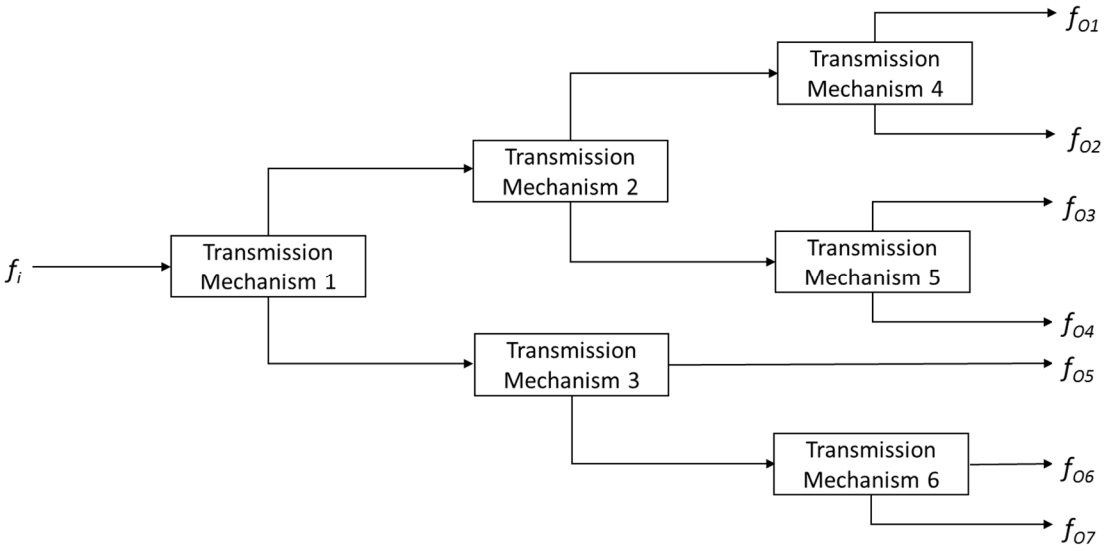

Fig. 41. Generically transmission tree composed by one input, seven outputs and six differential elements.

The transmission tree can be exploited with all differential mechanisms presented in the previous section. In particular, in the next sections, major focus is given on a serial transmission tree based on movable pulleys.

Floating platform transmission

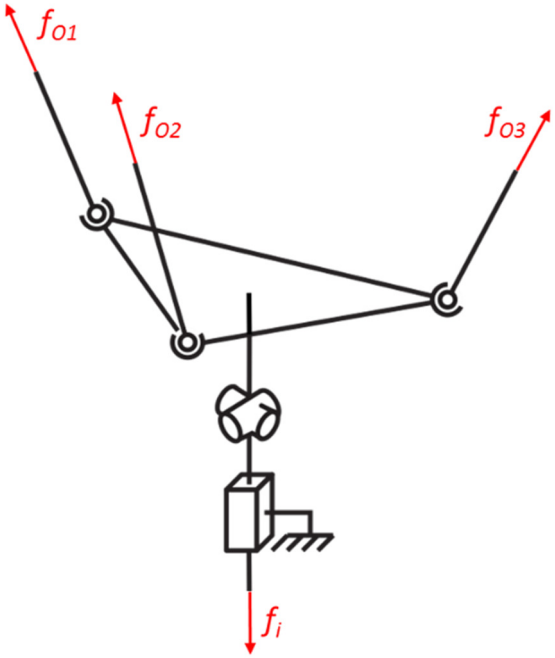

Fig. 42. A schematic of a floating platform transmission.

A floating platform transmission can be considered the direct evolution of the seesaw mechanism because it shares the same working principle except for the addition of a third output exploiting the third Cartesian dimension, as illustrated in Fig. 42. The floating platform can rotate around a 2-DOF joint and translate along a prismatic guide where the input force acts. The vertices of the platform transmit the output forces and according with the working principle of seesaws, the force distribution depends on the geometric parameters of mechanism and on the shape of outputs (fingers), as explained in (Lionel Birglen, Laliberté, and Gosselin 2008), (Myrand and Gosselin 2004) and (de Visser and Herder 2000). Such mechanisms show theoretical and practical limitations and drawbacks, such as, a not complete adaptation to the grasped object and a difficult prediction of the 3D motion. From the theoretical point of view, this kind of mechanism can be suitable for more than three outputs, but the need of a large number of joints and the complex design make its the implementation quite impossible.

Spring loaded slider

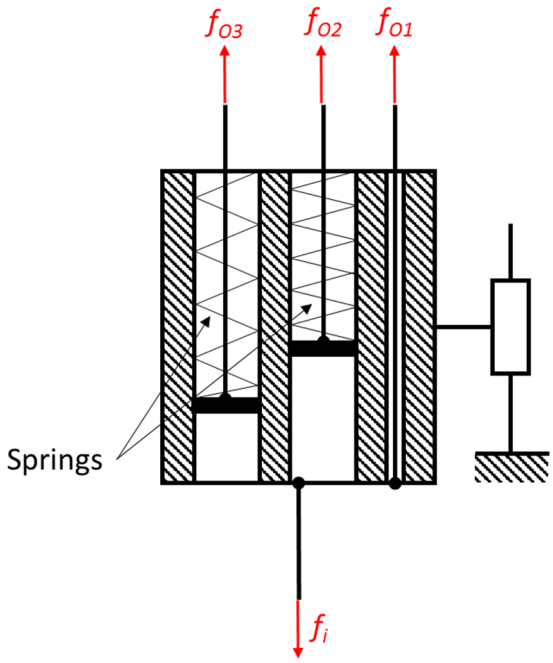

Fig. 43. Scheme of a spring-loaded 3-outputs slider.

Massa et al. in (Carrozza et al. 2004) propose another type of multiple output mechanism used for a three-finger prosthetic hand (Fig. 43 shows the adopted working principle for a three-outputs device). The intra-finger mechanism is composed by a translational slider where the force input (f_i) works, two wires attached to the slider

body by means of two compression springs (f_{O2} and f_{O3}) and one cable directly connected to the slider (f_{O1}). In this case, the differentiation of the outputs is given by the values of stiffness of the two compression springs. When a finger encounters an obstacle (or an object), its spring begins to compress and the slider continues its motion, allowing the other fingers to wrap the obstacle. In this particular case, also the springs' stiffness is part of the transmission equation, which is calculated as follows:

$$\begin{bmatrix} f_{O1} \\ f_{O2} \\ f_{O3} \end{bmatrix} = \begin{bmatrix} 1 & -F_2^S & -F_3^S \\ 1 & 0 & -F_3^S \\ 1 & -F_2^S & 0 \end{bmatrix} f_i \qquad (4.9)$$

Where F_i^S is the force generate by the $i-th$ spring, with $i = 2,3$. A similar mechanism is also used in the Arata et al. prototype (Arata et al. 2013) to allow the adaptability of the 12-DOF hand exoskeleton: in this case it is not used with cables but with linkages and elastic elements in order to permit the grasping adaptability.

4.2.3 Intra-finger underactuation

In the previous sections, the underactuation at inter-finger level has been described, but the same concept can be applied also at the intra-finger level. In this case it is possible to control all the fingers' DOFs (or a sub-set of them) related to the fingers with only one action. Usually, in the prosthetic field, the fingers' transmission mechanism assumes a *serial* configuration, according with the specific human limb. Contrarily to the inter-finger mechanisms, the intra-finger underactuted mechanisms are not easily generalizable, due to the large number of possibilities available. Currently the state of the art proposes several examples of underactuated fingers, both for exoskeletons and prosthetics. Concerning the exoskeletons, two of the most common solutions can be found in (Ho et al. 2011) and (A. Chiri et al. 2009). In particular, the Hand of Hope (Ho et al. 2011) exploits linkages in the finger module, whereas the HANDEXOS in (A. Chiri et al. 2009) exploits wires and pulleys, which is a typical solution in the field of prosthetics. Another intra-finger underactuated mechanism is presented in (Yamaura et al. 2009). This solution exploits a classical four-bar mechanism actuated by wires, in a very ingenious manner, the device combines the underactuation principle with the possibility to control both flexion and

extension of the PIP and DIP joints. This solution will be described in detail in the next chapter.

Chapter 5 ReHand

Even if they claim to be wearable, the traditional exoskeletons usually do not match the listed requirements of wearability and lightness. One of the main aspects of such a failure deals with the actuation. If all the degrees of freedom (DOFs) of the hand are actively assisted, the number of actuators and the mechanical complexity are very high, for instance in (Martin and Grossard 2014) a 24 DOFs hand is proposed, and it results heavy due for the large number of actuators. Different strategies have been envisaged in the past in order to reduce the number of actuators, dealing with single fingers. For example different DOFs are connected with rigid elements (one actuator activates several DOFs in a predetermined way) to realize an average grasping gesture of each finger (Shields et al. 1997)), or realizing underactuated mechanisms, that permit the finger to adapt to the grasped object (Arata et al. 2013). Usually underactuated solutions consist in mechanisms that exhibit a motor for each finger (K. Y. Tong et al. 2010). It is a quite common solution, also exploited in commercial hand prostheses. On the other hand, a possible solution for what concerns connecting multi-finger devices consists again in a rigid connection, in order to realize an average grasping gesture. Underactuation among different fingers is something not really investigated before in the field of exoskeletons, with the exception of (In et al. 2011). However, there are several examples of robotic hands, underactuated at the backhand level. ReHand applies the underactuation prosthetic hand background to exoskeletons, obtaining an underactuated hand exoskeleton.

5.1 ReHand Description

ReHand is a four-finger exoskeleton, actuated with one single motor, conceived and designed according to the underactuation principle. The mechanism, can adapt itself to whatever grasping gesture, transmitting a pre-determined fraction of the total actuating force to each phalange. The exoskeleton's architecture can be divided into two main modules: inter-finger and finger. Each finger assists the two more proximal phalanges, and is composed of a pair of consecutive four-bar mechanisms. The finger closing is tendon-driven, while the extension is performed by means of elastic elements. At the inter-finger level, a specific number of differential elements have been designed (5.1), in order to divide the single force input provided by the actuator into four outputs, one for each actuated finger.

$$n_{differential\ element} = n_{finger} - 1 \qquad (5.1)$$

Among all the possible differential elements, a scheme based on movable pulley elements has been adopted, in order to reproduce the typical force synergy of a cylindrical grasping gesture (Kuo et al. 2013). In the following sub-sections each module is described in detail.

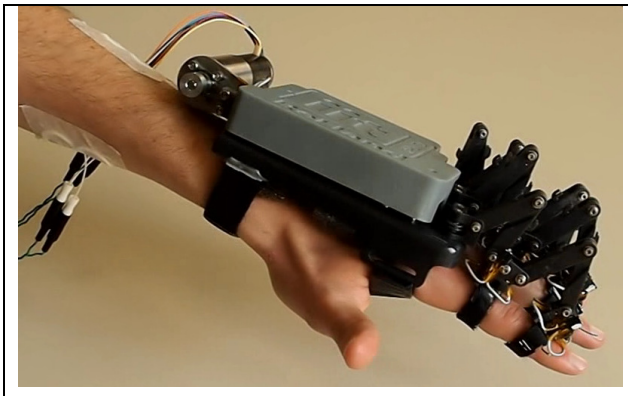

Fig. 44. ReHand prototype.

8 active DOFs (intra-finger and inter-finger underactuation);
4 passive adduction/abduction DOFs;
weight: 400 g (without motor);
material: ABS and steel;
actuator power: 36 W
actuator nominal torque: 0,44 Nm (η≈0,7)
compact;
customizable;
compliant;
ergonomic;
sEMG-driven.

5.1.1 Inter-finger module

Working principle

The underactuation module is the basis of the whole device: it is fixed to the hand body by means of Velcro straps; its bottom is modeled in order to match the anatomical surface of the backhand and for the most, it is technologically realized by means of 3D printing. The exoskskleton should not interfere with the wrist flexion/extension movement. It hosts the brushless DC motor and the gearbox (Faulhaber 2444 024 B and Faulhaber Planetary Gearhead Series 26/01 S), which transmits an actuating force to the underactuation module by means of dyneema wires, wounded on a pulley on the gearhead shaft. The underactuation module consists of three differential elements, in this case movable pulleys, mounted in a serial configuration. According to the definition of a differential element, each movable pulley divides the input action into two outputs. As explained, each pulley can shift along a direction coincident to input force application; moreover, the pulley can rotate about its axis, as a wire is wounded on it and connects the two outputs.

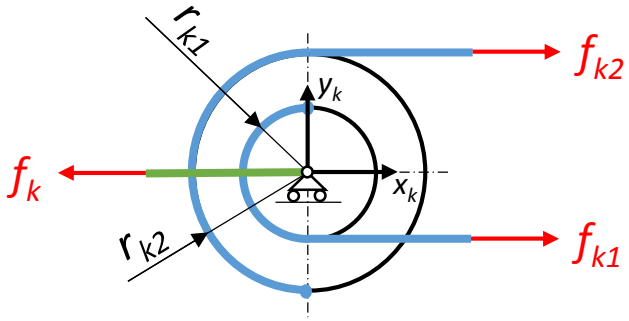

Fig. 45. Scheme of a generic pulley with different radii for the wounded output wires.

In Fig. 45 a generic scheme of the movable pulley is represented: the input force is f_k, while the two outputs are f_{k1} and f_{k2}, both parallel to f_k axis. To maintain the scheme general, the pulley exhibits different radii for the wounded output tendons. Under this assumption, the force transmission matrix (4.3) becomes:

$$\boldsymbol{T} = \begin{bmatrix} \dfrac{r_{k2}}{r_{k1} + r_{k2}} \\ \dfrac{r_{k1}}{r_{k1} + r_{k2}} \end{bmatrix} \tag{5.2}$$

The element can translate along its path (ideally, the same of f_k), and rotate about its own axis. In the following, the module design starting from the typical force synergy in a cylindrical grasp is shown.

The design

The inter-finger under-actuated structure is composed of three differential elements connected in a serial configuration as shown in Fig. 46.

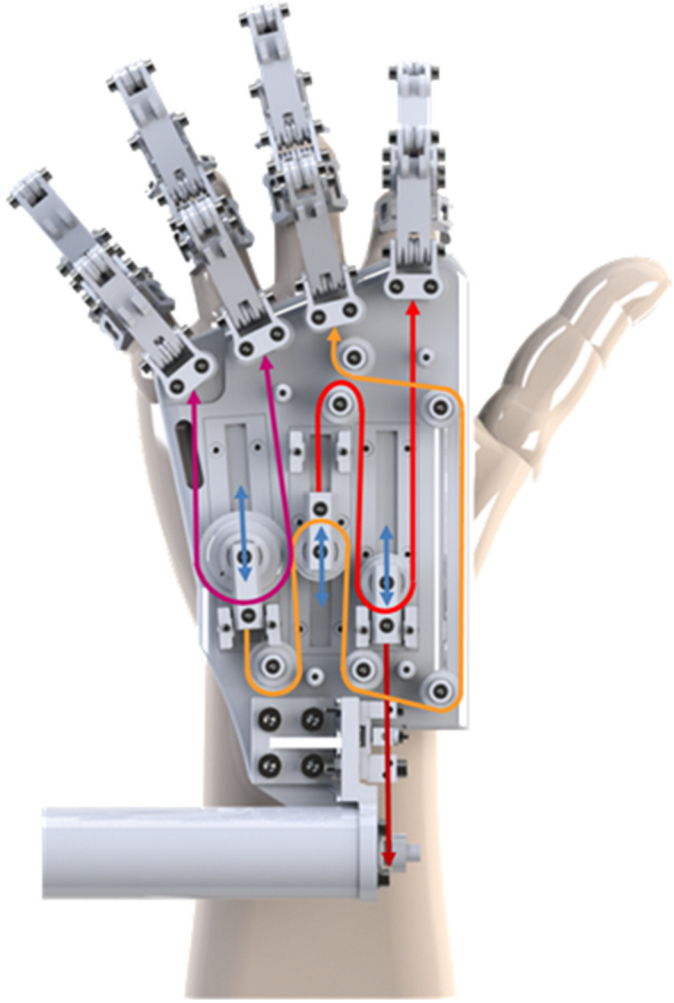

Fig. 46. Backhand configurations.

The geometrical dimensions and parameters of all the elements have been tuned in order to replicate the physiological force distribution (finger force synergy) among the four human fingers during a cylindrical grasp Fig. 47 (Kuo et al. 2013).

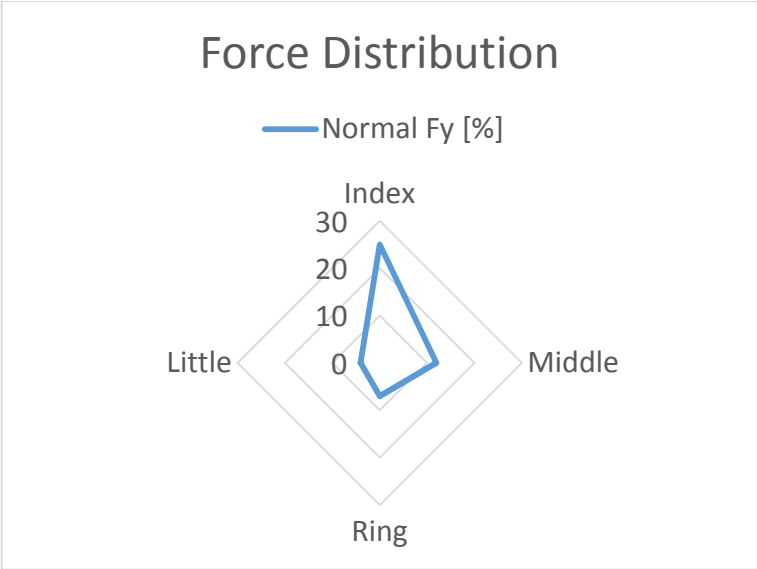

Fig. 47. Physiological force distribution during a cylindrical grasp, removing the thumb contributions.

Removing the contribution of the thumb, currently not actuated, the elements of the matrix $[S]_{\text{hand}}$ are reported in (5.3). Starting from these values, all other relevant parameters can be obtained using the following equation (5.3).

$$[\boldsymbol{S}]_{\boldsymbol{hand}} = \begin{bmatrix} 0.50 \\ 0.25 \\ 0.15 \\ 0.10 \end{bmatrix} = \begin{bmatrix} \dfrac{r_{A_2}}{(r_{A_1} + r_{A_2})} \\ \dfrac{r_{A_1} r_{B_2}}{(r_{A_1} + r_{A_2})(r_{B_1} + r_{B_2})} \\ \dfrac{r_{A_1} r_{B_1} r_{C_2}}{(r_{A_1} + r_{A_2})(r_{B_1} + r_{B_2})(r_{C_1} + r_{C_2})} \\ \dfrac{r_{A_1} r_{B_1} r_{C_1}}{(r_{A_1} + r_{A_2})(r_{B_1} + r_{B_2})(r_{C_1} + r_{C_2})} \end{bmatrix} \tag{5.3}$$

The previous transmission matrix allows to define the pulleys radii starting from the force distribution and the inter-finger-mechanism maximum size.

5.1.2 Fingers module

Working principle

The architecture of each of the four fingers is identical among them: the abduction/adduction of the MCP joint is allowed, but not actively assisted, while the MCP and PIP flexion are actuated. On the other hand, the return is passively

guaranteed by elastic elements (springs). By pulling the cable, the finger closes. The track of the tendon is given in Fig. 48 (each joint has an idle pulley, to decrease friction). At the end, the tendon is fixed to the second phalange. The kinematics of each finger joint realizes a four-bar mechanism: it is a well-known solution, for instance in (Wege and Hommel 2005) and (Yamaura et al. 2009), chosen as it is quite simple and lightweight. Each phalange element is attached to the human phalange by means of Velcro straps.

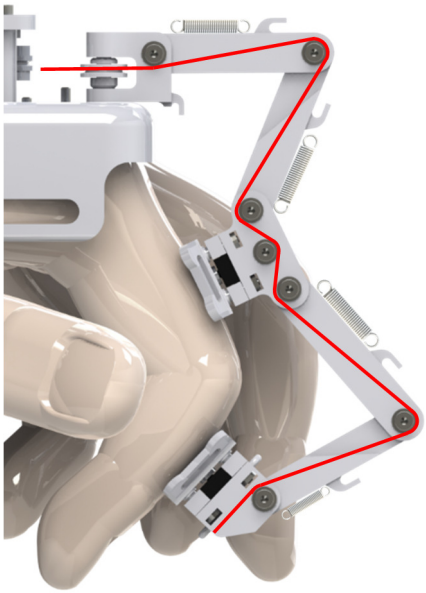

Fig. 48. Finger mechanism, in red line the tendon's path.

The design

In order to couple the exoskeleton with the human finger it necessary to use a mechanism that allows to interact with the user without any interference. In this dissertation the common planar four-bar mechanism is used, in particular one mechanism is used for each assisted joint. For the ReHand prototype, two mechanisms are considered sufficient, in order to drive the metacarpophalangeal (MCP) and proximal interphalangeal (PIP) joints. With reference to Fig. 49 it is possible to notice that the mechanism is composed by: two external linkages (p_{ji_1} and p_{ji_2}), two virtual links correlated with the phalanges and the position of exoskeleton on them (p_{ji_3} and p_{ji_4}) and three external coupling and the physiological joint. The figure represents the scheme of a generic four-bar mechanism, applied to the $j-$ th phalange of the $i-$ th finger. A local reference system centered in O_{ji_1} is applied, with the x_{ji} axis along the

direction of the segment as $\overline{O_{J\iota_1}O_{J\iota_4}}$. The angles φ_{ji_s}, positive along the counter-clockwise direction and with s from 1 to 3, describe the orientation of each segment $\overline{O_{J\iota_s}O_{J\iota_{s+1}}}$, whose length is p_{ji_s}.In particular, the configuration depicted in Fig. 49 is characterized by a negative φ_{ji_2} angle, according to the chosen positive angular rotation.

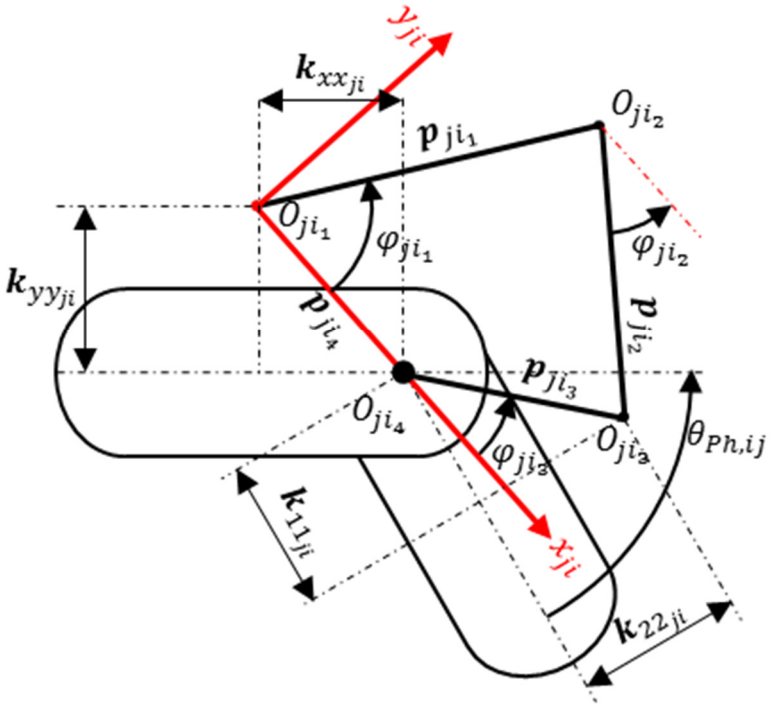

Fig. 49. Scheme of the four-bar mechanism for a generic finger phalange.

The previous figure is the basis for the following kinematic resolution, where, given the angle rotation of the phalange, the four-bar configuration is univocally determined. Starting from the reference frames definition, as in Fig. 49, it is possible to write the position equations as follows:

$$X: -p_{ji_1}cos(\varphi_{ji_1}) - p_{ji_2}cos(\varphi_{ji_2}) + p_{ji_4} + p_{ji_3}cos(\varphi_{ji_3}) = 0 \quad (5.4)$$

$$Y: -p_{ji_1}sin(\varphi_{ji_1}) - p_{ji_2}sin(\varphi_{ji_2}) + p_{ji_3}sin(\varphi_{ji_3}) = 0 \quad (5.5)$$

The previous equations can be transform in Freudenstein's form as follows:

$$k_1(\varphi_{ji_3})\sin(\varphi_{ji_1}) + k_2(\varphi_{ji_3})\cos(\varphi_{ji_1}) + k_3(\varphi_{ji_3}) = 0 \quad (5.6)$$

Where:

$$k_1 = -2p_{ji_1}p_{ji_2}\sin(\varphi_{ji_3}) \tag{5.7}$$

$$k_2 = -2 \cdot p_{ji_1}\left(p_{ji_4} + p_{ji_3}\cos(\varphi_{ji_3})\right) \tag{5.8}$$

$$k_3 = p_{ji_4}^2 + p_{ji_1}^2 - p_{ji_2}^2 + p_{ji_3}^2 \tag{5.9}$$

Substituting the trigonometric functions with the parametric form, it is possible to find the following solution:

$$\varphi_{ji_1}(\varphi_{ji_3}) = 2 \cdot atan2\left(-k_1 \pm \sqrt{k_1^2 + k_2^2 - k_3^2}, k_3 - k_2\right) \tag{5.10}$$

$$\varphi_{ji_2}(\varphi_{ji_1}, \varphi_{ji_3}) = \\ = atan2\left(-p_{ji_1}sin(\varphi_{ji_1}) + p_{ji_3}sin(\varphi_{ji_3}), p_{ji_4}\right. \\ \left. - p_{ji_1}cos(\varphi_{ji_1}) + p_{ji_3}cos(\varphi_{ji_3})\right) \tag{5.11}$$

$$\theta_{Ph,ij} = \varphi_{ji_3} - \text{atan}\left(\frac{k_{22_{ji}}}{k_{11_{ji}}}\right) - \left|\text{atan}\left(\frac{k_{yy_{ji}}}{k_{xx_{ji}}}\right)\right| \tag{5.12}$$

Deriving the previous equations (5.4) and (5.5) and organizing them in a matrix form (5.13). It is possible to find velocity equations:

$$\begin{bmatrix} p_{ji_1}\sin(\varphi_{ji_1}) & p_{ji_2}\sin(\varphi_{ji_2}) \\ -p_{ji_1}\cos(\varphi_{ji_1}) & -p_{ji_2}\cos(\varphi_{ji_2}) \end{bmatrix} \cdot \begin{Bmatrix} \dot{\varphi}_{ji_1} \\ \dot{\varphi}_{ji_2} \end{Bmatrix} = \begin{bmatrix} p_{ji_3}\sin(\varphi_{ji_3}) \\ -p_{ji_3}\cos(\varphi_{ji_3}) \end{bmatrix} \cdot \dot{\varphi}_{ji_3} \tag{5.13}$$

It is possible to calculate the velocities of the angle mechanism:

$$\begin{Bmatrix} \dot{\varphi}_{ji_1} \\ \dot{\varphi}_{ji_2} \end{Bmatrix} = \begin{bmatrix} S_1(\varphi_{ji_1}, \varphi_{ji_2}, \varphi_{ji_3}) \\ S_2(\varphi_{ji_1}, \varphi_{ji_2}, \varphi_{ji_3}) \end{bmatrix} \cdot \dot{\varphi}_{ji_3} \tag{5.14}$$

Where:

$$S_1(\varphi_{ji_1}, \varphi_{ji_2}, \varphi_{ji_3}) = \frac{p_{ji_3}\sin(\varphi_{ji_2} - \varphi_{ji_3})}{p_{ji_1}\sin(\varphi_{ji_2} - \varphi_{ji_1})} \tag{5.15}$$

$$S_2(\varphi_{ji_1}, \varphi_{ji_2}, \varphi_{ji_3}) = \frac{-p_{ji_3}\sin(\varphi_{ji_1} - \varphi_{ji_3})}{p_{ji_2}\sin(\varphi_{ji_2} - \varphi_{ji_1})} \tag{5.16}$$

Deriving equation (5.12) in time, it is possible to obtain the physiological angle velocity:

$$\dot{\theta}_{Ph,ij} = \dot{\varphi}_{ji_3} \tag{5.17}$$

The acceleration analysis is obtained differentiating the equation (5.13) and the result is reported below:

$$\begin{bmatrix} p_{ji_1}\sin(\varphi_{ji_1}) & p_{ji_2}\sin(\varphi_{ji_2}) \\ -p_{ji_1}\cos(\varphi_{ji_1}) & -p_{ji_2}\cos(\varphi_{ji_2}) \end{bmatrix} \cdot \begin{Bmatrix} \ddot{\varphi}_{ji_1} \\ \ddot{\varphi}_{ji_2} \end{Bmatrix} + \begin{bmatrix} \dot{\varphi}_{ji_1} p_{ji_1}\cos(\varphi_{ji_1}) & \dot{\varphi}_{ji_2} p_{ji_2}\cos(\varphi_{ji_2}) \\ \dot{\varphi}_{ji_1} p_{ji_1}\sin(\varphi_{ji_1}) & \dot{\varphi}_{ji_2} p_{ji_2}\sin(\varphi_{ji_2}) \end{bmatrix} \cdot \begin{Bmatrix} \dot{\varphi}_{ji_1} \\ \dot{\varphi}_{ji_2} \end{Bmatrix} = \begin{bmatrix} p_{ji_3}\sin(\varphi_{ji_3}) \\ -p_{ji_3}\cos(\varphi_{ji_3}) \end{bmatrix} \cdot \ddot{\varphi}_{ji_3} + \begin{bmatrix} \dot{\varphi}_{ji_3} p_{ji_3}\cos(\varphi_{ji_3}) \\ \dot{\varphi}_{ji_3} p_{ji_3}\sin(\varphi_{ji_3}) \end{bmatrix} \cdot \dot{\varphi}_{ji_3} \tag{5.18}$$

In compact form:

$$\begin{Bmatrix} \ddot{\varphi}_{ji_1} \\ \ddot{\varphi}_{ji_2} \end{Bmatrix} = \begin{bmatrix} S_1(\varphi_{ji_1}, \varphi_{ji_2}, \varphi_{ji_3}) \\ S_2(\varphi_{ji_1}, \varphi_{ji_2}, \varphi_{ji_3}) \end{bmatrix} \cdot \ddot{\varphi}_{ji_3} + \begin{bmatrix} \dot{S}_1(\varphi_{ji_1}, \varphi_{ji_2}, \varphi_{ji_3}) \\ \dot{S}_2(\varphi_{ji_1}, \varphi_{ji_2}, \varphi_{ji_3}) \end{bmatrix} \cdot \dot{\varphi}_{ji_3} \tag{5.19}$$

Where:

$$\dot{S}_1(\varphi_{ji_1}, \varphi_{ji_2}, \varphi_{ji_3}) = = \frac{(S_2 - 1)p_{ji_3}\cos(\varphi_{ji_2} - \varphi_{ji_3}) \cdot [p_{ji_1}\sin(\varphi_{ji_2} - \varphi_{ji_1})]}{[p_{ji_1}\sin(\varphi_{ji_2} - \varphi_{ji_1})]^2} - \frac{[p_{ji_3}\sin(\varphi_{ji_2} - \varphi_{ji_3})](S_2 - S_1)p_{ji_1} cos\left((\varphi_{ji_2} - \varphi_{ji_1})\right)}{[p_{ji_1}\sin(\varphi_{ji_2} - \varphi_{ji_1})]^2} \tag{5.20}$$

$$\dot{S}_2(\varphi_{ji_1}, \varphi_{ji_2}, \varphi_{ji_3}) = = \frac{[p_{ji_3}\sin(\varphi_{ji_1} - \varphi_{ji_3})](S_2 - S_1)p_{ji_2}\cos(\varphi_{ji_2} - \varphi_{ji_1})}{[p_{ji_2}\sin(\varphi_{ji_2} - \varphi_{ji_1})]^2} - \frac{(S_1 - 1)p_{ji_3}\cos(\varphi_{ji_1} - \varphi_{ji_3}) \cdot [p_{ji_2}\sin(\varphi_{ji_2} - \varphi_{ji_1})]}{[p_{ji_2}\sin(\varphi_{ji_2} - \varphi_{ji_1})]^2} \tag{5.21}$$

The acceleration of the physiological angle is then:

$$\ddot{\theta}_{Ph,i} = \ddot{\varphi}_{ji_3} \tag{5.22}$$

The position analysis is used to define a four-bar synthesis suitable for each exo-finger.

5.1.3 Four-bar synthesis

The four-bar synthesis is based on an optimization algorithm called Simulated Annealing Algorithm (SAA). The algorithm uses a series of four indicators in order to obtain the best geometry set. The optimization uses a kinematic function, implemented from the equations (5.10) (5.11) and (5.12), where the geometric set is known and the ϑ varies from zero degrees to a possible maximum value compatible with the physiological and mechanical constraints. In particular, the four indicators are: the ROM (range of motion), the mechanism's size, the contact between finger and mechanism and finally the distance from the singularity configuration by means of the well-known GCI (Global Conditioning Index) introduced by Gosselin at al. in (Gosselin and Angeles 1991).

Range of motion indicator

The first indicator concerns the mechanism's range of motion (ROM). The ROM can be evaluated as a global indicator because it is strictly connected only with the mechanism's geometry and not with a local configuration. The indicator can be considered as a normalized error expressed by the following equation:

$$y = \frac{\Delta\vartheta - \Delta\vartheta_{REF}}{\Delta\vartheta_{REF}} \tag{5.23}$$

Where $\Delta\vartheta$ is the mechanism's ROM, instead $\Delta\vartheta_{REF}$ is the reference ROM. The following chart shows the curve behavior exposed in (5.23), the co-domain is limited in the $[-1;\ 1]$ interval. From a physical point of view, the curve shows the behavior between errors from -100% (mechanism ROM equal to zero degrees) to $+100\%$ (mechanism ROM equal to twice the reference range of motion). The chart (Fig. 50) can give important information about the behavior of solution's goodness, in terms of ROM.

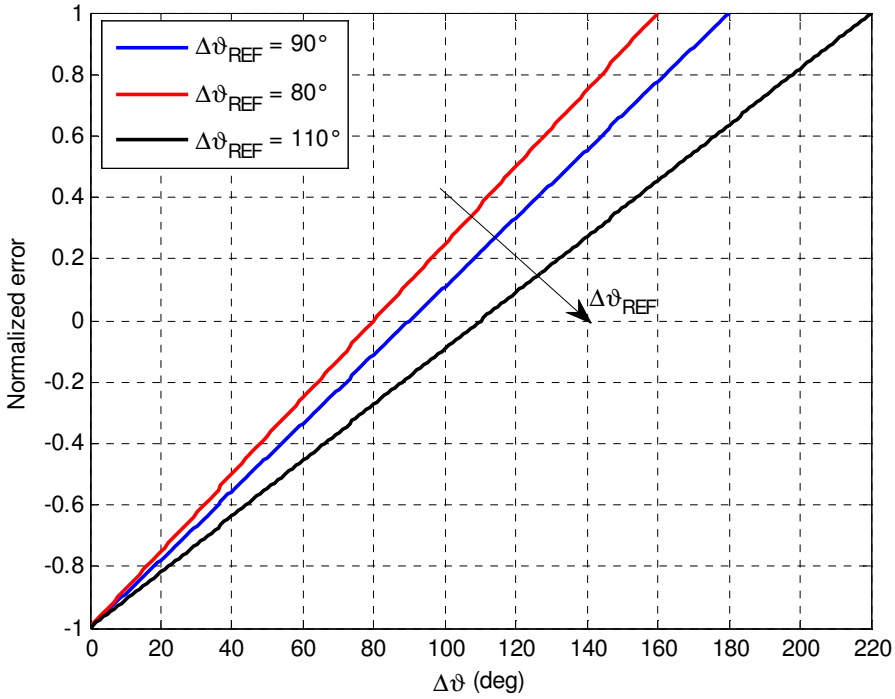

Fig. 50. Range of the motion indicator behaviors as a function of the reference ROM.

Dimension indicator

The requirement of a compact and compliant exoskeleton is necessary in order to develop a rehabilitation and empowerment device. It is so necessary to use a dimension indicator as a fundamental indicator about the size of the device (in first approximation, it is possible to consider the size directly proportional to weight). The computation of the second indicator is similar to the previous one, and it is reported in the following equation:

$$y = \frac{h_1}{\frac{\Delta\vartheta_{REF}}{\frac{K_f \cdot l_f}{1}}} \qquad (5.24)$$

Where, h_1 is the height calculated in zero configuration, $\Delta\vartheta_{REF}$ is the reference amplitude of ROM, l_f and K_f are respectively the finger length and the percentage of finger length compared with the ROM=1 rad. The dimension h_1 can be calculated as in (5.25).

$$h_1 = p_{ji_1} sin\left[\left|\varphi_{ji_1,0}\right| - \left|atan\left(\frac{k_{xx_{ji}}}{k_{yy_{ji}}}\right)\right|\right] + k_{xx_{ji}} \quad (5.25)$$

The angle $\varphi_{ji_1,0}$ denotes the angle φ_{ji_1} when the physiological angle is zero. The following diagram shows the curves' behaviors in terms of $\frac{h_1}{\Delta\vartheta_{REF}}$ and for different values of the K_f parameter.

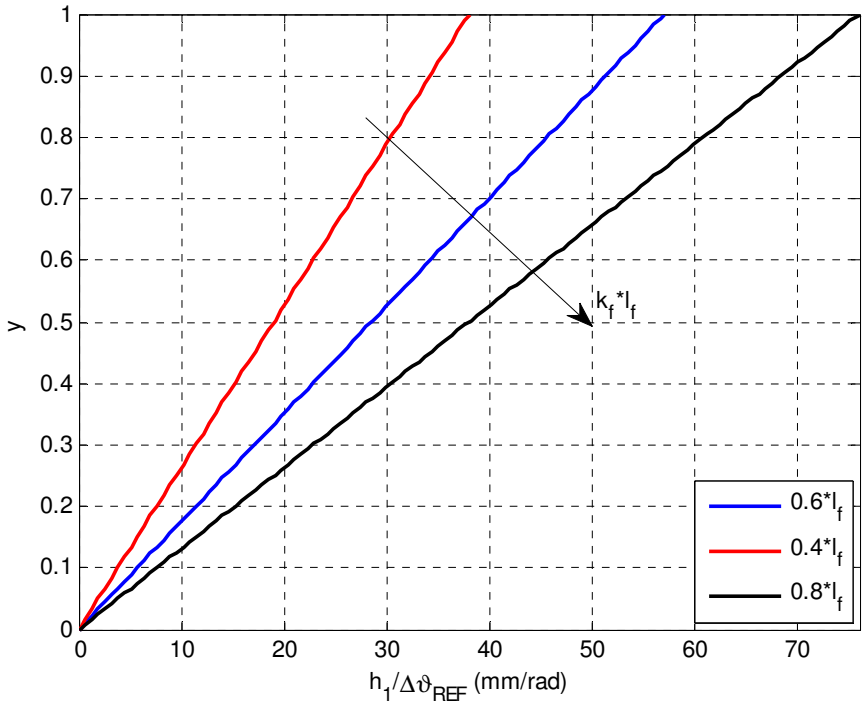

Fig. 51. Variation of the dimension indicator $\frac{h_1}{\Delta\vartheta_{REF}}$ as a function of the coefficient K_f.

Distance indicator

The third used indicator concerns the distance between the knuckle and the exoskeleton's mechanical links, as shown in the figure below (Fig. 52).

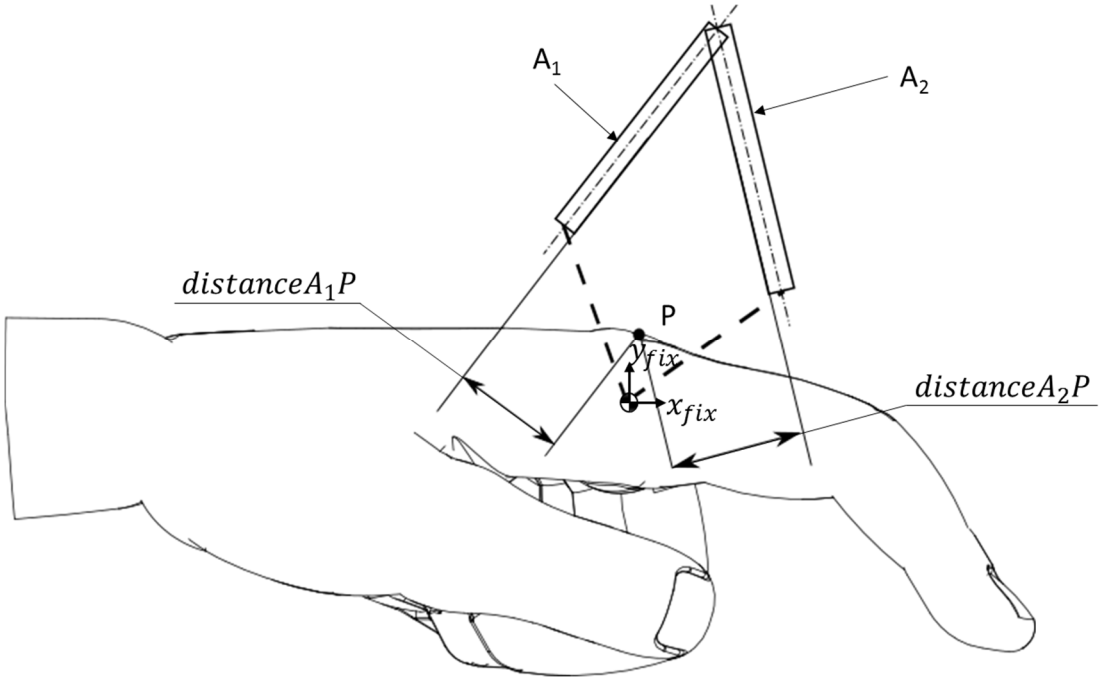

Fig. 52. Physical interpretation of the distance indicator.

The calculation and normalization of the distance indicator is expressed as follows:

$$y = \frac{\frac{\Delta\vartheta_{REF}}{dist}}{\frac{1}{K_f \cdot l_f}} \tag{5.26}$$

Where: $\Delta\vartheta_{REF}$ as previously, is the reference amplitude of ROM, $dist$ is the distance between the knuckle and links calculated as reported in the following (5.27), and the denominator is the reciprocal of the dimension indicator denominator. The calculation of the distance $dist$ is:

$$dist = min(min(distanceA_1P), min(distanceA_2P)) \tag{5.27}$$

The graph (Fig. 53) below shows the curve at the variation of the ratio $\frac{\Delta\vartheta_{REF}}{dist}$ and of the parameter K_f.

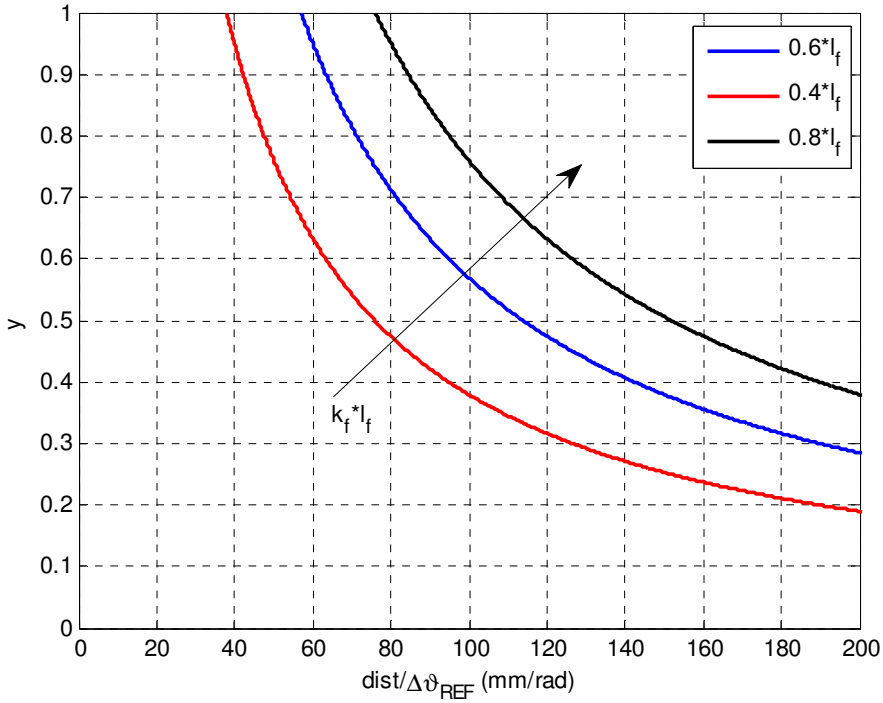

Fig. 53. Variations of the distance indicator as a function of the parameter K_f.

The function $distanceA_iP$ is calculate for each point for the RoM as:

$$distanceA_iP = \frac{\left|y_P - \left(m_{A_i}x_P + q_{A_i}\right)\right|}{\sqrt{1 + m_{A_i}^2}} \tag{5.28}$$

Where $(x, y)_P$ are the coordinates of the point P respect to the fixed reference frame, m_{A_i} and q_{A_i} are respectively the slope and intercept of the line pass through the internal side of the A_i link.

Global Condition Index (GCI)

In order to evaluate the quality of the found solution a classical kinematics index is used. The kinematics performance index is connected with the mechanism's Jacobian matrix. An example of kinematics index is the distance from a singularity configuration which has been computed by means of a Jacobian matrix determinant. The distance from a singularity configuration is strictly connect with a certain joint's position, so it is a local property of the manipulators. Usually it is preferable to use global property, so the Jacobian determinant can be substituted with the Global

Condition Index (GCI). Gosselin and Angeles proposed the GCI in (Gosselin and Angeles 1991), as a measure of distance form singularity configuration "mediated" in the workspace. In many other papers, the same indicator is used to evaluate parameters such as manipulator dexterity (Krovi, Ananthasuresh, and Kumar 2002) and (Lara-Molina, Rosario, and Dumur 2011), for example. The equation below shows the general GCI computation:

$$GCI = \frac{\int_{WS} \frac{1}{k(J)} dWS}{\int_{WS} dW\,S} \tag{5.29}$$

Where $k(J)$ is the condition number based on the Jacobian matrix $[J]$ and WS is the mechanism workspace. According to the computation method, the condition number is limited as shows below:

$$0 \leq \frac{1}{k(J)} \leq 1 \tag{5.30}$$

From a physical point of view, near null values mean that the mechanism is near to a singularity configuration, instead when the value approaches the unit value, it means that the Jacobian matrix is well-conditioned and it is far away from a singularity configuration. In terms of GCI:

$$0 \leq GCI \leq 1 \tag{5.31}$$

When the GCI is close to zero the workspace has bad GCI, that means the workspace is anisotropic, instead when the GCI is next to unit value, the workspace has a good GCI and the number can be interpreted as the neighbor to an isotropic workspace. It is possible to perform a numerical computation of GCI, substituting the integral with a summation:

$$y = GCI = \frac{\delta\vartheta \cdot \sum_i \frac{1}{k_i(J)}}{\delta\vartheta \cdot \sum_i i} \tag{5.32}$$

The condition number, based on J matrix, can be computed as follow:

$$k(J) = \|J\| \cdot \|J^{-1}\| = \sqrt{tr(J \cdot N \cdot J^T)} \cdot \sqrt{tr\left((J^{-1}) \cdot N \cdot (J^{-1})^T\right)} \quad (5.33)$$

Where the matrix called N, is defined by the following equation (5.34):

$$N = \frac{1}{n} \cdot [I]_{n \times n} \quad (5.34)$$

For simplicity the Jacobian matrix is a square matrix with dimension $n \times n$. Instead, $[I]$ is the identity matrix with the same size. Other articles consider also the possibility of using a non- square Jacobian matrix in order to generalize the discussion.

Weight function

The weight function, defined in this section, is common for all indices and represent a global indicator of the solution's goodness. The weight function is similar to a Harrington desirability function, in particular the "one-sided" function (Harrington 1965). The difference between the original and the proposed one is in the linear transformation, where the modulus function is applied at the input value y_j in order to have the same response for both negative and positive values. As introduce by Harrington, the function can be written from the knowledge of two pairs of (y_{j1}, d_1) and (y_{j2}, d_2) with the criteria values, y_j, given in actual response units. The response values can be scaled using the followed equations:

$$\begin{aligned} Y'_{j1}(\underline{x}) &= -ln(-ln(d_1)) \\ Y'_{j2}(\underline{x}) &= -ln(-ln(d_2)) \end{aligned} \quad (5.35)$$

The scaled criteria value $Y'_j(\underline{x})$ is obtained with the following linear transformation:

$$\mathrm{Y'_j}(\underline{\mathrm{x}}) = \left[\frac{\left|\mathrm{y_j}(\underline{\mathrm{x}})\right| - \mathrm{y_{j2}}}{\mathrm{y_{j1}} - y_{\mathrm{j2}}}\right] \cdot \left(\mathrm{Y'_{j1}}(\underline{\mathrm{x}}) - \mathrm{Y'_{j2}}(\underline{\mathrm{x}})\right) + \mathrm{Y'_{j2}}(\underline{\mathrm{x}}) \quad (5.36)$$

The weight function can be wrote as follow:

$$i_j\left(y_j(\underline{x})\right) = exp\left[-exp\left(-Y'_j(\underline{x})\right)\right] \quad (5.37)$$

For each indicator y_j, it is possible to compute the above-mentioned equation, in order to obtain a weighted indicator. The figure below shows the behavior of the function i_j, for the both cases, $d_{j1} > d_{j2}$ and $d_{j1} < d_{j2}$:

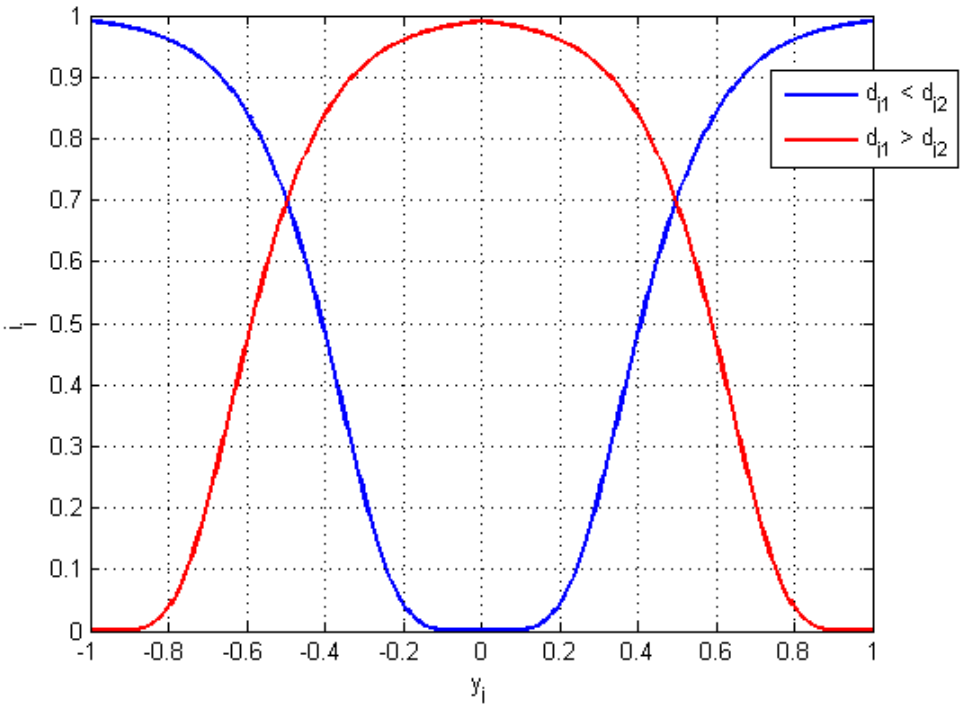

Fig. 54. First case: $y_{j1} > y_{j2}$

The chosen values of the mentioned couples (Y_{ji}, d_i), with $i = 1,2$, can be selected as proposed in (Derringer), where the importance of performance indicator compared to the others is discussed. The global performance indicator, indicated with the simple W can be defined as:

$$W = \sum_{j=1}^{N} \kappa_j i_j \quad (5.38)$$

Where the parameter called N is the number of considered indicator and κ_j is a constant, which depends on the importance of the indicator. Obviously, this function is the simplest one, and it is suitable for the mono-objective optimization problem.

Optimization problem and results

Now, it is possible to formulate the problem optimization in order to find the best geometry set. As seen before, the cost function W depends on the geometry set, so with the variation of mechanism lengths, we obtain different values of cost function. Under these assumptions, the optimization problem can be summarized as follows:

$$\min_{\underline{x}_l \le \underline{x} \le \underline{x}_u} \{W(\underline{x})\} \qquad (5.39)$$

The $\underline{x}_{ii}$ is the ii-geometry set, while the subscripts u and l denote respectively, the upper and lower limits of the mechanism dimensions. A stochastic algorithm, namely the Simulated Annealing Algorithm (SAA) (Greenwood 1986) and (Battezzato 2014), is implemented and used for an optimized synthesis. The flow chart below (Fig. 55) shows the strategy of the SAA for an iteration step.

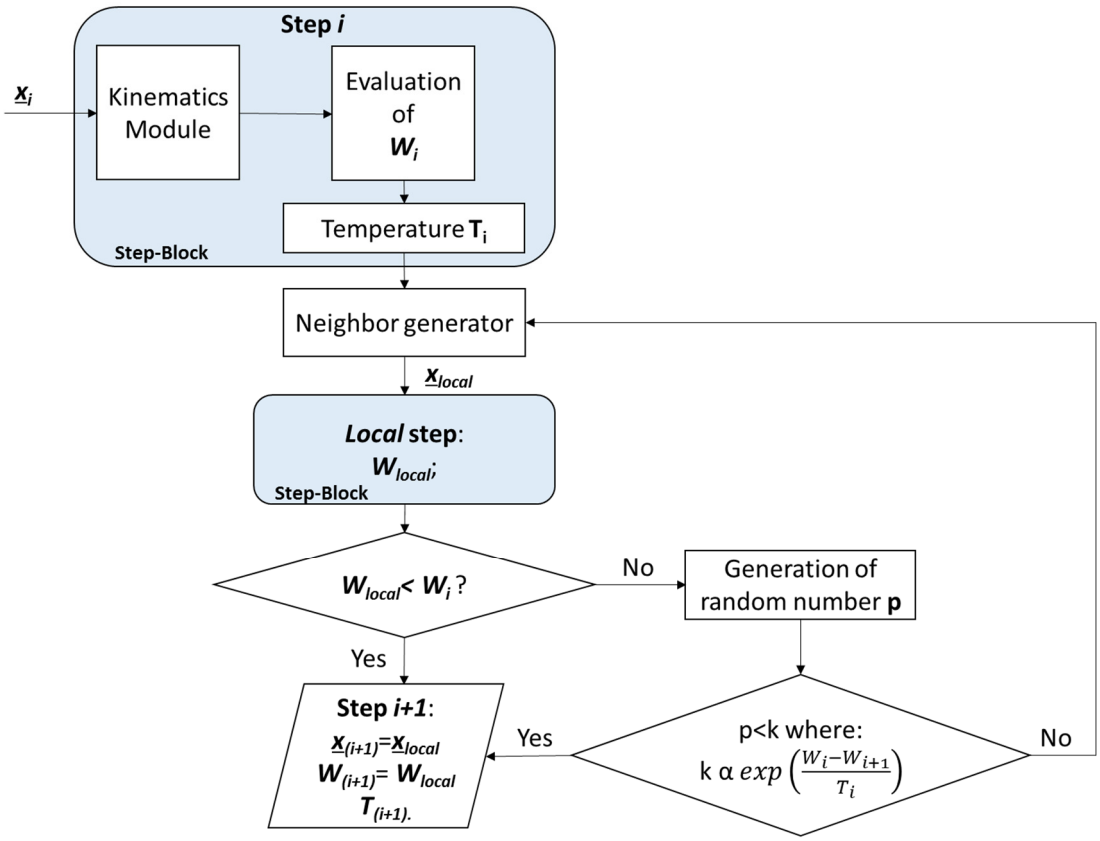

Fig. 55. Proposed optimization algorithm, based on SAA.

The used algorithm allows to minimize the objective function $W(\underline{x})$ considering a large number of variables, and also permits to find the global minimum by means of a random generation of variables. The temperature parameter, that controls the variables amplitude changing, is a historic heritage given by the original application field of statistical mechanics of annealing.

Starting from the previously introduced anthropometric data, the optimization results obtained for the MCP index finger's mechanisms are reported as example. It is important to keep in mind that hyperextension is neglected. Fig. 56 shows the notation used in the constraints defined in next table (Tab. 11).

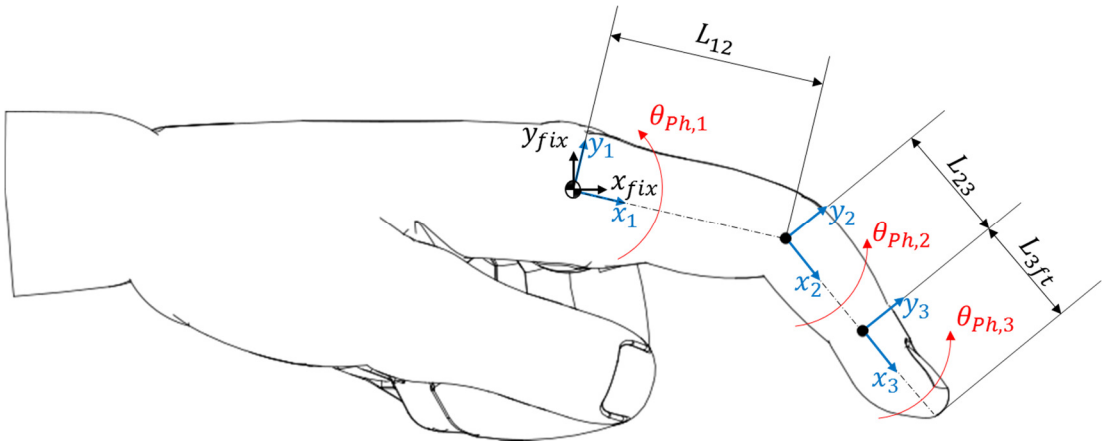

Fig. 56. Notation and reference frame applied to index finger.

For the index finger MCP mechanism, the constraints in Tab. 11 have been set:

Tab. 11. Upper and lower limits.

Lower limit (mm)		**Upper limit (mm)**
$\frac{1}{2}L_{12}$	$< k_{11_1} <$	$\frac{2}{3}L_{12}$
$\frac{3 \cdot h_d}{4}$	$< k_{22_1} <$	$\frac{h_d + 20}{2}$
25.00	$< p_{11_1} <$	40.00
25.00	$< p_{11_2} <$	40.00

5.1 ReHand Description

The constant parameters, used for the index MCP four-bar synthesis, are collected in the table below as well as the constant parameters k_j, which determines the priority of an indicator over the others.

Tab. 12. Constant parameters.

$\Delta\vartheta_{REF}$	90°
K_f	0.6
$\boldsymbol{h_d}$	20 *mm*
$\boldsymbol{k_{ROM}}$	1
$\boldsymbol{k_{dim}}$	1
$\boldsymbol{k_{dist}}$	1
$\boldsymbol{k_{GCI}}$	1

The optimization process, with the above constraints and constants produced the following results. In particular, the charts below show the behavior of interesting features as a function of links' length. The figures are referred to the index MCP mechanisms; the resulting figures are plotted keeping constant, respectively, lengths $k_{xx_{11}}$, $k_{yy_{11}}$ and varying the link lengths p_{11_1} and p_{11_2}in the first case, instead in the second case, the exoskeleton position on the phalanges is modifying by means of k_{11_1}, k_{22_1}.

Fig. 57 a) describes the behavior of the ROM on varying of the links length. A suitable solution for the exoskeleton can be obtained with p_{11_1} ranging from 25.0 mm to 30.5 mm and with p_{11_2} starting from 25.0 mm to 31.28 mm. The Fig. 57 b) shows the mechanism's dimension varying the link lengths. The worst performances are obtained with the couple composed by 36.79 mm and 39.9 mm where the dimension is around 59.89 mm. In contrast, the best dimension is obtained with the couple of link values of 35.22 mm and 26.57 mm. Fig. 57 c) describes the distance indicator, the best value is performed with the couple of lengths ranging from 31.29 mm to 40.0 mm for both link. Finally, the Fig. 57 d) shows the GCI, and it is possible to notice that the workspace is strictly anisotropic for all the chosen range of p_{11_1} and p_{11_2}.

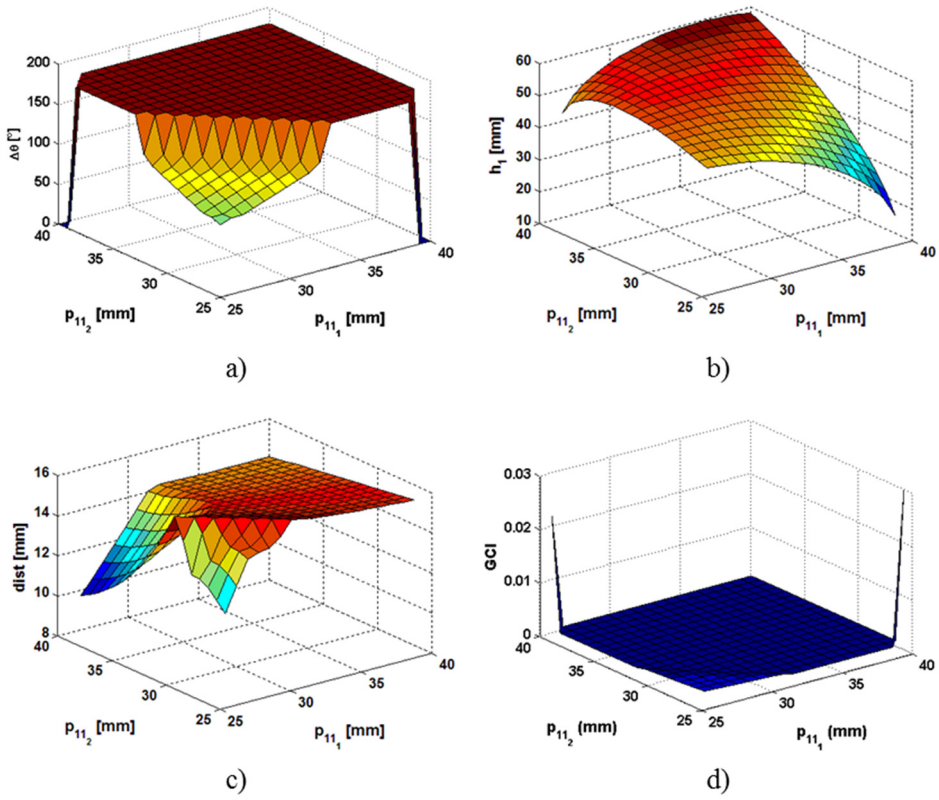

Fig. 57. Output of simulation #1, behavior of the four indicators of interest as a function of links lengths p_{11_1} and p_{11_2}, while k_{xx_1}, k_{yy_1}, k_{11_1} and k_{22_1} are kept constant. The ROM indicator is shown in a), b) shows the dimension indicator h_1, while $dist.$ and GCI are shown respectively in c) and d).

The following figure shows the behavior of the chosen indicators referred to the index MCP mechanism on varying of the values of k_{11_1}, k_{22_1} and maintaining constant the links lengths. As previously, the Fig. 58 a) describes the variation of ROM as a function of k_{11_1} and k_{22_1} lengths. Suitable ROM can be obtained with a couple of values from 22.45 mm to 23.15 mm concerning k_{11_1} and starting from 20 mm to 23.16 mm. The dimension indicator is strictly influenced by k_{11_1} and k_{22_1} values, in particular the best values of the dimension mechanism are obtained with k_{11_1}equal to 28.91 mm and k_{22_1} 21.06 mm. The best values of the indicator $dist$ are performed with k_{11_1} =25.51 mm and k_{22_1} =29.98 mm. In conclusion, the GCI (Fig. 58 d) shows that mechanism's workspace is anisotropic but is less anisotropic for the following values: 28.57 mm and 27.88 mm.

5.1 ReHand Description

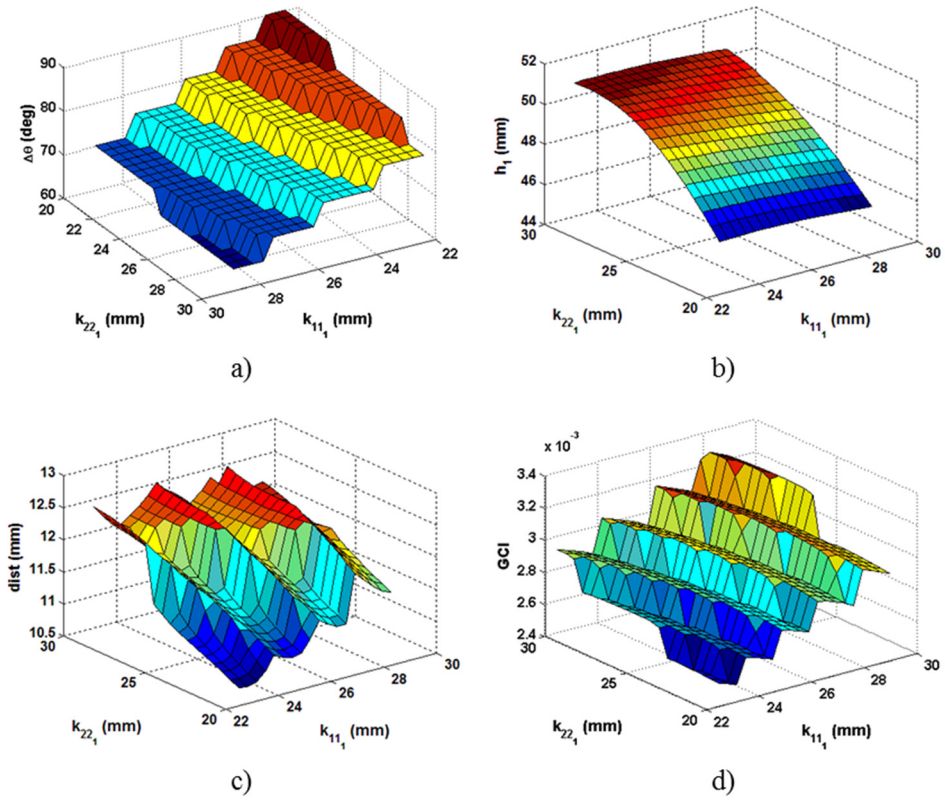

Fig. 58. Output of simulation #2, behavior of the four indicators of interest as a function of k_{11_1} and k_{22_1} values while k_{xx_1}, k_{yy_1}, p_{11_1} and p_{11_2} are kept constant. The variation of ROM indicator is reported in a), in b) is shown the h_1 dimension, in c) is reported the behavior of $dist.$ indicator, and finaly, in d) the GCI indicator.

Tab. 13. Realized geometry sets.

	Index (mm)	**Middle (mm)**	**Ring (mm)**	**Little (mm)**
$\boldsymbol{k_{xx_{1i}}}$	-10.0	-10.0	-10.0	-10.0
$\boldsymbol{k_{yy_{1i}}}$	26.0	26.0	26.0	26.0
$\boldsymbol{p_{1i_1}}$	32.0	38.5	33.0	32.0
$\boldsymbol{p_{1i_2}}$	34.0	40.0	33.0	30.0
$\boldsymbol{k_{11_{1i}}}$	9.5	12.5	10.0	8.5
$\boldsymbol{k_{22_{1i}}}$	26.0	26.0	26.0	26.0
$\boldsymbol{k_{xx_2i}}$	-9.5	-10.0	-9.5	-8.5
$\boldsymbol{k_{yy_2i}}$	26.0	26.0	26.0	26.0
$\boldsymbol{p_{2i_1}}$	35.0	34.0	35.0	30.0
$\boldsymbol{p_{2i_2}}$	32.0	37.0	32.0	32.0
$\boldsymbol{k_{11_{2i}}}$	10.5	12.0	11.0	10.0
$\boldsymbol{k_{22_{2i}}}$	26.0	26.0	26.0	26.0

The optimization results are obtained for a certain hand dimension and with strict tolerances. Exploiting the four bar property of adaption with different hand sizes, the best values are incremented by 10 %, in order to allow the donning and doffing of the device with different finger dimensions. In addition, the lengths have been rounded at 0.5 mm considering the resolution and tolerances of the additive manufacturing technology. The real geometry sets are reported in Tab. 13.

5.2 Kinetostatic model

This section presents the kinetostatic analysis of ReHand, which has been carried out by means of virtual power, in particular by means of the equivalence of virtual power along each finger. In the following, the bold lowercase notation will be used for the column vectors, while the matrices will be uppercase in square brackets. Considering the generic $K-th$ differential element, the relationship between the input and the $i-th$ output is the following:

$$f_{K_i} = k_{K_i} f_K \tag{5.40}$$

where k_{K_i} is a parameter, depending on the geometry and configuration of the differential mechanism. In particular, when considering the specific case of a pulley (Fig. 45), the angle $\alpha_{K_i} = 0, \forall i$ and the parameter k_{K_i} becomes equal to:

$$k_{K_i} = \frac{\sum_{t=1}^{2}\left[(-1)^t \, r_{K_t}(t-i)\right]}{\sum_{t=1}^{2}\left(r_{K_t}\right)}, \forall i \tag{5.41}$$

where r_{K_t} is the winding radius of the $t-$ th cable about the pulley. In particular, for the pulley the force subdivision is configuration-independent. Given that a single differential mechanism splits one input into two outputs, three mechanisms connected as previously described are necessary to drive the four fingers. In general, if there are N actuated fingers, $(N-1)$ differential elements are needed. The column vector $\boldsymbol{f}_{fin}$, collecting all the N forces f_i, where f_i represents the output of the ith under-actuated mechanism, becomes:

$$\boldsymbol{f}_{fin} = [S]_{hand} \cdot f_A \tag{5.42}$$

where f_A is the actuating input force and $[S]_{\text{hand}}$ is an $(N \times 1)$ matrix describing the inter-finger under-actuation. Equation (5.3), previously used in the design phase, shows the force transmission matrix structure, for the pulley case.

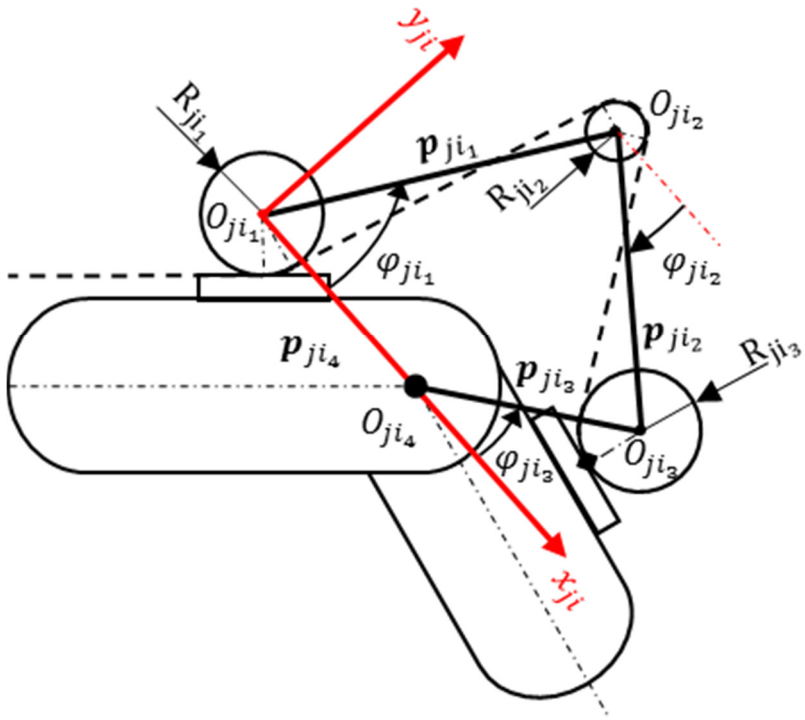

Fig. 59. Scheme of the four-bar mechanism for a generic finger phalange.

In order to relate the pulling force acting on the cable with the contact forces of the phalanges, it is necessary to know the exact configuration of each finger, as previously described. Recalling the four bar scheme, Fig. 59 shows the phalange's mechanism complete with the actuation, where R_{ji_s} is the radius of the pulley whose axis projection coincides with O_{ji_s}, and the vector of the joint velocities $\dot{\boldsymbol{\theta}}_i$, related to the $i-$th finger, describes the angular velocity of the $j-$th phalange $\dot{\theta}_{ji}$ in the $j-$th element. It has to be related to the vector $\dot{\boldsymbol{l}}_i$ describing the velocity of the cable along the whole finger; in detail, its component $\dot{l}_{ji}$ is the velocity of the cable due to only $\dot{\theta}_{ji}$ joint rotation. Since each phalange is actuated by means of a dedicated four-bar

mechanism, the total velocity of the actuating cable is a direct sum of the partial contributions coming from each phalange, i.e. the system is linear. Each contribution can be expressed as a function of the local angles and dimensions describing each four-bar mechanism:

$$\dot{l}_{ji} = R_{ji_1}\dot{\varphi}_{ji_1} + R_{ji_2}\left(\dot{\varphi}_{ji_1} - \dot{\varphi}_{ji_2}\right) + R_{ji_3}\left(\dot{\varphi}_{ji_3} - \dot{\varphi}_{ji_2}\right) \tag{5.43}$$

The equation (5.43) can be written in matrix form as follows:

$$\dot{l}_{ji} = A_{ji} \cdot \dot{\theta}_{ji} \tag{5.44}$$

Where the scalar A_{ji} can be computed as reported in the following relation:

$$A_{ji} = \begin{bmatrix} R_{ji_1} & R_{ji_2} & R_{ji_3} \end{bmatrix} \cdot \begin{bmatrix} 1 & 0 \\ 1 & -1 \\ t_{ji} & -1 \end{bmatrix} \cdot \begin{bmatrix} p_{ji_1}sin\left(\varphi_{ji_1}\right) & p_{ji_2}sin\left(\varphi_{ji_2}\right) \\ -p_{ji_1}cos\left(\varphi_{ji_1}\right) & -p_{ji_2}cos\left(\varphi_{ji_2}\right) \end{bmatrix}^{-1} \cdot \begin{bmatrix} p_{ji_3}sin\left(\varphi_{ji_3}\right) \\ -p_{ji_3}cos\left(\varphi_{ji_3}\right) \end{bmatrix} \tag{5.45}$$

In particular, $t_{ji} = \frac{p_{ji_1}\sin(\varphi_{ji_2} - \varphi_{ji_1})}{p_{ji_3}\sin(\varphi_{ji_2} - \varphi_{ji_3})}$ is a function of the dimensions and of the configuration of the four-bar mechanism. Combining the previous results for the different phalanges of the $i-$th finger, the following can be written:

$$\dot{\boldsymbol{l}}_i = [A]_i \dot{\boldsymbol{\theta}}_i \tag{5.46}$$

where $[A]_i$ is a single-row matrix with the terms A_{ji} in the first q positions, and zeroes from the $(q+1) - th$ element.

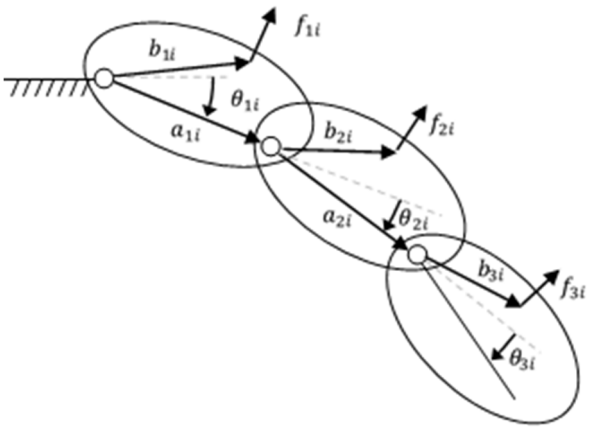

Fig. 60. Notation associated with the considered contact forces between the exoskeleton and the human finger phalanges.

The cable force f_i actuates the $i-$th finger and generates a distribution of forces on all the phalanges. Fig. 60 shows an equivalent scheme of the exo-finger, where the vectors $\boldsymbol{a}_{ji}$ denote the position of the biomechanical revolute joints, and the vectors $\boldsymbol{b}_{ji}$ describe the point of application of the contact forces $\boldsymbol{f}_{ji}$. All the $\boldsymbol{f}_{ji}$ forces are assumed to be perpendicular to the respective finger phalanges, while the tangential components are neglected. The unit vector $\boldsymbol{i}_{ji}$ describes the direction of $\boldsymbol{a}_{ji}$, i.e. it is also $\boldsymbol{f}_{ji} \cdot \boldsymbol{i}_{ji} = 0$. The angular rotations of the phalanges θ_{ji} are also indicated, positive according to the clockwise direction. Considering the equivalence of virtual powers along each finger, the following dot product can be written:

$$\sum_{j=1}^{3} (\boldsymbol{f}_{ji} \cdot \boldsymbol{v}_{ji}) = f_i \sum_{j=1}^{q} \dot{l}_{ji} \tag{5.47}$$

where the vector $\boldsymbol{v}_{ji}$ expresses the velocity of the application point of the contact force on the $j-$th phalange of the $i-$th human finger, and it is related to the angular joint velocities $\dot{\boldsymbol{\theta}}_i$. Equation (5.47) can be written in a matrix form obtaining:

$$\boldsymbol{f}_{phal\_i}{}^{T} [B]_i \dot{\boldsymbol{\theta}}_i = f_i [U]_i{}^{T} \dot{\boldsymbol{l}}_i \tag{5.48}$$

where the column vector $\boldsymbol{f}_{phal\_i}$ collects the magnitude of the three forces $\boldsymbol{f}_{ji}$ acting on the phalanges of the $i-$th finger -even if only the first q elements are not null- and the matrix $[B]_i$ is:

$$[B]_i = \begin{bmatrix} \boldsymbol{b}_{1i} \cdot \boldsymbol{i}_{1i} & 0 & 0 \\ (\boldsymbol{a}_{1i} + \boldsymbol{b}_{2i}) \cdot \boldsymbol{i}_{2i} & \boldsymbol{b}_{2i} \cdot \boldsymbol{i}_{2i} & 0 \\ (\boldsymbol{a}_{1i} + \boldsymbol{a}_{2i} + \boldsymbol{b}_{3i}) \cdot \boldsymbol{i}_{3i} & (\boldsymbol{a}_{2i} + \boldsymbol{b}_{3i}) \cdot \boldsymbol{i}_{3i} & \boldsymbol{b}_{3i} \cdot \boldsymbol{i}_{3i} \end{bmatrix} \tag{5.49}$$

Finally,$[U]_i$ is a (3x1) matrix, whose generic $j-$th element is equal to 1 if the $j-$th phalange is assisted and moving, and zero otherwise. Substituting equation (5.46) into (5.48), it is:

$$\boldsymbol{f}_{phal\_i} = [S]_{phal\_i} f_i \tag{5.50}$$

where $[S]_{phal\_i} = [B]_i^{-T}[A]_i^T[U]_i$ is a matrix describing the intra-finger underactuation. Finally, expressing the equation for all the assisted fingers, it becomes:

$$\boldsymbol{f}_{phal} = [S]_{phal}\boldsymbol{f}_{fin} \tag{5.51}$$

where $\boldsymbol{f}_{phal}$ is a column vector of size $(3N \times 1)$, obtained as the combination of the N vectors $\boldsymbol{f}_{phal\_i}$. On the other hand, the vector $\boldsymbol{f}_{fin}$ collects the N terms f_{i}. The $[S]_{phal}$ matrix presents the $[\mathrm{S}]_{\mathrm{phal\_i}}$ in the $i-th$ column and from $i-th$ to $(i+2)-th$ rows, with all the other terms equal to zero. Finally, defining $[S]_{glob} = [S]_{phal}[S]_{hand}$, the whole intra- and inter-finger underactuated system and the relationship between the input force f_A and the $\boldsymbol{f}_{phal}$ vector can be described as:

$$\boldsymbol{f}_{phal} = [S]_{glob}f_A \tag{5.52}$$

Starting from the previous mathematical model, it is possible to predict and validate the whole system. It is then possible to calculate the force exchanged between the system (hand plus exoskeleton) and the external word. In particular, it is possible create maps (for each actuated finger) and evaluate the force as a function of the angular position of the phalanges. An example of the exchanged forces of the actuated index is reported below:

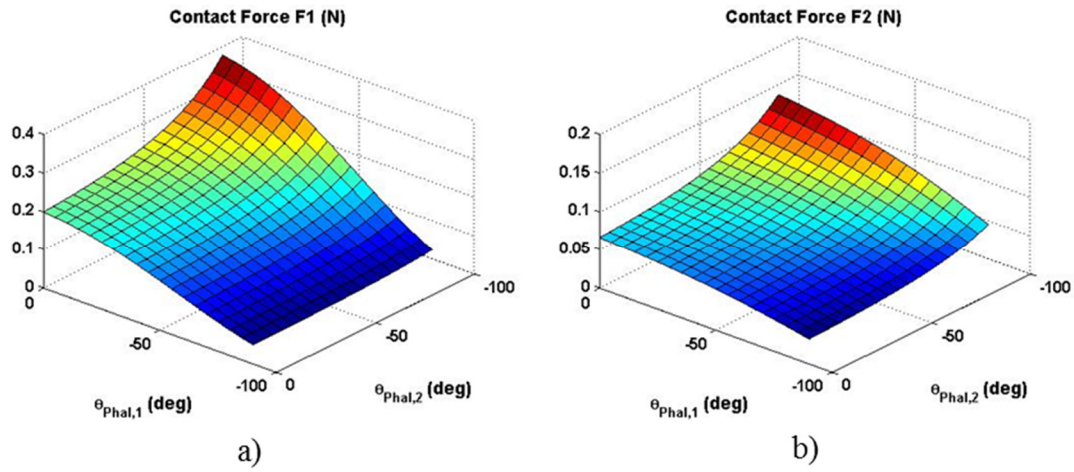

Fig. 61. Contact forces on first phalange a) and on the second one b) varying the angular position of the finger's phalanges.

5.3 Mechanical characterization

The prototype has been tested in order to verify the feasibility of the whole system. The performed tests have regarded the following features:

1) kinematical validation: it is a qualitative test, used to verify the device's adaptability to different grasps without constraining the user's hand;

2) kinetostatic validation: to numerically validate the correspondence between the experimentally measured mechanical response and the theoretically predicted values;

5.3.1 The test bench and kinetostatic validation

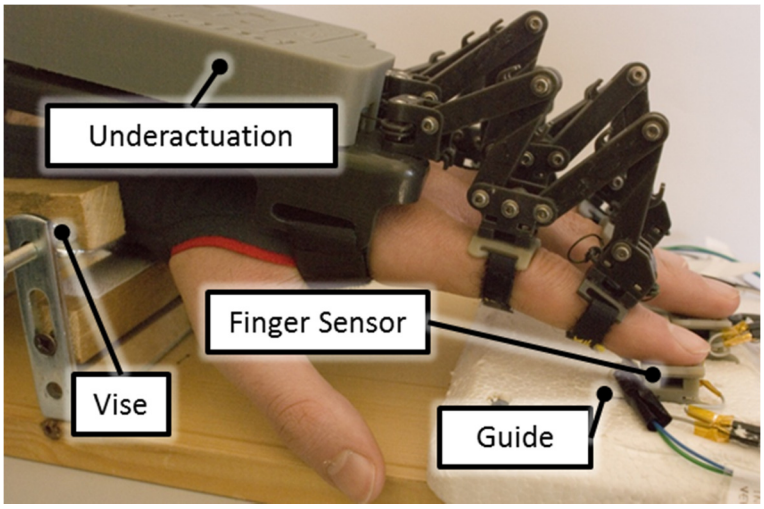

Fig. 62. Test setup for mechanical validation.

Fig. 62 shows a test bench developed for the mechanical evaluation. A vise mechanism immobilized the wrist of the subject, while a series of load cells measured the forces generated by the hand plus exoskeleton system. A single contact point between each finger and the test bench was imposed, and thus a single force was considered per fingertip. Therefore, referring to the equations in the previous section, the following parameters have been set: $N = 4$, $q = 1$ and $f_{ij} = 0 \; \forall i,j \neq 3$. The tests were performed in static conditions, i.e. without any displacement generated, and thus all geometrical parameters remained constant. The fingertip forces were measured using four commercial piezoresistive load cells (operating force 0 – 15 N, sensitivity 0.012 V/N, FSS1500NSB, Honeywell, FS Series, NJ). The sensors were integrated in a custom designed support (Fig. 63), promoting the exchange of force with the fingers

and allowing customization to different hand sizes by means of guides to change position of fingertip.

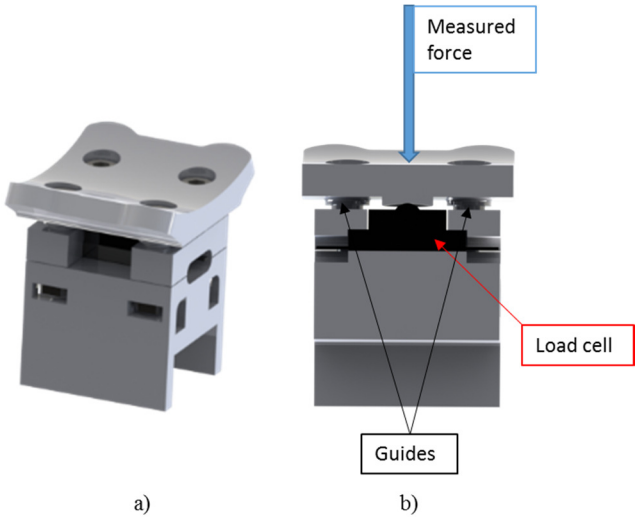

Fig. 63. Rendering a) and scheme of the finger force sensor b), the embedded sensor allow to measure force range between 0 - 15 N.

The position of the subject's wrist and the guides were adjusted for each subject individually so that the fingers could be extended and the fingertips would correctly land on the force sensors. Another load cell was integrated within the exoskeleton between the actuator and the inter-finger modules (Fig. 64) in order to measure the tension of the actuating tendon. It should be highlighted that this component is not required for the control of the exoskeleton, but it was used only for the characterization of the prototype.

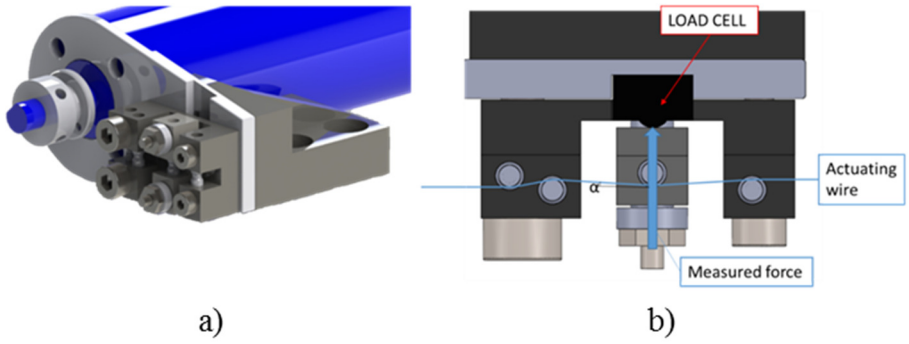

Fig. 64. Method of measurement of actuating force, a) rendering of the measurement setup, b) the scheme of the measurement unit. The α angles are calculated in order to have the limit of the load cell coincident with the maximum of the actuation force allowed by the motor shaft.

5.3 Mechanical characterization

A DAQ card (NI PCe 6363, National Instruments Corp.) received force signals as analog inputs, while the control parameters and command references were sent from the host PC to the motor using a standard RS232 communication link. A torque control and the sensors acquisition have been implemented using LabVIEW (National Instruments Corp.) (Fig. 65), in order to investigate the system behavior on a range of input forces.

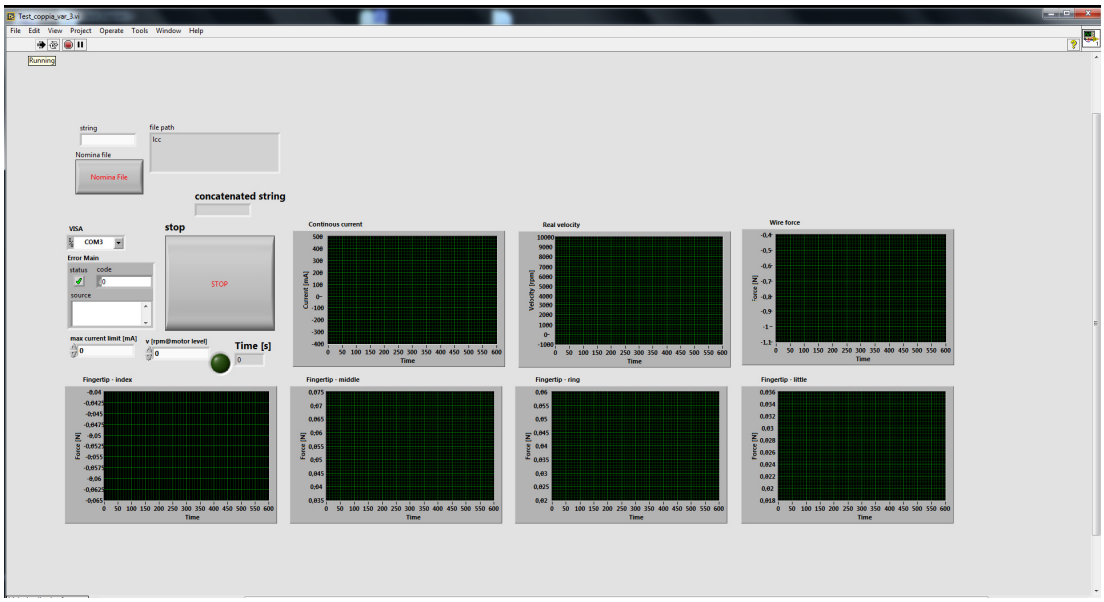

Fig. 65. Labview front panel.

In particular, the torque control was obtained by tuning the current limit of the inner control loop of the DC motor. In particular, a predefined ramp of currents, between 100 mA and 1000 mA, was sent to motor (Fig. 66).

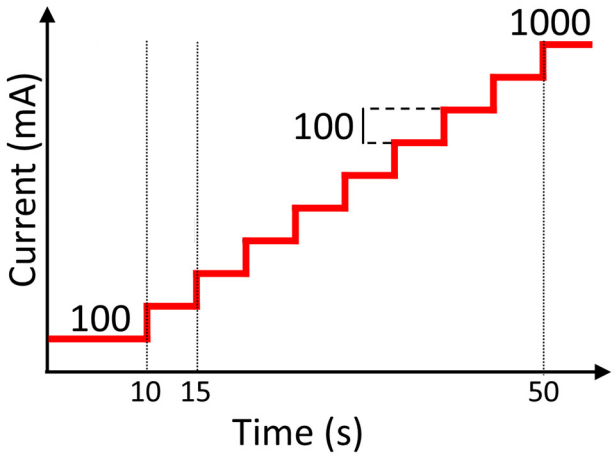

Fig. 66. Motor current reference for the mechanical validation.

Mechanical characterization was performed on three volunteer subjects (males, 29 yrs. average). The exoskeleton was attached to the subject's hand and placed in position as previously described. The validation comprised 8 cycles of closing actuation imposed by the exoskeleton (subject passive). The full extension was actively performed by the subject within the rest intervals in-between the flexion cycles. The reference profile for the motor current consisted of a staircase signal increasing from 100 mA to 1000 mA in increments of 100 mA, where all the steps lasted 5 seconds except for the first one, which lasted 10 seconds and served to measure offset and noise (Fig. 66). The average value of the latter was then subtracted from the acquired signals.

5.4 Preliminary results

In this section the results of kinetostatic and kinematic tests are reported and discussed. The trials have been conducted on eight healthy volunteers (6 males and 2 females, aged between 26 and 35), who participated in the study after providing written informed consent. The qualitative kinematic validation has the aim to show the mechanism's ability to adapt itself to a different object shapes. The quantitative tests are performed by the so-called kinetostatic tests.

5.4.1 Kinematical validation

The goal of this test was to demonstrate the adaptability, flexibility and compliance of the device to different grasps and objects, always leaving the user free of constraints. Fig. 67 shows the pictures of the accomplished tasks, organized according to the classification reported in (Cutkosky and Howe 1990). All subjects were able to perform all the tasks without dropping the grasped objects. No subject reported feeling any constraints imposed by the exoskeleton while performing the grasps. No subject complained about pain, although some subjects did report slight discomfort in the fingers, due to the distal finger-exoskeleton interface.

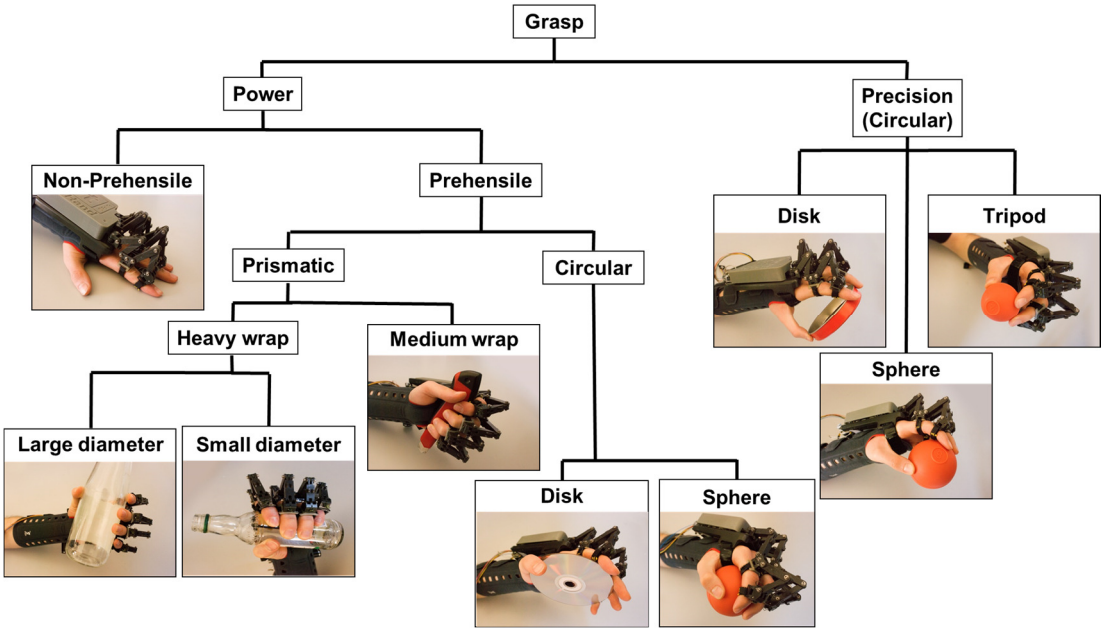

Fig. 67. Different grasps generated by the exoskeleton organized according to the classification reported in (Cutkosky and Howe 1990).

5.4.2 Kinetostatic validation

The kinematic validation consisted in giving a current trajectory to the motor and measuring the force at the fingertip level. Fig. 68 shows the comparison among the nominal (continuous red line) and the measured current (blue dots). The supplied current allows the motor to generate an output torque and a consequent actuation force developed on the tendon, which is measured by the load cell embedded into backhand mechanism and depicted in (Fig. 64) as f_A (green dots).

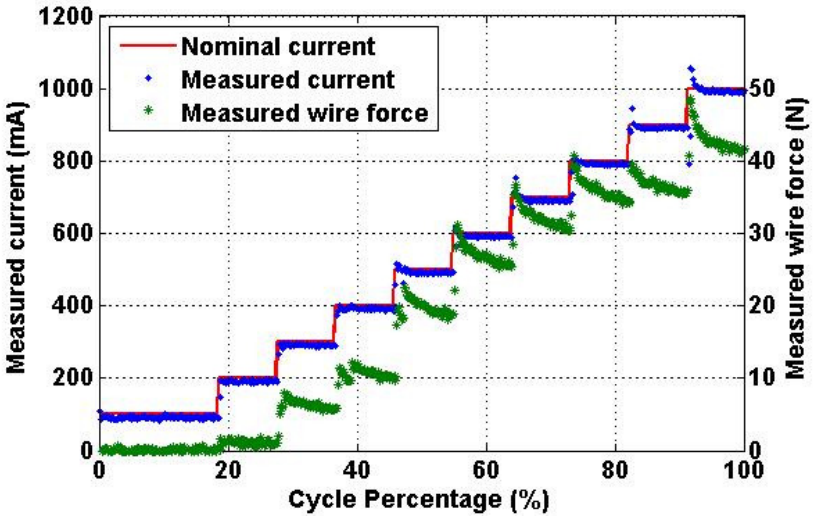

Fig. 68. Comparison between the nominal current of the motor (red line) and the measured one (blue dots) and the measurement of the consequent wire actuation force (green dots).

Obviously, there is a direct relationship between the supplied current and the measured tendon actuation force. However, for the lower current level, the servomotor does not generate enough torque to overcome friction and other non-idealities, resulting in almost no output wire tension. The previous kinetostatic model allows to predict the theoretical fingertip force $\boldsymbol{f}_{phal}$ and compare the results with the measured one. The latter $\boldsymbol{f}_{phal}$ was directly provided by the load cells (Fig. 63), whereas the theoretical behaviors were obtained by applying (5.52) to the measured wire force f_A. The comparison is shown in the following Fig. 69.

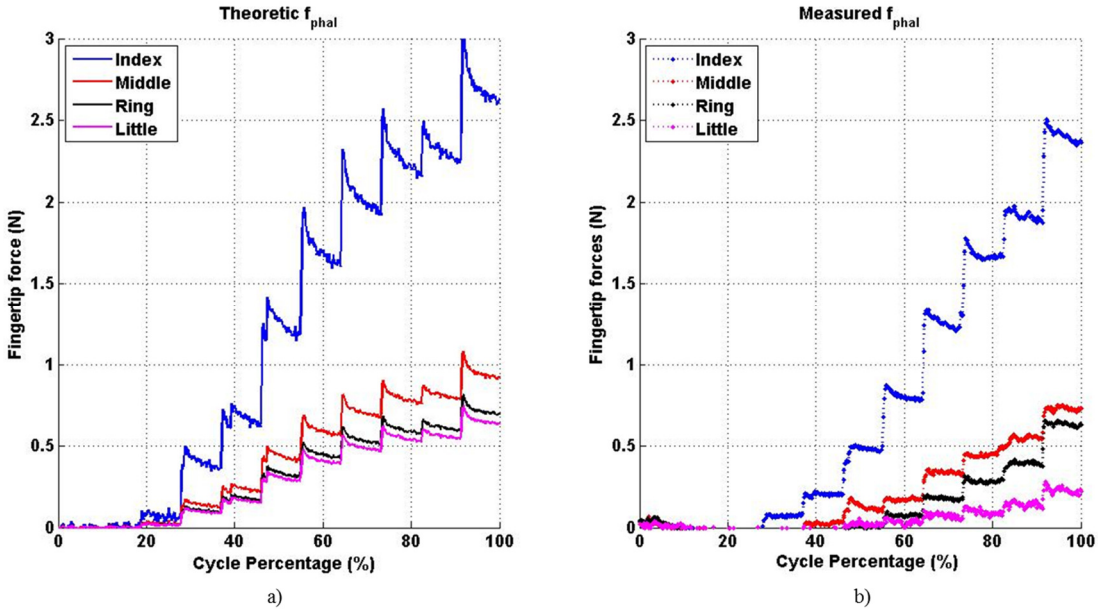

Fig. 69. The profiles of the theoretically predicted a) and experimentally measured b) fingertip forces

The measured forces are, as expected, lower than the theoretical values, due to friction effects and other non-idealities (tangential contact forces, moments and the non-ideality of tendons and knots under load and the unwanted motion between exoskeleton and human phalanges). Moreover, the measured forces did not exhibit the spiking behavior during step changes which is visible in the theoretical estimates. This could be due to the finite stiffness of the transmission system, acting partially as a low-pass filter.

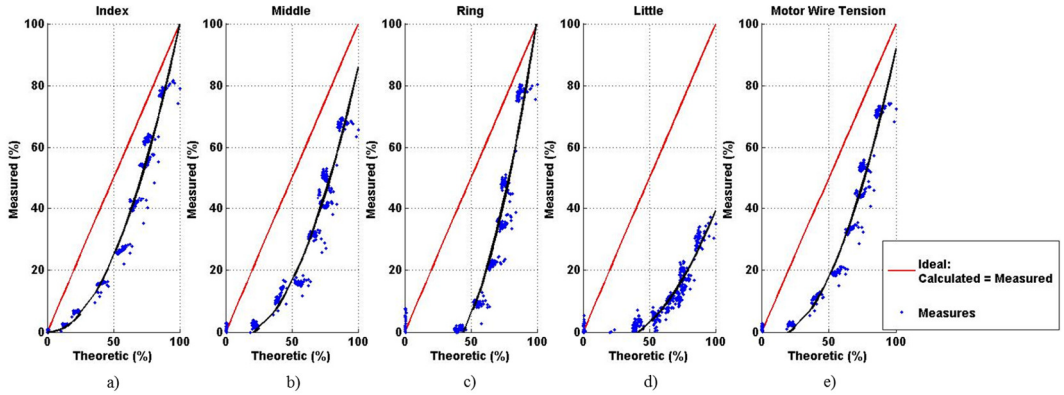

Fig. 70. Comparison between the measured (y axis) and the theoretical (x axis) fingertip forces and deviation between measured and calculated actuation wire force.

Fig. 70 a) to d) depict the measured fingertip force (y-axis) and the theoretical estimates (x axis) for each finger. The red line represents an ideal correspondence between the model and the reality, in which the theoretical and the measured forces are equal. The blue dots are the experimentally obtained data, interpolated to obtain the trend (black line). All four plots highlight a strong influence of un-modeled elements for low force values, while the measurements become more similar to the theoretical predictions when the actuation force increases. The non-idealities have different impact among fingers, due to the chosen inter-finger transmission. In fact, the serial configuration on the backhand module influences more the distal outputs, in particular from the figures it is possible notice that the forces measured on the index are more similar to the ideal ones (smallest total deviation), whereas the little finger exhibits the worst behavior.

Fig. 70 e) compares the measured actuation force f_A, with the calculated one, obtained from the measured fingertip forces $\boldsymbol{f}_{phal}$ by inverting the equation (5.52). As it is possible to notice, the deviation becomes lower as the actuation force increases due to the effect of non-idealities. Among the causes of such deviation there are friction, the non-ideal positioning and the unwanted motion of the exoskeleton on the finger phalanges. From the experimental tests, it is possible to evaluate the friction force around 12.10 N. This value is measured by means of the load cell embedded in the backhand module, when the motor is powered but the exoskeleton does not produce any forces on the test bench load cells. Other non-idealities consist in the sliding of the straps along the finger phalanges and in the rotation of the exoskeleton phalanges about

their contact points, generating a tangential component of force, which is difficult to model.

5.5 Some considerations about ReHand

ReHand is conceived starting from the knowledge acquired during the design and validation of an assistive exoskeleton for aerospace tasks, in particular to assist astronauts during the E.V.A. (Extra Vehicular Activities) missions. The skills have been then transferred to the rehabilitation sector and to assistance of impaired people during ADL (Activities of Daily Life). The performed tests have demonstrated the adaptability of the device to different hand sizes and various objects, which is essential in order to perform ADL. The ergonomy and wearability allow ReHand to be donned and doffed in less than 12 minutes and to be worn by the subjects for an hour, without causing pain or notable discomfort. Then, the mechanical validation investigated the efficacy of the device in transmitting adequate forces to the human phalanges in steady-state conditions. Given the kinetostatic model of the architecture, the experimental results showed that the ability of the system to transmit an assistive force from the actuator to the fingers is optimal for the index finger, while it decreases slightly for the middle and ring and more substantially for the little finger. Such behavior is due to the initial design choice of adopting a serial configuration (Fig. 46): as the little finger is the farthest element in the chain, it is the most prone to friction and other non-idealities. This is however acceptable considering the minor contribution of the little finger in grasping and pinching tasks (Hasser 1995). The presented system distributes the forces among the fingers imposing a human-like force synergy using an underactuated mechanism. Importantly, this resembles a contemporary model of human motor control, as presented in literature (D'Avella, Saltiel, and Bizzi 2003) In addition, ReHand can be controlled through the detection of the motion intention using the electromyography (EMG). This key point allows to simplify the user's interface. The implemented EMG control strategy, based on threshold control, consists in the use of two surface EMG (sEMG) sensors placed on the forearm (Fig. 71 a) into a mirrored configuration (Fig. 71 b) (Loconsole et al. 2013).

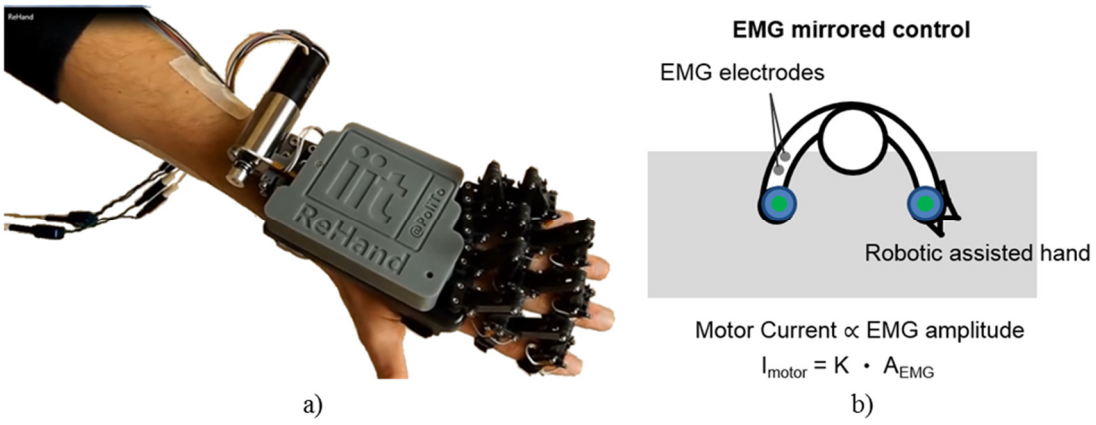

Fig. 71. Placement of the sEMG electrodes on the same forearm a), and a scheme of EMG mirrored control b), where the motor current is linear proportional to the EMG amplitude of the other forearm.

The particular placement of the electrodes on finger flexor and extensor muscles, avoids motor activation consequent to wrist muscles activation . In order to improve the rehabilitation features of ReHand, a series of medical doctors and physiotherapists have been interviewed about the exoskeleton. Generally, they have replied in enthusiastic way about the idea to merge two enabling technologies, as the functional rehabilitation (given by the underactuation) and the sEMG. On the contrary, they have highlighted some critical aspects such as the low wearability and ergonomy and most of all the absence of a controlled fingers' extension. Firstly, the exoskeleton should be donned and doffed from an impaired user in in less than 5 minutes without any help, so the wearability must be improved in order to have an efficient treatment without wasting time in the wearing phase. Secondly, comfort is another important aspect to consider when rehabilitation/assistive devices are designed. Above all, comfort is extremely important in assistive devices because the exoskeleton has to be worn for hours (up to an entire day), so the backhand frame must be modified in order to improve comfort. Thirdly, the last issue identified by the MDs concerns the passive elements to perform the fingers extension, the use of elastic elements to perform extension or flexion could induce muscles spasms, which would worsen the rehabilitation treatments. All those medical advices have been implemented in a new prototype, which is described in the next chapter. ReHand2 is the natural evolution of the previous exoskeleton, and it has been designed, realized and tested. In particular, ReHand2 implements some improvements in wearability and ergonomy, as well as some improvements in the wire tensioning and in the reduction of weight, but most of

all it introduces the idea and the concept of a wire-driven bidirectional underactuated mechanism.

Chapter 6 ReHand2: the evolution of the species

This chapter describes the evolution of the previously introduced ReHand, to the new version ReHand2, which is developed maintaining two cornerstones: the underactuation principle and the type of the finger structure. In addition, it presents interesting feature of a controlled bidirectional motion by tendon driven mechanism, maintaining a single actuator and dyneema wires. The chapter describes the general principles used in order to obtain the wanted bidirectional effect using a simple tendon driven strategy. The application of such principles is then described on inter- and intra-finger modules. In addition, the dynamic model of the structure concerning both intra- and inter-finger modules is described, and the chapter is concluded with the implementation of the Simulink model and the preliminary simulation results.

6.1 ReHand2: Description

ReHand2 (Fig. 72) is the evolution of the previous hand exoskeleton, maintaining most features such as the adaptability and the lightness, but overcoming the well-known limitations. ReHand2 proposes an innovative bidirectional tendon-driven underactuated inter-finger mechanism conceived for wearable robotics, but not limited to this field. The bidirectional four-finger exoskeleton, actuated through a single motor, is conceived, designed and realized. As ReHand, also ReHand2 maintains the capability to adapt itself to whatever grasping gesture, transmitting a predetermined

fraction of the actuation force to each finger. Also in this case, the mechanism can be considered as composed of two main parts:

- Backhand module;
- Finger module.

For the backhand module (or inter-finger), a predetermined number of differential elements (5.1) have been designed, in order to divide the single force input provided by the actuator into several outputs: three differential elements are used in order to power four fingers. Concerning the finger module, each finger assists the opening (extension) and the closing (flexion) of the two more proximal phalanges, and is composed of a pair of consecutive tendon-driven four-bar mechanisms.

Fig. 72. Proof of concept of a bidirectional tendon-driven underactuated hand exoskeleton, namely ReHand2

It is important keeping in mind that ReHand project was born with the aim to develop a portable rehabilitation device. As mentioned in the previously chapters, the traditional therapy is often carried out by manipulations. Fig. 73 shows a classical sequence of manipulation action performed by physiotherapists. Usually, the rehabilitation of a spastic hand requires to perform the extension of the fingers. As will be describe in the following, using a particular tendon's path for the fingers extension, it is possible obtain a sequence of actions equal to the traditional manipulation therapy.

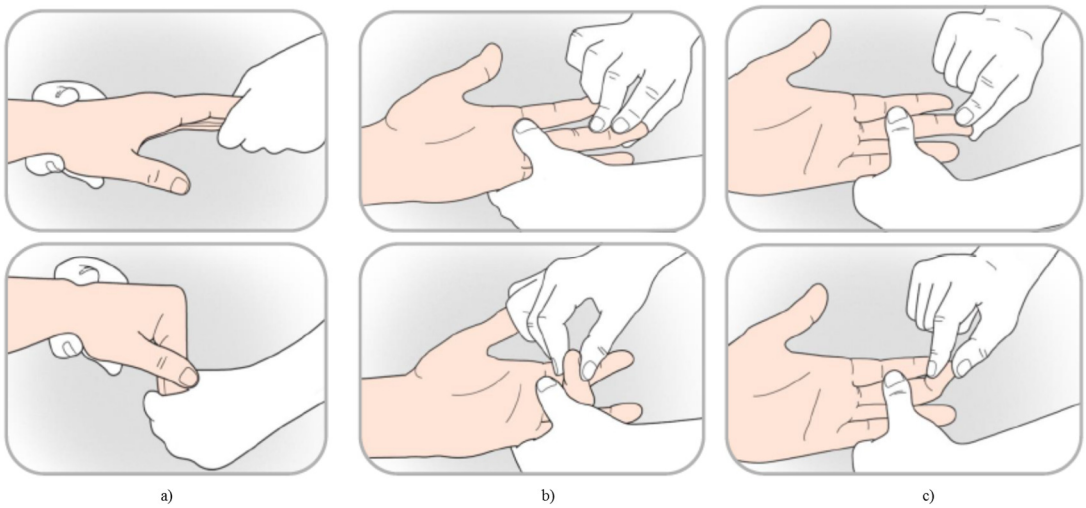

Fig. 73. Sequence of actions for the traditional manipulation therapy: a) MCP joint, b) PIP joint and c) DIP joint.

6.1.1 Tech specs

The table below (Tab. 14) shows the comparison between ReHand and ReHAnd2. Both of them have common properties and components as the DC servomotor, but as it can be seen, ReHand2 improves some fundamental aspects such as the active extension and better performance in terms of donning and doffing time.

From a rehabilitation point of view, the active flexion/extension is more safe compared springs, because in case of transmission failure, the user's hand is not subjects to unpredictable movements. The bidirectional mechanism, which will be describe in the following, permits to improve also the wearing time reducing the time of the setup phase: in fact, the use of a closed path of the wire avoids the boring issue of the wires slipping off the pulleys.

6.1 ReHand2: Description

Tab. 14. Comparison between the two versions of ReHand.

	ReHand	**ReHand2**
N° of actuated fingers	4	4
N° of active DOFs	8 ($MCP_{f/e}$ and $PIP_{f/e}$)	8 ($MCP_{f/e}$ and $PIP_{f/e}$)
N° of passive DOFs	4 ($MCP_{a/a}$)	4 ($MCP_{abd/add}$)
Fingers flexion	Tendon-driven	Tendon-driven
Fingers extension	Passive (elastic elements)	Tendon-driven
$MCP_{a/a}$	Not adaptable	Adaptable, with passive return in the rest position
Materials	ABS and steel	ABS, aluminum alloy and steel
Exoskeleton weight (without actuator)	452 g	304 g
Exoskeleton volume[6]	0.236 dm^3	0.238 dm^3
Average donning and doffing[7]	~12 minutes	~7 minute
Output power (@30000 rpm)	36 W	36 W
Motor weight	100 g	100 g
Gearbox	Faulhaber Planetary Gearhead Series 26/01 S	Faulhaber Planetary Gearhead Series 26/01 S
Reduction ratio	43:1	43:1
Gearbox weight	139 g	139 g
Control strategy	sEMG-driven	sEMG-driven

[6] Volume estimation performed by CAD software.
[7] The time considers also the setup phase and has been measured on 8 healthy subjects.

6.2 Inter-finger module

6.2.1 Design

The core of the ReHand2 mechanism is the inter-finger (or backhand) module. This module distributes the input action in four outputs, according with chosen geometry. Differently from the previously mechanism (section 5.1.1), this one embeds a second transmission in order to drive the outputs in both directions. This module comprises the sustaining platform, the actuator, and the underactuation module (with the differential elements). The platform is a frame where all components are attached. It is connected to the hand by means of two Velcro straps; its bottom is modelled in order to fit the anatomical hand surface and in addition, a soft and adaptable material, like rubber foam, can be inserted to give greater comfort to the user. The platform hosts the DC servomotor, which transmits the actuation input to the underactuation module by means of tendons, wounded on a pulley located on the motor shaft.

Starting from the concepts introduced in section (5.1.1) and from the need requirement of a mechanism that allows the finger flexion and extension using a single motor, a bidirectional mechanism has been conceived. The idea at the basis was the introduction of a second distinct tendon-driven transmission (Fig. 74).

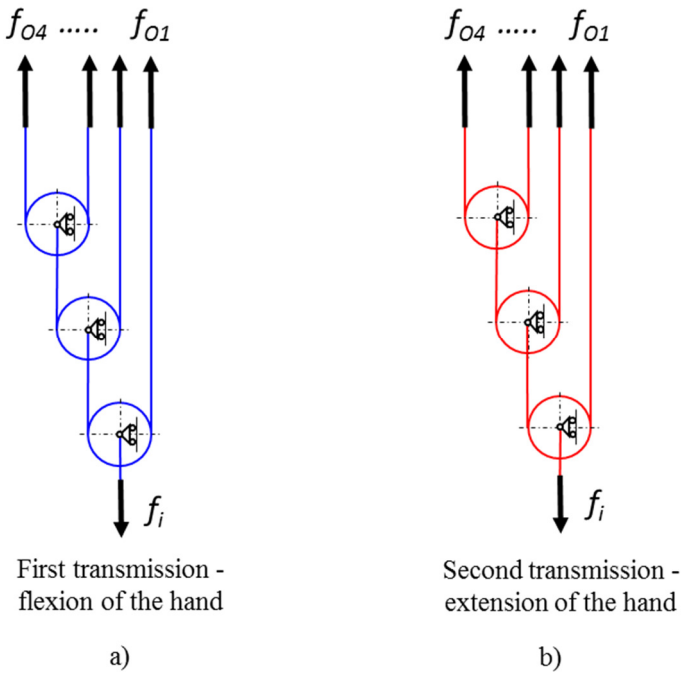

Fig. 74. Embedded phase zero: the inter-finger module has two separately transmission, a) flexion and b) extension of the fingers.

6.2 Inter-finger module

Introducing a second distinct transmission in the backhand module would causes an increase in weight and volume of the device and it would require a second actuator in order to drive the second chain, which is identical to the first one, in order to have the same action distribution in both movements. The solution as such would not be suitable for a hand exoskeleton because it violates the constraints presented in section 3.3. From Fig. 74 it is possible to notice some similarities, e.g. the direction of the actuating and output actions. Exploiting these similarities it is possible to joint the two transmissions and to use only one actuator, as depicted in the following scheme (Fig. 75)

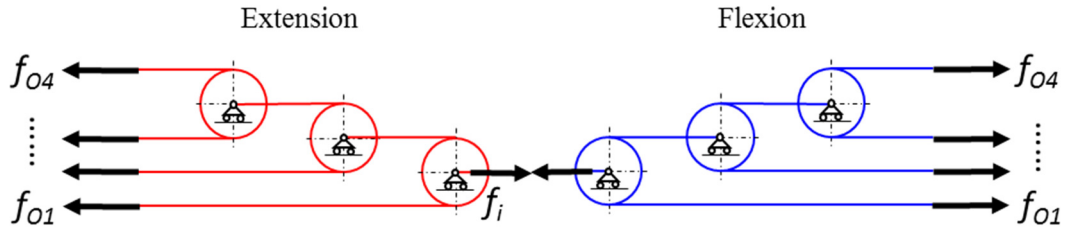

Fig. 75. Embedded phase one: the two transmission mechanisms share the same actuator.

Considering the different activation of the mechanisms during the motion or the grasp, it is possible not only to share the actuation but also to use the same differential elements. The scheme is reported in the following figure.

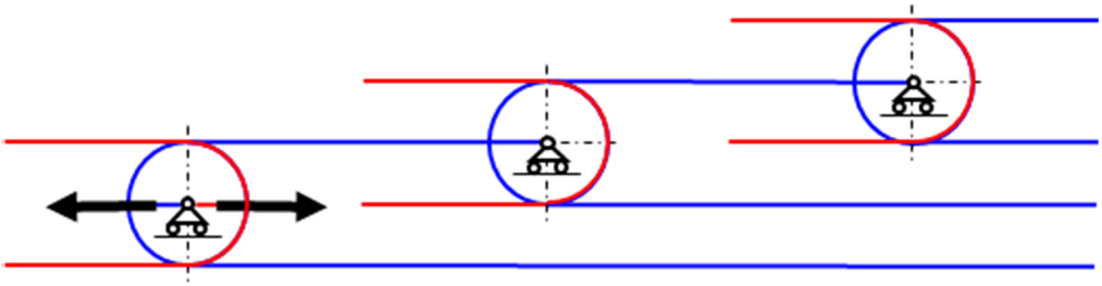

Fig. 76. Embedded phase two: the transmission mechanisms are integrated in one.

The integration of the two mechanisms requires the introduction of three idle pulleys for each differential element. The final scheme is shown in the figure below (Fig. 77)

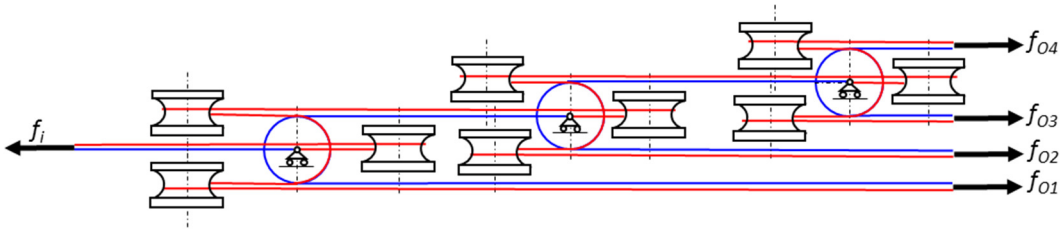

Fig. 77. Final integration phase: the single transmission mechanism allows the bidirectional movement of the fingers.

In conclusion, applying this concept to ReHand allows to obtain a self-adaptable underactuated bidirectional device. In the case of ReHand2, a serial configuration at the inter-finger level has been adopted; but different configurations are also possible without affecting the validity of the current reasoning. Fig. 78 shows the real path of the tendons: continuous lines are represent the paths concerning the fingers' flexion; instead, the dashed lines show the tendon routings regarding the fingers' extension.

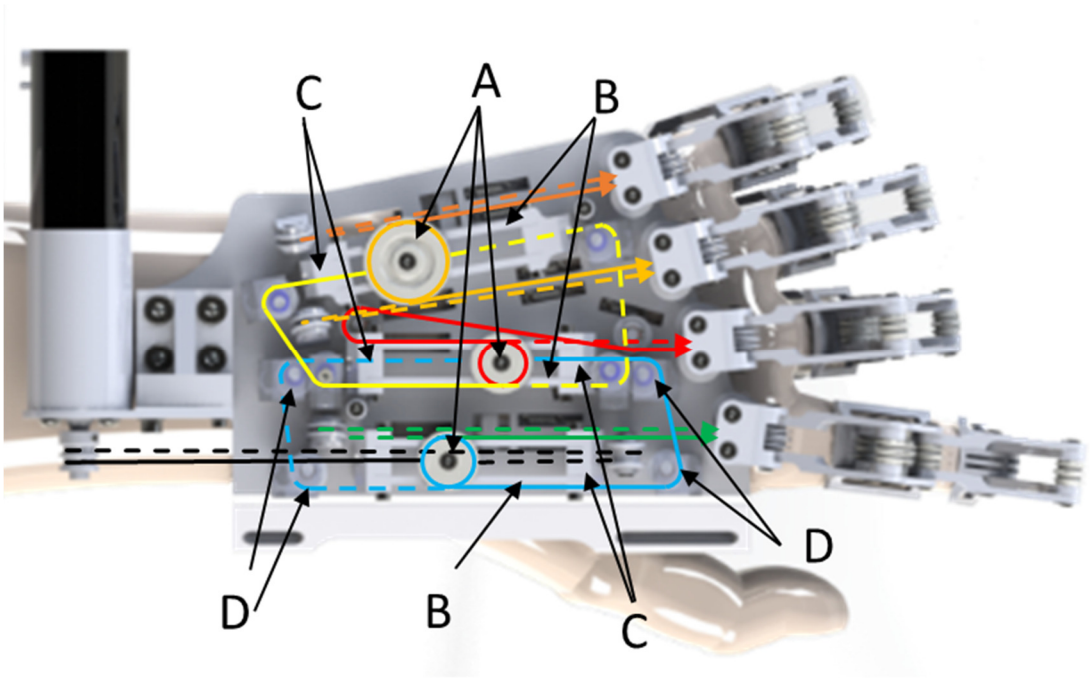

Fig. 78. Rendering of the inter-finger module with the wire paths, with continuous line are represented the tendons path for the flexion of the fingers, while dashed lines design the extension.

From Fig. 78 it is possible to notice the location of the differential elements (A) with their guides (B) and supports (C). Each differential element is composed by two pulleys made integral together and rotating with a coaxial shaft. This part (composed of pulleys and shaft) is connected to the slider by means of a bushing element. The

slider is then pulled at its extremities by the wires. It also is possible to notice the position of the idle pulleys (D), with their different structures. Each of them embeds bushings in order to limit the rotation friction. Concerning the pulleys dimension, the radii are chosen in order to obtain a force distribution which imitates the one of a cylindrical power grasp, in particular, the transmission matrix is reported in (5.3):

$$[\boldsymbol{S}]_{\boldsymbol{hand}} = \begin{bmatrix} 0.50 \\ 0.25 \\ 0.125 \\ 0.125 \end{bmatrix} \tag{6.1}$$

The proposed force distribution allows to simplify the last differential element. In fact, in this case the last pulley has a single radius, in order to simplify the construction of the element, which is already complex by the presence of the second tendons routing.

6.2.2 Kinematical and dynamical analysis

In this section the dynamical analysis of the inter-finger module is described, starting from the analysis of a generic movable pulley. As shown in Fig. 78, the inter-finger module is mainly composited by three differential elements in a serial configuration. From a kinematic analysis, as in (Rossi and Savino 2014), it is possible to written the following relations for a generic single movable pulley, depicted in the scheme below (Fig. 79), which shows a generic single movable pulley.

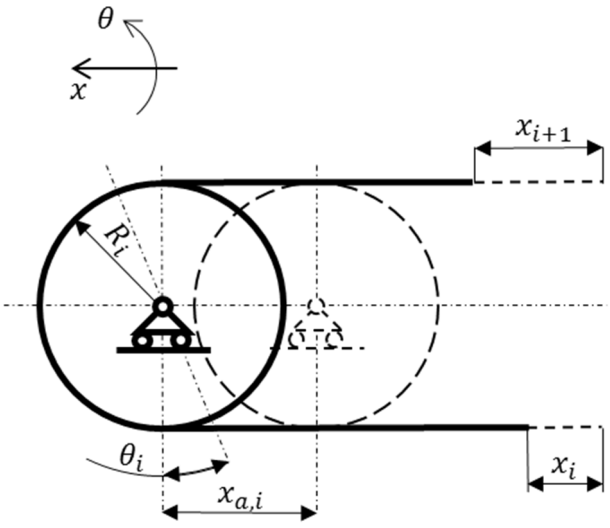

Fig. 79. Movable pulley.

Where: $x_{a,i}$ is the displacement of actuation slider, x_i and x_{i+1} is the tendons displacement, R_i is the constant radius of the pulley and θ_i is the pulley rotation.

$$x_i = x_{a,i} - \theta_i \cdot R_i \tag{6.2}$$

$$x_{i+1} = x_{a,i} + \theta_i \cdot R_i \tag{6.3}$$

$$\theta_i = \frac{x_{i+1} - x_i}{2 \cdot R_i} \tag{6.4}$$

$$x_{a,i} = \frac{x_i + x_{i+1}}{R_i} \tag{6.5}$$

The previous relations show that if the two displacements x_i and x_{i+1} are equal, the pulley does not rotate ($\theta_i = 0$), while, if they are different, the pulley rotates ($\theta_i \neq 0$) to a suitable angle in order to ensure the desired configuration of the fingers or more generally of the utilities. Obviously, differentiating the equations (6.2), (6.3), (6.4) and (6.5) in time once and twice, it is possible to obtain the velocity and the acceleration relationships, respectively:

$$\dot{x}_i = \dot{x}_{a,i} - \dot{\theta}_i \cdot R_i \tag{6.6}$$

$$\dot{x}_{i+1} = \dot{x}_{a,i} + \dot{\theta}_i \cdot R_i \tag{6.7}$$

$$\dot{\theta}_i = \frac{\dot{x}_{i+1} - \dot{x}_i}{2 \cdot R_i} \tag{6.8}$$

$$\dot{x}_{a,i} = \frac{\dot{x}_i + \dot{x}_{i+1}}{R_i} \tag{6.9}$$

$$\ddot{x}_i = \ddot{x}_{a,i} - \ddot{\theta}_i \cdot R_i \tag{6.10}$$

$$\ddot{x}_{i+1} = \ddot{x}_{a,i} + \ddot{\theta}_i \cdot R_i \tag{6.11}$$

$$\ddot{\theta}_i = \frac{\ddot{x}_{i+1} - \ddot{x}_i}{2 \cdot R_i} \tag{6.12}$$

$$\ddot{x}_{a,i} = \frac{\ddot{x}_i + \ddot{x}_{i+1}}{R_i} \tag{6.13}$$

In the previous chapter the statical analysis of several differential elements was presented. In this section a dynamical model for the movable pulley is described and written in order to perform the dynamical analysis of the whole inter-finger module as well as the finger module. Fig. 80 shows the notation and the dynamical actions on the

differential element. In the model also the presence of sliding and pin joint frictions is considered.

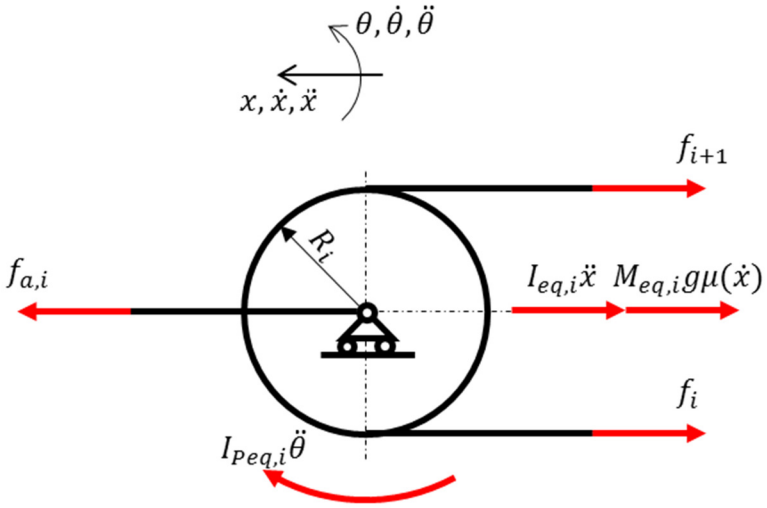

Fig. 80. Dynamical actions on the movable pulley.

Where: $f_{a,i}$ is the actuation force, f_i and f_{i+1} are the output forces, $I_{eq,i}$ is the equivalent inertia of the translational bodies, $M_{eq,i}$ is the equivalent mass of the translational bodies, g is the gravity acceleration, $\mu(\dot{x})$ is the coefficient of sliding friction modelled as function of the translational velocity and ρ is the coefficient of the pin joint friction. Finally, $I_{Peq,i}$ is the equivalent inertia of the rotating bodies (pulleys and bushings). Fig. 80 allows to write the following dynamical equilibrium on translation and rotation:

$$f_{a,i} - f_i - f_{i+1} - I_{eq,i}\ddot{x} - M_{eq,i}g\mu(\dot{x}) = 0 \tag{6.14}$$

$$f_i \cdot \left(R_i - sign(\dot{\theta}_i) \cdot \rho\right) - f_{i+1} \cdot \left(R_i + sign(\dot{\theta}_i) \cdot \rho\right) - I_{Peq,i} \cdot \ddot{\theta}_i = 0 \tag{6.15}$$

Concerning the coefficient of translational friction $\mu(\dot{x})$ it is modeled as a function of relative velocity and it is assumed to be the sum of Stribeck, Coulomb and viscous dissipation as reported in the equation (6.16):

$$\mu(\dot{x}) = (\mu_C + (\mu_{brk} - \mu_C)e^{-(c_v|\dot{x}_{a,i}|)} + \mu_v\dot{x}_{a,i} \tag{6.16}$$

Where: μ_C is the coefficient of Coulomb friction, μ_{brk} is the breakaway coefficient, c_v is a coefficient of the transition between the static and the Coulombus friction and

$\mu_v$is the viscous friction coefficient (neglected in the next study). The approximation on the friction model is too idealistic, but a more complex friction model derogate from the intended purposes.

Considering the backhand configuration (Fig. 78), it is easy to generate the mathematical model of the complete inter-finger mechanism. In particular, repeating three times the differential element calculation cell, is possible to create the mathematical model of the entire system. In the argumentation of the model, ideal behavior of the tendons and idle pulleys is assumed.

6.2.3 Simulink implementation

The previously introduced model has been implemented in Simulink environment, in order to simulate the inter-finger mechanism action. In the following Fig. 81 the entire backhand module is reported.

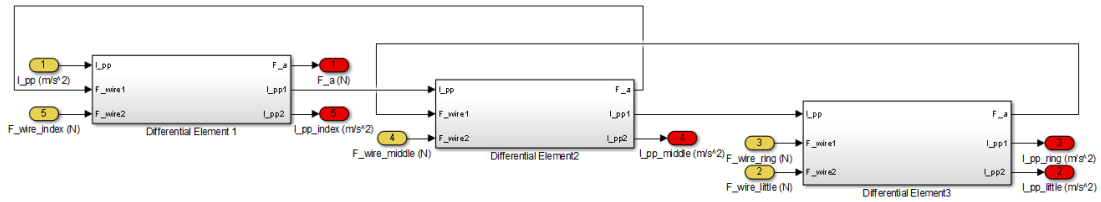

Fig. 81. Simulink model of the inter-finger (or backhand) module, with yellow background are indicated the input actions; instead, the red ones are the outputs.

It is possible to notice in the figure above, that the backhand module consists in the succession of three differential elements, and as mentioned above, that the idle pulleys are neglected. The input values are indicated in Fig. 81 with yellow background and they are respectively, the kinematic action coming from the actuator (input 1), the and the reaction forces coming from the fingers (input from 2 to 5). Concerning the outputs (red background) they represent, respectively, the kinematic action sent to the finger (output from 2 to 5) and the actuation force (output 1), which is sent to the actuator model. In Fig. 82 the details of the implementation in Simulink of the differential element are shown:

6.2 Inter-finger module

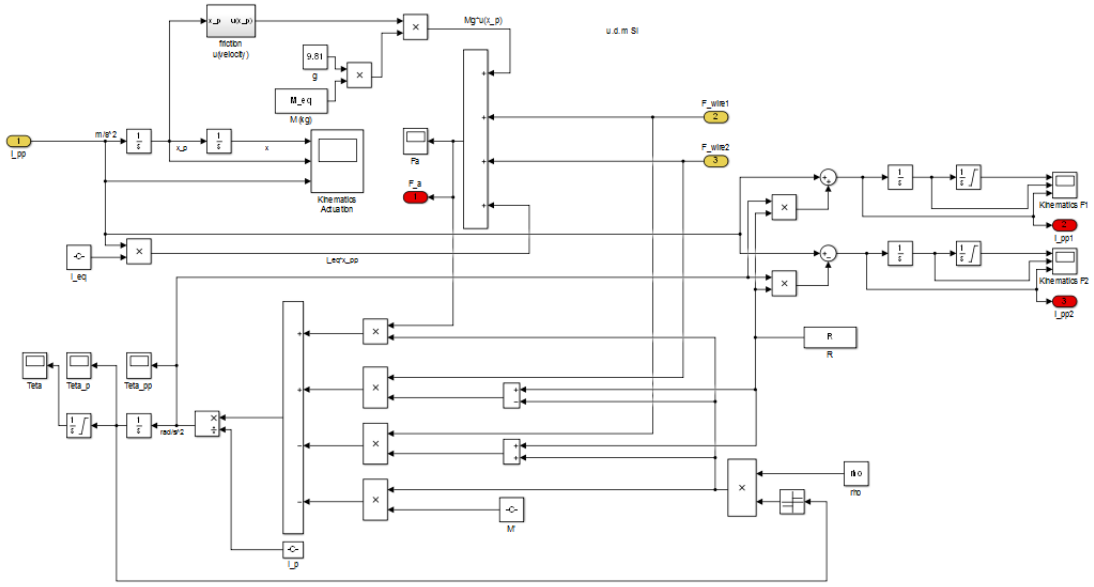

Fig. 82. Implementation of the differential element in Simulink, the input are represented with yellow background, in contrast the outputs are indicated with the red background.

From Fig. 82 is possible to notice that the movable pulley receives as inputs, the kinematic output coming from the actuator or from one of the outputs of the previous element (input 1) and the forces acting on the tendons coming from the fingers and/or the following pulley (input 2 and 3). The outputs of the module are instead represented by the linear acceleration of the output wires (output 2 and 3) sent to the following modules (fingers and/or following pulley) and the actuating force (output 1), sent to the actuator of the previous differential element. Another important aspect regards the saturation of the integrator in order to consider the physical limitation imposed by the mechanical stops. In the upper left corner it is also possible to notice, the presence of the friction model, implemented as in (6.16). In the following figure the scheme is shown:

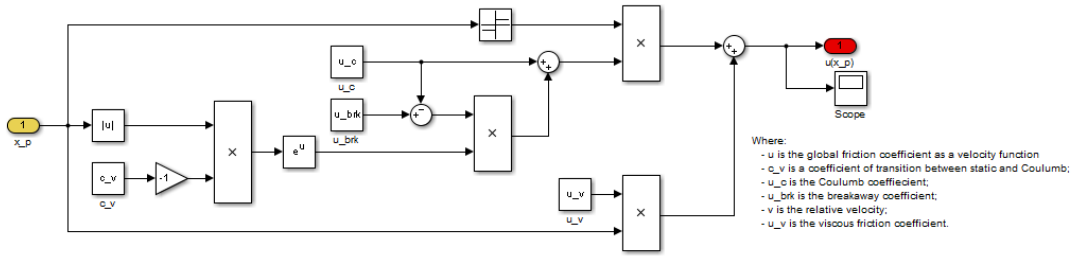

Fig. 83. Friction model implemented in Simulink, in yellow is indicated the velocity input, instead, in red the output represented by the friction coefficient.

Both scheme (Fig. 82 and Fig. 83) are implemented using Simulink blocks, instead of *Matlab function blocks* in order limit the computational cost, already expensive due to the interpretation of the *Matlab* function implemented for the fingers' dynamics.

6.3 Intra-finger module

6.3.1 Design

Concerning the finger module, the architecture is already explained in the previous chapter (section 5.1.2) as well as the synthesis and the optimization (section 5.1.3). In fact, the links' lengths are the same of the previous demonstrator ReHand device. The choice of maintaining the four bar structure is due to its simplicity, lightness and adaptability to be worn by hands of different sizes. Also in this case the MCP (metacarpophalangeal) and PIP (proximal interphalangeal) joints are actuated, but in contrast with the previously prototype both joints are assisted in both flexion and extension. The Tokyo hand structure, previous described in the state of the art (Yamaura et al. 2009), inspires the finger module and the actuation.

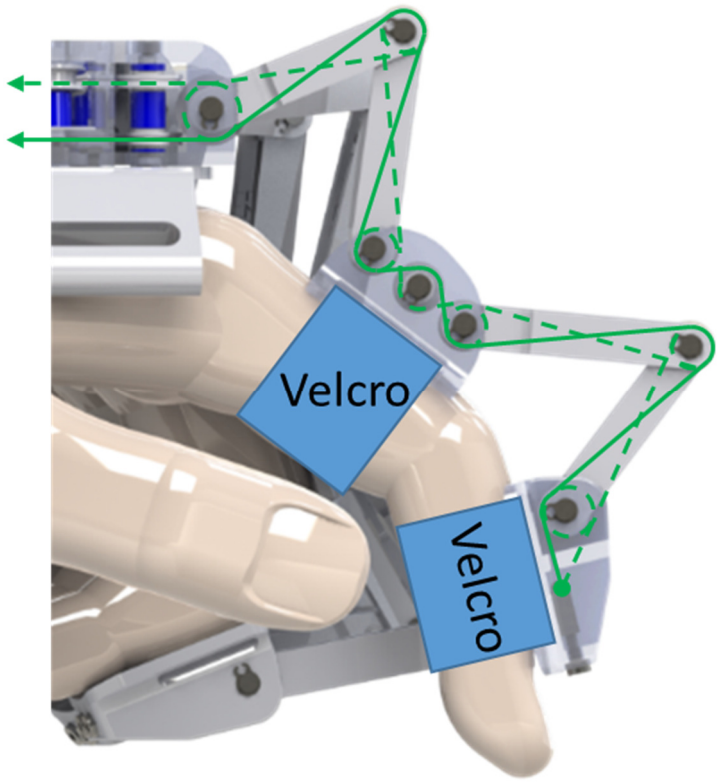

Fig. 84. Rendering of the middle finger mechanism, with continues line is represented the tendon routing for the flexion motion, while the dashed green line shows the routing for the extension.

6.3 Intra-finger module

By pulling the flexion cable (continuous green line in Fig. 84), the finger closes and the extension wire (dashed green line) is released. In the opposite way, when the dashed blue line is pulling, the finger opens and the continuous tendon is released to allow the movement. Both tendon paths are shown in Fig. 84. The each mechanical joint integrates the two different pulleys, in order to allow the different wires' motion. The pulleys embed also two bushings to reduce the friction on the shaft. At the end, the tendons are fixed to the more distal phalange by means of tensioners, which allow small regulation on the wires and the wires' pre-load. The pre-load is very important in order to have synchronous movements of the fingers and phalanges. In fact, an incorrect pre-load of the wires causes an undesired delay among the fingers, risking not to complete the finger motion. The finger exoskeleton allows also the passive abduction/adduction of the MCP joint. In particular, the $MCP_{a/a}$ mechanism allows the adaptation when an external load is exerted, and returns to the rest condition when the external action is over. The abduction/adduction mechanism is shown in Fig. 85 and Fig. 86. The direction of the input tendons on the finger can vary with respect to the finger, due to abd/add rotation. In order to maintain the tendons always near to the abd/add axis and to maintain them coplanar to the finger flexion/extension pulleys, two different-radius pulleys with vertical axis have been inserted. They can rotate about themselves, while their vertical axes are linked to phalange 0. In order to improve the adaptability of the hand exoskeleton during grasping phase, a mechanism with passive springs is introduced for each finger. Examined from the bottom view (Fig. 86), the abd/add mechanism consists in a pulley, linked to the body phalange 0, and two antagonistic springs linked to each other by wires (red line in figures). The mechanism has the aim to allow the adaptation of the finger at the abd/add joint during a grasp, driving the return to the rest position by means of the elastic elements. When the abd/add joint rotates, the springs change their length. In particular, one extends and the other decreases its length, generating a return torque towards the rest position.

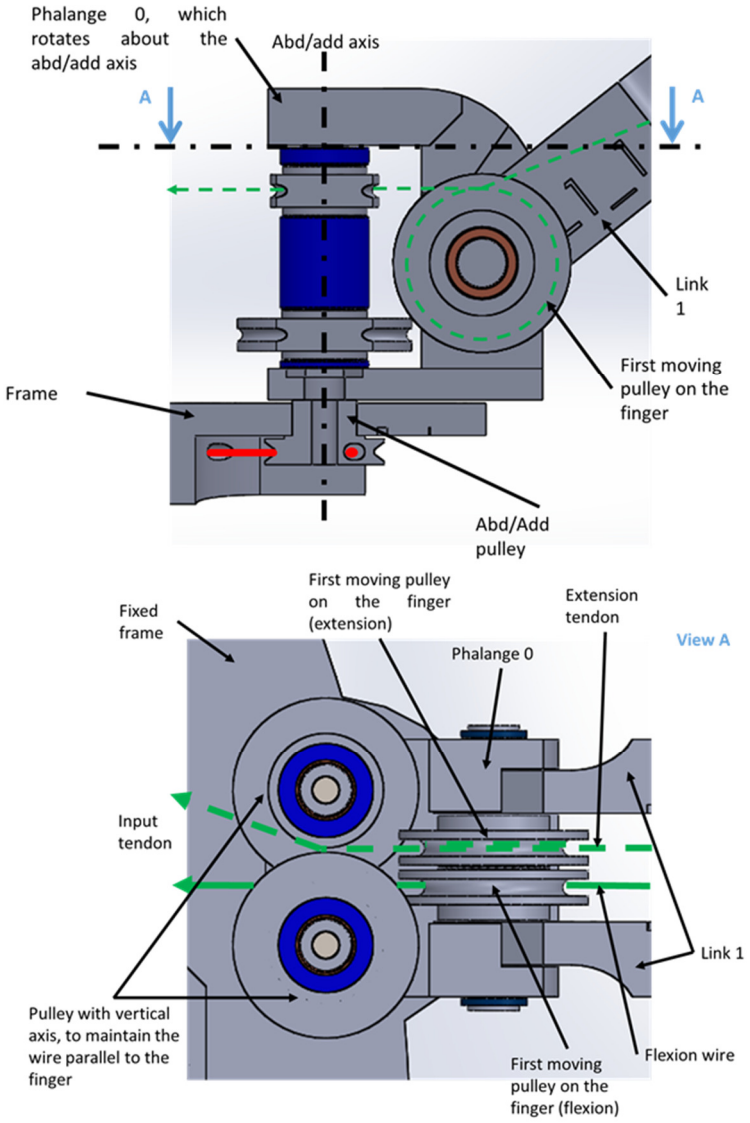

Fig. 85. MCP abduction/adduction mechanism, phalange 0 view.

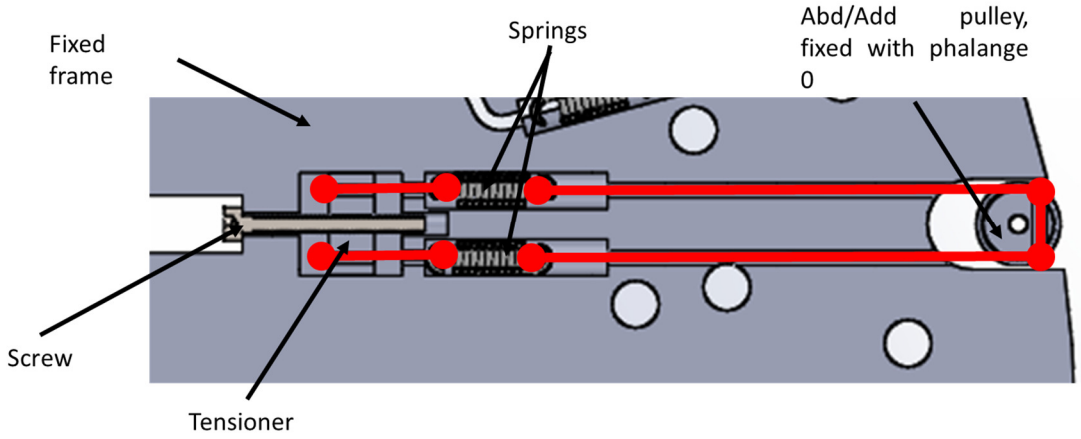

Fig. 86. Section of the MCP abd/add mechanism, the red lines represent the wires connected with the elastic elements.

6.3.2 Dynamical analysis

The kinematical analysis of a generic four bar mechanism, which can be implemented for the entire finger exoskeleton system, is described in the previous chapter (5.2). In this section, the dynamical model of a finger exoskeleton based on the Lagrange approach is presented, briefly explaining steps performed in order to obtain the dynamic equation of the $i-th$ finger exoskeleton system. Several simplifications are adopted for the dynamic system: with respect to the finger kinematics, the metacarpus is considered fixed. Moreover, the following are neglected: the $MCP_{a/a}$ articulation the weight properties of the external links (Appendix 1), the friction, the viscosity and the dissipative terms of the human muscles. Based on the convention shown in FIG.87, the dynamical model is obtained; the reference frame is deployed in the MCP joint ($\mathcal{R}_1$) and all the equations are written with respect to it. In the following, the i subscript is omitted for brevity.

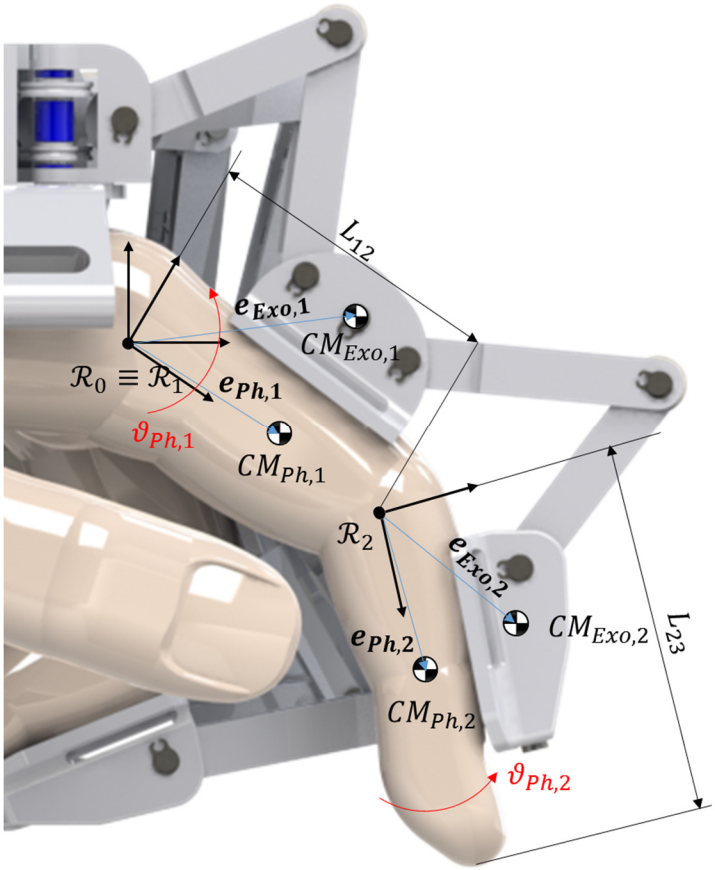

Fig. 87. Generic finger with the used notation for the dynamic analysis.

The Euler-Lagrange approach requires the calculation of the energies of the elements that form the analyzed structure. In the following, the kinetics and potential energies are obtained. Kinematic energy is obtained starting from the position vector of the center of mass of each phalange with respect to the base reference frame. The coordinates of the $j-th$ center of mass (CM) with respect to the $j-th$ reference frame $\mathcal{R}_j$ are:

$$\boldsymbol{e_{fing,j}} = [e_{jx} \quad e_{jy}]^T \tag{6.17}$$

$$\boldsymbol{e_{exo,j}} = [e_{exo,jx} \quad e_{exo,jy}]^T \tag{6.18}$$

The mass of the $j-th$ body is defined as m_j and the respective moment of inertia calculate about $z-axis$ of the $\mathcal{R}_j$ is namely I_j. The generic position vector of the generic $j-th$ CM with the reference frame $\mathcal{R}_0$ is:

$$\boldsymbol{c_{fing,j}} = \begin{bmatrix} e_{jx}\, cos(q_j + q_{j-1}) - e_{jy} sin(q_j + q_{j-1}) \\ e_{jx}\, sin(q_j + q_{j-1}) + e_{jy}\, cos(q_j + q_{j-1}) \end{bmatrix} + \begin{bmatrix} cos(q_{j-1}) \\ sin(q_{j-1}) \end{bmatrix} L_{j-1,j} \tag{6.19}$$

$$\boldsymbol{c_{exo,j}} = \begin{bmatrix} e_{exo,jx}\, cos(q_j + q_{j-1}) - e_{exo,jy} sin(q_j + q_{j-1}) \\ e_{exo,jx}\, sin(q_j + q_{j-1}) + e_{exo,jy}\, cos(q_j + q_{j-1}) \end{bmatrix} + \begin{bmatrix} cos(q_{j-1}) \\ sin(q_{j-1}) \end{bmatrix} L_{j-1,j} \tag{6.20}$$

Where, according to Fig. 87, $L_{01} = 0$ and the angular coordinates are changing as follow:

$$q_0 = 0\ ;\ q_1 = \vartheta_{Ph,1}\ ;\ q_2 = \vartheta_{Ph,2} \tag{6.21}$$

Differentiating the position vector (6.19) and (6.20), the velocity of the $j-th$ CM can be written as:

$$\boldsymbol{v_{fing,j}} = (\dot{q}_j + \dot{q}_{j-1}) \begin{bmatrix} -e_{jx}\, sin(q_j + q_{j-1}) - e_{jy} cos(q_j + q_{j-1}) \\ e_{jx}\, cos(q_j + q_{j-1}) - e_{jy}\, sin(q_j + q_{j-1}) \end{bmatrix} + \begin{bmatrix} -sin(q_{j-1}) \\ cos(q_{j-1}) \end{bmatrix} \dot{q}_{j-1} L_{j-1,j} \tag{6.22}$$

$$\boldsymbol{v_{exo,j}} = (\dot{q}_j + \dot{q}_{j-1})\begin{bmatrix} -e_{exo,jx}\, sin(q_j + q_{j-1}) - e_{exo,jy} cos(q_j + q_{j-1}) \\ e_{exo,jx}\, cos(q_j + q_{j-1}) - e_{exo,jy}\, sin(q_j + q_{j-1}) \end{bmatrix} + \begin{bmatrix} -sin(q_{j-1}) \\ cos(q_{j-1}) \end{bmatrix} \dot{q}_{j-1} L_{j-1,j} \tag{6.23}$$

Finally, the total kinetic energy of the system can be calculated as:

$$T = \frac{1}{2}\sum_{j=1}^{2}\left[\left(m_{fing,j}\left\|\boldsymbol{v_{fing,j}}\right\|^2 + m_{exo,j}\left\|\boldsymbol{v_{exo,j}}\right\|^2 + \left(I_{fing,j} + I_{exo,j}\right)\left(\dot{q}_j + \dot{q}_{j-1}\right)^2\right)\right] \tag{6.24}$$

The potential energy can be calculated as the sum of the gravitational potential energy and the elastic potential energy. The gravitational potential energy can be calculated starting from the knowledge of the mass properties of the considered body and the CM position respect to $\mathcal{R}_1$ arbitrary position. Concerning the elastic potential energy, it is possible to define an average value for the joints stiffness k_j, starting from Milner and Franklin's work (Milner and Franklin 1998). Defining $\boldsymbol{g}$ as the vector acceleration of gravity, the potential energy can be expressed as follows:

$$U = \sum_{j=1}^{2}\left[\left(-m_{fing,j}\boldsymbol{g^T}\cdot\boldsymbol{c_{fing,j}}\right) + \left(-m_{exo,j}\boldsymbol{g^T}\cdot\boldsymbol{c_{exo,j}}\right) + \frac{1}{2}k_j\left(q_j - q_{j-1}\right)\right] \tag{6.25}$$

The Lagrangian function can be easily expressed as:

$$\mathcal{L} = T - U \tag{6.26}$$

In order to consider the non-conservative contribution caused by the muscles viscosity, a Rayleight dissipation function is used:

$$R = \sum_{j=1}^{2}\frac{1}{2}\beta_j\left(\dot{q}_j - \dot{q}_{j-1}\right) \tag{6.27}$$

Where $\beta_j$is the damping constant, which models the non–conservative contribution of the human muscles and $\dot{q}_0 = 0$. It is also necessary to keep in mind that the non-conservative forces contribute less than the 10 % of the total force. Considering, the two generalized coordinates q_j, the Euler-Lagrange equations can be expressed as follows:

$$\frac{d}{dt}\left(\frac{\partial \mathcal{L}}{\partial \dot{q}_j}\right) - \frac{\partial \mathcal{L}}{\partial q_j} + \frac{\partial R}{\partial \dot{q}_j} = \tau_j \; ; \;\; j = 1{,}2 \qquad (6.28)$$

The term τ_j collects all the external actions applied on the $j - th$ phalange system. In particular, τ_j can be expressed as:

$$\tau_j = \tau_{m,j} + \tau_{exo,j} + \{[J(\boldsymbol{q})]^T \cdot \boldsymbol{f}_{ext}\}_j \qquad (6.29)$$

Where, $\tau_{m,j}$ is the action applied by muscles, $\tau_{exo,j}$ is the action exerted by the exoskeleton and finally $\{[J(\boldsymbol{q})]^T \cdot \boldsymbol{f}_{ext}\}_j$ is the $j - th$ force produced by the contact force applied on the $j - th$ phalange to the point defined by the Jacobian matrix $[J(\boldsymbol{q})]$ (proposed by (Laliberté, Birglen, and Gosselin 2003)). According to the virtual work principle, the equation to calculate the action $\boldsymbol{\tau}_{exo}$ can be expressed as follows (Tsai 1995) and (Tsai):

$$\delta W = F_{wire}\delta l_{wire} + \boldsymbol{\tau}_{exo}{}^T \cdot \delta \boldsymbol{q} = 0 \qquad (6.30)$$

Where F_{wire} is the actuation force acting on the wire (or tendon), δl_{wire} is the infinitesimal variation of the wire length, $\boldsymbol{\tau}_{exo}$ is a column vector of dimension (2×1) and $\delta \boldsymbol{q}$ is the infinitesimal variation of the generalized coordinates. The relation between the infinitesimal variation of length and generalized coordinates is expressed by:

$$\delta l_{wire} = [A(\boldsymbol{q})]\delta \boldsymbol{q} \qquad (6.31)$$

Where $[A(\boldsymbol{q})]$ is a (1×2) matrix, which can be calculated as follows for $j = 1$:

$$[A(\boldsymbol{q})] =$$

$$= \begin{bmatrix} R_{j_1} & R_{j_2} & R_{j_3} & R_{j+1_1} & R_{j+1_2} & R_{j+1_3} \end{bmatrix} \cdot \begin{bmatrix} 1 & 0 & & \\ 1 & -1 & [0]_{3x2} & \\ t_j & -1 & & \\ & & 1 & 0 \\ [0]_{3x2} & & 1 & -1 \\ & & t_{j+1} & -1 \end{bmatrix}$$

$$\cdot \begin{bmatrix} p_{j_1} sin(\varphi_{j_1}) & p_{j_2} sin(\varphi_{j_2}) & [0]_{2x2} & \\ -p_{j_1} cos(\varphi_{j_1}) & -p_{j_2} cos(\varphi_{j_2}) & & \\ [0]_{2x2} & & p_{j+1_1} sin(\varphi_{j+1_1}) & p_{j+1_2} sin(\varphi_{j+1_2}) \\ & & -p_{j+1_1} cos(\varphi_{j+1_1}) & -p_{j+1_2} cos(\varphi_{j+1_2}) \end{bmatrix}^{-1} \quad (6.32)$$

$$\cdot \begin{bmatrix} p_{j_3} sin(\varphi_{j_3}) & [0]_{2x1} \\ -p_{j_3} cos(\varphi_{j_3}) & \\ [0]_{2x1} & p_{j+1_3} sin(\varphi_{j+1_3}) \\ & -p_{j+1_3} cos(\varphi_{j+1_3}) \end{bmatrix}$$

The terms of the vector $\boldsymbol{q}$ are nestled in all the angles φ as shown in the kinematical model (5.1.2). The terms t_j and t_{j+1} can be expressed as follows:

$$t_k = \frac{p_{k_1} \sin(\varphi_{k_2} - \varphi_{k_1})}{p_{k_3} \sin(\varphi_{k_2} - \varphi_{k_3})}; \; k = 1,2 \quad (6.33)$$

Substituting the equation (6.31) in (6.30), it is possible to calculate the exoskeleton's action on the finger's joints as follows:

$$\boldsymbol{\tau}_{exo} = -[A(\boldsymbol{q})]^T \cdot F_{wire} \quad (6.34)$$

In Appendix 2, it is demonstrated that $[A(\boldsymbol{q})]$ matrix, calculated for the flexion path, is related to $[A(\boldsymbol{q})]_{ext}$, calculated on the extension routing, by this relationship:

$$[A(\boldsymbol{q})]_{ext} = -[A(\boldsymbol{q})]_{flex} \quad (6.35)$$

The Jacobian matrix, can be written according to the reasoning proposed by (Laliberté, Birglen, and Gosselin 2003) as follows for $j = 1$:

$$[J(\boldsymbol{q})] = \begin{bmatrix} d_j & 0 \\ d_{j+1} + L_{j-1,j}(cosq_{j+1} + \mu_{j+1} sinq_{j+1}) & d_{j+1} \end{bmatrix} \quad (6.36)$$

Where the μ_k is the friction coefficient of contact, while the values d_k and l_k are depicted in the next figure (Fig. 88).

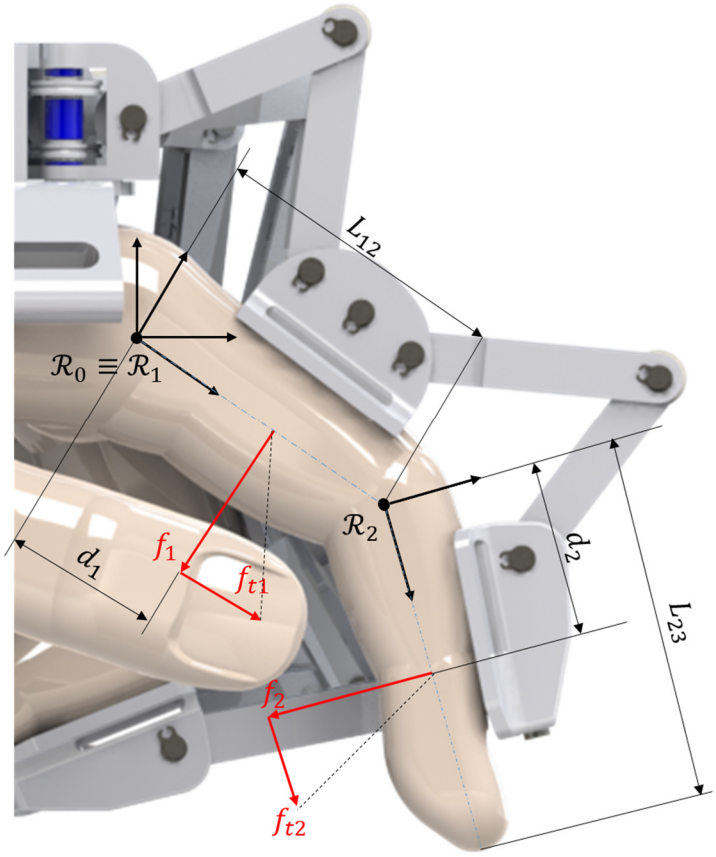

Fig. 88. Indication of the values appeared in equation (6.36)

Finally, neglecting the dissipation function and the finger stiffness, which are less than the 10 % of the total ammount, the dynamical finger exoskeleton model can be expressed in the following matrix form:

$$\begin{bmatrix} H_{11} & H_{12} \\ H_{21} & H_{22} \end{bmatrix} \cdot \ddot{\boldsymbol{q}} + \begin{bmatrix} C_{11} & C_{12} \\ C_{21} & C_{22} \end{bmatrix} \cdot \dot{\boldsymbol{q}} + \begin{bmatrix} G_{11}(\boldsymbol{q}) \\ G_{21}(\boldsymbol{q}) \end{bmatrix} = -[A(\boldsymbol{q})]^T \cdot F_{wire} + \boldsymbol{\tau}_m + [J(\boldsymbol{q})]^T \cdot \boldsymbol{f}_{ext} \tag{6.37}$$

For brevity, the calculation of the matrix elements is reported in Appendix 3. In order to accord with the outputs of the differential elements, the finger model has to be modified including the kinematics input. Considering the relation between the wire and the physiological velocity it is possible to write the following expression:

$$\dot{q}_2 = \frac{1}{A_{12}}\dot{l} - \frac{A_{11}}{A_{12}}\dot{q}_1 \tag{6.38}$$

Where A_{11} and A_{12} are the elements of the matrix presented in (6.32). Differentiating the previous equation (6.32) and substituting it in (6.37) is possible obtain the following system:

$$\begin{aligned}
&\ddot{q}_1 \\
&= -\frac{\left[\frac{H_{12}}{A_{12}} - \frac{A_{11}}{A_{12}}\frac{H_{22}}{A_{12}}\right]}{\left[H_{11} - H_{12}\frac{A_{11}}{A_{12}} - \frac{A_{11}}{A_{12}}\left(H_{21} - \frac{H_{22}A_{11}}{A_{12}}\right)\right]}\ddot{l} \\
&- \frac{H_{12}\left(\frac{\dot{A}_{12}\cdot A_{11}}{{A_{12}}^2} - \frac{\dot{A}_{11}}{A_{12}}\right) + C_{11} - \frac{C_{12}A_{11}}{A_{12}} - \frac{A_{11}}{A_{12}}\left[C_{21} + H_{22}\left(\frac{\dot{A}_{12}\cdot A_{11}}{{A_{12}}^2} - \frac{\dot{A}_{11}}{A_{12}}\right)\right]}{\left[H_{11} - H_{12}\frac{A_{11}}{A_{12}} - \frac{A_{11}}{A_{12}}\left(H_{21} - \frac{H_{22}A_{11}}{A_{12}}\right)\right]}\dot{q}_1 \\
&- \frac{\left[-H_{12}\left(\frac{\dot{A}_{12}}{{A_{12}}^2}\right) + \frac{C_{12}}{A_{12}} + \frac{A_{11}}{A_{12}}\left(H_{22}\frac{\dot{A}_{12}}{{A_{12}}^2}\right)\right]}{\left[H_{11} - H_{12}\frac{A_{11}}{A_{12}} - \frac{A_{11}}{A_{12}}\left(H_{21} - \frac{H_{22}A_{11}}{A_{12}}\right)\right]}\dot{l} \\
&- \frac{\left[G_{11} - \frac{A_{11}}{A_{12}}G_{21} + \frac{A_{11}}{A_{12}}\tau_{m,2} - \frac{A_{11}}{A_{12}}\{[J(\boldsymbol{q})]^T\cdot\boldsymbol{f}_{ext}\}_2 - \tau_{m,1} + \{[J(\boldsymbol{q})]^T\cdot\boldsymbol{f}_{ext}\}_1\right]}{\left[H_{11} - H_{12}\frac{A_{11}}{A_{12}} - \frac{A_{11}}{A_{12}}\left(H_{21} - \frac{H_{22}A_{11}}{A_{12}}\right)\right]}
\end{aligned} \tag{6.39}$$

$$\begin{aligned}
F_{wire} = &-\frac{1}{A_{12}}\left(H_{21} - \frac{H_{22}A_{11}}{A_{12}}\right)\ddot{q}_1 - \frac{1}{A_{12}}\frac{H_{22}}{A_{12}}\ddot{l} \\
&- \frac{1}{A_{12}}\left[C_{21} + H_{22}\left(\frac{\dot{A}_{12}\cdot A_{11}}{{A_{12}}^2} - \frac{\dot{A}_{11}}{A_{12}}\right)\right]\dot{q}_1 + \frac{1}{A_{12}}\left(H_{22}\frac{\dot{A}_{12}}{{A_{12}}^2}\right)\dot{l} \\
&- \frac{1}{A_{12}}G_{21} + \frac{1}{A_{12}}\tau_{m,2} - \frac{1}{A_{12}}\{[J(\boldsymbol{q})]^T\cdot\boldsymbol{f}_{ext}\}_2
\end{aligned} \tag{6.40}$$

$$\ddot{q}_2 = \frac{1}{A_{12}}\ddot{l} - \left(\frac{\dot{A}_{12}}{{A_{12}}^2}\right)\dot{l} - \frac{A_{11}}{A_{12}}\ddot{q}_1 + \left(\frac{\dot{A}_{12}\cdot A_{11}}{{A_{12}}^2} - \frac{\dot{A}_{11}}{A_{12}}\right)\dot{q}_1 \tag{6.41}$$

The system reported in expression (6.39), (6.40) and (6.41) is implemented in the Simulink model, as described in the next section.

6.3.3 Simulink implementation

The intra-finger dynamical model, has been implemented in a Simulink model using a *Matlab function block* Fig. 89.

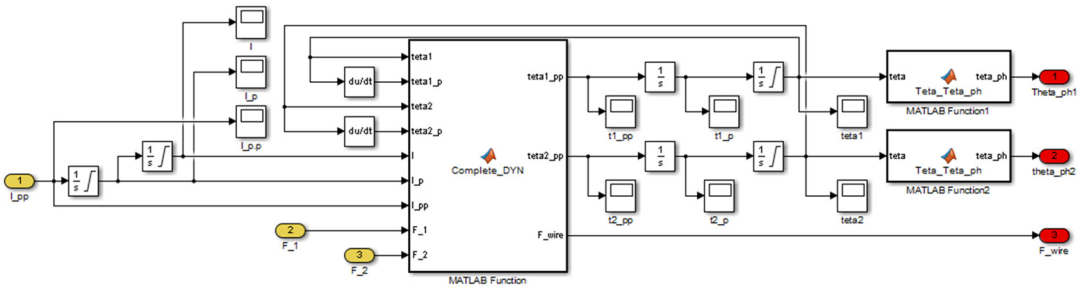

Fig. 89. Simulink model of finger's system. In the "MATLAB Function block" is implemented the kinematic and dynamic model.

The function requires as input the kinematics values of the wire (position, velocity and acceleration), the external forces acting on the phalanges and finally, the position and the velocities of the two articulations of the finger. Consequently, the function provides as outputs the phalanges acceleration and the corresponding wire force. The phalange accelerations are integrated in order to obtain the velocities and the angular positions, in addition, the model uses a series of limited integrators in order to consider the mechanical stops of the finger exoskeleton and the physiological constraints of the finger. The flow chart of the implemented function is reported in the following figure (Fig. 90).

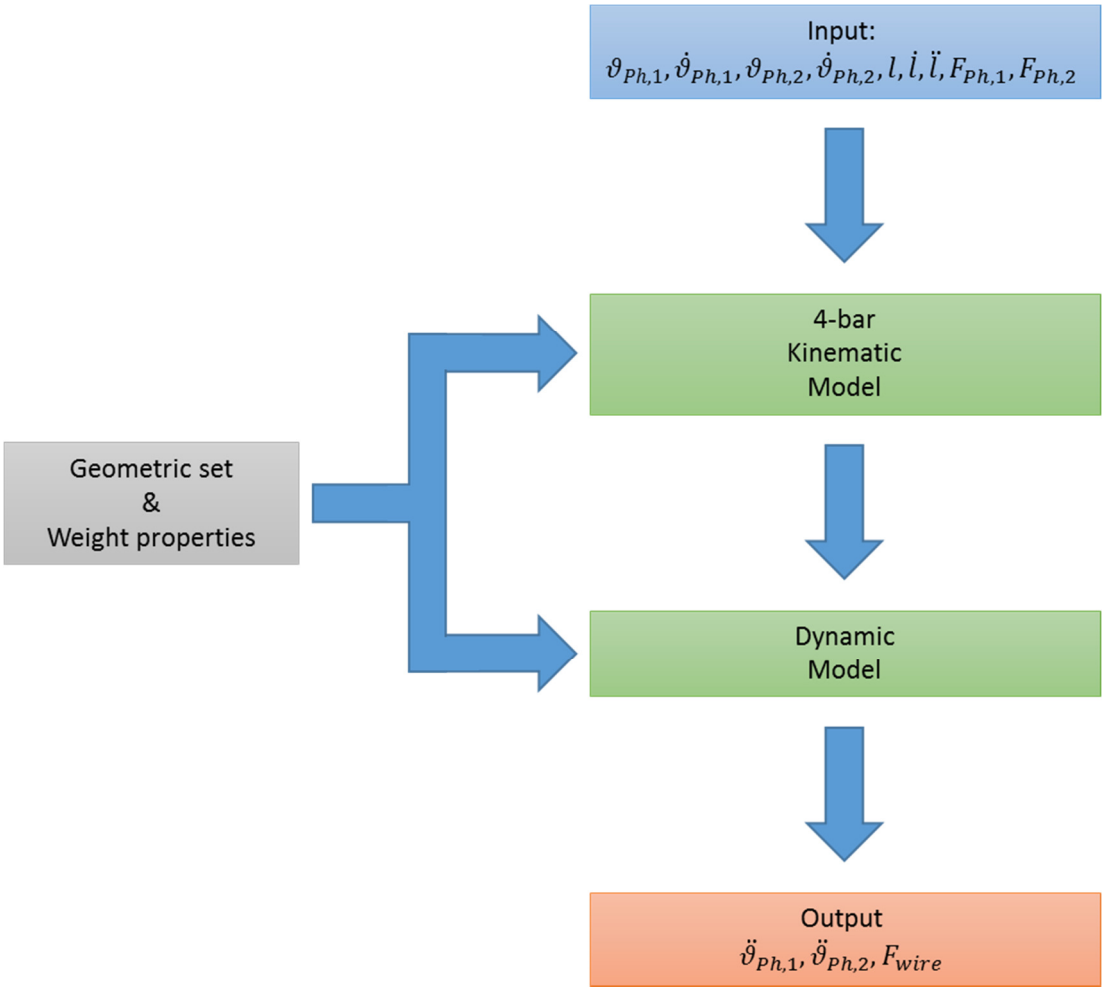

Fig. 90. Flow chart of the function implemented in "MATLAB Function block".

As shown in the flow chart, after the input management, a kinematic model that provides the mechanism's angles used for the calculation of the $[A(\boldsymbol{q})]$ as expressed in (6.32). Finally, the dynamics is resolved by the three equations (6.39), (6.40) and (6.41).

6.4 ReHand2 Simulink model

The entire ReHand2 model is presented in Fig. 91. Complete Simulink model of ReHand2. The Simulink model, obviously, consists of the inter-finger mechanism model, fingers and in addition, the DC/gearmotor and the "object" models.

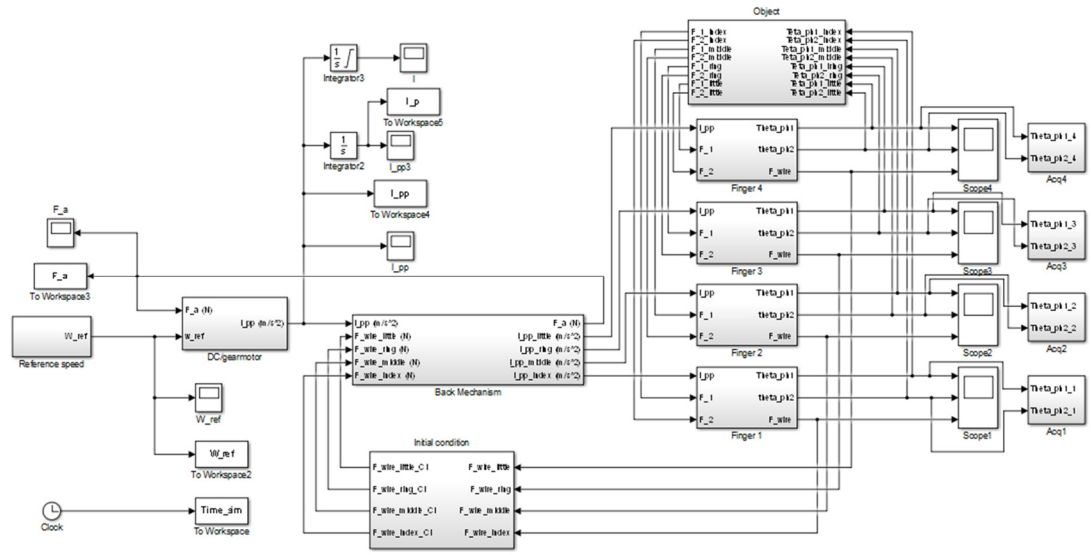

Fig. 91. Complete Simulink model of ReHand2.

The DC/gearmotor is a scholastic Simulink model of a DC motor followed by a series gain that consider the reduction steps and the efficiency of the motor and the gearbox (Fig. 92). The model require a velocity signal as input, this reference signal is regulated by means of two PID controllers, for the velocity and current loops respectively. The electrical part of the DC motor, as well as the mechanical one, are modeled by a simple second order transfer function and requires the equivalent external torque. The speed and the acceleration are then multiplied for the reduction ratios and efficiency, and finally, the velocity is translated in the linear velocity of the tendon.

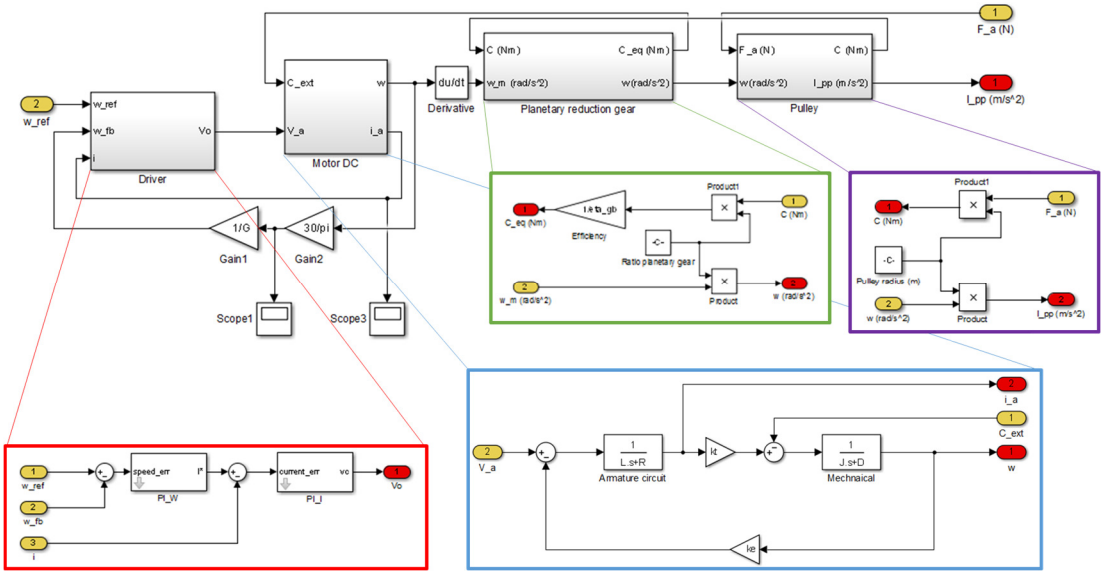

Fig. 92. Simulink model of DC/gearmotor.

Another interesting part of the model is the "object", which provides as output a contact force that is one of the inputs of the finger module. The contact force is modelled with a damping-spring model, in order to consider the finger-object deformation during the contact. The model intervenes when the phalange angle is equal or major than a reference one otherwise the model remains inactive. The constraints of the model can be expressed as follows:

$$\begin{cases} -90° \leq \vartheta_{Ph,ij}(t) \leq 0° \\ \vartheta_{OB,ij} \qquad\qquad \forall \vartheta_{OB,ij} \in ROM_{ij} \end{cases} \tag{6.42}$$

Where $\vartheta_{OB,ij}$ is the contact reference angle, expressed in degrees, for the phalange $j-th$ of the finger $i-th$. That angle has to belong to the phalange's range of motion. The contact force, instead can be expressed as:

$$f_{ext_{ij}} = c(\dot{\vartheta}_{Ph,ij}(t) - \dot{\vartheta}_{OB,ij}) + k(\vartheta_{Ph,ij}(t) - \vartheta_{OB,ij}) \tag{6.43}$$

The difference $\vartheta_{Ph,ij}(t) - \vartheta_{OB,ij}$ allows to discriminate in the model the different condition of touch and no-touch by means of a switch, in particular, in no contact mode, the difference is forced to be zero, in the other case instead it is the real result. In the figure below (Fig. 93) the generation of the external force for $j-th$ phalange of the $i-th$ finger is reported.

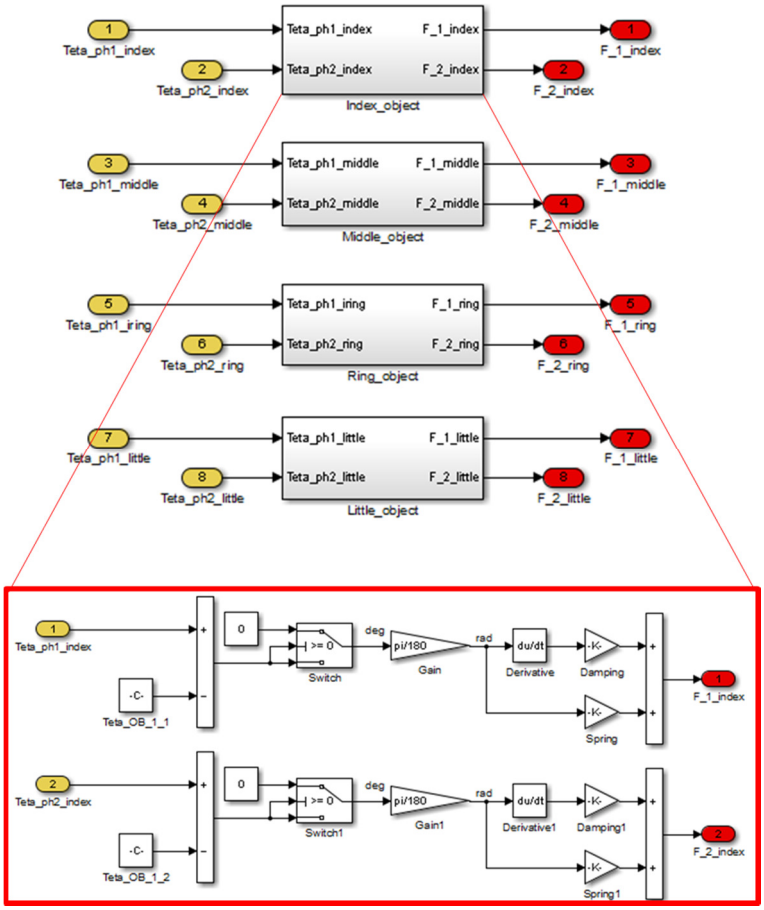

Fig. 93. Simulink model of the grasped object, the position reference is set independently for each phalange.

The presented model is used to perform a validation of ReHand2 during tests phase. The model allows to compare the simulation results with the experimental behavior, in the next chapter. As mentioned before, in the model are assumed some idealities, for instance, the friction on the finger mechanism is neglected as well as pre-loaded issue on the inter-finger mechanisms.

Chapter 7 ReHand2: v for validations

This chapter shows the validation of demonstrator ReHand2. Moreover, the chapter describes all the parts of the test bench and force and bending sensors. The used methodology is described, with a support of picture and detailed scheme as well as comparisons between experimental and simulated results.

7.1 The test bench

In order to characterize ReHand2 a suitable test bench was design and realized. The test bench consists in sensorized platform, a dummy hand, a motor control and an acquisition software implemented in LabVIEW enironment. In the following sections more details about the test bench are given before entering in the details of the experimental measurement setup, protocol and results.

7.1.1 Dummy hand

The ReHand2 structure does not permit a stand alone use so, in order to evaluate the entire mechanism, a dummy hand is realized and characterized. The dummy hand (Fig. 94) is based on an open access project called Flexy-Hand by Gyrobot, (http://www.thingiverse.com/thing:242639) which is licensed under the Attribution and Non-Commercial purpose.

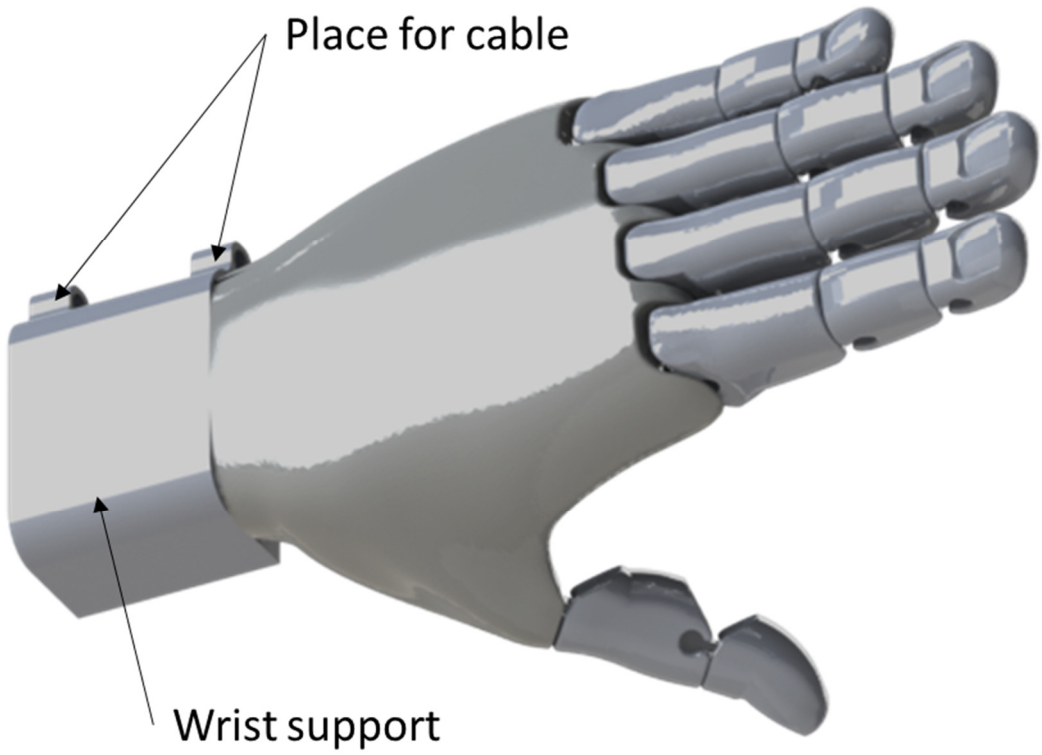

Fig. 94. Rendering of the dummy hand.

The Flexy-Hand is a printable cosmetic hand, which is modelled to fit with the human hand size. Flexy-hand allows the fingers motion due the presence of three joints for the long fingers (MCP, PIP and DIP) and two for the thumb (MCP and PIP), instead the fingers abduction/adduction is neglected.

The hand's body parts are made by a stereo-lithography 3D printer, with the Transparent RDG 720 (http://www.stratasys.com/materials/polyjet/transparent), which has good mechanical properties; the joints are made with Tango Black (http://www.stratasys.com/materials/polyjet/rubber-like) by additive manufacturing. The Tango Black is a rubber-like material, which allow the bend, for this reason it is used in articulation joints with the aim to reproduce the hand anatomy during motion and grasps. Despite the rubbery behavior of the Tango Black, the resistance to motion is negligible when inserted between the hand's links. In the original project is added a fixed platform, "wrist", which allows the positioning in different configurations and mechanical stops in order to limit the finger hyperextension. In addition, the phalanges

are modified in order to allow the integrations with eight bending sensors (Flex Sensor 2.2” powered by Spectra Symbol) one for each assisted phalange of long finger. The figure (Fig. 95) shows the section of a long finger and the location of the embedded bending sensors.

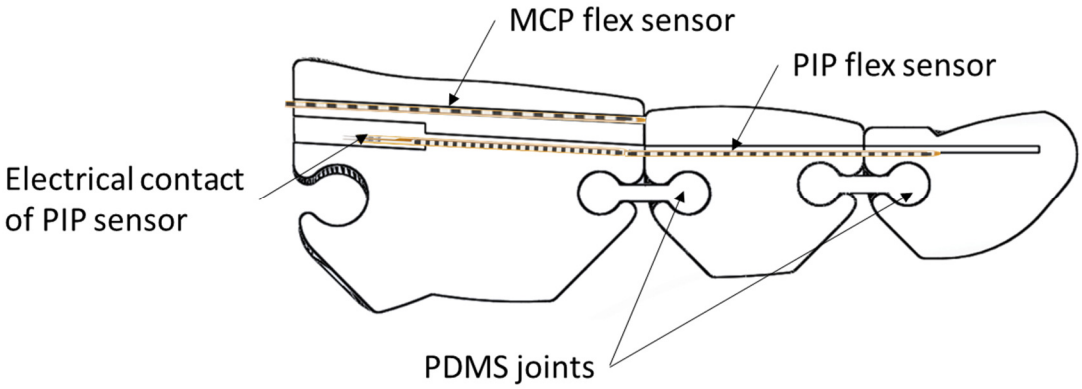

Fig. 95. Long finger's section.

The Flex sensor 2.2” (Fig. 96), produced by Spectra Symbol, can be used for detect the angle position of the dummy hand. The sensor is printed using a polymeric ink, which contained conductive particles in it. When the sensor is s straight, the particles give to ink a nominal resistance. While the sensor is bending, the consequent deformation change the distribution of the conductive particles that increase the resistance. When the sensor straightens out again, the resistance returns to the original value. Measuring the resistance variation it is possible determine how much the sensor is being bent.

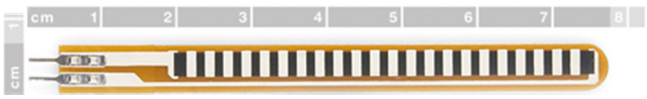

Fig. 96. Flex sensor 2.2” powered by Spectra Symbol.

From datasheet, the FS can be powered with a voltage of 5 V, and the resistance varying from 30 kΩ ±30 % in flat position and its resistance increase up to 50 kΩ, when the sensor is bent to 90°. The simplest way to use this sensor is with the impedance buffer circuit, as shown in the figure below (Fig. 97), which is presented in flex sensors datasheet.

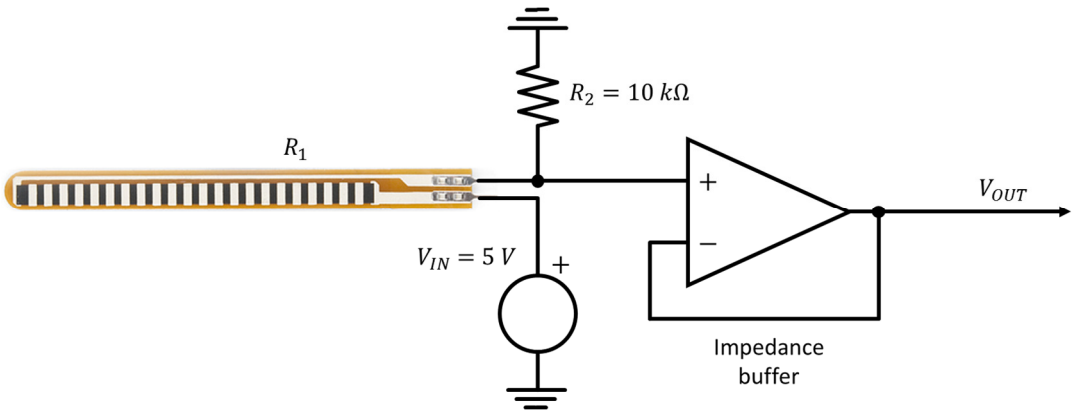

Fig. 97. Basic flex sensor circuit.

The implementation of the basic flex sensor circuit requires a single sided operational amplifier (Texas Instrument LM358) and a 10 kΩ resistance; they are assembled as shown in Fig. 97. The use of LM358 permits to reduce the error, due to flex sensor source impedance as voltage divider, thanks to the low current bias of the operational amplifier. Considering the scheme, it is easy calculate the V_{OUT} as follow:

$$V_{OUT} = \left(\frac{R_2}{R_1 + R_2}\right) V_{IN} \qquad (7.1)$$

Using the readout circuit, it is possible characterize the sensor; in particular, the transducer is calibrated in static conditions before and after the insertion on the dummy hand. The calibration is performed using a classical workshop goniometer using the test bench presented in Fig. 98.

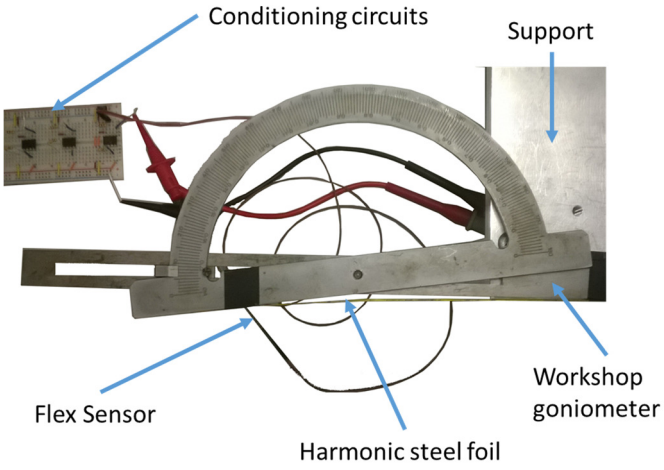

Fig. 98. Flex sensor calibration: test bench.

The sensor, under calibration, is attached by means of biadhesive tape on a harmonic steel foil, which is covered by kapton tape. The kapton tape is used in order to isolate electrically the sensor from the rest of test bench. One of the extremity of harmonic foil is attached to stationary arm of the goniometer, instead, the other end is left free to adapt to the movable arm. The calibration is performed with three rising and falling cycles, for each sensor, moving the movable arm of the goniometer between 0° and 90°, reading the output voltage. This kind of calibration is necessary in order to study the linearity of the sensors, after the insertion of sensors on the dummy hand, another calibration is needed in order to evaluate the gain and offset variations. The estimation of the inertial and weight properties are reported in the table below (Tab. 15):

Tab. 15. Weight properties of hand dummy realized by Transparent RDG 720, the thumb mass and inertia are neglected for obvious reasons.

Part name	Mass (g)	Inertia (g mm^2)
Index proximal phalange	14.82	2138.63
Index middle and distal phalanges	11.43	2385.03
Middle proximal phalange	15.71	2549.07
Middle distal and middle phalanges	13.74	3551.91
Ring proximal phalange	12.92	1925.63
Ring middle and distal phalanges	11.93	2779.67
Little proximal phalange	9.35	1021.34
Little middle and distal phalanges	6.87	1147.30

The values reported in Tab. 15 are implemented in the previously dynamical model (6.4) in order to compare the experimental behavior with the theoretical one during tests.

7.1.2 Platform

Another important part of the test bench is the platform, already used in the previously version of ReHand, in particular for kinetostatic tests. The platform provides a mechanisms with guide that immobilized the dummy wrist, while four load cells measure the forces generate by the exoskeleton system at the fingertip level. The load cells are the commercial piezoresistive FSS1500NSB, Honeywell, FS Series, NJ able to measure the perpendicular force ranging from 0 to 15 *N*. The readout circuit (ROC)

foreseen the presence of a single-supply differential amplifier (AD626) in order to change the gain of full Wheatstone bridge an obtain the out signal varying from 0 to 3.6 *V*. The simple ROC is shown in (Fig. 99).

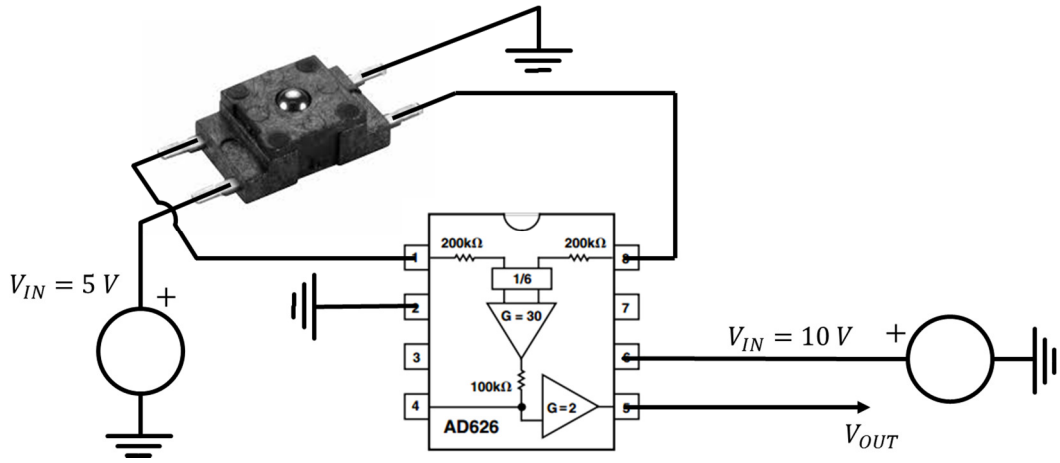

Fig. 99. Readout circuit for FSS1500NSB, Honeywell, FS Series, NJ. The AD626 is the differential amplifier, used in the single-supply configuration.

The load cells are characterize after the introduction of the sensors in the ad hoc structures as shown previously in (Fig. 63). As in the previously case, the calibration is performed with three cycles increasing and decreasing the load applied for each sensor.

7.1.3 The software and the interfaces

The analogic sensor signals are acquired by a DAQ card (NI PCe 6363, National Instruments Corp.), which receive the force and phalanges position voltages. An appropriate software is implemented in LabVIEW (National Instruments Corp.) environment in order to manage the voltages inputs. The software have also the aim to command the DC motor, both in current or velocity depending on the type of test. The communication between software and motor drive occur by a RS232 interface. The software has also the aim to record the signal for post processing analysis. In figure (Fig. 100) is shown the front panel and the block diagram of the software.

Fig. 100 a) shows the front panel of the acquisition/command software. Front panel can is composed by five columns, the first one concerns name file and path following by the choice of the test types (kinetostatic or dynamic) and real current consumption

and real velocity graphs acquired directly by the motor drive. The other columns regard the four long fingers (from index to little) and the chart following the same succession of force signal, MCP and PIP position signals respectively. Concerning the block diagram, Fig. 100 b) presents the opening of communication port, instead in the *while* cycle is reported the motor command, the acquisition of the sensors and creation of data file for successive post processing.

a)

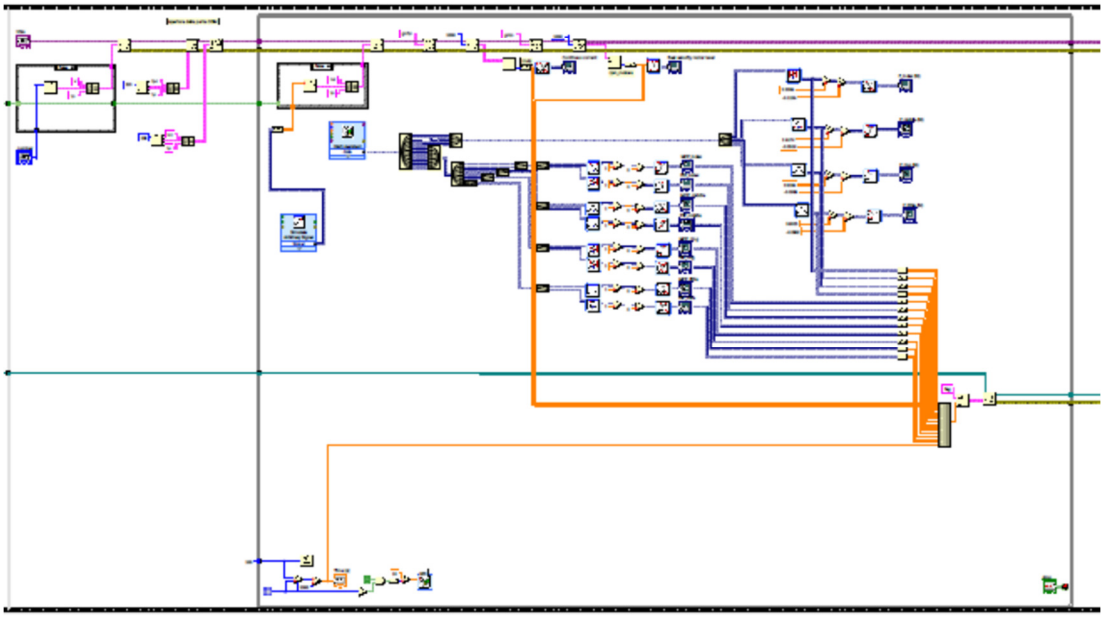

b)

Fig. 100. Implemented LabVIEW program: a) the front panel, where is possible see the graphs in real time and b) the block diagram.

7.2 Exoskeleton: ergonomy and adaptability

Qualitative tests are performed in order to evaluate the ergonomy and fitting of ReHand2 with different hand size. In addition, in the same time, with this test is demonstrated the intrinsic capability of the underactuated device to adapt itself to different hand dimension and several types of grasps.

The test is carry out on eight healthy subjects (six males and two females, ranging from 26 to 37 years old). Concerning the ergonomy and wearability, the protocol foreseen after about one-hour test where the subject wears and drags the exoskeleton to grasp different object, according with the Cutkoski classification (Cutkosky and Howe 1990) followed by an interview. Fig. 101 shows the pictures of the accomplished tasks.

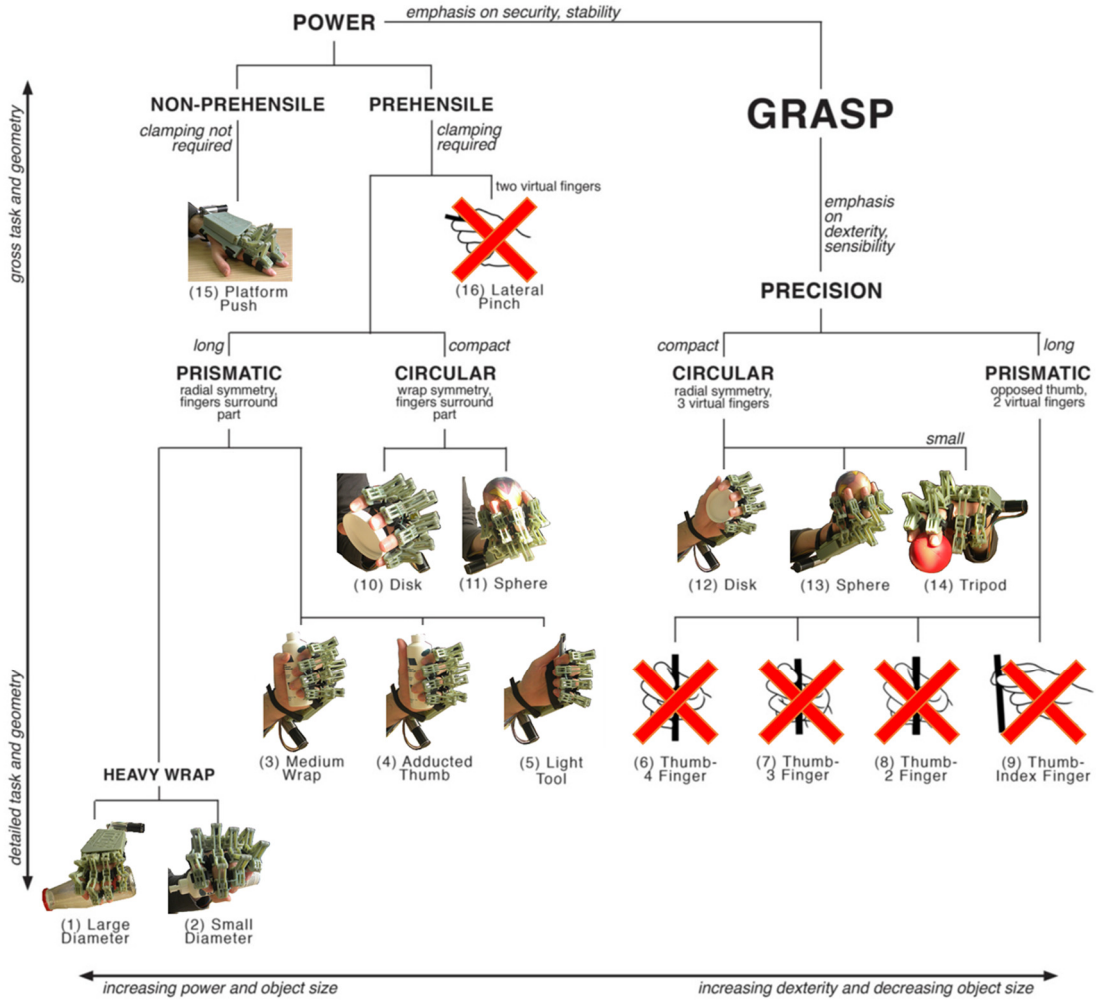

Fig. 101. Different grasps generated by ReHand2 organized according to the classification reported in (Cutkosky and Howe 1990)*, the red cross is referred to not done grasps.*

All subjects were able to perform all the given tasks, and no constraints imposed by the exoskeleton while performing the grasps and no complained about pain were not reported by test subjects. Compare to the previously version of ReHand, subjects do not report any kind of discomfort due to exoskeleton shape. Negative feedbacks reborted by subjects are related to uncomfortable location of the DC motor due to wrist ROM, which motor involves, and the position of the motor's center of mass that generate a torque action about the wrist axis.

7.3 Kinetostatic validation

As for the previously prototype, a kinetostatic validation of ReHand2 is performed. In contrast with the previously kinetostatic tests, where the exoskeleton was worn by a healthy subject, in this series of tests ReHand2 is attached to the sensorized dummy hand. The kinetostatic validation is achieved in two different hand configurations. The first one is a non-prehensile configuration; instead, the second is a generic hand shape that will be explain in the following. In the tests carried out with the dummy, the exoskeleton is stucked on the hand phalanges in order to reduce the boring displacements caused by the presence of Velcro straps.

7.3.1 Non-prehensile hand shape

Using the dummy hand associated with the sensorized platform, it is possible to conduct the kinetostatic validation of ReHand2. The picture below (Fig. 102) shows the test bench setup used.

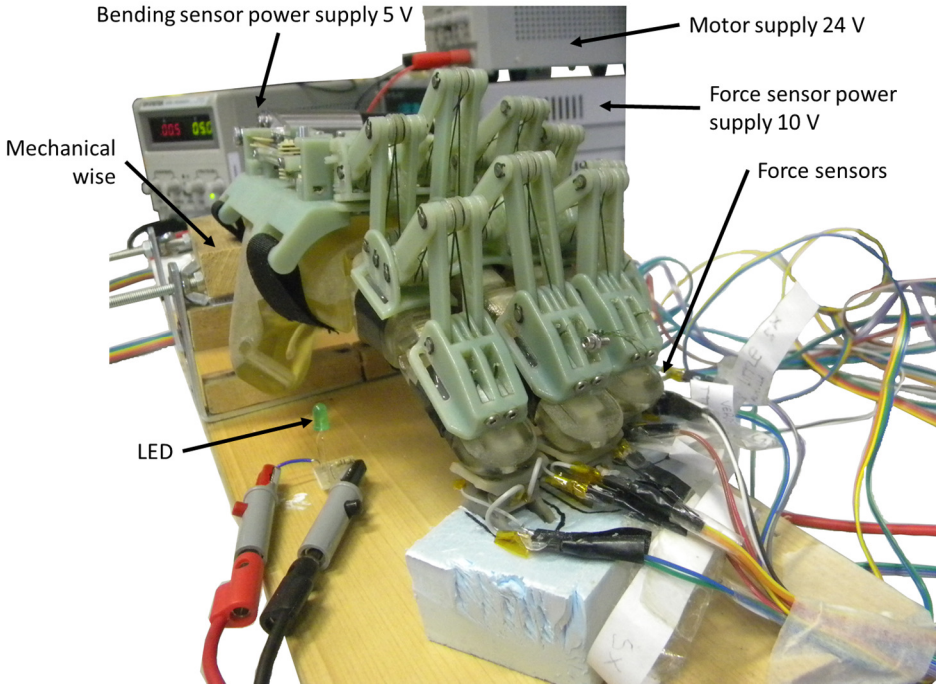

Fig. 102. ReHand2 attached to the sensorized hand in a non-prehensile configuration, the sensors are deployed at the fingertips level, and measure the exchanging force between the finger and the "object".

The dummy hand is positioned in a non-prehensile configuration, where the wrist is locked in position by the vise mechanism and the fingertips are in contact with the load cells. The protocol involves sending a current step trajectory (ranging from 100 *mA* to 500 *mA* with steps of 50 *mA*) to the DC motor, maintaining constant the reference speed (100 *rpm* at motor shaft). The figures (Fig. 103) below show, an example of real current consumption, compare with the current reference and real motor speed, which are acquired by the motor driver.

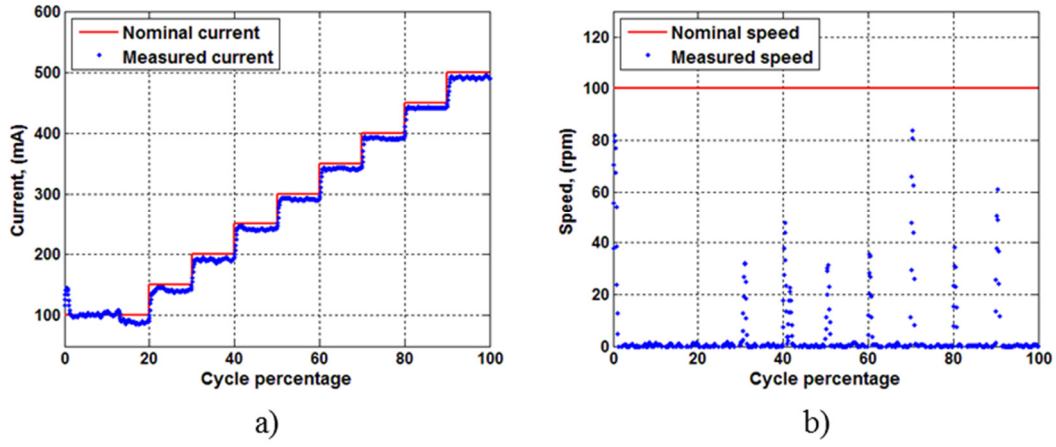

Fig. 103. Comparison between the nominal (red line) and measured (blue dots) conditions, respectively for current a) and motor speed b).

The motor torque and the consequent input wire force are dependent to current consumption by the following relationship:

$$F_{wire} = k_M \cdot \eta_m \cdot i \cdot \eta_i \cdot I \cdot \frac{1}{R_p} \cdot 10^{-3} \quad (7.2)$$

Where F_{wire} is the actuating force acting on the input wire of the system, expressed in *N*; k_M is the constant torque expressed in *mNm/A*,; η_m is the DC motor efficiency ; i is the reduction ratio; η_i is the gearbox efficiency; I represents the current consumption expressed in *A* and finally, R_p is the radius of the action pulley, where the wire is wrapped, expressed in *m*.

The value of these constant are reported in the following table:

Tab. 16. Electrical and mechanical constant of Faulhaber DC-Servomotor 2444 024 B, Faulaber Planetary Gearheads Series 26/1S and pulley radius.

Constant	Value	SI units
k_M	9.8	*mNm/A*
η_m	0.77	-
i	1/43	-
η_i	0.7	-
R_p	$3.75 \cdot 10^{-3}$	*m*

Starting from the previously values, the wire force is reported in the figure (Fig. 104), where is superimposed with the measured current consumption.

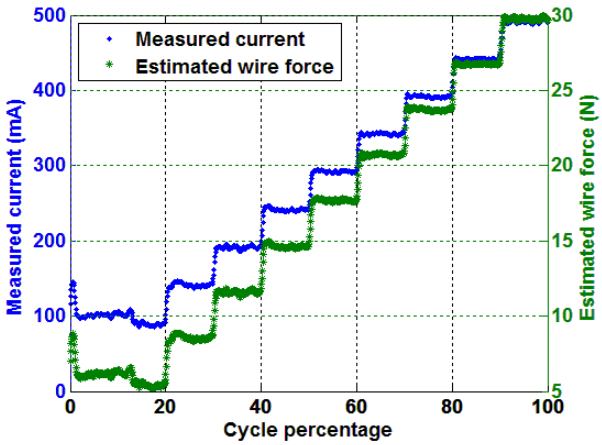

Fig. 104. Comparison between the measured current (blue dots) and the consequent wire actuation force (green dots) estimated as in (7.2).

In the kinetostatic tests, it is possible to consider the ReHand2 mechanism as force distributor, because of in the isostatic condition of the hand, the motor develops the maximum torque according to current consumption.

Observing the cycle percentage of the actuating force (Fig. 104) comparing with the experimental $\boldsymbol{f}_{phal}$ (Fig. 105 b)), it is possible notice that for current lower than *200 mA* the DC motor does not generate sufficient torque/force on wire to overcome the internal friction and exoskeleton dissipations. According with the kinetostatic model, presented in Chapter 5, it is possible compare the predicted behavior of the $\boldsymbol{f}_{phal}$ with the measured one provided by the load cells. The theoretical behavior is the result of the equation (5.52). The wire force f_A is estimated by the relationship between force

and current consumption (7.2). The comparison is shown in the following figure (Fig. 105).

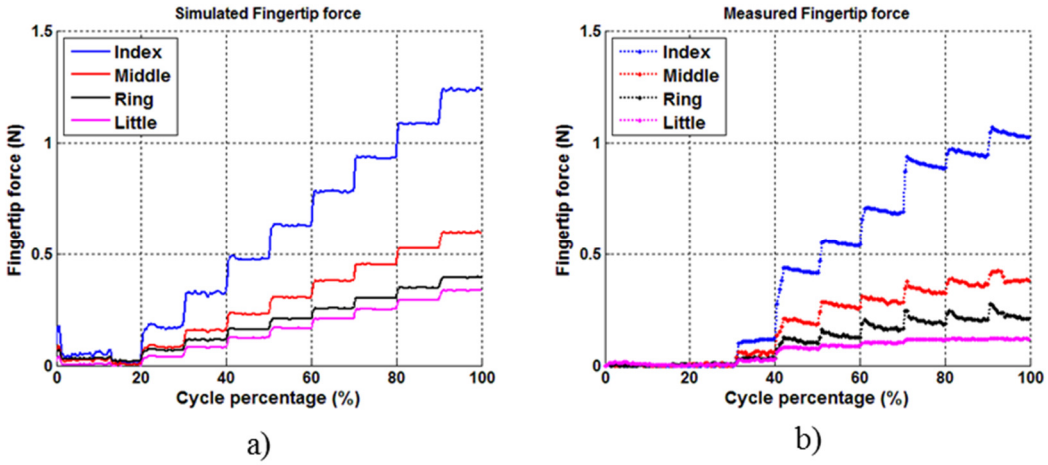

Fig. 105. Profile of the theoretical predicted a) and experimental measured b) fingertip forces generated by ReHand2.

In the left chart is presented the theoretical behavior instead the right graph shows the experimental measures. As expected, the comparison shows that the experimental values are lower than the simulated one. The different behavior is caused by the following reasons:

1. Friction between the transmission components;
2. Non-ideality of the tendons;
3. Deformation of tendon clamps under load;
4. Non-perfect tendons' pre-load.

The graph below (Fig. 106) and the table (Tab. 17) show the experimental behavior with the standard deviation calculated on eight consecutive tests. The standard deviation value depends precisely by exoskeleton non-idealities and from the load cells. It is possible also note that these non-idealities are not constant for every fingers but depend also from the chosen transmission tree. In fact, ring and little fingers, which are the last outputs of the transmission tree, are the most affected by the friction and by the not perfect tendon's pre-load.

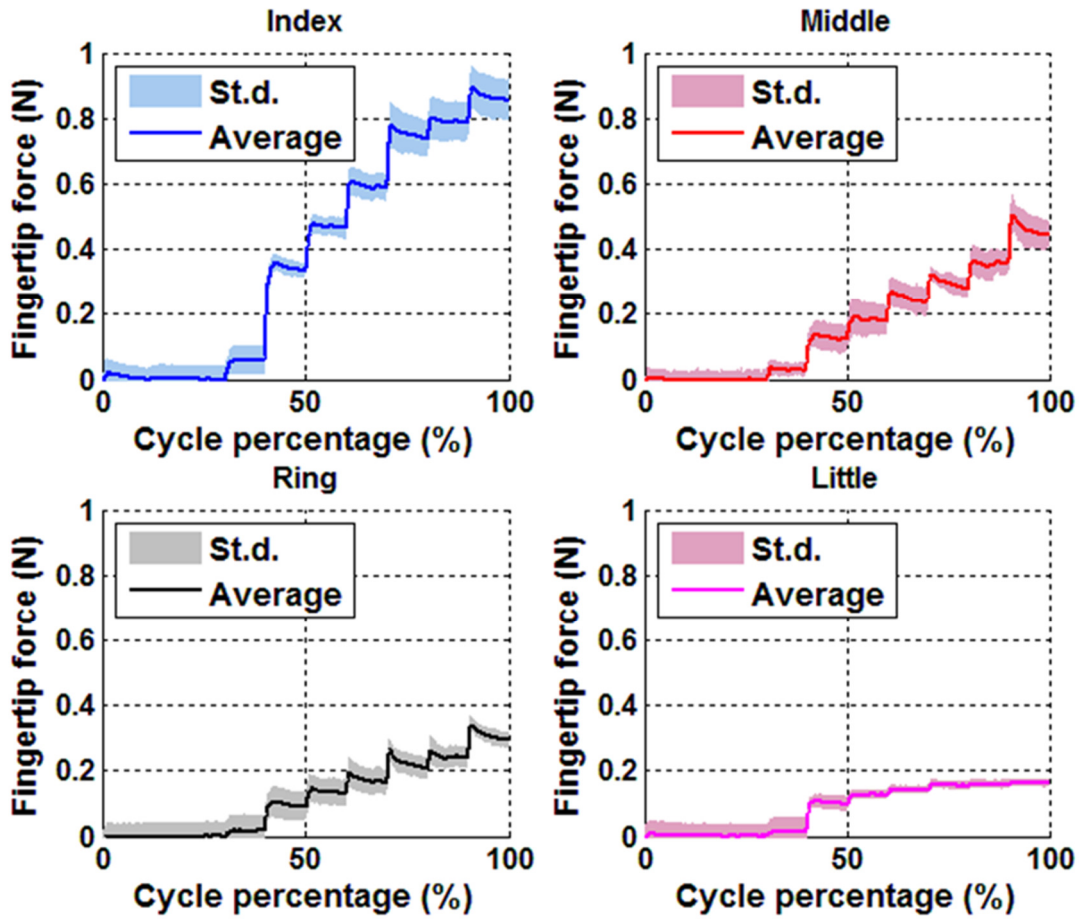

Fig. 106. Average of measured fingertip forces (on eight tests) and the consequent standard deviation.

The repeatability is associated with the percentage of Variation Coefficient (CV). This coefficient is the ratio between standard deviation, calculated on the tests, and the average measured value at each fingertip force step. The table (Tab. 17) below reports the minimum and the maximum value for each finger.

Tab. 17. Minimum and maximum Coefficient of Variation (CV) expressed in percentage.

	Index	**Middle**	**Ring**	**Little**
min. CV (%)	2.70	5.31	8.28	6.67
max. CV (%)	12.72	25.55	21.06	30.53

Fig. 107 describes deviation between the measured fingertip force and the expected one for each finger. The charts depict the theoretical estimates (x-axis) and the measured fingertip force (y-axis) for each finger. The bisector line represents the ideal

behavior (solid red line), where there is a correspondence between theoretical simulation and the experimental values. The experimental data are reported with blue dots; instead, the black line represents the trend line obtained interpolated the experimental data.

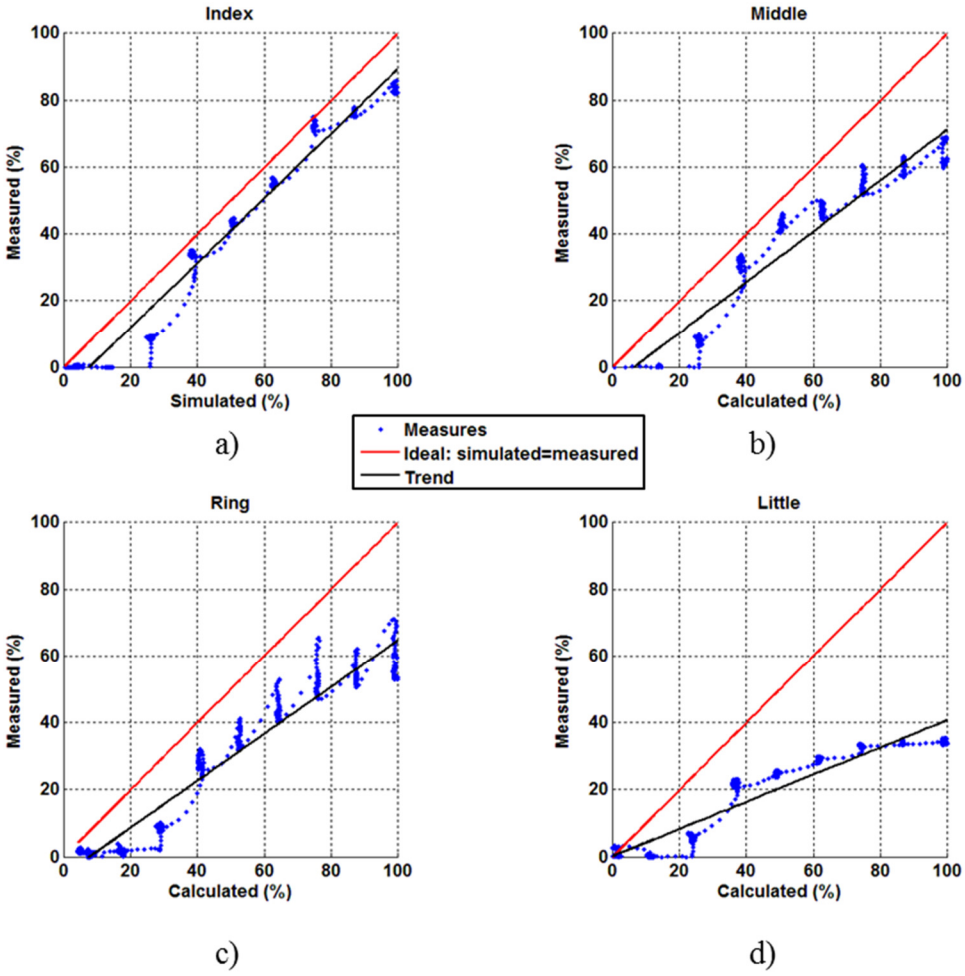

Fig. 107. Comparison between the experimental (y axis), simulated (x axis) fingertip forces.

All the four graphs show how the non-idealities have different impact and influence among the fingers; in particular, that influence is most relevant for the more distal output (little finger) due to the serial configuration. This behavior is due tofrictions summation that acts on the differential elements and idler pulley. The difference between theoretical and experimental is quite constant during the test for the index finger, while for the other fingers the deviation become more relevant for high force.

Finally, in Fig. 108 the previously logic is followed in order to compare the real actuation force generate by the actuator with the estimated one. The latter f_A is calculated starting from the measured fingertip forces $\boldsymbol{f}_{phal}$.

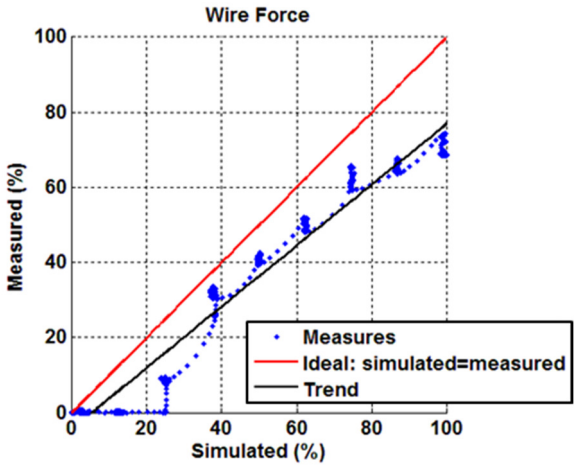

Fig. 108. Comparison between measured (y-axis) and simulated (x-axis) actuation force.

Inverting the previously concept and the equation (5.52) it is possible compare the measurement of the actuating wire with the estimated one (Fig. 108), starting by the fingertip measurements $\boldsymbol{f}_{phal}$. Also in this case, it is possible verify that the gap between the two curves is caused by non-idealities neglected in the mathematical model. In both figures (Fig. 107 and Fig. 108) is possible underline the higher influence of static friction for low forces.

7.3.2 Generic hand shape

This test has the aim to verify the ReHand2 behavior in a generic finger position. The protocol and the analysis are identic to the previously one, except for the position of the fingers on the load cells.

The table below reported the generic position of the fingers' articulations.

Tab. 18. Generic position of the hand's articulations, divided per finger.

Finger	MCP angle (deg)	PIP angle (deg)
Index	-20 °	-43 °
Middle	-10 °	-5 °
Ring	-15 °	-8 °
Little	-20 °	-10 °

The current consumption and the consequent force is reported in the figure (Fig. 109) below. In addition, the figure reported also the velocity diagram, which is around zero considering that the tests are conducted in an isostatic conditions.

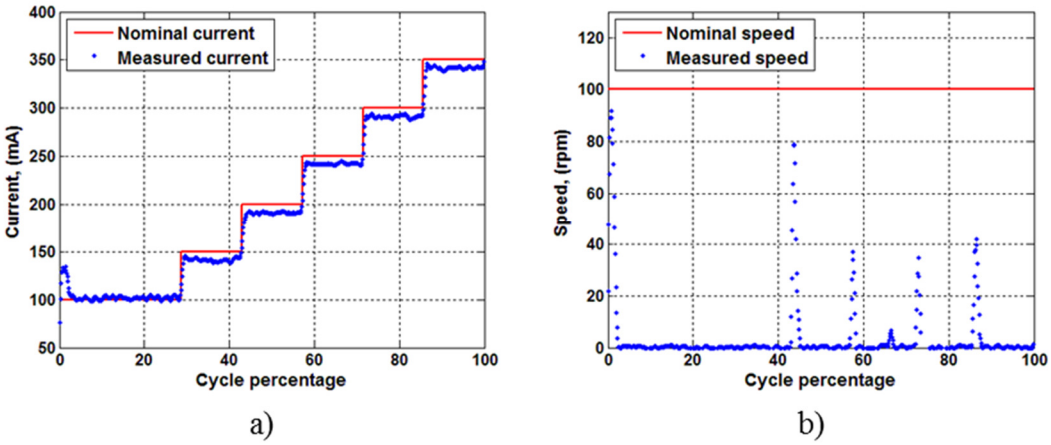

Fig. 109. Current and speed conditions during the tests conduct in a generic hand shape, respectively the comparison between nominal and measured current a) and motor speed b).

Fig. 110 shown the well-known relation between torque and the actuation force estimated by current measurement.

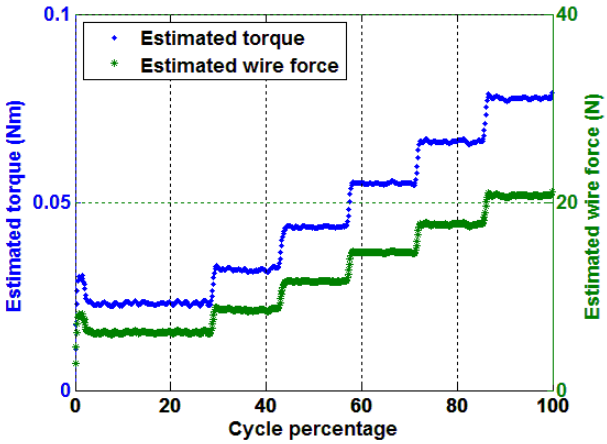

Fig. 110. Relation between torque generated by the electrical motor and the consequent force that acts on actuation wire.

7.3 Kinetostatic validation

Applying the angular values, reported in Tab. 18, to the kinetostatic model, it is possible compare the theoretical values of $\boldsymbol{f}_{phal}$ (Fig. 111 a) with the experimental measurements (Fig. 111 b).

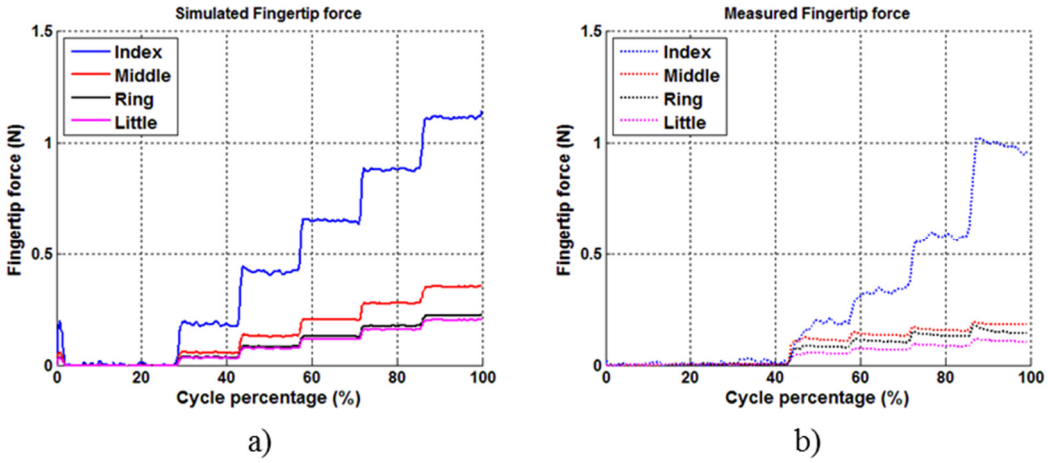

Fig. 111. Comparison between theoretical a) and experimental measurements b) at fingertip level for a generic hand shape.

As in the previously case, the DC motor does not generate sufficient torque, to overcome the internal and external friction until 200 mA. After that value of current, the actuator starts to generate force at fingertip level. Observing the behavior of the fingertip force is possible notice that the measured and expected force are influenced to the same finger position, according to the equation (5.50).

In order to verify the repeatability of force distribution on this type of hand shape, nine consecutive tests are performed. The Fig. 112 shows the average of the fingertip force and the standard deviation overlapped to it.

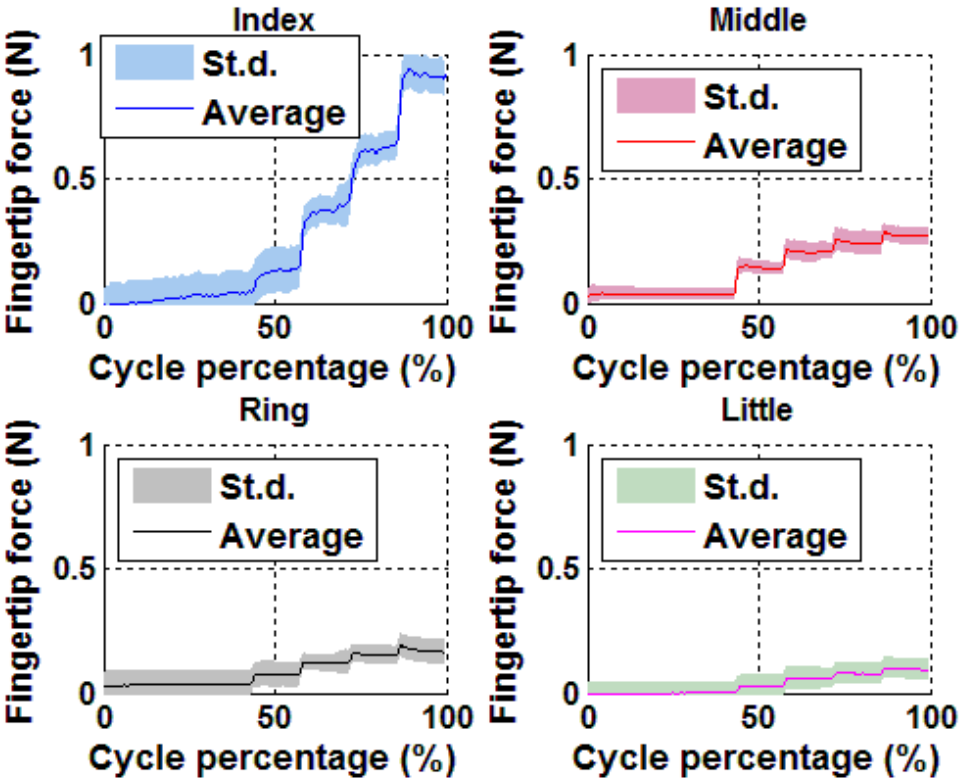

Fig. 112. Average of measured fingertip forces (on nine tests) and the consequent standard deviation obtained for a generic hand shape.

The amplitude of the standard deviation depend only on the relative displacement between fingertips and load cells jointed to the already mentioned non-idealities as the wire's pre load. The post processing on the kinetostatic analysis performs also the normalized comparison among the fingers and the actuating force. Fig. 113 shows five graphs, one for each finger and one for the force acting on the input wire.

The charts shows the deviation between the real measurements with the theoretical behavior. It is possible to notice how non-idealities are influenced by finger-position. As in previously case, it is reported the trend line obtained by the experimental data.

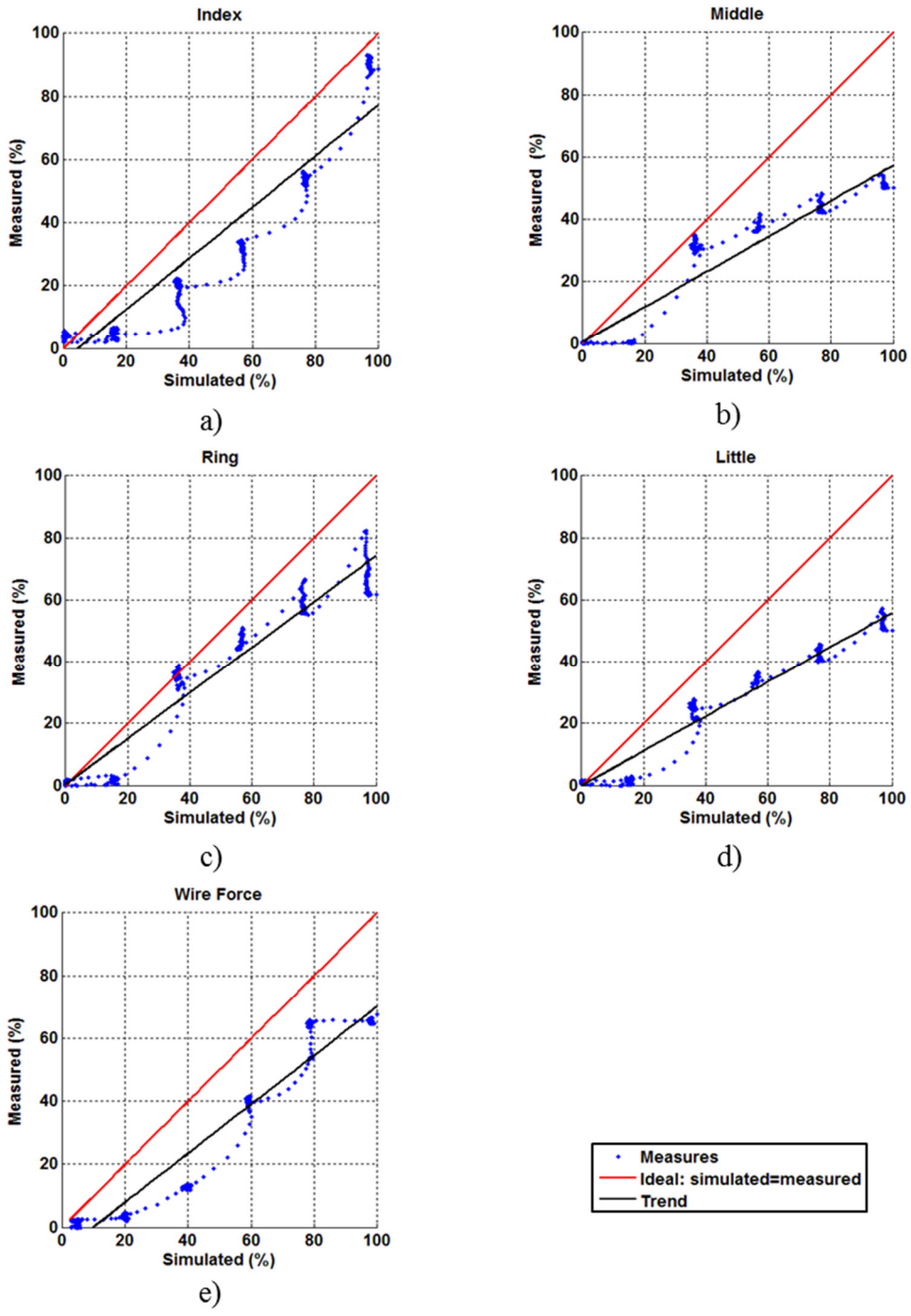

Fig. 113. Comparison between the measurements (y axis), simulated (x axis) fingertip forces (a – d) and the comparison between measured and simulated actuation force (e).

In conclusion, it is possible compare the behavior of the device in the two different position and generalize some considerations. In particular, according with the kinetostatic model, the phalanges forces are position-depending as well as the force at the fingertip level. In addition, it is possible seen, the role that friction plays in the

finger module, in particular comparing the results of the two different hand shape, the deviation between the theoretical and real data is increase.

7.4 Free motion tests

The main feature of ReHand2 concern the possibility to control both flexion and extension movements with the use of a single actuator using the underactuation principle as described in the previously chapter. In order to validate this property a free motion tests are performed. The tests foreseen the vertical hand position, as shown in the picture (Fig. 114):

Fig. 114. Free motion test setup.

The protocol consists to give a predetermined speed trajectory to DC motor and measure the finger's articulations during free motion. In this analysis is evaluated the influence of different motor speed and different current limitation. In fact, the experiment is conducted with different maximum motor speed, repeated at least five

time, and different current limitation. Fig. 115 shows the normalized reference speed trajectory:

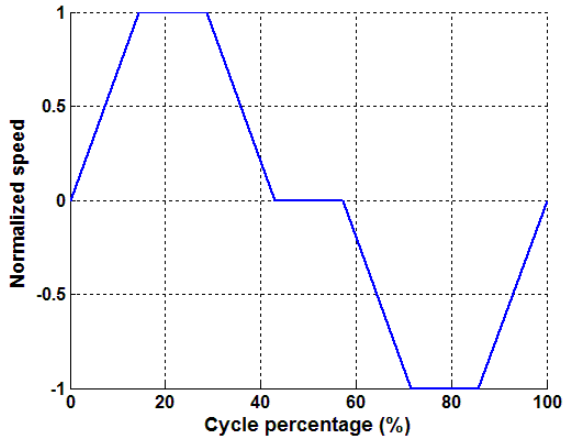

Fig. 115. Normalized reference speed trajectory

The reference trajectory is multiply by a gain in order to report the normalized values to *rpm*. In Fig. 116 is reported the reference speed in blue line while the real motor output is shown with red dots.

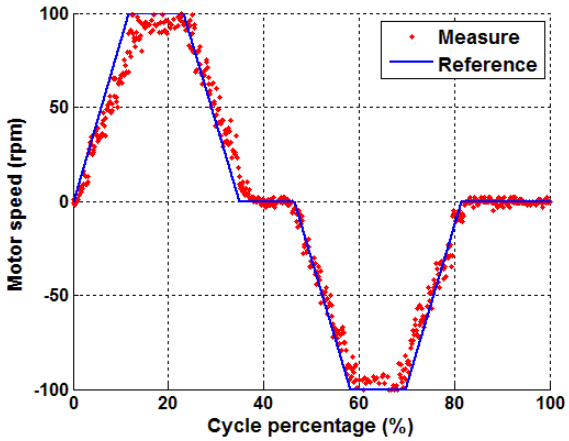

Fig. 116. Comparison between reference speed and real motor output.

The articulation angles, consequent to the speed signal, are shown in the figure below (Fig. 117).

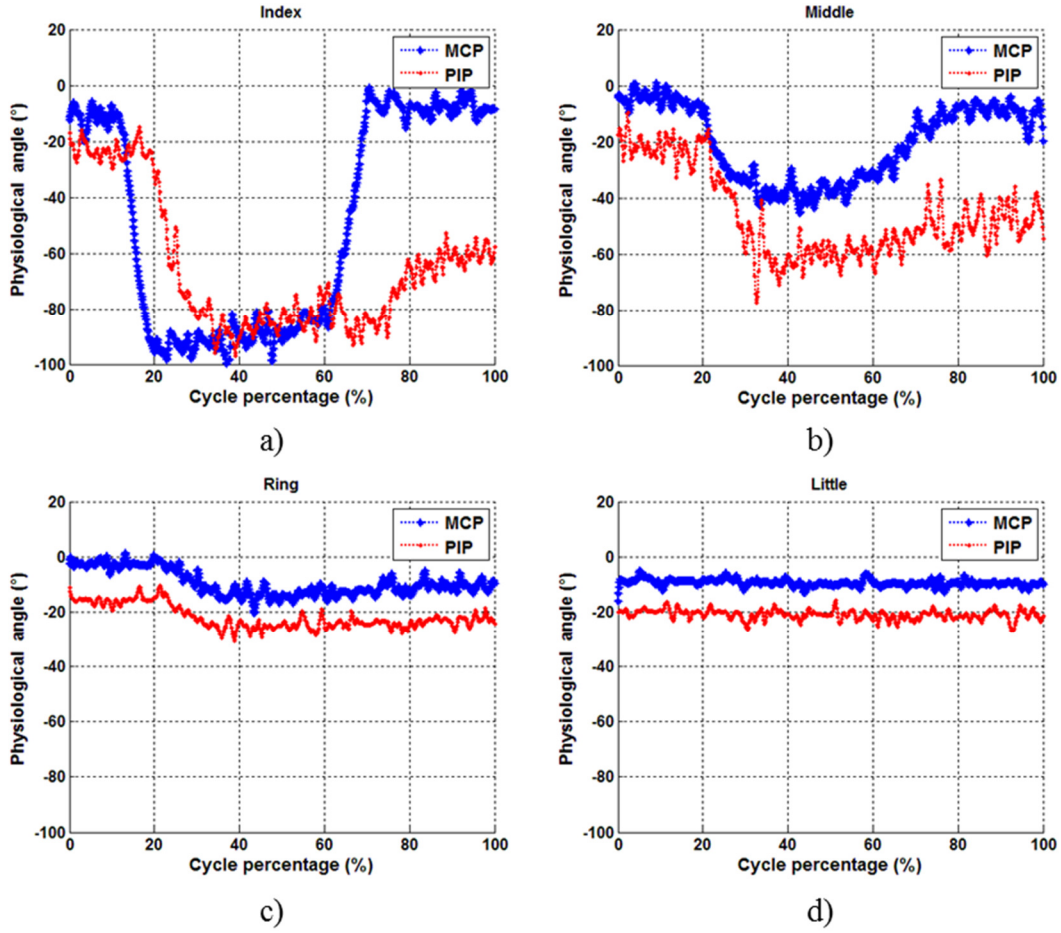

Fig. 117. Measured physiological angles for each finger, in blue lines are represented the MCP joints while the red ones are indicated the PIP joints. The current consumption limitation on the test is 750 mA while the maximum reference speed, at the motor shaft, is 100 rpm.

Comparing the reference speed with the finger motion, it is possible observe the influence of the tendon's preload. The loose wire involves a delay between the input and the outputs, estimable in about *12 s*. It is possible notice the influence of dynamic friction on ring and little fingers (Fig. 117 c) and d)).

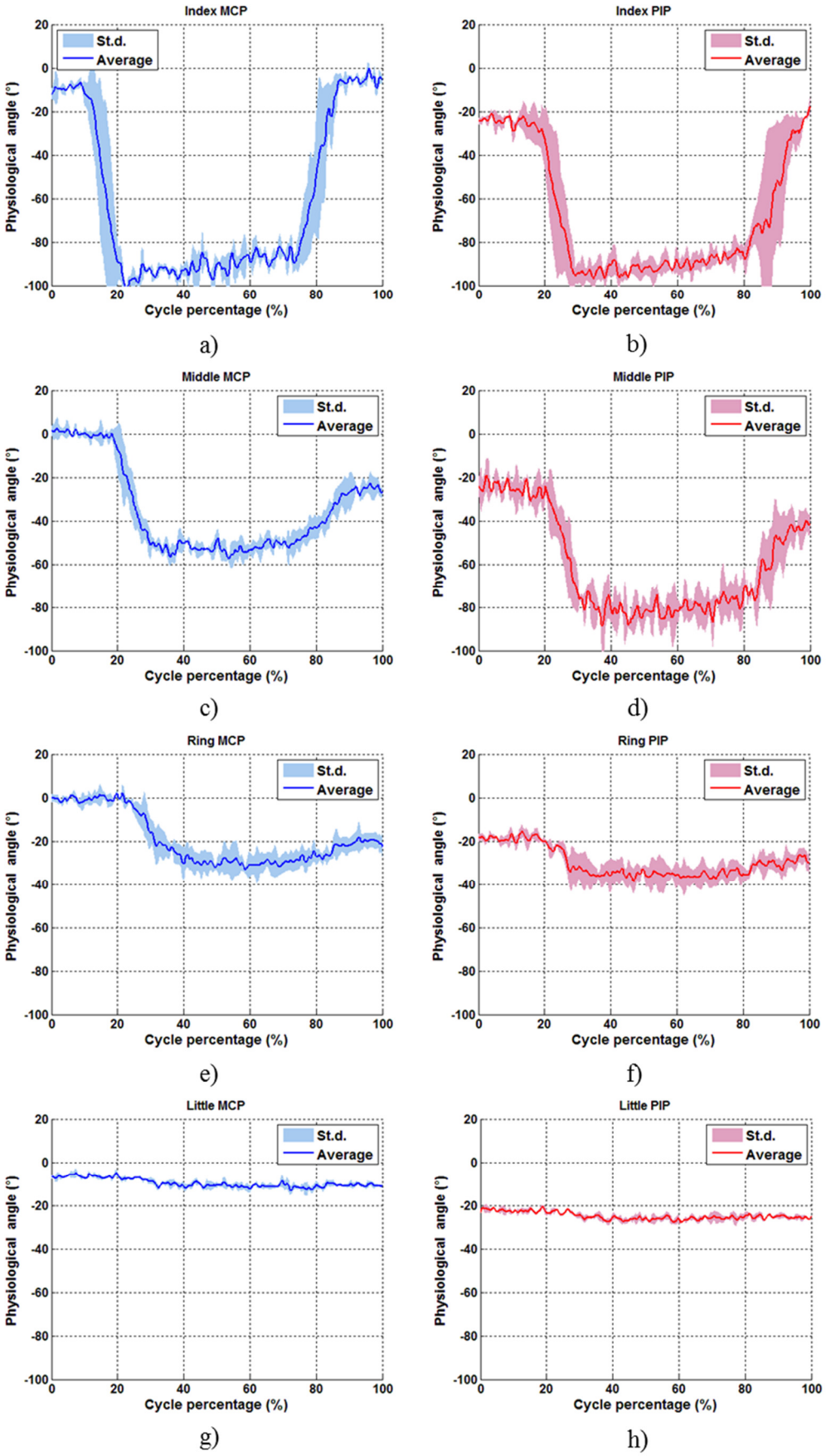

Fig. 118. Average of measured physiological angle (on five tests with the following conditions 150 rpm and current limitation 750 mA) and the consequent standard deviation obtained for each finger.

Despite the presence and the influence of non-linearity, the repeatability of the mechanism motion is good. Fig. 118 shows the repeatability of the finger motion calculated on five test. Despite the presence of the non-idealities and not perfect pre-load of the tendons, the device responds in a very repeatable manner. The percentage of repeatability error, during free motion, can be summarize in the following table:

Tab. 19. Average Coefficient of Variation (CV) for actuated MCP and PIP joints.

Finger	MCP CV (%)	PIP CV (%)
Index	9.21	9.56
Middle	9.51	11.77
Ring	22.35	15.85
Little	14.00	5.55

Changing the gain of the reference trajectory it is possible to evaluate the influence of the maximum motor speed on the fingers' motion. In the next figure (Fig. 119) an example of flexion/extension behavior is reported.

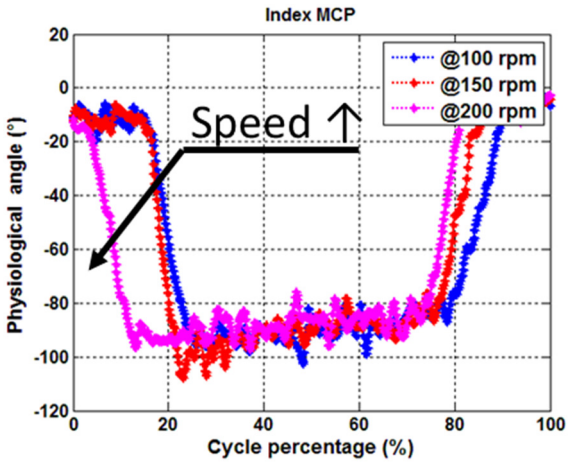

Fig. 119. Flexion/extension variation according to the motor speed changing. The motor speed is increase from 100 rpm to 200 rpm with a step of 50 rpm and maintaining constant the current consumption limitation at 750 mA.

The percentage of cycle is reported on *x-axis*, instead, the angle values, expressed in degrees (°), are reported on *y-axis*. Each finger joints have a similar behavior so it is possible conclude that maximum speed does not change the shape of the response.

Much more interesting is the behavior at the current variation.

The system is influenced by dissipations, for instance: friction on the differential elements, dissipation on the wire's paths and in general the friction due by all the parts in relative motions. The influence of the current limitation on the exoskeleton hand is evaluated performing the same test, varying the current consumption limitation from 750 *mA* to 1 *A*, maintaining constant the motor speed (150 *rpm*).

The figure (Fig. 120) reports the variations of the finger phalanges position for a variation on the current level. It is possible notice that the index finger is less influenced by this parameter, instead, all the other fingers increase their maximum position value increasing the current level. As already seen in the kinetostatic tests, this fact is due to serial configuration adopted in the transmission tree. The serial configuration foreseen the first output (index finger) on the first movable pulley and as the consequent is effected only by the friction caused by the first differential element and from itself. Contrary, the other outputs (starting from middle to little finger) are always influenced by their own friction and by all dissipations introduced in all upstream elements.

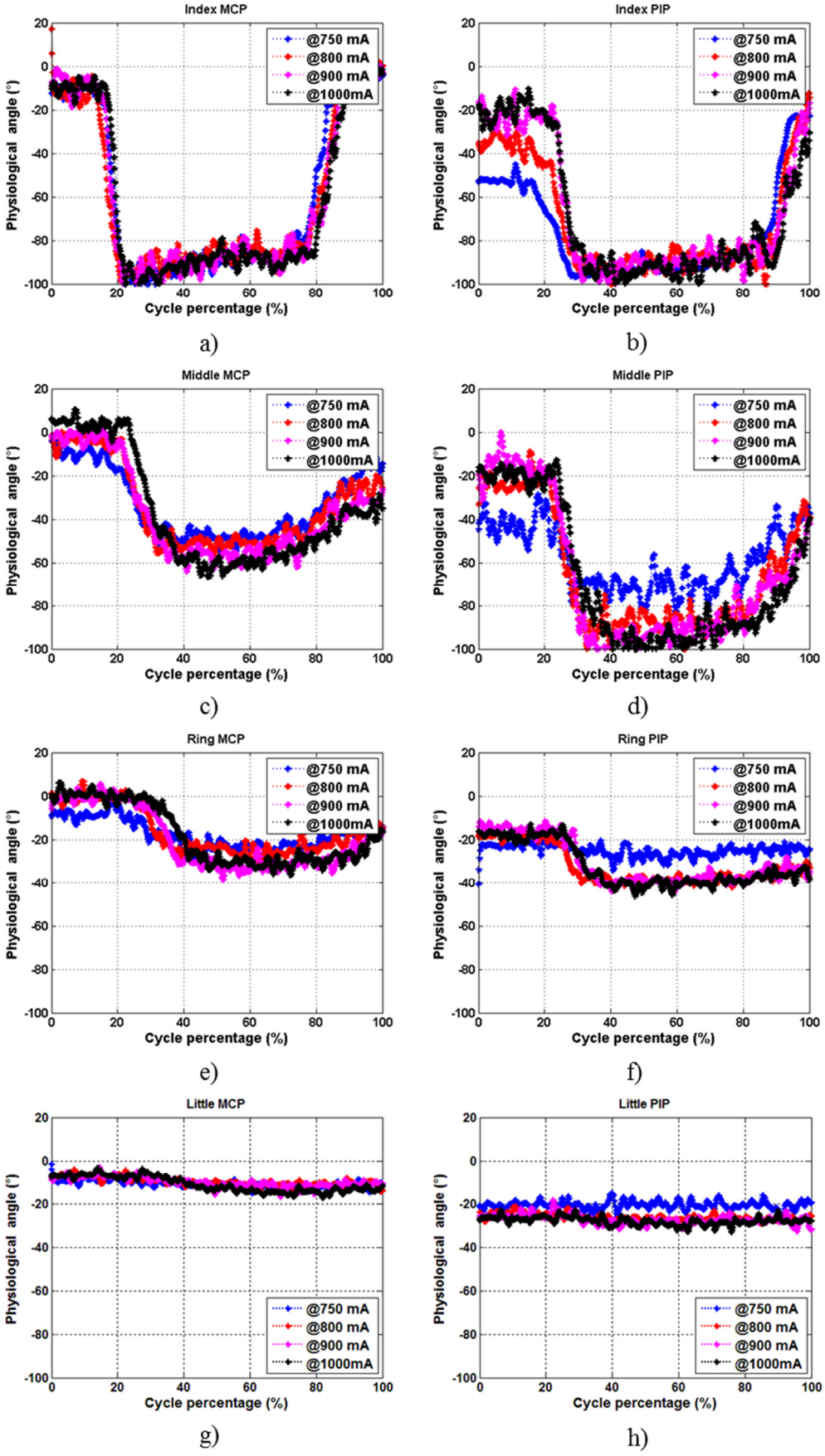

Fig. 120. Influence of current consumption on the finger phalange values. The motor speed during the test is constant at 150 rpm.

Considering the weight properties of the dummy hand, it is possible compare the simulated behavior with the experimental one for the each finger movement.

The figure below (Fig. 121) shows the comparison between the simulated and the experimental behavior of physiological angles for each actuated finger. In particular, Fig. 121 a) reported the angle of index finger; in continues blue line is represented the MCP angle joint while solid red line the PIP one; both of them are obtained by mathematical model. Fig. 121 b) reported the same variables obtained by the experiments: blue dots line is the experimental value of MCP joint while the red dots line is the PIP one. Analogue representation is followed for middle finger (c and d), ring (e and f) and finally little (g and h).

It is possible to highlight a good correlation between theoretical and experimental trend. Nevertheless, it is possible notice also, how the wire pre-loaded influence startup and final phases. In fact, a weak pre-load create a delay between input kinematic action and output ones. Pre-load affects all fingers and the most distant one, for instance little, are mainly affected by it. The low wires' pre-load influence also the finger ROM, it is possible notice this behavior around 50 % of cycle percentage. This effect is explainable as follow: when the movable pulley starts to move before pull, the wire have to stretch it and only after that, the pulling wire moves the fingers or the other differential elements. In addition, we have to keep in mind presence of internal frictions due to sliding friction and to sliding cable on different routing. It is remarkable that also in this case a major impact occurs for ring and little fingers.

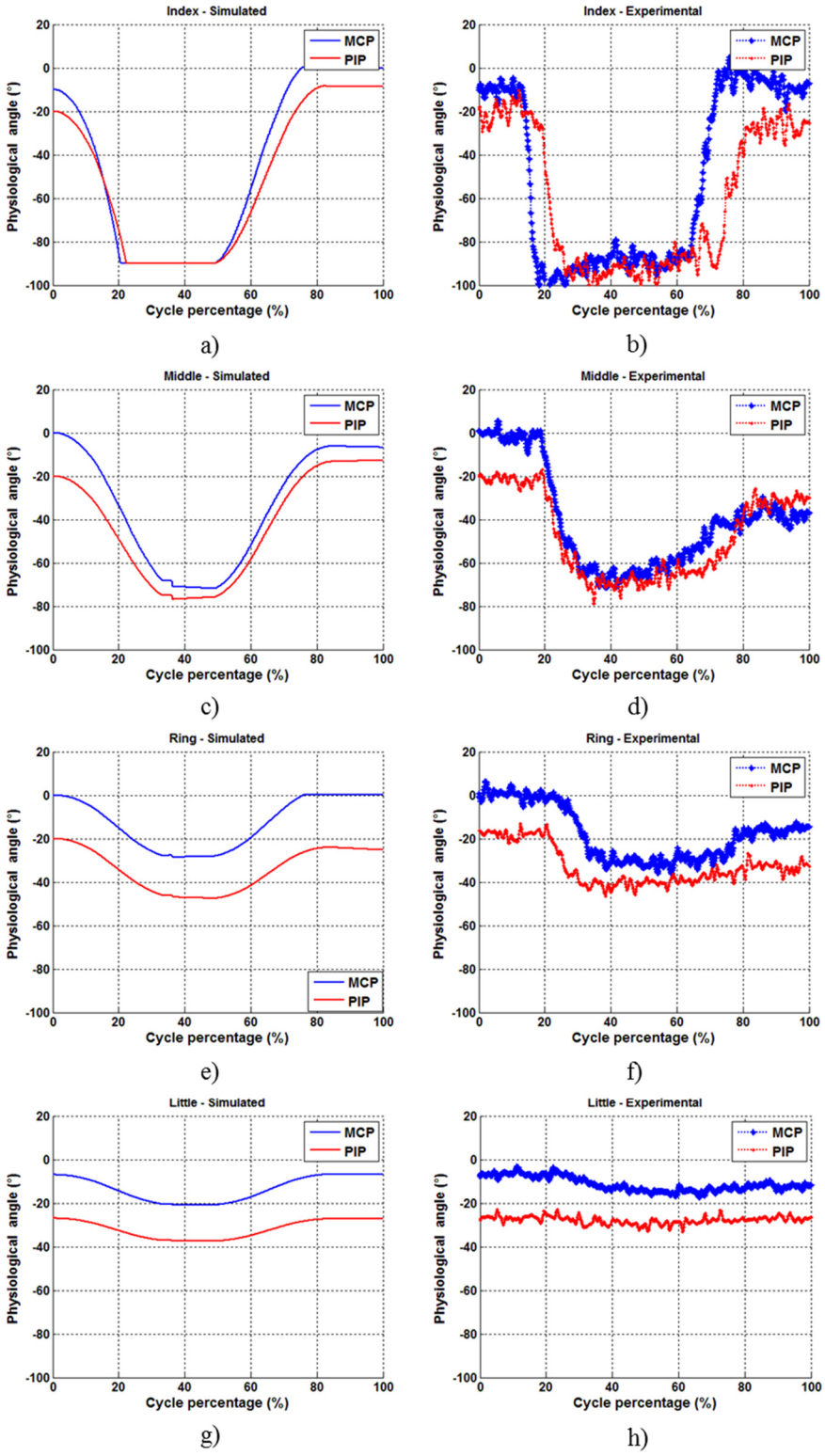

Fig. 121. Comparison between the simulated and experimental behavior of ReHand2 fingers. Graph a), c) e) and g) show the physiological angles of metacarpal phalangeal (MCP, blue lines) and proximal interphalangea (PIP red lines) given by the mathematical model for each finger while b), d), f) and h) represent the experimental data. The experimental data are represented the MCP with blue dots lines and PIP with dots red lines.

7.5 sEMG-control tests

For what concerns the sEMG part, an armband of six dry electrodes is placed around the forearm of the subject. A scheme of the sEMG armband is shown in the figure below (Fig. 122). The use of armband is more simple and comfortable respect to the positioning of two electrodes but require a calibration. The sEMG band calibration allows to identify two groups of electrodes, respectively related to the muscles, which will drive the finger extension and flexion.

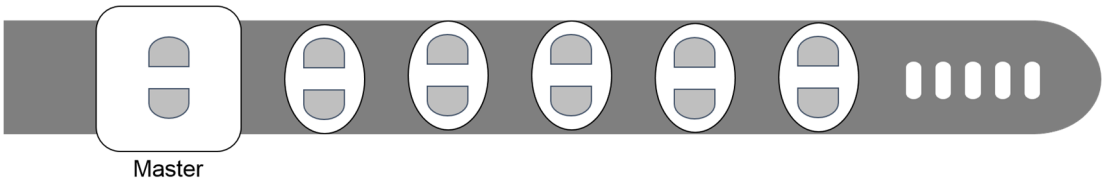

Fig. 122. Concept of sEMG armband. The armband is composed by six dry-electrodes and one of them is the master, which provide also the signal conditioning and the appropriate gains.

The control strategy is currently the industrial state-of-the-art of myoelectric hand prosthesis. When the detected myoelectric signal, associated to finger flexion, exceeds a threshold, it means that the subject has begun a closing gesture and a velocity signal is given to the actuator. When the hand is closing, independently from the configuration due to the grasped object, an amount of force is transmitted to the subject. A software-imposed limitation of current on the actuator translates into a torque –and then in force- limitation on the device. This closing force is provided even if the detected sEMG signal, after the actuator activation, goes to zero. In other words, the subject wearing the exoskeleton is not required to exert continuously force to maintain the assistance from the device. When the subject activates the extension muscles and the sEMG electrodes detect this activity, the actuating force decreases and changes the sign in order to help the extension of the fingers. In the below scheme (Fig. 123) is reported a conceptual scheme using in the sEMG-control.

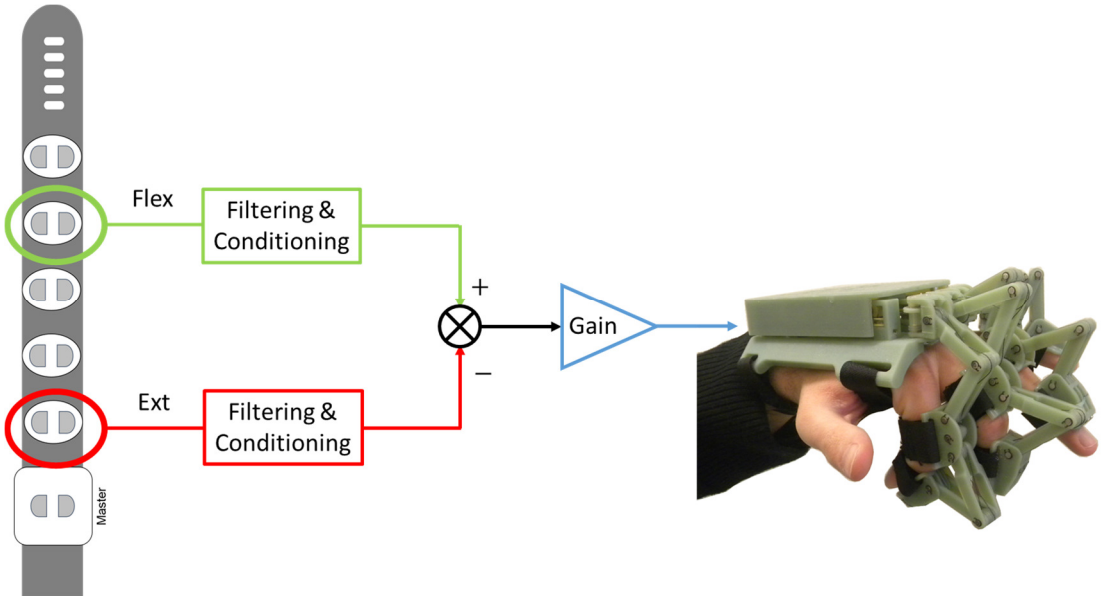

Fig. 123. Conceptual scheme of the sEMG-control. The filtering & conditioning blocks are composited by filter in order to remove the 50 Hz noise, the introduction of death band and saturation as well as gain. Finally, the last gain consists to refer the generated muscle signal to speed or current reference signal to motor.

Tests with the sEMG-control on ReHand2 are ongoing. The sEMG tests foreseen two different types of tests, one with the dummy hand and the second using a mirrored control as the predecessor. At present, some preliminary tests are performed with the dummy hand, but it is believed that the available data are not sufficient for an exhaustive presentation.

7.6 Discussion

In this chapter are presented the preliminary results obtained with the demonstrator ReHand2. The experimental results starting from the kinetostatic tests performed in two different hand shapes, following by the evaluation of the system's performance obtained in hand free motion, and finally, the dynamic tests.

These tests have shown interesting performances that can be optimized by changing the material (i.e. using low friction materials) and modifying the robustness of some critical components as well as the necessity to foresee wire tensioner not only on the fingertip but also in the backhand mechanism. These improvements can determine an increase on whole system performances.

7.6 Discussion

The experimentation with healthy human hand, which wears ReHand2, will provide also the introduction and tests of the sEMG control.

It is better to keep in mind that the ReHand2 mechanism can be exploited also in order to develop assistive and/or empower devices. In comparison with the state-of-the-art technology, the main advantages of ReHand2 can be summarized in the following three cornerstones:

1. Bidirectional underactuation;
2. Adaptable to grasping object.

The main aspect involves the bidirectional underactuation solution, which permits to drive the flexion and extension of fingers in a controlled way, with only one actuator. Considering the whole system, for example the Hand of Hope (K Y Tong et al. 2013), as well as other exoskeletons present on the market or research prototypes (A. Chiri et al. 2012) (Cempini et al. 2013) (Wege and Hommel 2005) and (Yamaura et al. 2009), even if they usually present underactuation at the finger level of each finger, they do not exploit the underactuation at the inter-finger level or a tendon-driven bidirectional underactuation.
This fact implies an increase in weight, bulk, power consumption, cost and the use of complexity control logic. This complexity increases in an user-driven control, where the human-machine interface (HMI) of the robotic system has to be capable of detecting the subject intentions to move the hand. For this purpose, the system can be sensorized by deploying pressure/force or bent sensors in the finger phalanges: when the human finger exerts force or move the finger, the exoskeleton detects it and the actuator drives the exoskeleton in order to assist the human one. This strategy adapts well when there is one –or more- motors for each finger. The main drawback is the increase in cost and complexity: lots of sensors, lots of cable connections and conditioning circuits, and a control logic for each actuator. Moreover, the force/position triggering cannot be applied in the patients that are highly disabled and thereby unable to generate finger movements.

The latter case can be addressed by using surface electromyography (sEMG) to detect the subject's intention, even when the muscle is unable to produce detectable forces, residual electrical activity might still be present. This strategy involves the use of EMG signals to detect the flexion/extension of the hand fingers. Detecting the single finger

movement using sEMG electrodes is a very difficult task; while it is quite plain to understand when the hand is globally closed or opened even in dynamic condition, (this technique of two sEMG electrodes is currently applied to drive commercial hand prostheses for amputees). Thus, with only two sEMG electrodes and an exoskeleton with a motor for each finger, it is necessary to translate the global opening/closing signal into command signals for each finger actuator, realizing some sort of synergy (or coordination) among the fingers. This translation is implemented in the software control logic and, as such, is a design choice, hence consisting in a compromise, based on somewhat arbitrary assumptions and always prone to errors.

Chapter 8 Conclusion and discussion

8.1 Conclusion

The concept, design and preliminary validation for a hand exoskeleton namely ReHand2 is described in this dissertation. ReHand2 is a wearable active exoskeleton; it aims to improve rehabilitation, both in clinical and home environments, and acts as support to individuals suffering for hand impairment following a neurological disorder or injury in daily life activities.

This dissertation is opened describing the context where ReHand2 would place. In particular, 200000 strokes happen every year in Italy, with 20 % of mortality and about 130000 people are affected by lost of upper limbs mobility. In addition, the traditional manipulation recover only about 50 - 65 % of upper limb mobility often neglecting the hands, because the cost overcome the benefits. In this depicted scenario, arises the idea to develop a compact, lightweight, intrinsically safe and compliant hand exoskeleton with the aim to help physiotherapists during the patients' rehabilitation.

As the second step the analysis of the bio-mechanic of the hand, where the hands' size are described as well as static and dynamic constraints, are analyzed. Afterward, the state of the art on current technologies for hand exoskeleton are introduced before entering in the detailed on the developed prototypes and commercialized products. The proposed classification of the state of art, allows to develop a series of constraint and

guidelines useful during the design of a new hand exoskeleton. The guidelines can be list in the following points:

I. Range of motion:
II. Compactness;
III. Energy consumption;
IV. Comfortability and wearability;
V. Force level;
VI. HMI (Human Machine Interface);
VII. Safety.

Based on these aspects, it was proposed and studied the underactuation. Exploiting the underactuation principle, it was developed ReHand. ReHand is a wearable hand exoskeleton, which assists the finger's flexion. The tester is composed by the sequence of two modules: finger and inter-finger. The backhand (or inter-finger module) is composed by a series of three differential elements, which split the single input action into four outputs. Also the finger module is based on underactuation concept using a series of classical four bar mechanisms. The mechanism assisted the finger flexion; instead, the extension is guarantee passively by the presence of elastic elements. The synthesis design is performed with a stochastic algorithm (Simulated Annealing Algorithm) and the mechanism geometry is optimized in terms of range of motion, dimension, GCI and interference. The finger exoskeleton foreseen also the passive abduction/adduction of the MCP joint, which is necessary to adapt the system to grasp object with different size and shape. During ReHand conceived phase a kinetostatic model is developed. Then the prototype is realized with 3D printing technology and successively validate with kinetostatic tests and sEMG-control.

ReHand shows some limitations concerning the wires loss, the wearability and the comfortability for both modules. Discussions with physiotherapists and clinical engineers, underling the necessity to develop a control extension of the hand in order to transform the assistive device in a rehabilitation one. The advices, coming from physiotherapist, pushed us to conceive a new underactuated hand exoskeleton, namely ReHand2.

ReHand2 is conceived using the underactuation, as its predecessor, but introduce and implement a new tendon-driven mechanism for the backhand module. The backhand

mechanisms allows to drive both flexion and extension of the fingers using a tendon mechanism. According with bidirectional backhand module, also finger module is updated. For both modules are implemented and studied the design and develop a dynamical model. From the idea to the realization, ReHand2 demonstrator is manufactured at mechanical workshop (MWS@IIT) of the Italian Institute of Technology (Genova), and then the device was delivered to Artificial Physiology Lab (APLab) at IIT@PoliTo (Torino) for assembled and successive validation. Different experimental tests are done in order to characterize ReHand2 using a sensorized dummy hand and test bench.

Results obtained by experiments are promising and demonstrate the usability of proposed exoskeleton system for hand training in grasping tasks, but there are also underling its actual limits. Typical issues of tendon driven mechanism are connected with wires tensioning, and this mechanism does not exception. In particular, actual tensioner are not sufficient to guarantee a sufficient pre-load on backhand module, instead, for the finger the tensioning of the wires is suitable and sufficient compact. Another aspect to evaluate carefully, it is the choice of the material in order to decrease, where possible, the slip friction between the parts. Despite, the demonstrator's limitations has shown great potentiality of the concept for the wearable and the empower robotics. In particularly, compactness conjoint to the limited weight and the great adaptability make ReHand an interesting demonstrator for the future generation of rehabilitation device for both home and clinics. It is better keep in mind that ReHand can be adapted also for assistive but above all for the empower tasks.

In conclusion, the originality of ReHand2 respect to the current state of the art can be summarized in the following points:

I. *Lightweight and energy optimized design*: the underactuation principle exploits only one actuator for the both tendon-driven flexion and extension of fingers, significantly reducing weight since actuators are often the heaviest components. In particular, the weight of current prototype is about 300g without actuator and about 550g with it.
II. *High performance capabilities to interact with environment*: the mechanical structure is designed to adapt itself, while grasping, to the held object.
III. *Dexterous device with limited encumbrance*: the entire palm of the hand and the fingertips are left free from the exoskeleton, thus leaving the user the

possibility to manipulate objects. Moreover, the mechanical structure does not force the hand in predefined positions, and the fingers are free to move along the degrees of freedom which are not actuated.

IV. *Intrinsically safe mechatronic systems*: ReHand2 exploits mechanical strategies for patients' safety, because it implements a backdriveability mechanism.

V. *Low cost realization*, it is possible reduce the realization cost and in the same time obtain a robust and lightweight structure using polymeric materials and only one actuator (the cost of the prototype is less than 2500€ plus actuator). The cost can decrease in the case of a small series mostly for the metallic parts.

VI. *High interaction with the* user: EMG interface detects the user's intention and allows for an easy interaction with the user.

8.2 Further developments

Prototype validation on healthy subjects as well as trials on relevant environment, such as clinical and hospital, on post stroke patients, it is essential to in order to perform a clinical validation on impaired patient. In particular, these tests will be performed with a sEMG-control in order to improve the rehabilitation using not only the adaptability of the device (task-oriented rehabilitation) but also exploit the patient's intention of movement, in order to stimulate the patient to perform actively the assigned tasks.

The developed ReHand2 has shown interesting properties, and it has made an opening to future development and improvements. Firstly, ReHand2 requires an active thumb, as well as implementation of several force synergies (or force distributions), with aim to help the user with different tasks of the ADLs. Concerning the thumb's design: different strategies will be considered, starting from the use of underactuated principles at the inter-finger and intra-finger level as the use of independent actuators, in order to perform also the thumb rehabilitation. Introduce several force distribution is not really new, in fact several prototype of undercatuated prosthesis implement different force synergies but this fact require to increase the number of actuators with the consequent increasing of weight. The challenge is to use only one actuator with a sort of "gearbox" and control different force distributions. Secondly, the development of an active wrist, which allows at least the flexion and the extension movements completely independent

form hand module actuator. The wrist module should allow to optimize the location of the DC motor as well as the improvement of the volumetric exploitation coefficient on the hand mechanism.

Appendix 1

Considering a generic distal phalange it is possible wrote the entire dynamical model as follow:

$$T_{Fing} = \frac{1}{2}\left(m_{Fing} \cdot \|\boldsymbol{v_{fing}}\|^2 + I_{Fing} \cdot \dot{\vartheta}_{Ph}^2\right)$$

$$T_{Exo} = \frac{1}{2}\left(m_{Exo} \cdot \|\boldsymbol{v_{exo}}\|^2 + I_{Exo} \cdot \dot{\vartheta}_{Ph}^2\right)$$

$$T_{p_{j+1_1}} = \frac{1}{2}\left(m_{p_{j+1_1}} \cdot \left\|\boldsymbol{v_{p_{j+1_1}}}\right\|^2 + I_{p_{j+1_1}} \cdot \dot{\varphi}_{j+1_1}{}^2\right)$$

$$T_{p_{j+1_2}} = \frac{1}{2}\left(m_{p_{j+1_2}} \cdot \left\|\boldsymbol{v_{p_{j+1_2}}}\right\|^2 + I_{p_{j+1_2}} \cdot \dot{\varphi}_{j+1_2}{}^2\right)$$

$$T_{tot} = T_{Fing} + T_{Exo} + T_{p_{j+1_1}} + T_{p_{j+1_2}}$$

Where m_{Fing} and I_{Fing} are respectively the mass and the inertia of finger phalange, m_{Exo} and I_{Exo} are the weight properties of exoskeleton phalange, while $m_{p_{j+1_k}}$ is the bar mass and $I_{p_{j+1_k}}$ is the link inertia. The velocity can be computed as follow:

$$\|\boldsymbol{v_{fing}}\| = \|\boldsymbol{e}_{fing}\| \cdot \dot{\vartheta}_{Ph} \rightarrow \|\boldsymbol{v_{fing}}\|^2 = \|\boldsymbol{e}_{fing}\|^2 \cdot \dot{\vartheta}_{Ph}^2$$

$$\|\boldsymbol{v_{exo}}\| = \|\boldsymbol{e}_{exo}\| \cdot \dot{\vartheta}_{Ph} \rightarrow \|\boldsymbol{v_{exo}}\|^2 = \|\boldsymbol{e}_{exo}\|^2 \cdot \dot{\vartheta}_{Ph}^2$$

$$\left\|\boldsymbol{v_{p_{j+1_1}}}\right\| = \left\|\boldsymbol{e_{p_{j+1_1}}}\right\| \cdot S_1\left(\varphi_{j+1_1}, \varphi_{j+1_2}, \vartheta_{Ph}\right) \cdot \dot{\vartheta}_{Ph}^2 \rightarrow \left\|\boldsymbol{v_{p_{j+1_1}}}\right\|^2 = \left\|\boldsymbol{e_{p_{j+1_1}}}\right\|^2 \cdot \left(S_1\left(\varphi_{j+1_1}, \varphi_{j+1_2}, \vartheta_{Ph}\right)\right)^2 \cdot \dot{\vartheta}_{Ph}^2$$

$$\left\|\boldsymbol{v_{p_{j+1_2}}}\right\|^2 = p_{j+1_1}{}^2 \dot{\varphi}_{j+1_1}{}^2 + \left\|\boldsymbol{e_{p_{j+1_2}}}\right\|^2 \dot{\varphi}_{j+1_2}{}^2 + 2p_{j+1_1}\left\|\boldsymbol{e_{p_{j+1_2}}}\right\| \dot{\varphi}_{j+1_1}\dot{\varphi}_{j+1_2}\cos(\varphi_{j+1_1} - \varphi_{j+1_2})$$

Appendix 1

Still:

$$\left\|\boldsymbol{v}_{\boldsymbol{p}_{j+1_2}}\right\|^2$$
$$= \left[{p_{j+1_1}}^2 \left(S_1\left(\varphi_{j+1_1}, \varphi_{j+1_2}, \vartheta_{Ph}\right)\right)^2 + \left\|e_{p_{j+1_2}}\right\|^2 \left(S_2\left(\varphi_{j+1_1}, \varphi_{j+1_2}, \vartheta_{Ph}\right)\right)^2\right.$$
$$+ 2p_{j+1_1} \left\|e_{p_{j+1_2}}\right\| \left(S_1\left(\varphi_{j+1_1}, \varphi_{j+1_2}, \vartheta_{Ph}\right)\right)^2 \left(S_2\left(\varphi_{j+1_1}, \varphi_{j+1_2}, \vartheta_{Ph}\right)\right)^2 cos(\varphi_{j+1_1}$$
$$\left. - \varphi_{j+1_2})\right] \cdot \dot{\vartheta}_{Ph}^2$$

Where $L_{Cp_{j+1_k}}$ is the norm of the $k-th$ link center of mass vector, and p_{j+1_k} is the length of $k-th$ link. Calling:

$$I_{fing,eq} = \frac{1}{2}\left(m_{Fing} \cdot \left\|\boldsymbol{e}_{fing}\right\|^2 + I_{Fing}\right)$$

$$I_{exo,eq} = \frac{1}{2}\left(m_{Exo} \cdot \|\boldsymbol{e}_{exo}\|^2 + I_{Exo}\right)$$

$$I_{p_{j+1_1},eq} = \frac{1}{2}\left(m_{p_{j+1_1}} \cdot \left\|\boldsymbol{e}_{\boldsymbol{p}_{\boldsymbol{j+1_1}}}\right\|^2 + I_{p_{j+1_1}} + m_{p_{j+1_2}} \cdot {p_{j+1_1}}^2\right)$$

$$I_{p_{j+1_2},eq} = \frac{1}{2}\left(m_{p_{j+1_2}} \cdot \left\|\boldsymbol{e}_{\boldsymbol{p}_{\boldsymbol{j+1_2}}}\right\|^2 + I_{p_{j+1_2}}\right)$$

$$P_1 = 2m_{p_{j+1_2}} p_{j+1_1} \left\|\boldsymbol{e}_{\boldsymbol{p}_{\boldsymbol{j+1_2}}}\right\|$$

$$C_1 = cos\left(\varphi_{j+1_1} - \varphi_{j+1_2}\right)$$

The total kinetic energy of the entire system is:

$$T_{tot} = \left[I_{fing,eq} + I_{exo,eq} + I_{p_{j+1_1},eq}\left(S_1\left(\varphi_{j+1_1}, \varphi_{j+1_2}, \vartheta_{Ph}\right)\right)^2\right.$$
$$+ I_{p_{j+1_2},eq}\left(S_2\left(\varphi_{j+1_1}, \varphi_{j+1_2}, \vartheta_{Ph}\right)\right)^2$$
$$\left. + P_1 C_1 \left(S_1\left(\varphi_{j+1_1}, \varphi_{j+1_2}, \vartheta_{Ph}\right)\right)\left(S_2\left(\varphi_{j+1_1}, \varphi_{j+1_2}, \vartheta_{Ph}\right)\right)\right] \cdot \dot{\vartheta}_{Ph}^2$$

Neglecting the gravitational potential energy, the Lagrangian can be wrote as:

$$\mathcal{L} = T_{tot}$$

The Euler-Lagrange equation can be computed as follow:

$$\frac{d}{dt}\left(\frac{\partial \mathcal{L}}{\partial \dot{\vartheta}_{Ph}}\right) - \left(\frac{\partial \mathcal{L}}{\partial \vartheta_{Ph}}\right) = \tau_{\vartheta}$$

Then:

$$H(\vartheta_{Ph}) \cdot \ddot{\vartheta}_{Ph} + C\left(\vartheta_{Ph}, \dot{\vartheta}_{Ph}\right) \cdot \dot{\vartheta}_{Ph} + G(\vartheta_{Ph}) = \tau_{\vartheta}$$

Where:

$$H(\vartheta_{Ph})$$
$$= 2\left[I_{Fing,eq} + I_{Exo,eq} + I_{L_1,eq}\left(S_1\left(\varphi_{j+1_1}, \varphi_{j+1_2}, \vartheta_{Ph}\right)\right)^2\right.$$
$$+ I_{L_2,eq}\left(S_2\left(\varphi_{j+1_1}, \varphi_{j+1_2}, \vartheta_{Ph}\right)\right)^2$$
$$\left. + P_1 C_1\left(\varphi_{j+1_1}, \varphi_{j+1_2}\right)\left(S_1\left(\varphi_{j+1_1}, \varphi_{j+1_2}, \vartheta_{Ph}\right)\right)\left(S_2\left(\varphi_{j+1_1}, \varphi_{j+1_2}, \vartheta_{Ph}\right)\right)\right]$$

$$C\left(\vartheta_{Ph}, \dot{\vartheta}_{Ph}\right)$$
$$= \left\{2I_{L_1,eq}\left(S_1\left(\varphi_{j+1_1}, \varphi_{j+1_2}, \vartheta_{Ph}\right)\right) \cdot \left[2A_1 - \frac{\partial}{\partial \vartheta_{Ph}}\left(S_1\left(\varphi_{j+1_1}, \varphi_{j+1_2}, \vartheta_{Ph}\right)\right)\right]\right.$$
$$+ I_{L_2,eq}\left(S_2\left(\varphi_{j+1_1}, \varphi_{j+1_2}, \vartheta_{Ph}\right)\right)\left[2A_2 - \frac{\partial}{\partial \vartheta_{Ph}}\left(S_2\left(\varphi_{j+1_1}, \varphi_{j+1_2}, \vartheta_{Ph}\right)\right)\right] + P_1$$
$$\cdot \left[2A_3\left(S_1\left(\varphi_{j+1_1}, \varphi_{j+1_2}, \vartheta_{Ph}\right)\right)\left(S_2\left(\varphi_{j+1_1}, \varphi_{j+1_2}, \vartheta_{Ph}\right)\right)\right.$$
$$+ 2C_1\left(\varphi_{j+1_1}, \varphi_{j+1_2}\right)A_1\left(S_2\left(\varphi_{j+1_1}, \varphi_{j+1_2}, \vartheta_{Ph}\right)\right)$$
$$+ 2C_1\left(\varphi_{j+1_1}, \varphi_{j+1_2}\right)\left(S_1\left(\varphi_{j+1_1}, \varphi_{j+1_2}, \vartheta_{Ph}\right)\right)A_2$$
$$- \left(\frac{\partial}{\partial \vartheta_{Ph}}\left[C_1\left(\varphi_{j+1_1}, \varphi_{j+1_2}\right)\right]\left(S_1\left(\varphi_{j+1_1}, \varphi_{j+1_2}, \vartheta_{Ph}\right)\right)\left(S_2\left(\varphi_{j+1_1}, \varphi_{j+1_2}, \vartheta_{Ph}\right)\right)\right.$$
$$+ C_1\left(\varphi_{j+1_1}, \varphi_{j+1_2}\right)\frac{\partial}{\partial \vartheta_{Ph}}\left[\left(S_1\left(\varphi_{j+1_1}, \varphi_{j+1_2}, \vartheta_{Ph}\right)\right)\right]\left(S_2\left(\varphi_{j+1_1}, \varphi_{j+1_2}, \vartheta_{Ph}\right)\right)$$
$$\left.\left.\left. + C_1\left(\varphi_{j+1_1}, \varphi_{j+1_2}\right)\left(S_1\left(\varphi_{j+1_1}, \varphi_{j+1_2}, \vartheta_{Ph}\right)\right)\frac{\partial}{\partial \vartheta_{Ph}}\left(S_2\left(\varphi_{j+1_1}, \varphi_{j+1_2}, \vartheta_{Ph}\right)\right)\right)\right]\right\} \cdot \dot{\vartheta}_{Ph}$$

$$G(\vartheta_{Ph}) = 0$$

$$\frac{d}{dt}\left(S_1\left(\varphi_{j+1_1}, \varphi_{j+1_2}, \vartheta_{Ph}\right)\right) = A_1\dot{\vartheta}_{Ph}$$

$$\frac{d}{dt}\left(S_2\left(\varphi_{j+1_1}, \varphi_{j+1_2}, \vartheta_{Ph}\right)\right) = A_2\dot{\vartheta}_{Ph}$$

$$\frac{d}{dt}\left(C_1\left(\varphi_{j+1_1}, \varphi_{j+1_2}\right)\right) = A_3\dot{\vartheta}_{Ph}$$

Simplifying the mathematical model, neglecting the weight properties of the external links, the total kinetic energy can be wrote as:

$$T_{tot} = \left[I_{Fing,eq} + I_{Exo,eq}\right] \cdot \dot{\vartheta}_{Ph}^2$$

The Euler-Lagrangian can be wrote as follow:

$$2\left[I_{Fing,eq} + I_{Exo,eq}\right] \cdot \ddot{\vartheta} = \tau_{\vartheta}$$

The comparison between both models can be observed in the following figure:

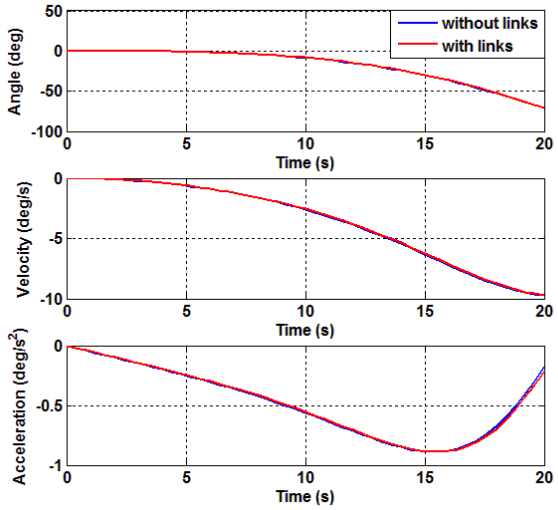

Fig. 124. Comparison between simulation results obtained considering the external links (red line) and without considering the weight properties of them.

Fig. 124 shows the comparison between the behaviors the equation of the motion for the imposed condition considering the weight properties of external links (red line) and neglecting them (blue line). From this comparison, it is possible neglect the external links weight properties committing a negligible error.

Appendix 2

The wire length can be wrote, for the generic path as:

$$l_{wire} = R_{j_1} \cdot \gamma_1 + R_{j_2} \cdot \gamma_2 + R_{j_3} \cdot \gamma_3 + \sqrt{{p_{j_1}}^2 - \left(R_{j_1} + R_{j_2}\right)^2} + \sqrt{{p_{j_2}}^2 - \left(R_{j_2} + R_{j_3}\right)^2} + R_{j+1_1} \cdot \gamma_5 + R_{j+1_2} \cdot \gamma_6 + R_{j+1_3} \cdot \gamma_7 + \sqrt{{p_{j+1_1}}^2 - \left(R_{j+1_1} + R_{j+1_2}\right)^2} + \sqrt{{p_{j+1_2}}^2 - \left(R_{j+1_2} + R_{j+1_3}\right)^2} + Constant$$

Differentiating on time:

$$\dot{l}_{wire} = R_{j_1} \cdot \dot{\gamma}_1 + R_{j_2} \cdot \dot{\gamma}_2 + R_{j_3} \cdot \dot{\gamma}_3 + R_{j+1_1} \cdot \dot{\gamma}_5 + R_{j+1_2} \cdot \dot{\gamma}_6 + R_{j+1_3} \cdot \dot{\gamma}_7$$

That can be wrote also in this compact form:

$$\dot{l}_{wire} = [A(\boldsymbol{\vartheta})] \cdot \dot{\boldsymbol{\vartheta}}$$

For the flexion path, it is possible wrote the following winding angle on the idler pulleys:

$${\gamma_1}^F = \left\| atan\left(\frac{k_{xx_j}}{k_{yy_j}}\right) \right\| + \varphi_{j_1} - \varepsilon_{j_1}$$

$${\gamma_2}^F = \pi - \varphi_{j_2} + \varphi_{j_1} - \varepsilon_{j_1} - \varepsilon_{j_2}$$

$${\gamma_3}^F = \vartheta_{Ph,1} - \varphi_{j_2} - \varepsilon_{j_2} + atan\left(\frac{k_{11_j}}{k_{22_j}}\right)$$

$${\gamma_5}^F = \left\| atan\left(\frac{k_{xx_{j+1}}}{k_{yy_{j+1}}}\right) \right\| + \varphi_{j+1_1} - \varepsilon_{j+1_1}$$

$${\gamma_6}^F = \pi - \varphi_{j+1_2} + \varphi_{j+1_1} - \varepsilon_{j+1_1} - \varepsilon_{j+1_2}$$

Appendix 2

$$\gamma_7{}^F = \vartheta_{Ph,2} - \varphi_{j+1_2} - \varepsilon_{j+1_2} + atan\left(\frac{k_{11_{j+1}}}{k_{22_{j+1}}}\right)$$

Where:

$$\varepsilon_{j_k} = \frac{R_{j_k} + R_{j_{(k+1)}}}{p_{j_k}}$$

$$\varepsilon_{j+1_k} = \frac{R_{j+1_k} + R_{j+1_{(k+1)}}}{p_{j+1_k}}$$

Differentiating the winding angle on time, it is possible obtain the following relationship:

$$\dot{\gamma}_1{}^F = \dot{\varphi}_{j_1}$$

$$\dot{\gamma}_2{}^F = \dot{\varphi}_{j_1} - \dot{\varphi}_{j_2}$$

$$\dot{\gamma}_3{}^F = \dot{\vartheta}_1 - \dot{\varphi}_{j_2}$$

$$\dot{\gamma}_5{}^F = \dot{\varphi}_{j+1_1}$$

$$\dot{\gamma}_6{}^F = \dot{\varphi}_{j+1_1} - \dot{\varphi}_{j+1_2}$$

$$\dot{\gamma}_7{}^F = \dot{\vartheta}_2 - \dot{\varphi}_{j+1_2}$$

Similar reasoning can be performed on the extension path. The extension's winding angle on the idler pulleys can be wrote as reported below:

$$\gamma_1{}^E = 3\pi - \varepsilon_{j_1} - \varphi_{j_1} - \left\| atan\left(\frac{k_{xx_j}}{k_{yy_j}}\right) \right\|$$

$$\gamma_2{}^E = 3\pi - \varepsilon_{j_1} - \varepsilon_{j_2} - \left(\varphi_{j_1} - \dot{\varphi}_{j_2}\right)$$

$$\gamma_3{}^E = 3\pi - \varepsilon_{j_2} - atan\left(\frac{k_{11_j}}{k_{22_j}}\right) - \left(\vartheta_{Ph,1} - \dot{\varphi}_{j_2}\right)$$

$$\gamma_5{}^E = 3\pi - \varepsilon_{j+1_1} - \varphi_{j+1_1} - \left\| atan\left(\frac{k_{xx_{j+1}}}{k_{yy_{j+1}}}\right) \right\|$$

$$\gamma_6{}^E = 3\pi - \varepsilon_{j+1_1} - \varepsilon_{j+1_2} - \left(\varphi_{j+1_1} - \varphi_{j+1_2}\right)$$

$$\gamma_7{}^E = 3\pi - \varepsilon_{j+1_2} - atan\left(\frac{k_{11_{j+1}}}{k_{22_{j+1}}}\right) - \left(\vartheta_{Ph,2} - \varphi_{j+1_2}\right)$$

Differentiating on time:

$$\dot{\gamma}_1{}^E = -\dot{\varphi}_{j_1}$$

$$\dot{\gamma}_2{}^E = -\left(\dot{\varphi}_{j_1} - \dot{\varphi}_{j_2}\right)$$

$$\dot{\gamma}_3{}^E = -\left(\dot{\vartheta}_1 - \dot{\varphi}_{j_2}\right)$$

$$\dot{\gamma}_5{}^E = -\dot{\varphi}_{j+1_1}$$

$$\dot{\gamma}_6{}^E = -\left(\dot{\varphi}_{j+1_1} - \dot{\varphi}_{j+1_2}\right)$$

$$\dot{\gamma}_7{}^E = -\left(\dot{\vartheta}_2 - \dot{\varphi}_{j+1_2}\right)$$

In conclusion, considering both wire paths it is possible verify the relationship between finger flexion matrix and extension one.

$$[A(\boldsymbol{\vartheta})]_{ext} = -[A(\boldsymbol{\vartheta})]_{flex}$$

In particular, the $[A(\boldsymbol{\vartheta})]$ matrix for the flexion's path is:

Appendix 2

$$[A(\boldsymbol{\vartheta})]_{flex} =$$

$$= \begin{bmatrix} R_{j_1} & R_{j_2} & R_{j_3} & R_{j+1_1} & R_{j+1_2} & R_{j+1_3} \end{bmatrix} \cdot \begin{bmatrix} 1 & 0 & & & \\ 1 & -1 & & [0]_{3x2} & \\ t_j & -1 & & & \\ & & 1 & 0 & \\ [0]_{3x2} & & 1 & -1 & \\ & & t_{j+1} & -1 & \end{bmatrix}$$

$$\cdot \begin{bmatrix} p_{j_1} sin\left(\varphi_{j_1}\right) & p_{j_2} sin\left(\varphi_{j_2}\right) & & \\ -p_{j_1} cos\left(\varphi_{j_1}\right) & -p_{j_2} cos\left(\varphi_{j_2}\right) & [0]_{2x2} & \\ & & p_{j+1_1} sin\left(\varphi_{j+1_1}\right) & p_{j+1_2} sin\left(\varphi_{j+1_2}\right) \\ [0]_{2x2} & & -p_{j+1_1} cos\left(\varphi_{j+1_1}\right) & -p_{j+1_2} cos\left(\varphi_{j+1_2}\right) \end{bmatrix}^{-1}$$

$$\cdot \begin{bmatrix} p_{j_3} sin\left(\varphi_{j_3}\right) & \\ -p_{j_3} cos\left(\varphi_{j_3}\right) & [0]_{2x1} \\ & p_{j+1_3} sin\left(\varphi_{j+1_3}\right) \\ [0]_{2x1} & -p_{j+1_3} cos\left(\varphi_{j+1_3}\right) \end{bmatrix}$$

While the matrix for extension:

$$[A(\boldsymbol{\vartheta})]_{ext} =$$

$$= \begin{bmatrix} R_{j_1} & R_{j_2} & R_{j_3} & R_{j+1_1} & R_{j+1_2} & R_{j+1_3} \end{bmatrix} \cdot \begin{bmatrix} -1 & 0 & & & \\ -1 & 1 & & [0]_{3x2} & \\ -t_j & 1 & & & \\ & & -1 & 0 & \\ [0]_{3x2} & & -1 & 1 & \\ & & -t_{j+1} & 1 & \end{bmatrix}$$

$$\cdot \begin{bmatrix} p_{j_1} sin\left(\varphi_{j_1}\right) & p_{j_2} sin\left(\varphi_{j_2}\right) & & \\ -p_{j_1} cos\left(\varphi_{j_1}\right) & -p_{j_2} cos\left(\varphi_{j_2}\right) & [0]_{2x2} & \\ & & p_{j+1_1} sin\left(\varphi_{j+1_1}\right) & p_{j+1_2} sin\left(\varphi_{j+1_2}\right) \\ [0]_{2x2} & & -p_{j+1_1} cos\left(\varphi_{j+1_1}\right) & -p_{j+1_2} cos\left(\varphi_{j+1_2}\right) \end{bmatrix}^{-1} \cdot$$

$$\begin{bmatrix} p_{j_3} sin(\varphi_{j_3}) & \\ -p_{j_3} cos(\varphi_{j_3}) & [0]_{2x1} \\ & p_{j+1_3} sin(\varphi_{j+1_3}) \\ [0]_{2x1} & -p_{j+1_3} cos(\varphi_{j+1_3}) \end{bmatrix}$$

Appendix 3

Using a similar notation of previously appendixes, it is possible wrote the simplified finger dynamical model, the Euler-Lagrangian equations can be wrote in matrix form as:

$$\begin{bmatrix} H_{11} & H_{12} \\ H_{21} & H_{22} \end{bmatrix} \ddot{\boldsymbol{q}} + \begin{bmatrix} C_{11} & C_{12} \\ C_{21} & 0 \end{bmatrix} \dot{\boldsymbol{q}} + \begin{bmatrix} G_{11} \\ G_{21} \end{bmatrix} = - \begin{bmatrix} A_{11} \\ A_{12} \end{bmatrix} F_{wire} + \boldsymbol{\tau}_m + [J(\boldsymbol{q})]^T \cdot \boldsymbol{f}_{ext}$$

The subscript 1 refers to the proximal phalange values, while the 2 subscript concerns the middle phalange values. The elements of inertia matrix $[H]$ can be wrote as:

$$H_{11} = \Big(I_{fing,1_{eq}} + I_{fing,2_{eq}} + 2 \Big(m_{fing,2} L_{12} e_{fing2,x} \cos\big(\vartheta_{Ph,2}\big) + m_{exo,2} \cdot \big(L_{12} e_{exo2,x} \cos(q_2) - L_{12} e_{exo2,y} \sin(q_2) \big) \Big) \Big)$$

$$H_{12} = \Big(\Big(m_{fing,2} L_{12} e_{fing2,x} \cos(q_2) + m_{exo,2} \big(L_{12} e_{exo2,x} \cos(q_2) - L_{12} e_{exo2,y} \sin(q_2) \big) \Big) \Big)$$

$$H_{21} = I_{fing,2_{eq}} + \Big(m_{fing,2} L_{12} L_{CFing,2} \cos(q_2) + m_{exo,2} \big(L_{12} e_{exo2,x} \cos(q_2) - L_{12} e_{exo2,y} \sin(q_2) \big) \Big)$$

$$H_{22} = I_{fing,2_{eq}}$$

The equivalent inertia can be computed as:

$$I_{fing,1_{eq}} = \big(m_{fing,1} {e_{Fing1,x}}^2 + I_{fing,1} + m_{exo,1} \|\boldsymbol{e}_{exo1}\|^2 + I_{exo,1} + \big(m_{fing,2} + m_{exo,2} \big) {L_{12}}^2 \big)$$

Appendix 3

$$I_{fing,2_{eq}} = \left(m_{fing,2} e_{Fing2,x}{}^2 + I_{fing,2} + m_{exo,2}\|\boldsymbol{e}_{exo2}\|^2 + I_{exo,2}\right)$$

$$C_{11} = \Big(2\dot{q}_2 \Big(-m_{fing,2} L_{12} e_{fing2,x}\, sin(q_2) + m_{exo,2}\big(-L_{12} e_{exo2,x}\, sin(q_2) - L_{12} e_{exo2,y} cos(q_2)\big)\Big)\Big)$$

$$C_{12} = \Big(\Big(-m_{fing,2} L_{12} e_{Fing2,x}\, sin(q_2) + m_{exo,2}\big(-L_{12} e_{exo2,x}\, sin(q_2) - L_{12} e_{exo2,y} cos(q_2)\big)\Big)\dot{q}_2\Big)$$

$$G_{11} = \Bigg[-m_{fing,1}[0 \quad -g]\begin{bmatrix} -sin(q_1) \\ cos(q_1) \end{bmatrix} e_{Fing1,x} - m_{fing,2}[0 \quad -g]\begin{bmatrix} -sin(q_1) L_{12} - sin(q_1 + q_2) e_{Fing2,x} \\ cos(q_1) L_{12} + cos(q_1 + q_2) e_{Fing2,x} \end{bmatrix} - m_{exo,1}[0 \quad -g]\begin{bmatrix} -e_{exo1,x} sin(q_1) - e_{exo1,y} cos(q_1) \\ e_{exo1,x} cos(q_1) - e_{exo1,y} sin(q_1) \end{bmatrix} - m_{exo,2}[0 \quad -g]\begin{bmatrix} -sin(q_1) \cdot L_{12} - e_{exo2,x} sin(q_1 + q_2) - e_{exo2,y} cos(q_1 + q_2) \\ cos(q_1) \cdot L_{12} + e_{exo2,x} cos(q_1 + q_2) - e_{exo2,y} sin(q_1 + q_2) \end{bmatrix}\Bigg]$$

$$C_{21} = -\Big(-m_{fing,2} L_{12} e_{Fing2,x}\, sin(q_2) + m_{exo,2}\big(-L_{12} e_{exo2,x}\, sin(q_2) - L_{12} e_{exo2,y}\, cos(q_2)\big)\Big)\dot{q}_1$$

$$G_{21} = \Bigg(-m_{fing,2}[0 \quad -g]\begin{bmatrix} -sin(q_1 + q_2) \\ cos(q_1 + q_2) \end{bmatrix} e_{Fing2,x} - m_{exo,2}[0 \quad -g]\begin{bmatrix} -e_{exo2,x} sin(q_1 + q_2) - e_{exo2,y} cos(q_1 + q_2) \\ e_{exo2,x} cos(q_1 + q_2) - e_{exo2,y} sin(q_1 + q_2) \end{bmatrix}\Bigg)$$

Considering now, the equation deriving from the wire path, it is possible wrote the following relation:

$$\ddot{q}_2 = \frac{1}{A_{12}}\ddot{l} - \frac{\dot{A}_{11}}{A_{12}}\dot{q}_1 - \frac{A_{11}}{A_{12}} q_1 - \frac{\dot{A}_{12}}{A_{12}}\left(\frac{1}{A_{12}}\dot{l} - \frac{A_{11}}{A_{12}}\dot{q}_1\right)$$

$$= \frac{1}{A_{12}}\ddot{l} - \left(\frac{\dot{A}_{12}}{A_{12}}\frac{1}{A_{12}}\right)\dot{l} - \frac{A_{11}}{A_{12}}\ddot{q}_1 + \left(\frac{\dot{A}_{12}}{A_{12}}\frac{A_{11}}{A_{12}} - \frac{\dot{A}_{11}}{A_{12}}\right)\dot{q}_1$$

$$= \frac{1}{A_{12}}\ddot{l} - \left(\frac{\dot{A}_{12}}{A_{12}{}^2}\right)\dot{l} - \frac{A_{11}}{A_{12}}\ddot{q}_1 + \left(\frac{\dot{A}_{12} \cdot A_{11}}{A_{12}{}^2} - \frac{\dot{A}_{11}}{A_{12}}\right)\dot{q}_1$$

Where A_{11} and A_{12} are the elements of $[A(\boldsymbol{\vartheta})]$ matrix while $\dot{A}_{11}$ and $\dot{A}_{12}$ are their derivatives. Substituting the previously equation in the second Euler-Lagrange equation, it is possible obtain:

$$H_{21}\ddot{q}_1 + H_{22}\left[\frac{1}{A_{12}}\ddot{l} - \left(\frac{\dot{A}_{12}}{{A_{12}}^2}\right)\dot{l} - \frac{A_{11}}{A_{12}}\ddot{q}_1 + \left(\frac{\dot{A}_{12}A_{11}}{{A_{12}}^2} - \frac{\dot{A}_{11}}{A_{12}}\right)\dot{q}_1\right] + C_{21}\dot{q}_1 + G_{21} = -A_{12}F_{wire} + \{\boldsymbol{\tau}_m\}_2 - \{[J(\boldsymbol{q})]^T \cdot \boldsymbol{f}_{ext}\}_2$$

Developing the calculations:

$$\left(H_{21} - \frac{H_{22}A_{11}}{A_{12}}\right)\ddot{q}_1 + \frac{H_{22}}{A_{12}}\ddot{l} + \left[C_{21} + H_{22}\left(\frac{\dot{A}_{12}A_{11}}{{A_{12}}^2} - \frac{\dot{A}_{11}}{A_{12}}\right)\right]\dot{q}_1 - \left(H_{22}\frac{\dot{A}_{12}}{{A_{12}}^2}\right)\dot{l} + G_{21} = -A_{12}F_{wire} + \{\boldsymbol{\tau}_m\}_2 - \{[J(\boldsymbol{q})]^T \cdot \boldsymbol{f}_{ext}\}_2$$

Similarly, on the first equation it is possible obtain, after developing the calculation:

$$\begin{aligned}\left[H_{11} - H_{12}\frac{A_{11}}{A_{12}} - \frac{A_{11}}{A_{12}}\left(H_{21} - \frac{H_{22}A_{11}}{A_{12}}\right)\right]\ddot{q}_1 + \left[\frac{H_{12}}{A_{12}} - \frac{A_{11}}{A_{12}}\frac{H_{22}}{A_{12}}\right]\ddot{l} \\ + \left\{H_{12}\left(\frac{\dot{A}_{12}A_{11}}{{A_{12}}^2} - \frac{\dot{A}_{11}}{A_{12}}\right) + C_{11} - \frac{C_{12}A_{11}}{A_{12}}\right. \\ \left. - \frac{A_{11}}{A_{12}}\left[C_{21} + H_{22}\left(\frac{\dot{A}_{12}A_{11}}{{A_{12}}^2} - \frac{\dot{A}_{11}}{A_{12}}\right)\right]\right\}\dot{q}_1 \\ + \left[-H_{12}\left(\frac{\dot{A}_{12}}{{A_{12}}^2}\right) + \frac{C_{12}}{A_{12}} + \frac{A_{11}}{A_{12}}\left(H_{22}\frac{\dot{A}_{12}}{{A_{12}}^2}\right)\right]\dot{l} + G_{11} - \frac{A_{11}}{A_{12}}G_{21} \\ + \frac{A_{11}}{A_{12}}\{\boldsymbol{\tau}_m\}_2 - \frac{A_{11}}{A_{12}}\{[J(\boldsymbol{q})]^T \cdot \boldsymbol{f}_{ext}\}_2 - \{\boldsymbol{\tau}_m\}_1 + \{[J(\boldsymbol{q})]^T \cdot \boldsymbol{f}_{ext}\}_1 = 0\end{aligned}$$

Finally, the mathematical model can be wrote as:

$$\ddot{q}_1 = -\frac{\left[\frac{H_{12}}{A_{12}} - \frac{A_{11}}{A_{12}}\frac{H_{22}}{A_{12}}\right]}{\left[H_{11} - H_{12}\frac{A_{11}}{A_{12}} - \frac{A_{11}}{A_{12}}\left(H_{21} - \frac{H_{22}A_{11}}{A_{12}}\right)\right]}\ddot{l}$$
$$- \frac{H_{12}\left(\frac{\dot{A}_{12}A_{11}}{{A_{12}}^2} - \frac{\dot{A}_{11}}{A_{12}}\right) + C_{11} - \frac{C_{12}A_{11}}{A_{12}} - \frac{A_{11}}{A_{12}}\left[C_{21} + H_{22}\left(\frac{\dot{A}_{12}A_{11}}{{A_{12}}^2} - \frac{\dot{A}_{11}}{A_{12}}\right)\right]}{\left[H_{11} - H_{12}\frac{A_{11}}{A_{12}} - \frac{A_{11}}{A_{12}}\left(H_{21} - \frac{H_{22}A_{11}}{A_{12}}\right)\right]}\dot{q}_1$$
$$- \frac{\left[-H_{12}\left(\frac{\dot{A}_{12}}{{A_{12}}^2}\right) + \frac{C_{12}}{A_{12}} + \frac{A_{11}}{A_{12}}\left(H_{22}\frac{\dot{A}_{12}}{{A_{12}}^2}\right)\right]}{\left[H_{11} - H_{12}\frac{A_{11}}{A_{12}} - \frac{A_{11}}{A_{12}}\left(H_{21} - \frac{H_{22}A_{11}}{A_{12}}\right)\right]}\dot{l}$$
$$- \frac{\left[G_{11} - \frac{A_{11}}{A_{12}}G_{21} + \frac{A_{11}}{A_{12}}\tau_{m,2} - \frac{A_{11}}{A_{12}}\{[J(\boldsymbol{q})]^T \cdot \boldsymbol{f}_{ext}\}_2 - \tau_{m,1} + \{[J(\boldsymbol{q})]^T \cdot \boldsymbol{f}_{ext}\}_1\right]}{\left[H_{11} - H_{12}\frac{A_{11}}{A_{12}} - \frac{A_{11}}{A_{12}}\left(H_{21} - \frac{H_{22}A_{11}}{A_{12}}\right)\right]}$$

$$F_{wire} = -\frac{1}{A_{12}}\left(H_{21} - \frac{H_{22}A_{11}}{A_{12}}\right)\ddot{q}_1 - \frac{1}{A_{12}}\frac{H_{22}}{A_{12}}\ddot{l}$$
$$- \frac{1}{A_{12}}\left[C_{21} + H_{22}\left(\frac{\dot{A}_{12}A_{11}}{{A_{12}}^2} - \frac{\dot{A}_{11}}{A_{12}}\right)\right]\dot{q}_1 + \frac{1}{A_{12}}\left(H_{22}\frac{\dot{A}_{12}}{{A_{12}}^2}\right)\dot{l} - \frac{1}{A_{12}}G_{21}$$
$$+ \frac{1}{A_{12}}\tau_{m,2} - \frac{1}{A_{12}}\{[J(\boldsymbol{q})]^T \cdot \boldsymbol{f}_{ext}\}_2$$

$$\ddot{q}_2 = \frac{1}{A_{12}}\ddot{l} - \left(\frac{\dot{A}_{12}}{{A_{12}}^2}\right)\dot{l} - \frac{A_{11}}{A_{12}}\ddot{q}_1 + \left(\frac{\dot{A}_{12}A_{11}}{{A_{12}}^2} - \frac{\dot{A}_{11}}{A_{12}}\right)\dot{q}_1$$

The notation $\{\boldsymbol{a}\}_t$ considers only the $t-th$ element of $\boldsymbol{a}$ vector.

List of figures

List of tables

List of tables

Bibliography

Alexander, R McN. 1990. “Three Uses for Springs in Legged Locomotion.” *The International Journal of Robotics Research* 9 (2): 53–61.

An, K N, L J Askew, and E Y Chao. 1986. “Biomechanics and Functional Assessment of Upper Extremities.” In *Trends in Ergonomics/human Factors III*, 573–580.

Arata, Jumpei, Keiichi Ohmoto, Roger Gassert, Olivier Lambercy, Hideo Fujimoto, and Ikuo Wada. 2013. “A New Hand Exoskeleton Device for Rehabilitation Using a Three-Layered Sliding Spring Mechanism:” 3902–3907.

Atkins, Michal S, Jane M Baumgarten, Yuriko Lynn Yasuda, Rodney Adkins, Robert L Waters, Pierre Leung, and Philip Requejo. 2008. “Mobile Arm Supports: Evidence-Based Benefits and Criteria for Use.” *The Journal of Spinal Cord Medicine*.

Battezzato, Alessandro. 2014. “Towards an Underactuated Finger Exoskeleton: An Optimization Process of a Two-Phalange Device Based on Kinetostatic Analysis.” *Mechanism and Machine Theory* 78: 116–130. doi:10.1016/j.mechmachtheory.2014.03.007. http://dx.doi.org/10.1016/j.mechmachtheory.2014.03.007.

———. 2015. “Kinetostatic Analysis and Design Optimization of an N-Finger Underactuated Hand Exoskeleton.” *Mechanism and Machine Theory* 88: 86–104. doi:10.1016/j.mechmachtheory.2014.12.007. http://dx.doi.org/10.1016/j.mechmachtheory.2014.12.007.

Bien, Z Zenn, and Dimitar Stefanov. 2004. *Advances in Rehabilitation Robotics: Human-Friendly Technologies on Movement Assistance and Restoration for People with Disabilities*. Vol. 306. Springer Science & Business.

Birglen, L., and Clement M. Gosselin. 2006. “Force Analysis of Connected Differential Mechanisms: Application to Grasping.” *The International Journal of Robotics Research* 25: 1033–1046. doi:10.1177/0278364906068942.

Birglen, Lionel, and Clément M. Gosselin. 2004. “Kinetostatic Analysis of Underactuated Fingers.” *IEEE Transactions on Robotics and Automation* 20 (2): 211–221. doi:10.1109/TRA.2004.824641.

Birglen, Lionel, Thierry Laliberté, and Clément Gosselin. 2008. *Underactuated Robotic Hands*. *Springer Tracts in Advanced Robotics*. Vol. 40. doi:10.1007/978-3-540-77459-4.

Biryukova, E V, and V Z Yourovskaya. 1994. “A Model of Human Hand Dynamics.” *Advances in the Biomechanics of the Hand and Wrist*: 107–122.

Bizzi, E, V C K Cheung, A d’Avella, P Saltiel, and Me Tresch. 2008. “Combining Modules for Movement.” *Brain Research Reviews* 57 (1): 125–133.

Bizzi, Emilio, and Vincent C K Cheung. 2013. “The Neural Origin of Muscle Synergies.”

Carrozza, Maria Chiara, C Suppo, Fabrizio Sebastiani, Bruno Massa, Fabrizio Vecchi, Roberto Lazzarini, Mark R Cutkosky, and Paolo Dario. 2004. “The SPRING Hand: Development of a Self-Adaptive Prosthesis for Restoring Natural Grasping.” *Autonomous Robots* 16 (2): 125–141.

Catalano, Manuel G, Giorgio Grioli, Alessandro Serio, Edoardo Farnioli, Cristina Piazza, and Antonio Bicchi. 2012. “Adaptive Synergies for a Humanoid Robot Hand.” In *Humanoid Robots (Humanoids), 2012 12th IEEE-RAS International Conference on*, 7–14.

Cempini, Marco, Student Member, Stefano Marco, Maria De Rossi, Tommaso Lenzi, Mario Cortese, Francesco Giovacchini, Nicola Vitiello, and Maria Chiara Carrozza. 2013. “Kinematics and Design of a Portable and Wearable Exoskeleton for Hand Rehabilitation.”

Chen Chen, Fai, Silvia Appendino, Alessandro Battezzato, Alain Favetto, Mehdi Mousavi, and Francesco Pescarmona. 2013. “Constraint Study for a Hand Exoskeleton: Human Hand Kinematics and Dynamics.” *Journal of Robotics* 2013.

Chiri, a., F. Giovacchini, N. Vitiello, E. Cattin, S. Roccella, F. Vecchi, and M.C. Carrozza. 2009. “HANDEXOS: Towards an Exoskeleton Device for the Rehabilitation of the Hand.” *2009 IEEE/RSJ International Conference on Intelligent Robots and Systems* (October): 1106–1111. doi:10.1109/IROS.2009.5354376.

Chiri, Azzurra, Nicola Vitiello, Student Member, Francesco Giovacchini, Stefano Roccella, Fabrizio Vecchi, Maria Chiara Carrozza, and Associate Member. 2012.

"Mechatronic Design and Characterization of the Index Finger Module of a Hand Exoskeleton for Post-Stroke Rehabilitation" 17 (5): 884–894.

Cobos, Salvador, Manuel Ferre, and Javier Ortego. 2008. "Efficient Human Hand Kinematics for Manipulation Tasks." *Direct*: 22–26.

Cobos, Salvador, Manuel Ferre, MA Sánchez-Urán, and Javier Ortego. 2007. "Constraints for Realistic Hand Manipulation." *Proc. Presence 2007*: 369–370.

Curtiss, Ellen T., and Eustis Susan. 2014. "Rehabilitation Robots, Active Prostheses, and Exoskeletons Market Shares, Strategies, and Forecasts, Worldwide, 2014 to 2020: Markets To Reports." *Jul 31*.

Cutkosky, Mark R, and Robert D Howe. 1990. "Human Grasp Choice and Robotic Grasp Analysis." *Dextrous Robot Hands* 1: 5–31.

d'Avella, Andrea, Philippe Saltiel, and Emilio Bizzi. 2003. "Combinations of Muscle Synergies in the Construction of a Natural Motor Behavior." *Nature Neuroscience* 6 (3): 300–308.

Darling, WARREN G, and KELLY J Cole. 1990. "Muscle Activation Patterns and Kinetics of Human Index Finger Movements." *Journal of Neurophysiology* 63 (5): 1098–1108.

De Luca, A, S Iannitti, R Mattone, and G Oriolo. 2002. "Underactuated Manipulators: Control Properties and Techniques." *Machine Intelligence and Robotic Control* 4 (3): 113–125.

de Visser, H, and J L Herder. 2000. "Force-Directed Design of a Voluntary Closing Hand Prosthesis." *Journal of Rehabilitation Research and Development* 37 (3): 261–271.

Derringer, George C. "MAXIMIZING USE OF RECYLED MATERIALS IN FORMULATION PRODUCTS."

Dictionary, Oxford English. 1989. "Oxford: Oxford University Press."

Dollar, Aaron M, and Robert D Howe. 2007. "The SDM Hand as a Prosthetic Terminal Device: A Feasibility Study." In *Rehabilitation Robotics, 2007. ICORR 2007. IEEE 10th International Conference on*, 978–983.

Dollar, Aaron M., and Hugh Herr. 2008. "Lower Extremity Exoskeletons and Active Orthoses: Challenges and State-of-the-Art." *IEEE Transactions on Robotics* 24 (1): 144–158. doi:10.1109/TRO.2008.915453.

Edwards, Sandra J, Donna J Buckland, and Jenna McCoy-Powlen. 2002. *Developmental & Functional Hand Grasps*. Slack Thorofare.

Ertas, Ismail Hakan, Elif Hocaoglu, Duygun Erol Barkana, and Volkan Patoglu. 2009. "Finger Exoskeleton for Treatment of Tendon Injuries." *2009 IEEE International*

Conference on Rehabilitation Robotics (June): 194–201. doi:10.1109/ICORR.2009.5209487.

Favetto, Alain. 2014. "Glove Exoskeleton for Extra-Vehicular Activities: Analysis of Requirements and Prototype Design." Politecnico di Torino.

Feix, Thomas, Javier Romero, Heinz-Bodo Schmiedmayer, Aaron M Dollar, and Danica Kragic. "The GRASP Taxonomy of Human Grasp Types."

Fontana, Marco, Andrea Dettori, Fabio Salsedo, and Massimo Bergamasco. 2009. "Mechanical Design of a Novel Hand Exoskeleton for Accurate Force Displaying." In *Robotics and Automation, 2009. ICRA'09. IEEE International Conference on*, 1704–1709.

Foumashi, Mohammad Mozaffari, Marco Troncossi, and Vincenzo Parenti Castelli. 2011. "State-of-the-Art of Hand Exoskeleton Systems.".

Garrett, J. W. 1970. "Anthropometry of the Hands of Male Air Force Flight Personnel." *Report No. AMRL-TR-69-42*.

———. 1971. "Anthropometry of the Hands of Female Air Force Flight Personnel." *Applied Ergonomics* 2 (4): 244. doi:10.1016/0003-6870(71)90119-0.

Gosselin, C., and J. Angeles. 1991. "A Global Performance Index for the Kinematic Optimization of Robotic Manipulators." *Journal of Mechanical Design* 113 (September 1991): 220. doi:10.1115/1.2912772.

Greenwood, C T. 1986. "Simulated Annealing Algorithms: An Overview" (x): 102–104.

Habib, Sahar Refaat, and Nashwa Nabil Kamal. 2010. "Stature Estimation from Hand and Phalanges Lengths of Egyptians." *Journal of Forensic and Legal Medicine* 17 (3): 156–160.

Harrington, E C. 1965. "The Desirability Function." *Industrial Quality Control* 21 (10): 494–498.

Hasegawa, Yasuhisa, Yasuyuki Mikami, Kosuke Watanabe, and Yoshiyuki Sankai. 2008. "Five-Fingered Assistive Hand with Mechanical Compliance of Human Finger." *2008 IEEE International Conference on Robotics and Automation* (May): 718–724. doi:10.1109/ROBOT.2008.4543290.

Hasser, Christopher J. 1995. "Force-Reflecting Anthropomorphic Hand Masters." *Technical Report, Crew Systems Directorate, Biodynamics and Biocommu-Nications Division, Armstrong Laboratory* (July).

Heo, Pilwon, Gwang Min Gu, Soo-jin Lee, Kyehan Rhee, and Jung Kim. 2012. "Current Hand Exoskeleton Technologies for Rehabilitation and Assistive Engineering." *International Journal of Precision Engineering and*

Manufacturing 13 (5) (May 4): 807–824. doi:10.1007/s12541-012-0107-2.

Hirose, Shigeo, and Shugen Ma. 1991. "Coupled Tendon-Driven Multijoint Manipulator." *Proc. IEEE International Conference on Robotics and Automation ICRA* (April): 1268–1275. doi:10.1109/ROBOT.1991.131786.

Hirose, Shigeo, and Yoji Umetani. 1978. "The Development of Soft Gripper for the Versatile Robot Hand." *Mechanism and Machine Theory* 13 (3): 351–359. doi:10.1016/0094-114X(78)90059-9.

Ho, N S K, K Y Tong, X L Hu, K L Fung, X J Wei, W Rong, and E a Susanto. 2011. "An EMG-Driven Exoskeleton Hand Robotic Training Device on Chronic Stroke Subjects: Task Training System for Stroke Rehabilitation." *IEEE ... International Conference on Rehabilitation Robotics : [proceedings]* 2011 (January): 5975340. doi:10.1109/ICORR.2011.5975340.

Hogan, Neville. 1985. "Impedance Control: An Approach to Manipulation: Part II - Implementation." *Journal of Dynamic Systems, Measurement, and Control* 107 (1): 8–16.

Hu, X L, K Y Tong, X J Wei, W Rong, E A Susanto, and S K Ho. 2013. "The Effects of Post-Stroke Upper-Limb Training with an Electromyography (EMG)-Driven Hand Robot." *Journal of Electromyography and Kinesiology* 23 (5): 1065–1074.

Iberall, Thea. 1997. "Human Prehension and Dexterous Robot Hands." *The International Journal of Robotics Research* 16 (3): 285–299.

IFToMM Commission. 1991. "Terminology for the Theory of Machines and Mechanisms." *Mechanism and Machine Theory* 26 (5): 435–539.

In, HyunKi, Kyu-Jin Cho, KyuRi Kim, and BumSuk Lee. 2011. "Jointless Structure and under-Actuation Mechanism for Compact Hand Exoskeleton." In *Rehabilitation Robotics (ICORR), 2011 IEEE International Conference on*, 1–6.

Iqbal, Jamshed, and Khelifa Baizid. 2015. "Stroke Rehabilitation Using Exoskeleton-Based Robotic Exercisers: Mini Review." *Biomedical Research (India)* 26 (1): 197–201.

Iqbal, Jamshed, Nikos G Tsagarakis, and Darwin G Caldwell. 2011. "A Multi-DOF Robotic Exoskeleton Interface for Hand Motion Assistance." *Conference Proceedings : Annual International Conference of the IEEE Engineering in Medicine and Biology Society. IEEE Engineering in Medicine and Biology Society. Conference* 2011 (January): 1575–8. doi:10.1109/IEMBS.2011.6090458. http://www.ncbi.nlm.nih.gov/pubmed/22254623.

Jones, Christopher L, Furui Wang, Robert Morrison, Niladri Sarkar, and Derek G Kamper. 2014. "Design and Development of the Cable Actuated Finger Exoskeleton for Hand Rehabilitation Following Stroke." *Mechatronics,*

IEEE/ASME Transactions on 19 (1): 131–140.

Kamakura, Noriko, Michiko Matsuo, Harumi Ishii, Fumiko Mitsuboshi, and Yoriko Miura. 1980. "Patterns of Static Prehension in Normal Hands." *American Journal of Occupational Therapy* 34 (7): 437–445.

Kapandji I.A. 1970. *The Physiology of the Joints: Upper Limb. British Journal of Surgery*. Vol. 1. John Wiley & Sons, Ltd. doi:10.1002/bjs.1800570821. http://dx.doi.org/10.1002/bjs.1800570821.

Krovi, Venkat, G. K. Ananthasuresh, and Vijay Kumar. 2002. "Kinematic and Kinetostatic Synthesis of Planar Coupled Serial Chain Mechanisms." *Journal of Mechanical Design* 124 (2): 301. doi:10.1115/1.1464563.

Kuo, Li-Chieh, Shih-Wei Chen, Chien-Ju Lin, Wei-Jr Lin, Sheng-Che Lin, and Fong-Chin Su. 2013. "The Force Synergy of Human Digits in Static and Dynamic Cylindrical Grasps." *PloS One* 8 (3): e60509.

Laliberté, Thierry, Lionel Birglen, and M. Clément Gosselin. 2003. "Underactuation in Robotic Grasping Hands." *Machine Intelligence & Robotic Control* 4 (3): 1–11.

Laliberté, Thierry, and Clément M Gosselin. 2001. "Underactuation in Space Robotic Hands." In *International Symposium on Artificial Intelligence, Robotics and Automation in Space, Montr{é}al, Canada*, 18–21.

Landsmeer, J M F. 1962. "Power Grip and Precision Handling." *Annals of the Rheumatic Diseases* 21 (2): 164.

Lara-Molina, F.A., J.M. Rosario, and D. Dumur. 2011. "Multi-Objective Optimization of Stewart-Gough Manipulator Using Global Indices:" 79 –85. doi:10.1109/AIM.2011.6026996.

Lin, John, Ying Wu, and Thomas S Huang. 2000. "Modeling the Constraints of Human Hand Motion." In *Human Motion, 2000. Proceedings. Workshop on*, 121–126.

Loconsole, Claudio, D Leonardis, Michele Barsotti, Massimiliano Solazzi, Antonio Frisoli, Marco Bergamasco, M Troncossi, M Mozaffari Foumashi, C Mazzotti, and V Parenti Castelli. 2013. "An EMG-Based Robotic Hand Exoskeleton for Bilateral Training of Grasp." In *World Haptics Conference (WHC), 2013*, 537–542.

Lowe, B D, Y Kong, and J Han. 2006. "Development and Application of a Hand Force Measurement System." In *Proceedings of the XVIth Triennial Congress of the International Ergonomics Association*.

Lu, Yi, Gazell Mapili, Gerry Suhali, Shaochen Chen, and Krishnendu Roy. 2006. "A Digital Micro-Mirror Device-Based System for the Microfabrication of Complex, Spatially Patterned Tissue Engineering Scaffolds." *Journal of Biomedical*

Materials Research Part A 77 (2): 396–405.

Martin, J., and M. Grossard. 2014. "Design of a Fully Modular and Backdrivable Dexterous Hand." *The International Journal of Robotics Research* 33 (5): 783–798. doi:10.1177/0278364913511677.

Milner, Theodore E, and David W Franklin. 1998. "Characterization of Multijoint Finger Stiffness: Dependence on Finger Posture and Force Direction." *Biomedical Engineering, IEEE Transactions on* 45 (11): 1363–1375.

Mulas, Marcello, Michele Folgheraiter, and Giuseppina Gini. 2005. "An EMG-Controlled Exoskeleton for Hand Rehabilitation." In *Rehabilitation Robotics, 2005. ICORR 2005. 9th International Conference on*, 371–374.

Myrand, Mathieu, and CM Gosselin. 2004. "Dynamic Simulation of an Underactuated Hand for Space Applications." *CISM-IFToMM Symposium on Robot.*

Pons, José L. 2008. *Wearable Robots: Biomechatronic Exoskeletons*. John Wiley & Sons.

Rossi, Cesare, and Sergio Savino. 2014. "An Underactuated Multi-Finger Grasping Device." *International Journal of Advanced Robotic Systems* 11 (1). doi:10.5772/57419.

Saliba, Michael A, Duncan Camilleri, and Matthew J Farrugia. 2005. "Development of an Anthropomorphic Robot Hand and Wrist for Teleoperation Applications:" 203–208.

Santello, Marco, Martha Flanders, and John F Soechting. 1998. "Postural Hand Synergies for Tool Use." *The Journal of Neuroscience* 18 (23): 10105–10115.

Seifried, Robert. 2014. *Dynamics of Underactuated Multibody Systems*. Vol. 205. doi:10.1007/978-3-319-01228-5. http://link.springer.com/10.1007/978-3-319-01228-5.

Shields, Bobby L, John A Main, Steven W Peterson, and Alvin M Strauss. 1997. "An Anthropomorphic Hand Exoskeleton to Prevent Astronaut Hand Fatigue during Extravehicular Activities." *Systems, Man and Cybernetics, Part A: Systems and Humans, IEEE Transactions on* 27 (5): 668–673.

Skerik, Sharon K, Madge W Weiss, and Adrian E Flatt. 1971. "Functional Evaluation of Congenital Hand Anomalies." *The American Journal of Occupational Therapy: Official Publication of the American Occupational Therapy Association* 25 (2): 98.

Stergiopoulos, Panagiotis, Philippe Fuchs, and Claude Laurgeau. 2003. "Design of a 2-Finger Hand Exoskeleton for VR Grasping Simulation." *Eurohaptics, Dublin, Ireland*: 80–93.

Tang, T, D Zhang, T Xie, and X Zhu. 2013. “An Exoskeleton System for Hand Rehabilitation Driven by Shape Memory Alloy.” In *Robotics and Biomimetics (ROBIO), 2013 IEEE International Conference on*, 756–761. doi:10.1109/ROBIO.2013.6739553.

Taylor, Craig L, and Robert J Schwarz. 1955. “The Anatomy and Mechanics of the Human Hand.” *Artificial Limbs* 2 (2): 22–35.

Tjahyono, Arief P, Kean C Aw, Harish Devaraj, Wisnu Surendra, Enrico Haemmerle, and Jadranka Travas-Sejdic. 2013. “A Five-Fingered Hand Exoskeleton Driven by Pneumatic Artificial Muscles with Novel Polypyrrole Sensors.” *Industrial Robot: An International Journal* 40 (3): 251–260.

Tong, K Y, P M K PANG, M Chen, S K Ho, H ZHOU, and D T W CHAN. 2013. “Wearable Power Assistive Device for Helping a User to Move Their Hand.” Google Patents. http://www.google.ch/patents/US8574178.

Tong, K. Y., S. K. Ho, P. M K Pang, X. L. Hu, W. K. Tam, K. L. Fung, X. J. Wei, P. N. Chen, and M. Chen. 2010. “An Intention Driven Hand Functions Task Training Robotic System.” *2010 Annual International Conference of the IEEE Engineering in Medicine and Biology Society, EMBC’10*: 3406–3409. doi:10.1109/IEMBS.2010.5627930.

Tsai, Lung-Wen. “Robot Analysis - The Mechanics of Serial and Parallel Manipulator.”

———. 1995. “Design of Tendon-Driven Manipulators.” *Journal of Vibration and Acoustics*. doi:10.1115/1.2838680.

Van Ham, Ronald, Thomas G. Sugar, Bram Vanderborght, Kevin W. Hollander, and Dirk Lefeber. 2009. “Compliant Actuator Designs.” *IEEE Robotics & Automation Magazine* 16 (3): 81–94. doi:10.1109/MRA.2009.933629.

Vanderborght, B., A. Albu-Schaeffer, A. Bicchi, E. Burdet, D. G. Caldwell, R. Carloni, M. Catalano, et al. 2013. “Variable Impedance Actuators: A Review.” *Robotics and Autonomous Systems* 61 (12): 1601–1614. doi:10.1016/j.robot.2013.06.009.

Wege, Andreas, and Günter Hommel. 2005. “Development and Control of a Hand Exoskeleton for Rehabilitation of Hand Injuries.” In *Intelligent Robots and Systems, 2005.(IROS 2005). 2005 IEEE/RSJ International Conference on*, 3046–3051.

Wege, Andreas, Konstantin Kondak, and Guenter Hommel. 2006. “Force Control Strategy for a Hand Exoskeleton Based on Sliding Mode Position Control.” In *Intelligent Robots and Systems, 2006 IEEE/RSJ International Conference on*, 4615–4620.

Wyndaele, M, and J-J Wyndaele. 2006. “Incidence, Prevalence and Epidemiology of Spinal Cord Injury: What Learns a Worldwide Literature Survey?” *Spinal Cord*

44 (9): 523–529. doi:10.1038/sj.sc.3101893.

Xu, Kai, Huan Liu, Zenghui Liu, Yuheng Du, and Xiangyang Zhu. 2015. "A Single-Actuator Prosthetic Hand Using a Continuum Differential Mechanism." In *Robotics and Automation (ICRA), 2015 IEEE International Conference on*, 6457–6462.

Yamaura, Hiroshi, Kojiro Matsushita, Ryu Kato, and Hiroshi Yokoi. 2009. "Development of Hand Rehabilitation System for Paralysis Patient - Universal Design Using Wire-Driven Mechanism." *Proceedings of the 31st Annual International Conference of the IEEE Engineering in Medicine and Biology Society: Engineering the Future of Biomedicine, EMBC 2009*: 7122–7125. doi:10.1109/IEMBS.2009.5332885.

Zheng, Joshua Z., Sara De La Rosa, Aaron M. Dollar, and Sara De La Rosa. 2011. "An Investigation of Grasp Type and Frequency in Daily Household and Machine Shop Tasks." *Proceedings of the 2011 IEEE International Conference on Robotics and Automation (ICRA)*: 4169–4175. doi:10.1109/ICRA.2011.5980366. citeulike-article-id:9457399.